

UNIVERSITÉ VICTOR SEGALEN BORDEAUX 2

and

CHARLES UNIVERSITY IN PRAGUE

1<sup>st</sup> Faculty of Medicine



**NON-CANONICAL BIOENERGETICS OF THE CELL**

DOCTORAL THESIS

PRAGUE 2009

Katarína Smolková

This thesis was elaborated in cooperation of the Membrane Transport Biophysics, laboratory of Institute of Physiology, Academy of Sciences of the Czech Republic and the laboratory U688 Physiopathologie Mitochondriale of INSERM, Bordeaux, France, supported by postgraduate fellowship provided by French government in the program entitled “Doctorat en co-tutelle”. Foreign stage was further supported by foundation “Nadání Josefa, Marie a Zdeňky Hlávkových”, foundation “Dagmar a Václava Havlových VIZE 97”, and Fond Mobility UK.

PHD studies proceeded from October 2005 PHD in study program Biochemistry and Pathobiochemistry.

Author: Mgr. Katarína Smolková  
Supervisors: Rodrigue Rossignol, PhD.  
RNDr. Petr Ježek, DrSc.

Prague, June 2009

.....  
Katarína Smolková

## **AKNOWLEDGEMENTS**

I would like to express my grateful thanks to supervisors Petr Ježek and Rodrigue Rossignol for giving me the opportunity to work with their groups and introducing me to the most exciting field of research. I appreciate their kind supervising, patience, enthusiasm and support.

Thanks belong also to Thierry Letellier, head of the department U688 in Bordeaux for permitting me to work in his laboratory. I must also thank to authors of the presented articles, namely Lukáš Alán, Eva Valoušková, Martin Modrianský and Jitka Šantorová.

Special thanks to all people I met in both laboratories for great time I spent with them and for making my time in lab really enjoyable.

# CONTENT

LIST OF FIGURES AND TABLES.....	1
1. INTRODUCTION.....	3
1.1. Significance of non-canonical bioenergetics.....	3
1.2. Specific aspects of presented studies.....	5
1.3. Aims.....	7
2. BACKGROUND.....	8
2.1. Mitochondria – general features.....	8
2.1.1. Mitochondria, their structure and composition.....	8
2.1.2. Mitochondrial biogenesis.....	10
2.1.3. Function of mitochondria.....	11
2.1.3.1. Oxidative phosphorylation.....	11
2.1.3.2. Energy metabolism.....	12
2.1.3.3. Apoptosis.....	13
2.2. Basic facts for CIDE proteins.....	14
2.2.1. Expression.....	14
2.2.2. Biological function.....	15
2.2.3. Interaction with UCP1.....	16
2.2.4. Possible migration of CIDE proteins into mitochondria and consequences.....	16
2.3. Bioenergetics of cancer cells.....	18
2.3.1. Energy metabolism of cancer cells.....	18
2.3.1.1. Warburg effect.....	18
2.3.1.2. Variability.....	18
2.3.1.3. Dysfunctional mitochondria and alterations in cancer cells.....	19
2.3.1.4. Crabtree effect.....	20
2.3.2. Possible origin of cancer metabolic remodeling.....	22
2.3.2.1. Hypoxia: Adaptation and survival in low oxygen.....	22
2.3.2.1.1. Tumor oxygenation.....	22
2.3.2.1.2. Respiration at low oxygen.....	24
2.3.2.1.3. HIF pathway.....	25
2.3.2.1.4. AMPK pathway NFkB, mTOR participation in hypoxia.....	32
2.3.2.2. Oncogenes in metabolic reprogramming.....	33
2.3.2.3. Proliferation rate.....	36
2.3.2.4. Metabolism of glutamine in cancer cells, glucose deprivation.....	38
2.3.2.5. Reversal to fetal phenotype.....	40
2.4. Mitochondrial uncoupling protein isoforms.....	42
2.4.1. Uncoupling by uncoupling proteins.....	42
2.4.2. Possible physiological roles of mitochondrial uncoupling proteins UCP2 to 5.....	45
2.4.2.1. UCP2 and diabetes.....	45
2.4.2.2. UCP2 and immunity response.....	46
2.4.2.3. UCP2 and atherosclerosis.....	46
2.4.2.4. UCP2 and neuroprotection.....	47
2.4.3. Minute protein amount expression of uncoupling proteins and its consequences.....	47
2.4.4. Existing transcript quantifications for mitochondrial uncoupling proteins UCP2 to 5.....	48
3. METHODS.....	50
3.1. Methods A.....	50
3.1.1. Cell cultures.....	50
3.1.1.1. Culturing conditions.....	50
3.1.1.2. Hypoxic cultivation.....	50
3.1.2. Cell proliferation.....	50
3.1.3. Neutral red assay.....	51
3.1.4. Microscopy.....	51
3.1.5. Lowry assay.....	51

3.1.6.	ATP measurement.....	52
3.1.7.	Western blotting .....	52
3.1.7.1.	Sample preparation.....	52
3.1.7.2.	Electrophoresis.....	52
3.1.7.3.	Protein transfer and immunodetection .....	53
3.1.7.4.	Western-blot detection of CIDEa .....	53
3.1.8.	Respirometry.....	54
3.1.8.1.	General use of oxygraph .....	54
3.1.8.2.	Instrumental background.....	54
3.1.8.3.	Measurement of oxygen kinetics .....	55
3.1.8.4.	Respiratory rate and respiratory states of intact cells .....	56
3.1.8.5.	Cell permeabilization.....	57
3.1.8.6.	Multiple substrate-inhibitor protocol with permeabilized cells.....	57
3.1.9.	Statistical analysis .....	57
3.2.	Methods B.....	58
3.2.1.	Experimental animals.....	58
3.2.2.	RNA preparation .....	58
3.2.2.1.	Total RNA isolation.....	58
3.2.2.2.	DNase treatment .....	58
3.2.2.3.	mRNA isolation.....	59
3.2.2.4.	Determination of RNA amount .....	59
3.2.3.	Quantitative real-time PCR .....	59
3.2.3.1.	Signal detection.....	59
3.2.3.2.	Design of LightCycler primers and hybridization probes.....	60
3.2.3.3.	Quantification method.....	60
3.2.3.4.	Performance of the real-time RT-PCR .....	60
3.2.4.	Statistical analysis .....	61
3.3.	Methods C.....	62
3.3.1.	Cell cultures.....	62
3.3.2.	Expression plasmids preparation .....	62
3.3.3.	Confocal microscopy .....	63
3.3.4.	Initiation of apoptosis .....	63
3.3.5.	Preparation of subcellular fractions.....	64
3.3.6.	Izolation of mitochondria.....	64
3.3.7.	Caspase-3 activity.....	64
3.3.8.	Western-blot detection of CIDEa .....	65
3.3.9.	<i>In situ</i> detection of apoptosis (TUNEL assay) .....	65
3.3.10.	Immunocytochemistry .....	65
3.3.11.	Cell death assay.....	65
3.3.12.	Quantitative RT-PCR.....	66
3.3.13.	Statistical analysis .....	66
4.	RESULTS.....	67
4.1.	Glucose deprivation .....	67
4.1.1.	Cell growth .....	67
4.1.2.	Cell viability upon mitochondrial inhibition .....	68
4.1.3.	Respiration .....	69
4.1.4.	ATP synthesis .....	73
4.1.5.	Expression of OXPHOS proteins .....	73
4.2.	Hypoxia .....	74
4.2.1.	Cell viability under the hypoxia.....	74
4.2.2.	Respiration .....	74
4.2.3.	OXPHOS proteins expression under hypoxia .....	75
4.3.	Mitochondrial network morphology .....	76
4.4.	Crabtree effect.....	77
4.5.	Absolute quantifications of UCP2 transcripts.....	78
4.6.	Absolute quantifications of UCP3 transcripts.....	78
4.7.	Absolute quantifications of UCP4 transcripts.....	78

4.8.	Absolute quantifications of UCP5 transcripts .....	79
4.9.	Quantification of UCPs transcript levels in UCP2-null mice tissues .....	79
4.10.	Quantification of GAPDH .....	80
4.11.	Quantification of CIDEA transcript level in rat tissues .....	80
4.12.	CIDEa overexpression leads to apoptosis in HeLa cells .....	81
4.13.	Cellular distribution of CIDEA upon its overexpression .....	82
4.14.	Role of CIDE-N and CIDE-C domain in subcellular localization .....	83
4.15.	CIDEa redistribution is associated with treatment of HeLa cells with apoptosis inducers ....	84
5.	DISCUSSION .....	85
6.	CONCLUSIONS .....	98
7.	SUMMARY .....	99
8.	REFERENCES .....	101
ABBREVIATIONS .....		114
LIST OF PUBLICATIONS .....		116
APPENDIX 1		
APPENDIX 2		
APPENDIX 3		

## LIST OF FIGURES AND TABLES

- FIG 2-1. Compartmentalization of a mitochondrion.  
FIG 2-2. Mitochondrial network.  
FIG 2-3. Mitochondrial DNA.  
FIG 2-4. Mitochondrial respiratory chain.  
FIG 2-5. Anaplerotic and cataplerotic flux of the TCA cycle.  
FIG 2-6. Models of mitochondrial permeability transition.  
FIG 2-7. Distribution of CIDE domains in CIDE and DFF proteins.  
FIG 2-8. Model for the inhibition and activation of DFF40.  
FIG 2-9. Distribution of hypoxic regions within tumor.  
FIG 2-10. Scheme of glutaminolysis.  
TAB 2-1. Overview of tumor oxygenation of selected tumor types 1.  
TAB 2-2. Overview of tumor oxygenation of selected tumor types 2.  
FIG 2-11. Uncoupling of respiration by uncoupling proteins, proposed models.
- FIG 3-1. HTB-125 and HTB-126.  
FIG 3-2. Oxygen signal calibration.  
FIG 3-3. Background calibration.  
FIG 3-4. Oxygen kinetics measurement.  
FIG 3-5. Cell permeabilization of HTB-126 GAL.  
FIG 3-6. Schematic model of real-time PCR quantification using fluorescent hybridization probes.  
FIG 3-7. Calibration for absolute quantification.  
TAB 3-1. Primer sets and fluorescent hybridization probes used for RT-PCR quantification of UCP mRNAs.  
FIG 3-8. Tetracycline-inducible expression.  
FIG 3-9. Scheme of CIDE-N and CIDE-C domain deletion by PCR.  
TAB 3-2. Primer sequences used for expression plasmids preparation.  
TAB 3-3. Primers and probes sequences used for Real-time quantification of rat CIDEa.
- FIG 4-1. Effect of mitochondrial inhibition on cell viability of cancer HTB-126 cells.  
FIG 4-2. Influence of cultivation conditions on cell respiration of normal and breast cancer cells.  
FIG 4-3. Influence of cultivation conditions on cell respiration of normal and breast cancer cells – oxygen kinetics.  
FIG 4-4. Influence of cultivation conditions on cell respiration of normal and breast cancer cells –  $C_{50}$ .  
FIG 4-5. Variation of  $C_{50}$  with respiratory flux.  
FIG 4-6. Respiratory ratios of HTB-125 and HTB-126 intact cells Glc vs. Gln/GAL; components of cellular respiration in intact cells.  
FIG 4-7. Respiratory ratios of permeabilized cancer cells; components of mitochondrial respiration in permeabilized cells.  
TAB 4-1. Quantification of respiratory ratios of permeabilized cells.  
FIG 4-8. ATP synthesis in HTB-126 Glc.  
FIG 4-9. Western-blot quantification of the respiratory chain content of normal and breast cancer cells upon glucose deprivation.  
FIG 4-10. Cell viability of HTB-125 and HTB-126 under normoxia and hypoxia.  
FIG 4-11. Effect of hypoxia on respiratory flux and medium pH of normal and breast cancer cells.

- FIG 4-12. Western-blot quantification of the respiratory chain content of breast cancer cells HTB-126 Glc grown under hypoxia.
- FIG 4-13. Mitochondrial network in HTB-125 and HTB-126 in normoxia and hypoxia.
- FIG 4-14. Demonstration of Crabtree effect occurring in breast cancer cells.
- FIG 4-15. Respiration of cancer cells upon glucose addition and removal, comparison of routine and uncoupled flux.
- TAB 4-2. Quantified  $c_{50}$  values and uncoupling phosphorylation ratios in response to glucose presence.
- FIG 4-16. Quantification of UCPn mRNA in rat tissues.
- FIG 4-17. Quantification of UCPn mRNA in mouse tissues.
- FIG 4-18. Quantification of UCPn mRNA in control and UCP2<sup>-/-</sup> mouse.
- FIG 4-19. Quantification of GAPDH mRNA in mouse and rat tissues.
- FIG 4-20. Absolute quantification of mRNA transcripts of CIDEA in rat tissues.
- FIG 4-21. Induction of CIDEa expression – western blot.
- FIG 4-22. TUNEL assay of HeLa cells expressing CIDEa.
- FIG 4-23. Mitochondrial localization of CIDEa in 293-HEK cells – confocal microscopy.
- FIG 4-24. Subcellular localization of CIDE $\Delta$ C in 293-HEK cells – confocal microscopy.
- FIG 4-25. Subcellular localization of CIDE $\Delta$ N in 293-HEK cells – confocal microscopy.
- FIG 4-26. Subcellular localization of CIDEa in HeLa cells treated with valinomycin and camptothecin.
- FIG 4-27. Redistribution of CIDEa from cytosolic to nuclear fraction of HeLa cells– western-blot.
- FIG 4-28. Effect of pan-caspase inhibitor on apoptosis induced by CIDEa overexpression.
- FIG 5-1. Proposed mechanism of downregulation of mitochondrial respiration in HTB-126 Glc.
- FIG 5-2. Proposed model of substrate distribution in HTB-126 GAL.

# 1. INTRODUCTION

## 1.1. SIGNIFICANCE OF NON-CANONICAL BIOENERGETICS

Canonical bioenergetics has explained on the basis of Mitchell chemiosmotic theory the mechanisms of ATP synthesis in mitochondria, chloroplasts, bacteria, and other entities, including the essential coupling of the electron flow through the complexes of the respiratory chain and concomitant proton pumping with the ATP synthesis by the ATP synthase. Protons are the intermediates of this coupling and a physical quantity called gradient of electrochemical potential of protons (across the inner mitochondrial membrane) taken at pH 7,  $\Delta\tilde{\mu}_{H^+}$ . When expressed in mV (divided by Faraday constant) the quantity is called according to Nobel Prize laureate Peter Mitchell, the protonmotive force,  $\Delta p$  ( $\Delta p = \Delta\psi_m - 60\Delta pH$ , in mV at 30 °C, where  $\Delta\psi_m$  is membrane potential). Yet, the canonical bioenergetics has recognized detail structure of huge respiratory chain complexes (pioneered by Hartmudt Michel as Nobel Prize laureate), rotatory mechanism of ATP synthesis as well as structure of the ATP synthase (other 1997 Nobel laureates, John Walker, Paul D Boyer) and numerous other findings including biogenesis and assembly of these complexes.

Nevertheless, canonical bioenergetics turned out to be unable to explain various physiological and pathological phenomena. Non-canonical bioenergetics concerns with those physiological and pathophysiological situations under which ATP synthesis is suppressed. The early findings of Otto Warburg (actually the first Nobel Prize laureate in bioenergetics) led to his hypothesis on the exclusively glycolytic phenotype of tumor cells. Since 1961 a brown adipose tissue has been discovered, a tissue deliberately dissipating energy into the heat. Subsequent discoveries of mitochondrial uncoupling protein-1 (UCP1), originally found specific for brown adipose tissue (today known with extended expression pattern), and the whole subfamily of uncoupling proteins (UCP2 to UCP5 plus three plant isoforms) have opened a new chapter of non-canonical bioenergetics, recognizing that a mild uncoupling may physiologically regulate superoxide formation of mitochondria, hence the redox signaling in mitochondria and cell (see below). A self-standing field concerns with the "tax for life", i.e. inevitable inherent formation of superoxide within the respiratory chain Complexes I and III. Superoxide is a species at the top of cascade of reactive oxygen species (ROS), creating oxidative stress if elevated. A constant ROS formation as an inevitable byproduct of respiration leads to aging and if pathogenically accelerated it causes numerous diseases. This field of oxidative stress however, has expanded into a vast field of redox regulations, recognizing "physiologically slight" ROS elevations as fundamentally initiating certain information signaling pathways. An exemplar prototype concerns with ROS-initiation of hypoxia-mediated-factor-signaling,

in fact representing oxygen sensing in hypoxia by the respiratory chain. Thus non-canonical bioenergetics of the cell is the science for years to come.

Related disciplines that might be also grouped under umbrella of non-canonical bioenergetics concern with the mitochondrial pathways of apoptosis and other forms of programmed cell death or mitochondrial biodegradation; and also with mitochondrial morphology and yet only genetic discipline unknown in details, genetics of mitochondrial DNA. Although accidentally reported by morphologists for decades, the fact that mitochondria form a reticular network within the cell has been recognized fully in the advent of confocal microscopy since 1990s. Colleagues in my Czech laboratory have recently mastered three-dimensional (3D) microscopy with higher (100 nm) resolution than conventional (250 at x,y, >700 at z axis) and demonstrated a rich 3D mitochondrial network nearly completely interconnected with uniform tubule diameter around 260 nm. The last decade has discovered several major proteins, termed mitodynamins, and numerous signaling pathways that concern with the dynamics and morphology of such mitochondrial network and its fission (disintegration) and fusion. The fission is indicating but not exclusively initiation of apoptosis. Small objects dividing from the network by fission are hypothetically considered to be marked for mitochondrial biodegradation. In turn, mitochondrial network physiologically disintegrates in G2 and M phases of the cell cycle. Mitochondrial DNA organized in nucleoids might be redistributed evenly or unevenly during transfer of mitochondrial material to the daughter cell. Uneven distribution might be fatal in case of extended heteroplasmy, when percentage of mutated mtDNA exceeds a certain threshold, causing fatal oxidative stress due to providing 13 VIP subunits (now mutated with impaired function) of the respiratory chain and ATP synthase. Besides the mtDNA impairment, also other pathology of mitochondria is frequently reflected just by the altered morphology of mitochondrial network and altered morphology of the inner mitochondrial membrane formed topologically rich sacks protruding to the matrix. These topological structures traditionally called cristae possess their own shape-forming machinery (not yet discovered) and also change upon physiological and pathophysiological stimuli. Classic electron microscopy is able to study mitochondrial tubule sections with sectioned cristae morphology, while thicker sections providing 3D images of "cristae sacks" results from the 3D electron tomography. Nevertheless, due to impossibility to combine many of such small cubes into an overall 3D image, future super-resolution (3D ~30 nm) microscopic techniques such as isoSTED or BiplaneFPALM will be required for imaging of both network and cristae morphology simultaneously.

During my PhD studies I have participated in two laboratories dealing with non-canonical bioenergetics. In Prague laboratory of the Institute of Physiology, under supervision of Dr. Petr Ježek, PhD., DSc., I have studied two sub-disciplines of the non-canonical bioenergetics, a role of mitochondrial uncoupling proteins as deduced from their transcript distribution in various tissues and

organs; and the role of yet not fully understood factor CIDEa in mitochondrial apoptosis. As a part of PHD studies of “co-tutelle” between France and the Czech Republic, supported by a grant from the French Government, I have spent nearly two years in the laboratory of my second supervisor Dr. Rodrigue Rossignol, at the Université Victor Segalen-Bordeaux 2, Bordeaux (France). Here I have studied specific bioenergetic phenotypes of cancer cells, hence the *par excellence* issue of the non-canonical bioenergetics. Together with my colleagues in both laboratories, I have attempted to summarize knowledge in sometimes confused field of bioenergetics during tumorigenesis (review Smolková et al, submitted invited review) and I have participated in another overview of non-canonical bioenergetics excluding tumorigenesis and dealing with basic physiological situations under which oxidative phosphorylation is suppressed (review Ježek et al, submitted invited review). These are not only phases of embryonic development prior to implantation (hence including bioenergetics of stem cells) and events following hypoxic adaptations of the cells, but even yet hypothetically predicted postprandial transient suppressions of oxidative phosphorylation upon insulin signaling due to the transient synthesis of nitric oxide by its mitochondrial synthase activated due to insulin-Akt2 signaling (*Finocchietto et al. 2008*). This hypothesis by Juan Poderoso elegantly explains the type-2 diabetes mellitus etiology as the impairment of the periodically elevated nitrosative stress and its pathological conversion into the progressive nitrosative and oxidative stress affecting insulin receptor and its signaling pathway itself and causing peripheral insulin resistance, as well as affecting mtDNA, hence causing another dysfunction of cell bioenergetics in peripheral tissues and impairment of glucose-stimulated insulin secretion in pancreatic beta cells. This hypothesis is yet to be supported by more experimental evidence. Nevertheless, it shows an enormous impact of non-canonical bioenergetics on biomedicine.

That is why I combined results of my studies in the two principal laboratories into one PhD thesis under umbrella of non-canonical bioenergetics. Although studies of uncoupling proteins, pro-apoptotic factor CIDEa, and cancer cell phenotypes might seem as unrelated diverse stories, the opposite is true. All these entities concerns with cellular bioenergetics when oxidative phosphorylation is by a certain extent suppressed and modified with enormous consequences as outlined above. Nevertheless, for simplicity, I present a common Introduction/Background and subsequently discuss these three issues in the separate three parts of my PhD thesis. I hope that this "non-canonical" set up will be warmly accepted by members of PhD committee.

## **1.2. SPECIFIC ASPECTS OF PRESENTED STUDIES**

High degree of genetic variability among cancer types along with enormous flexibility in term of assimilation to extreme environmental conditions of solid tumors, where nutrients and oxygen are limited, implies difficulty of cancer treatment. Growing body of evidence indicate large complexity in

alterations of energy pathways and its modulation by tumor microenvironment in cancer cells. Metabolic pathways adjustments are in turn reflected in elevated vitality and high probability to survive of otherwise detrimental conditions. Main objective of this part of thesis was *to analyze the strategies that cancer cells utilize in order to survive harsh conditions, namely glucose and oxygen limitation*, similar to those present in solid tumors. The biological question under investigation is of particular importance for a better understanding of cancer biology and energy metabolism regulation. There are well-defined general metabolic strategies, designated as metabolic phenotypes of cancer cells, classified according to the relative contribution of distinct metabolic pathways involved in energy production. However, there is a limited number of information concerning the exact pattern of mitochondrial functioning in process of metabolic remodeling. Thus, this study concentrated on characterization of bioenergetic parameters of mitochondrial oxidative phosphorylation in respect to selected conditions. In my thesis we focused on breast cancer because of the high incidence, which accounts for 2,000 deaths in Czech Republic every year. We have also chosen this type of malignant tumor since previous studies indicate that breast cancer microenvironment is typically aglycemic and hypoxic. Impact of glucose and oxygen deprivation on mitochondrial bioenergetic properties was analyzed in comparison to non-cancer cells. Thesis contains an overview of current knowledge about cancer cell metabolism and basic theories concerning strategies that facilitate cell survival and leads to cancer progression.

Uncoupling proteins (UCPs, UCPn) are members of SLC25 gene family of anion carrier proteins residing in the inner mitochondrial membrane. Likewise chemical uncouplers, UCPs uncouple respiration from ATP synthesis by their protonophoric activity. The mechanism for this protonophoric activity is not definitely resolved, but most probably free fatty acids are required to "activate" uncoupling function. Although various models propose principally different mechanisms, only the UCP1 isoform in brown adipose tissue is present in so excess that it can cause nearly complete uncoupling and concomitant heat production. Not only UCP1 is required for the thermogenic function but all stoichiometry of the respiratory chain, low content of the ATP synthase, etc. is composing the thermogenic function. This is clear e.g. from experiment where UCP1 has been overexpressed in the heart, and no uncoupling took place, probably due to a high concentration of ATP, ADP, and other inhibitory purine nucleotides. For the other UCP isoforms a concept of a "mild uncoupling" amounting only several mV changes has been developed. The physiological function of such a mild uncoupling might be suppression of mitochondrial ROS production, hence oxidative stress. In pancreatic  $\beta$ -cells UCP2 also serves as negative modulator of glucose-sensing function required for glucose-sensitive insulin secretion. Thus we cannot judge any definitive conclusions on the role of distinct UCP isoforms in various tissues. However, some light might be shed from the knowledge of their absolute amounts expressed in the tissues. Proteomics of UCPs is, however, extremely difficult as for all hydrophobic

integral membrane proteins, hence we can have some estimates from evaluations of mRNA for given UCPs. Indeed, UCPs are expressed in five distinct isoforms in mammals with various tissue distribution. Originally determined tissue distribution seems to be invalid, since novel findings show that UCP1 is not restricted exclusively to brown fat and that originally considered brain-specific isoforms UCP4 and UCP5 might have wider tissue distribution. Hence, in this part of thesis, I discuss consequences of findings of UCPn transcripts in the studied tissues.

Apoptosis is a natural, genetically controlled process of cell elimination. The mechanisms of its activation and regulation is a fundamental scientific question and a growing body of evidence reveal further molecular pathways of apoptotic machinery. The well-known caspase activation cascade along with pro- and anti-apoptotic members of BCL family is the basic structure of apoptotic machinery. However, side pathways of executive steps of apoptosis have been revealed, namely proteins with homology to nuclease DFF responsible for apoptotic DNA cleavage. In this part of thesis, we tried to elucidate another apoptotic pathway connected to mitochondria, independent of caspases.

### **1.3. AIMS**

In this regard, aims of the thesis were designed as follows:

- To analyze the impact of glucose and oxygen limitation on the overall survival of cancer cells and corresponding normal cells, mainly their bioenergetic profile and mitochondrial features.
- To present the quantification of mitochondrial uncoupling proteins transcripts in rat and mouse tissues brain, heart, kidney, liver, spleen, skeletal muscle and white adipose tissue.
- To elucidate cellular function of CIDEA protein, its possible migration between cellular compartments and organelles and thus attempt to determine its function in apoptosis.

## 2. BACKGROUND

### 2.1. MITOCHONDRIA – GENERAL FEATURES

#### 2.1.1. Mitochondria, their structure and composition

Mitochondria are historically described as kidney-shaped organelles, with two distinct membranes - outer (OMM) and inner mitochondrial membrane (IMM). Since OMM is permeable to ions and metabolites due to presence of VDAC/porin protein, transport of ions and metabolites across the IMM is conducted by a family of specific mitochondrial transporters and regulated channels. Impermeability of IMM for charged ions makes possible formation of proton gradient. Recent studies revealed a detailed structure of mitochondria and defined further mitochondrial compartments. Ultrastructural analysis of mitochondria established that cristae of 2D electron microscopic images in fact represent sacks protruding deeply into the central matrix space of the mitochondrial tubules (*Mannella 2006*). Consequently, the major morphologic features of mitochondrion can be distinguished: the outer membrane (OM), topologically contouring the tubular surface; the inner membrane (IM), with its peripheral IM part called inner boundary membrane (IBM) and intracristae parts (ICM); the intermembrane space, with its peripheral part (PIMS), located between OM and IBM, and intracristae part (cristae sacks interiors, ICS); and finally, the matrix, filling the IM-engulfed space. Sectioning the tubule, one can view either a unique peripheral sandwich OM-PIMS-IBM-matrix; or below OM one may point to cristae (sack) outlets and ICS, below which ICM and finally matrix layers are recognized (FIG 2-1), (*Ježek and Plecítá-Hlavatá 2009*). The inner membrane with its enormous surface capacity is the site of oxidative phosphorylation (OXPHOS), machinery of which is enriched in ICM (*Benard and Rossignol 2008*).

Traditional picture of mitochondria as isolated oval organelles is now considered to be just an intersection of a single mitochondrial tubule (FIG 2-2), (*Benard and Rossignol 2008*); instead the mitochondrion in reality most probably exists as a single mitochondrial reticulum network in a typical cell (*Plecítá-Hlavatá et al. 2008*). Mitochondria are, in fact, a dynamic reticulum maintained through a balanced mitochondrial fusion and fission events. The field of mitochondrial dynamics study dynamic changes of mitochondrial network in living cells, causes and consequences of such changes and mobility. The dynamics is regulated by so-called mitodynamins. Profusion proteins of OMM are mitofusins Mfn1/2, and Mgm1p/OPA1 for fusion of IMM and cristae morphology. Fis1p, and dynamin related protein 1 (Drp1) are pro-fission proteins. Principles of mitochondrial dynamics are summarized in several reviews (*Ježek and Plecítá-Hlavatá 2009; Benard and Rossignol 2008; Twig et al. 2008*). We recognize two extreme morphological situations, namely fragmented mitochondria and filamentous, highly interconnected mitochondrial network. Large diversity in mitochondrial network is linked to the

physiological and/or energy status of the cell. Changes of mitochondrial network have been observed in response to energy substrate, calcium signaling, or upon the inhibition of oxidative phosphorylation, energy status (*Benard et al. 2007; Plecítá-Hlavatá et al. 2008*) and apoptosis. Despite the significant effort, to predict or recognize exactly the ongoing cellular processes by contemplating mitochondrial network is not possible with present data as well as to set the rules that link mitochondrial network organization to particular physiological or pathological state.

Mitochondria bear their own genome. Proteins of electron transport chain (ETC) are encoded either by nuclear and mitochondrial DNA (mtDNA). mtDNA is 16.5 kbp circular molecule (FIG 2-3), (*Scarpulla 2008*), localized in mitochondrial matrix, typically present in approximately 1,000 copies per cell (but more than 20,000 copies in oocyte). mtDNA displays maternally inheritance pattern and cellular phenotype is determined by many mtDNA copies within the cell. In addition, because mtDNA is a multicopy genome, an individual cell may harbor more than a single sequence, a condition referred to as heteroplasmy. mtDNA contains 37 genes, including 13 genes encoding proteins that function as subunits for respiratory complexes I, III, IV, and V, and also the 22 tRNAs and 2 rRNAs necessary for the translation of these respiratory subunits within the mitochondrial matrix, for review see (*Scarpulla 2008*). mtDNA is mostly a coding region; the only non-coding region is the D-loop, the site of transcription initiation of divergent promoters (HSP, LSP). In order to protect, maintain, and propagate the mitochondrial genome accurately, mtDNA is packaged into protein-DNA assemblies called mitochondrial nucleoids. Concept of nucleoids is relatively recent, contradicting the general view of mtDNA without any structural proteins. mtDNA is effectively packaged into the compact, discrete structures of approximately 70 nm in diameter (*Iborra et al. 2004*), having a layered structure consisting of mtDNA with associated proteins (*Bogenhagen et al. 2008*). The most abundant structural protein is mtDNA transcription factor A (TFAM), major nucleoid organizing protein. TFAM is essential in regulating of mtDNA copy number (*Ekstrand et al. 2004*). Mitochondrial nucleoids contain approximately 6 copies of mtDNA per nucleoid (*Gilkerson et al. 2008*). Among other protein components of mitochondrial nucleoids, mtDNA-associated compounds have been characterized to participate in mtDNA maintenance and transcriprion/replication of mtDNA, including Twinkle helicase, mitochondrial polymerase  $\gamma$ , mitochondrial single-stranded binding protein (mtSSB) (*Garrido et al. 2003*) and ATAD3 (*He et al. 2007*), probably associated with D-loop in transcription and replication. Within mitochondrial network, nucleoids are localized in discrete units distributed regularly along the mitochondrial tubules (*Iborra et al. 2004*) and probably freely diffusing throughout the mitochondrial network. Interestingly, when fragmenting, each mitochondrion possesses at least one nucleoid (*Margineantu et al. 2002*). Conversely, mtDNA nucleoids can efficiently repopulate the mitochondrial DNA of mtDNA-deficient Rho<sup>0</sup> cells (*Legros et al. 2004*).

Partially known but not yet fully understood principles of mtDNA replication and transcription are summarized in reviews (*Clay Montier et al. 2009; Fernandez-Silva et al. 2003*).

Mitochondria possess more than 1500 proteins, the majority of which is nuclearly-encoded and imported into mitochondria. To depict important members of mitochondrial resident proteins besides proteins of respiratory chain, there is an enzymatic machinery of Krebs (TCA) cycle and  $\beta$ -oxidation in the mitochondrial matrix. The important members of IMM are mitochondrial transporter proteins, including the ADP/ATP carrier, phosphate carrier and uncoupling proteins. Both membranes are spanned by the translocation proteins of OMM and IMM.

The lipid component contains major classes of phospholipids found in all cell membranes. Mitochondrial membranes, however, lack cholesterol. Thus, both OMM and IMM consist of phosphatidylcholine, phosphatidylethanolamine (PE), phosphatidylinositol, phosphatidylserine, and phosphatidic acid, as well as phosphatidylglycerol (PG) and cardiolipin (CL). CL is located predominantly if not exclusively to the mitochondria (*Zinser et al. 1991*). PE, PG, and CL are synthesized "in house," whereas the others must be imported. Phospholipids play a fundamental role in the function and import of mitochondrial proteins, which in turn regulate the synthesis of these phospholipids.

### **2.1.2. Mitochondrial biogenesis**

A process involving formation of mitochondrial mass with complete mitochondrial protein machinery and membranes is termed mitochondrial biogenesis. It is a dynamic process which besides nuclear gene expression and addressing products to OMM, intermembrane space, IMM, or matrix, includes mtDNA replication, and simultaneous mitochondrial membrane formation. Most of references describe mitochondrial biogenesis as a process directly dependent on mtDNA replication, which may be wise, and consider a mitochondrial membrane formation secondary to mtDNA transcription process. However, mitochondrial membrane biogenesis requires a coordinated import and synthesis of proteins, as well as phospholipids. Mitochondria are not formed de novo, rather they grow and divide from the pre-existing mitochondrial pool, exactly from the pre-formed mitochondrial network. An increase in the mitochondrial mass does not necessarily correlate with the cell cycle. Rather, biogenesis of mitochondria occurs in response to various external stimuli, like exercise, caloric restriction and hormonal signaling (*Feige and Auwerx 2007*). Since mitochondrial OXPHOS has certain respiratory capacity, an increased energy demand is dependent on formation of new mitochondrial mass with enrichment of OXPHOS protein pool. Therefore, increase biogenesis of mitochondria in turn results in increased respiratory rate (*Wu et al. 1999*). Since mitochondrial OXPHOS proteins are both nuclearly and mitochondrially encoded, biogenesis requires the participation and coordination of the nuclear and mitochondrial genomes. Mechanisms, how cell regulate expression of OXPHOS complexes

simultaneously and how stoichiometry of mitochondrial-to-nuclear-encoded subunits is maintained, is poorly understood. Nevertheless, a coordinated action has been described for peri-OMM ribosomes and matrix ribosomes in order to form simultaneously parts of respiratory chain complexes where one subunit comes from the nuclear and the second one from the mitochondrial genome.

A central regulator of mitochondrial genes expression is PGC-1 which transmits the external stimuli into intracellular biogenesis pathway. PGC-1 activity is regulated at the level of expression. Additionally, PGC-1 interacts with other cellular targets and undergoes numerous modifications at the post-translational level, which regulate its activity (*Ventura-Clapier et al. 2008*). PGC-1 governs the expression of nuclear respiratory factors (NRF-1 and NRF-2) and estrogen-related receptors (ERR), which are transcription factors that trigger the expression of genes coding for both nuclear subunits of the respiratory chain and proteins involved in mitochondrial DNA transcription and replication. Expression of mitochondrial-encoded proteins is directed by TFAM (*Feige and Auwerx 2007; Scarpulla 2008*). Importantly, expression of TFAM is also regulated by NRFs. Biogenesis correlates with transcriptional activity of mtDNA, therefore the regulation of mtDNA transcription is essential in the regulation of mitochondrial biogenesis. Since mtDNA replication and transcription are most probably coupled processes, activation of biogenesis pathways results in increased expression of OXPHOS proteins and also mtDNA content.

### **2.1.3. Function of mitochondria**

#### **2.1.3.1. Oxidative phosphorylation**

During oxidative phosphorylation ATP is synthesized from ADP and inorganic phosphate (Pi). This reaction is driven by energy released from oxidation of reducing equivalents NADH and FADH<sub>2</sub> which are generated in cellular catabolic pathways. Electrons from NADH or FADH<sub>2</sub> are transferred via ETC (FIG 2-4) which consists of complex I (NADH:ubiquinone oxidoreductase), complex II (succinate:ubiquinone oxidoreductase), complex III (coenzymeQ:cytochrome c oxidoreductase), and complex IV (cytochrome c oxidase, COX). Complexes of ETC protrude in the inner mitochondrial membrane (except of complex II attached from the matrix side) and are organized according to the increasing redox potential. The final electron acceptor is molecular dioxygen (O<sub>2</sub>) which is then converted to molecule of water. According to Mitchell's chemiosmotic theory this process of electron flow is accompanied by conformational changes of Complex I, III, and IV leading to the proton pumping from the mitochondrial matrix into the intermembrane space via these respiratory complexes. This generates a proton-motive force ( $\Delta p$ ) which is composed of pH gradient ( $\Delta pH$ ) and electrical membrane potential ( $\Delta \psi_m$ ). Proton-motive force, in turn, is driving force for protons that drive F<sub>1</sub>F<sub>0</sub>-ATPase (complex V) to generate ATP. By the action of the ADP/ATP carrier, the generated

ATP can exit the mitochondria in exchange for ADP and this provides energy pool for various cellular processes.

Flow of electrons through the electron transport system can be regulated by  $\Delta p$ , since the electron transport is directly coupled to the proton translocation. For instance, when the energy demand is increased, cytosolic and subsequently the intramitochondrial concentration of ADP rises, causing discharge of the  $\Delta p$  as protons pass through  $F_1F_0$ -ATPase, regenerating the ATP pool. As a result, electron transport is substantially activated. Thus, the magnitude of the  $\Delta p$  reflects the energy charge of the cell and, importantly, regulates the electron transport rate. The rate of electron transport is usually measured by assessing the rate of oxygen consumption and is referred to as the mitochondrial respiratory rate.

Theoretically under experimental conditions when we measure the respiratory rates of isolated mitochondria, bioenergetics refers to the respiratory states (*Chance and Williams 1956*). The respiratory rate is known as the *state 2* rate when the energy charge is high, the concentration of ADP is low, and electron transport is limited by ADP. When ADP levels rise and inorganic phosphate is available, the flow of protons through  $F_1F_0$ -ATP synthase is elevated and higher rate of electron transport is observed; the resulting respiratory rate is known as the *state 3*. When ADP pool is depleted, state of inhibited respiration by lack of ADP is referred as *state 4*. Difference of state 2 and state 4 is the presence of ATP in state 4. When experimenting with intact cells, we refer to *endogenous* or routine respiration instead of state 3. Endogenous respiration is different than state 3 (also referred as as state 3½) as mitochondrial respiration is limited *in situ* by substrate delivery (including oxygen) and ADP content (while in isolated mitochondria both are given in excess). State 4 in intact mitochondria is the oligomycin-inhibited state, where ADP-regulated respiration is inhibited.

#### 2.1.3.2. Energy metabolism

Besides oxidative phosphorylation, mitochondrial matrix gathers other important pathways of energy metabolism, namely Krebs cycle (tricarboxylic acid, TCA cycle) and fatty acid oxidation. Within the TCA cycle, a glycolytic product pyruvate is further oxidized, resulting in a production of reduced equivalents NADH,  $FADH_2$ , and also GTP. Intermediates of TCA cycle can be exported from mitochondria and used as biosynthetic precursors in a process called cataplerosis of TCA cycle (FIG 2-5). Anaplerotic reactions replenish TCA cycle by metabolites. The citric acid cycle is a hub of metabolism, with degradative pathways leading in and anabolic pathways leading out and it is closely regulated in coordination with other pathways. One of the key TCA enzymes, succinate dehydrogenase (SDH) is also a complex of respiratory chain (complex II).

### 2.1.3.3. Apoptosis

Mitochondria are involved in regulation of programmed cell death, termed apoptosis, a sequence of processes that lead to cell elimination. It originates from intrinsic or extrinsic signals and progress in multiple pathways involving apoptotic proteins, and results in a transmission of the molecular signal, activation of caspases and eventual cell death. Mitochondria perform executive step in apoptotic control, permeability transition, during which, cytochrome c and other factors are liberated of mitochondria to trigger cytoplasmic part of apoptosis, apoptosome. Mitochondrial permeability transition is controlled by sensors of a bioenergetic status, components of the permeability transition pore (PTP), Bcl-2 family proteins, mitochondrial dynamins, and mitochondrial lipids (*Cheng et al. 2008*). So far, there are three general models of how permeability could transition occur: formation of yet unidentified permeability transition pore (*Halestrap 2005*), interaction of pro-apoptotic proteins of Bcl-2 family leading to BAX-BAK hexameric channels enabling cytochrome c release, and involvement of mitochondrial fission process (*Youle and Karbowski 2005*). Principles of these three models are depicted in FIG 2-6 (*Alirol and Martinou 2006*). Permeability transition is followed by formation of apoptosome and activation of caspases. Activated caspases initiate proteolytic cell destruction by cleaving DNA, nuclear and cytoplasmic structural proteins. Additional pathways that do not involve caspases activation, cell death independent of caspases, have been reported. This includes activation of EndoG nuclease, another mitochondrial protein, that mediates nuclear DNA degradation (*Lindholm et al. 2004*).

Next to the mitochondrial permeability transition, mitochondria also sequester numerous pro- and anti-apoptotic factors reside in mitochondria (*Kim et al. 2006b; Cheng et al. 2006*). Relay of information signaling, that involves mitochondria, is mediated by proteins possessing the ability to migrate between mitochondria and cytosol or other cell organelles or compartments, notably to the nucleus where subsequent signaling cascades may be initiated. On one hand, a “regular” protein import proceeds into mitochondrion (import of nuclear-coded mitochondrial proteins) bringing in either executive or regulatory proteins (*Baker et al. 2007*). Among the latter, PKC-, tyrosine- and other kinases were found to access at least the intermembrane space (*Salvi et al. 2005*). On the other hand, an export of signaling proteins into the cytosol or other cell organelles exists and plays an essential role in life and death (*Garrido et al. 2006; Cheng et al. 2006; Kim et al. 2006b*). Thus, protein export mechanisms for apoptosis mediators such as cytochrome c, Smac/Diablo, apoptosis-inducing factor or EndoG serve as well established, but not completely understood examples (*Vařecha et al. 2007; Kim et al. 2006b; Cheng et al. 2006*).

## 2.2. BASIC FACTS FOR CIDE PROTEINS

Executive part of apoptotic pathway involves the action of DNA fragmentation factor (DFF) protein in nucleus, a chief apoptotic DNA nuclease. DFF is important effector of apoptosis performing the final step of apoptosis – DNA fragmentation/chromatin condensation. It is a heteromultimeric protein (*Lechardeur et al. 2005*) that consists of the 40-kDa caspase-3-activated nuclease (DFF40, CAD), and its 45-kDa inhibitor (DFF45, inhibitor of CAD or ICAD). Cleavage of DFF complex by caspase-3 liberates the functional nuclease thus promoting the internucleosomal DNA fragmentation (*Inohara et al. 1999; Bayascas et al. 2004; Erdtmann et al. 2003*).

Sequence similarity searches revealed proteins homologous to DFF, CIDE proteins, with possible proapoptotic function (*Inohara et al. 1998*). CIDEs are related to N-terminal of both subunits of the DFF (FIG 2-7). There are three members of so-called cell death-inducing DFF45 (DNA fragmentation factor)-like effector (CIDE) protein family described: CIDEa (*Inohara et al. 1998; Zhou et al. 2003b*), CIDEb (*Inohara et al. 1998; Lugovskoy et al. 1999; Chen et al. 2000*) and CIDE-3/FSP27 (*Liang et al. 2003*). CIDEs are small proteins (~25kDa) expressed in two isoforms arising from alternative splicing (*Liang et al. 2003*). Complete three-dimensional structure of CIDE proteins is not established. However, we recognize two distinct protein domains in CIDE proteins, so-called CIDE-N and CIDE-C domains. Common feature among DFF and CIDE proteins is conserved CIDE-N domain, located in N-terminal half of the protein. CIDE-C domain, other specific feature of CIDE family, is not present in DFF proteins (FIG 2-7).

Structure of CIDE-N domain has been determined (*Lugovskoy et al. 1999*), consisting of about 75 amino acids forming of a twisted five-stranded  $\beta$ -sheet with two  $\alpha$ -helices arranged in an  $\alpha/\beta$  roll (*Lugovskoy et al. 1999*). Higher assembly features were also described - CIDE proteins seems to oligomerize by their CIDE-C domains to form dimers (*Chen et al. 2000*).

### 2.2.1. Expression

Although expression of CIDEa and CIDEb is not ubiquitous, their expression was detected in a wide variety of human and mouse tissues and cell lines. A complication to physiological studies may be the fact that the three CIDEs have different tissue distributions for their mRNA. Their physiological roles specific to given tissues are unknown. Besides, CIDEa and CIDEb exhibit tissue-specific non-overlapping expression pattern. CIDEa mRNA has been found namely in human heart, and at lower level in skeletal muscle, brain, lymph node, thymus, appendix and bone marrow as a 1.3 kb transcript, while 1 kb transcript was found at low levels in placenta and 7 kb transcript in kidney and at low levels in heart, brain, placenta and lung (*Inohara et al. 1998*). Detectable transcript levels were independently confirmed in brown adipose tissue, heart, brain, skeletal muscle, lymph nodes, appendix, and bone marrow (*Liang et al. 2003*). CIDEb mRNA, 1.3 kb transcript, was found in high

amounts in liver and small intestine (*Chen et al. 2000*) or in fetal liver (*Inohara et al. 1998*); a lower level in colon, kidney and spleen (*Chen et al. 2000*), 2.5 kb transcript was detected in low levels in spleen, peripheral blood lymphocytes, bone marrow, and fetal liver (*Inohara et al. 1998*). CIDE3 was found in small intestine, heart, colon, and stomach (*Chen et al. 2000*).

### **2.2.2. Biological function**

Existing information about CIDE proteins provides more confusing than determining proof of their cellular function. Their identification was based on homology to N-terminal domain (termed CIDE-N) of DFF45 (ICAD) (*Inohara et al. 1998*), which is known to inhibit DFF40 (CAD), the major cell death executor nuclease responsible for DNA fragmentation. Inactive DFF, which is constitutively targeted to nucleus, should consist of 2 molecules of CAD and 2 molecules of ICAD (*Lechardeur et al. 2005*), although exact stoichiometry is a matter of debate. Activation occurs upon caspase-3 cleavage of ICAD, liberating active nuclease CAD. CIDE-N domain seems to be responsible for oligomeric assembly of inactive DFF complex, as well as activated CAD oligomer.

Since their identification, studies of CIDE proteins were concentrated on tracing possible connection with control of apoptosis induction or progression. Overexpression of CIDE-A and CIDE-B results in induction of apoptosis and DNA fragmentation (*Inohara et al. 1998*). Importantly, CIDE-induced apoptosis was not inhibited by caspase inhibitors, but was inhibited by DFF45. Nuclease function of CIDE-A or CIDE-B proteins, such as for EndoG, was not reported. Instead, action of CIDE-A and CIDE-B proteins, is more likely connected to DFF40 and DFF45 and provides a possibility of regulation of DFF activation by domain interactions, and independently of caspases.

Structure analysis of CIDE-N domain of CIDE-B revealed surface (interface) and charge compatibility of individual CIDE-N domains and weak interaction of CIDE-N domains has been confirmed (between CIDE and DFF) (*Lugovskoy et al. 1999*). In contrast, CIDE-C was demonstrated to bind CIDE-C domains with high affinity resulting in stable dimer formation (*Chen et al. 2000*); and further to govern mitochondrial targeting. CIDE dimerization was reported to be likely required for induction of apoptosis caused by CIDEb (*Lugovskoy et al. 1999*).

With this background, one can assume a model of apoptosis regulation by CIDEA. The CIDE-N domain, common with DFF, can bind to the homologous domain on DFF45 opposing its inhibitory effect on DFF40 (*Lugovskoy et al. 1999*), FIG 2-8. However, it is not clear whether CIDE has higher affinity for DFF45 than DFF40 and is thus able to release DFF40 from the complex allowing it to exert its nuclease activity. One should also bear in mind other regulatory mechanisms of apoptosis, such as that DFF45 is synthesised in excess to DFF40 ensuring fine tuning of DFF activation and decreasing the probability of CIDE-N buffering by CIDE proteins.

### **2.2.3. Interaction with UCP1**

Other finding reports CIDEa interacting with UCP1 in mitochondria in mitochondria, CIDEa proteins were shown to interact with inner-membrane protein UCP1 (*Zhou et al. 2003b*). This important finding reports that protonophoric activity of UCP1 can be inhibited by CIDEa protein. *Zhou* and coworkers observed that CIDEa deficient mice had higher metabolic rate, lipolysis in BAT and core body temperature when subjected to cold treatment. They reported that these roles of CIDE-A are at least in part caused by its direct suppression of UCP1 activity.

### **2.2.4. Possible migration of CIDE proteins into mitochondria and consequences**

In processes of apoptosis activation, protein-protein interaction and subcellular localisation, CIDE domains play distinct roles. Unlike CIDE-C domain, without which apoptosis does not occur, responsible for CIDE-CIDE interaction, CIDE-N domain cooperates with other CIDE-N domains by homophilic interaction (both with CIDE or DFF proteins) and thus it is considered as a regulatory subunit of CIDE proteins.

Regarding subcellular targeting of CIDE proteins, various monitoring approaches revealed distinct subcellular localization. CIDEa and CIDEb were shown to be targeted either to mitochondria (*Chen et al. 2000; Liang et al. 2003*), cytoplasm and nucleus (*Iwahana et al. 2006*). Mitochondrial localization is strictly dependent by CIDE-C domain (*Chen et al. 2000*), since its removal causes redirection into cytoplasm. Surprisingly, recent findings uncovered also nuclear localization, which is dependent on glycosylation status of CIDE proteins (*Iwahana et al. 2006*) and that deglycosylation promotes translocation of CIDE-A into cytoplasm from nucleus.

Current consensus states that the CIDE-N domain of CIDE proteins is required for binding to DFF45 or DFF40 (*Inohara et al. 1998; Lugovskoy et al. 1999; Chen et al. 2000*), whereas the CIDE-C domain is required for mitochondrial localization and apoptosis (*Inohara et al. 1998; Chen et al. 2000*). The latter finding opposes the obligatory location of mitochondrial addressing sequences (pre-sequences or scattered motifs) within the N-terminus. Actually, none of the protein sorting software tools, e.g. PSORT, indicated the presence of any mitochondrial addressing sequence within CIDEa or CIDEb. It seems that the localization of CIDE proteins in mitochondria results from yet unknown addressing sequence or scattered motifs.

When considering interaction with DFF, problem lies in the evidenced localization of CIDEa (*Zhou et al. 2003b*), CIDEb (*Chen et al. 2000*), and CIDE3 (*Liang et al. 2003*) in mitochondria. Therefore, it is not known in which cellular compartment CIDE may interact with the DFF45&DFF40 complex. Nucleus is the most likely location because the entire DFF45&DFF40 complex is imported preferably into the nucleus (*Lechardeur et al. 2000*). Glycosylated CIDEb was demonstrated to reside in the nucleus, whereas the deglycosylated form is exported into the cytosol (*Iwahana et al. 2006*). Alternatively,

CIDE interacts with DFF45 or its short form lacking the nucleus localization sequence in the cytosol, thus preventing the import of free DFF45 into the nucleus. The third possibility is that the complex DFF45/DFF40 is disrupted by CIDE in the cytosol with consequent migration of free DFF40 into the nucleus. This model implies apoptosis regulation independently of caspases, because CIDE-induced apoptosis is not sensitive to caspase inhibitors but is inhibited by DFF45 (*Inohara et al. 1998*). CIDEs may bypass the caspase-dependent apoptosis due to a crosstalk between mitochondria and nucleus and as such they are important subjects of molecular physiology of the cell.

## 2.3. BIOENERGETICS OF CANCER CELLS

### 2.3.1. Energy metabolism of cancer cells

#### 2.3.1.1. Warburg effect

Based on proposal of Warburg (*Warburg 1956*), glycolysis of cancer cells is often highly enhanced even in the presence of oxygen, resulting in an excessive lactate production (Warburg effect, aerobic glycolysis). These findings lead investigators to consider oxidative phosphorylation of cancer cells to be necessarily impaired during carcinogenesis. Aerobic respiration from glucose produces 38 mol of ATP, 19 times more than glycolysis, although the rate of ATP production by the OXPHOS is less rapid than glycolysis (*Pfeiffer et al. 2001*). However, due to the high glycolytic turnover that cancer cells maintain, ATP production is sufficient to support the cell growth. In many aspects, Warburg effect resembles metabolic switch occurring as an adaptation to anaerobic conditions (chapter 2.3.2.1.) Based on the studies with FDG uptake (positron emission tomography imaging of 2-(<sup>18</sup>F) fluoro-2-deoxy-D-glucose) of human living tumoral tissues it was assumed that glucose uptake is largely elevated in cancer cells when compared to surrounding normal tissue (*Nakata et al. 2001; Mankoff et al. 2007*). Cancer cells have greater uptake of glucose but use a smaller fraction of this glucose for complete oxidation, even when oxygen is abundant. Rather, it is secreted as a lactate.

Despite obvious disadvantage in term of producing ATP, elevated glucose metabolism is considered to be somehow supportive in cell growth. It must be stressed that cellular metabolism, and particularly oxidative metabolism, is totally subverted to the needs of cancer cells in which proliferation is the primary function. Enhanced glycolysis is also considered a preconditioning for hypoxic conditions and high lactate concentrations as a product of glycolysis facilitate tumor invasion and suppress anticancer treatment. Besides rapid ATP production, cells benefits from glycolysis, as intermediates of glucose metabolism are source of pentose-phosphate pathway (PPP). It was proposed, that aerobic glycolysis is the essential step in cellular transformation (*Gatenby et al. 2007*). Later in this thesis, we present, that cancer cells utilize preferentially glucose to other energy sources. Some tumor cells are reported to be strictly dependent on glycolytic ATP (*Fantin et al. 2006*), so that proliferation with OXPHOS-derived ATP exclusively is attenuated.

#### 2.3.1.2. Variability

Despite the existence of aerobic glycolysis in numerous tumor types, OXPHOS activity within tumor cells is not necessarily attenuated considering numerous reports indicating strong OXPHOS activity and dependency on aerobic ATP production (*Moreno-Sánchez et al. 2007*). Therefore, Warburg hypothesis cannot be interpreted so strictly anymore, despite the indisputable fraction of tumors with

aerobic glycolysis; mitochondria of cancer cells are not dysfunctional in general, rather it operates at a low-capacity there. For instance, analysis of MCF-7 cells originating from a mammary gland epithelial adenocarcinoma revealed that ATP production is 80 % oxidative in glucose medium (*Guppy et al. 2002*). Likewise, in hepatoma cells mitochondrial respiration was found to be coupled to ADP phosphorylation and produced 40% of the total cellular ATP in glucose medium (*Nakashima et al. 1984*). More recently, it has been revealed that in HeLa and AS-30D young-spheroids, the contribution of OXPHOS to the total ATP supply was 60% (*Rodríguez-Enríquez et al. 2006*). They further studied this feature and evidenced a class of tumor cell lines in which the oxidative metabolism prevails over glycolysis. This situation has been extensively reviewed (*Moreno-Sánchez et al. 2007*), and the authors even conclude that "high glycolysis" is not a prerequisite of all cancer cells but could be acquired during the highest proliferative activity and/or in response to stringent micro-environmental conditions, such as intermittent hypoxia. Accordingly, a critical review of numerous studies comparing cancer cells with normal tissues concluded that several tumors derive most of their ATP from mitochondrial oxidative phosphorylation, in striking contrast to Warburg's hypothesis (*Zu and Guppy 2004*). Therefore, due to the genetic heterogeneity of tumor cells, OXPHOS capacity should be experimentally evaluated for each particular tumor type, to assess whether the enhanced glycolysis is indeed accompanied by a significant depression of mitochondrial function.

#### 2.3.1.3. Dysfunctional mitochondria and alterations in cancer cells

Numerous genetic rearrangements of mitochondrial and nuclear DNA-encoding mitochondrial ETC components have been referred to occur in cancer cells. There are cancer-related mitochondrial alterations (for review see (*Chatterjee et al. 2006*)) and mutations related to specific cancer cell type that arise with increasing degree of carcinogenesis in a process of mutation accumulation. mtDNA mutations may arise as a result of tumor progression (*Brandon et al. 2006*), but some mtDNA mutations might actively contribute to tumor progression. Likewise, mitochondrial defects imply increased glycolysis (*Ishikawa et al. 2008a*) and glucose uptake (*Lopez-Rios et al. 2007*) in human carcinoma cells. The expression of a mutant mtDNA-encoded complex I - subunit 2 concomitantly stimulates aerobic glycolysis, reactive oxygen species (ROS) production, and tumor growth (*Zhou et al. 2007*). The activity of other enzymes involved in oxidative phosphorylation is known to be decreased in cancer cells according to numerous reports. The  $\alpha$ -subunit of mitochondrial  $F_1F_0$ -ATPase has been shown to be downregulated in colorectal carcinomas (*Sakai et al. 2004; Shin et al. 2005*). Similarly, the defect of  $\beta$ -subunit of  $F_1F_0$ -ATPase expression in liver, kidney and colon carcinomas, lung, and breast (*Cuezva et al. 2002; Isidoro et al. 2004*) was associated with increased FDG uptake and poor prognostic outcome. These mutations have been also used as mitochondrial markers of cancer cells. Tumor mitochondria are often relatively small, lack cristae, and are deficient in the  $\beta$  subunit of the

$F_1F_0$ -ATPase (Lopez-Rios *et al.* 2007). Moreover, the reduced biogenesis is characterized by the decreased expression level of the PGC-1 found in lung (Bellance *et al.* 2009a) and breast cancer (Watkins *et al.* 2004) and of the mitochondrial TFAM protein. Decreased level of mtDNA has also been reported (Mambo *et al.* 2005). Decreased content of oxidative phosphorylation complexes (complexes II, III and IV of the respiratory chain, and  $F_1F_0$ -ATPase) has been associated with renal cell carcinoma (Simonnet *et al.* 2002). Mitochondrial mutations and subsequent ROS production have been shown to regulate cell growth and metastatic potential (Ishikawa *et al.* 2008b).

#### 2.3.1.4. Crabtree effect

Besides long-term metabolic adaptations known as Warburg effect, it was shown, that tumor cells are able to react rapidly to a presence of exogenous fuel. Acute inhibition of respiration by exogenous hexoses glucose and fructose (but not galactose) is known as Crabtree effect. Addition of glucose to cell culture induces immediate transition to anaerobic metabolism, lactate production (Burd *et al.* 2001) and, mainly, pronounced decrease of cellular respiratory rate. It was demonstrated for several tumor cell types and normal fast-proliferating cells. Mechanism of Crabtree effect is mostly unresolved. Up to date, there is no clear explanation or molecular mechanism proving, that during Crabtree effect, direct inhibition of mitochondrial respiratory system occurs; or if there is a regulatory mechanism at the level of substrate administration between aerobic and anaerobic metabolic pathways; or triggering of cellular signalization causing activation/inactivation of target enzymes involved.

Inhibition of mitochondrial respiration occurs in response to addition of glycolytic intermediates, including glucose-6-phosphate (G6P), fructose-6-phosphate (F6P), glyceraldehyde-3-phosphate, phosphoenolpyruvate (Melo *et al.* 1998). Elevated levels of glycolytic intermediates G6P, F6P, and fructose-1,6-bisphosphate (FBP) were reported during Crabtree effect (Rodríguez-Enríquez *et al.* 2001) along with decreased ATP/ADP ratio (metabolic link between glycolysis and OXPHOS). Addition of galactose, nonfermentable substrate, does not inhibit respiration (Rodríguez-Enríquez *et al.* 2001). Elevated glucose intermediates, particularly FBP, were suggested to affect respiratory complexes and respiration in yeast cells (Diaz-Ruiz *et al.* 2008). However, FBP influence activity of several enzymes of glycolytic pathway, including pyruvate kinase (PK) and phosphofructokinase (PFK), so allosteric activation of glycolysis is probably involved (Rodríguez-Enríquez *et al.* 2001). Lactate production is also elevated during Crabtree effect (Burd *et al.* 2001).

Crabtree effect has been also reported for proliferating thymocytes (Guppy *et al.* 1993). During transition from resting to proliferative state, thymocytes increases glycolysis and lactate production. In proliferating, but not resting cells, respiration was inhibited in the presence of glucose to the level of respiration of resting cells. ATP production is also shifted from aerobic to glycolytic in proliferating

cells, when glucose is present (*Guppy et al. 1993*). Proliferating cells are therefore, as well as tumor cells, able to readily react to exchange of exogenous substrate, and it was concluded that Crabtree effect might be a feature of proliferative rather than tumoral tissue. Another report describes the effect of extracellular pH on respiration of melanoma cells (*Burd et al. 2001*). Melanoma cells, which normally exhibit pronounced Crabtree effect, adapted to growth in low pH (6.7) exhibit glucose-stimulated increase of respiratory rate and decrease of lactate production (*Burd et al. 2001*). This is an important finding demonstrating that within a tumor, multiple regions of distinct metabolic activity may exist dependent on metabolite concentration, in this case lactate. By reversal of Crabtree effect, cells which grow in already acidic environment overcome further acidification and protect themselves by potentially harmful consequences of lactate production.

### **2.3.2. Possible origin of cancer metabolic remodeling**

It is clearly established that cancer cells undergo genetic and biochemical changes leading to so-called metabolic remodeling. Importantly, metabolic remodeling occurring in cancer cells depends on nutrient and substrate availability that in turn ultimately influence substrate distribution in tumor cells and determine cell functions. One of the demonstrations of this metabolic conversion is that cells become dependent on glucose for their survival when glucose is present, downregulated OXPHOS in some tumors or, conversely, upregulation of OXPHOS activity in others. In general, due to the genetic heterogeneity of tumor cells, there are multiple metabolic strategies that cancer cells utilize in order to support proliferation under the particular environmental and substrate conditions. Metabolic intermediates may in turn regulate enzymes of energy production pathways.

High rate of glycolysis is not only beneficial in hypoxic conditions but also supports the cell growth and proliferation. This presumes that the regulation of cellular energy production is multifactorial, very complex and flexible. An alternative energetic pathway of cancer cells that utilize mitochondrial oxidative phosphorylation is glutaminolysis, where cells use available glutamine as bioenergetic substrates along with glucose, or when glucose is no longer available will be described (chapter 2.3.2.4.). Aerobic glycolysis is also considered to result from reprogramming of metabolic genes to allow cancer cells to function more like fetal cells (2.3.2.5.) and to enable a greater fraction of glucose metabolites to be incorporated into macromolecule synthesis rather than burned to CO<sub>2</sub>.

In this chapter, I summarize general metabolic strategies engaged in order to survive nutrition variations, and genetic and environmental features that directly control metabolic phenotype of cancer cells will be described.

#### 2.3.2.1. Hypoxia: Adaptation and survival in low oxygen

##### *2.3.2.1.1. Tumor oxygenation*

Blood system organization and principal pattern of oxygen transport based on hemoglobin is described in all textbooks of physiology. Shortly, atmospheric pressure of air at the sea level is 760 mmHg, comprising of 20.93% of air (159 mmHg). Gaseous exchange between capillary blood of lung and alveolar air occurs across the “air-blood barrier”, which is the alveolar epithelium and capillary endothelium with their adherent basement membranes and epithelial cell cytoplasm. Oxygen is bound to hemoglobin of red blood cells in alveoli capillaries, where the partial oxygen pressure is near 100 mmHg and hemoglobin saturation the highest. Transport of oxygen to tissues is carried out by arterial blood with typical oxygen pressure of 80 – 100 mmHg. Partial oxygen pressure further decreases in tissues, as oxygen is released with decreasing hemoglobin saturation. Administration to

single cells within tissue is held by microvascular system. Oxygenation of well perfused tissues ranges of 30 – 60 mmHg (see TAB 2-1, 2-2). Homeostasis between oxygen demand of metabolically active tissue, oxygen delivery and release is regulated by blood flow variations, pH, and diffusion flux from the microvessels. On the contrary, tumor vasculature is often structurally and functionally impaired and provides an inadequate oxygen supply.

Acute or chronic regions of hypoxia or anoxia are often observed in solid tumors, i.e. large fraction of cervical, breast, head and neck carcinomas contain tissue fractions of  $p_{O_2}$  less than 10 mmHg (considered hypoxic). Acute (perfusion-limited) hypoxic regions are formed in response to increasing tumor mass without proper vascularization. Acutely hypoxic cells are believed to experience several short-term periods of hypoxia during their lifetime. The duration of these periods has been shown to range from less than a minute to several hours in experimental tumors (*Dewhirst et al. 1998*). Intermittent hypoxia gradually develops into chronic (diffusion-limited) hypoxia caused by increased oxygen diffusion distance due to the tumor expansion, which affect cells distant more than 100  $\mu\text{m}$  (FIG 2-9) from the nearest capillary (*Rijken et al. 2000*). Areas of severe hypoxia are often necrotic, containing cells which have lost their vital function.

Detection of hypoxia is of great clinical interest, since tumor hypoxia decreases treatment effectiveness; correlation was found between tumor hypoxia and survival after radiotherapy (*Brizel et al. 1997*). In addition to treatment resistance, hypoxia is considered to induce genomic instability (*Rofstad et al. 2000*) to promote metastatic dissemination (*Rofstad et al. 2005*) and being a selective pressure for metastatic phenotype within individual cells (*Subarsky and Hill 2003*). Hypoxic tumors have been observed to have elevated metastasis propensity and higher malignant potential (*Cairns et al. 2001*), resulting in poor overall prognosis (*Brizel et al. 1996; Johan et al. 2003*). There is to be considered, whether hypoxia is a cause or consequence of enormous vitality of cancer cells. Presumably, a combination of both scenarios would mean that hypoxia is the cause of increased aggressiveness since it promotes tumor progression, while at the same time being a consequence of aggressive malignant growth that leads to defective (“chaotic”) vascular morphology and function together with other alterations in the nonmalignant part of the tumor, thereby creating an environment which is adjusted to the pathophysiological demands of the tumor (*Subarsky and Hill 2003*). Routine detection of tumor oxygenation status and various hypoxic markers is therefore useful information about clinical stage of disease and prognostic information for optimization of treatment strategy. Methods for improvement of tumor oxygenation in order to obtain a better treatment outcome have been described, i.e. oxygen breathing or glucose administration to inhibit oxygen consumption (*Erickson et al. 2003*), because the respiratory activity of tumor can significantly influence tumor oxygenation.

A direct correlation between tumor size and oxygenation status is not usually observed, even small tumors contain hypoxic or anoxic fractions, and large tumors might contain numerous hypoxic fractions or none. In contrast to tissue of origin, in which oxygenation is regulated by variations of blood flow and therefore homogenous, spatial distribution of hypoxic regions within tumor is heterogeneous (there may be several hypoxic areas, even adjacent to tissue with normal oxygen tension) and reflects the variations in blood supply and vascular organization. Hypoxic tumor may contain different subpopulations of hypoxic cells (FIG 2-9), according to duration, severity of hypoxia and morphology of vascular network. The role of O<sub>2</sub> transport capacity of blood (hemoglobin content) has been also reported to impact tumor oxygenation (*Snyder et al. 2001; Baudelet and Gallez 2002*). Tumor oxygenation is also dependent on metabolic and respiratory activity of cellular subset, for instance when glycolysis impaired tumors (dependent on respiration) they still consume less oxygen and have a higher average p<sub>O<sub>2</sub></sub> because their individual cell growth rate is slower (*Helmlinger et al. 2002*). Oxygenation status of selected cancers is summarized in TAB 2-1, 2-2. For further overview of human tumor oxygenation, see reviews of Vaupel et al., e.g. (*Vaupel et al. 2007*).

#### 2.3.2.1.2. *Respiration at low oxygen*

In general, mitochondrial respiration rate is independent of oxygen when oxygen is abundant, but declines with declining oxygen pressure in low oxygen range (*Gnaiger et al. 1995*). Respiration in low oxygen pressure, as described by Chance (*Chance 1965*), is a hyperbolic function, with P<sub>50</sub> ranging from isolated mitochondria to intact cells. With development of steady-state oxygraphy applications it has become clear, that each point of aerobic-anoxic transition represents the steady-state respiration corresponding to the oxygen level. So, as a primary regulatory kinetic mechanism, oxygen flux through mitochondrial respiratory system is imposed by oxygen itself. Secondary adaptive changes to low oxygen pressure include complex redox-, cellular signalization and protein expression changes. It has been reported that cells grown under hypoxic conditions decrease their mitochondrial oxygen consumption; 24 hours hypoxia exposure resulted in 50% reduction of total cellular oxygen consumption either in primary human or immortalized mouse fibroblasts (*Papandreou et al. 2006*). Subarsky reported (*Subarsky and Hill 2008*) a reversal to normal oxygen consumption after 6 hours of growth in normoxia, so that expression pattern leading to suppression of respiration has been altered during this time. These experiments were performed under standard atmospheric conditions and describe alterations of OXPHOS system arising as an adaptation to hypoxia, similarly to results presented in this thesis. Further evaluation of cellular respiration of adapted cells under the hypoxic oxygen tension is required.

### 2.3.2.1.3. HIF pathway

The hypoxia-inducible factor is a transcriptional regulator essential for normal response to hypoxia. HIF is a heterodimeric transcription factor, consisting of HIF- $\alpha$  and HIF- $\beta$  subunit (aryl hydrocarbon nuclear receptor, ARNT) (Semenza 2002). Both subunits are constitutively expressed, although half-life of HIF- $\alpha$  subunit is dependent on oxygen level. Degradation of HIF- $\alpha$  occurs at normal oxygen conditions and it is mediated by action of cytosolic enzymes prolyl-hydroxylases (PHD), catalyzing O<sub>2</sub>-dependent hydroxylation of two proline residues located in oxygen-dependent degradation (ODD) domain of HIF- $\alpha$ . Besides oxygen, PHD requires Fe<sup>2+</sup> and  $\alpha$ -ketoglutarate ( $\alpha$ -KG) as cofactors. Hydroxylated prolines are in turn recognized by the von Hippel-Lindau protein (pVHL), which is a component of multi-protein E3 ubiquitin ligase, and targeted for proteosomal degradation. Stabilization of HIF- $\alpha$  occurs when oxygen level declines, because PHD mediated hydroxylation of HIF- $\alpha$  is inhibited by lack of oxygen, so that HIF-1 $\alpha$  is no longer degraded. Stabilized subunit dimerizes with  $\beta$ -subunit to form functional transcriptional factor, and along with p300/CBP transcription coactivator induces transcription of target genes by specific interaction with hypoxia-responsive element (HRE, 5'-RCGTG-3'), (Semenza 2007). Genetic knockout of either HIF-1 $\alpha$  or ARNT is lethal (Iyer et al. 1998; Maltepe et al. 1997) and impairs survival of derived cell strains under the hypoxia (Hänze et al. 2003; Welford et al. 2006), which is a demonstration of importance of HIF function in normal development.

- **Regulation of HIF activity by FIH**

Transactivation function of HIF- $\alpha$  is regulated by factor inhibiting HIF (FIH), asparaginyl-hydroxylase which hydroxylate asparagine residue of HIF. Similarly to prolyl-hydroxylases, FIH utilizes 2-oxoglutarate as cofactors and depends on oxygen availability. Modification of HIF- $\alpha$  by hydroxylation of Asn803 blocks the interaction of HIF- $\alpha$  C-terminal transactivation domain with coactivator p300/CBP, thus inhibiting assembly of functional transcriptional complex (Lando et al. 2002). In addition to controlling of stability of HIF, oxygen level regulates directly the ability of HIF to initiate transcription of the target genes.

- **Regulation of HIF- $\alpha$  stabilization by ROS**

Several lines of evidence depicted relationship between redox signaling originating at the complex III of the respiratory chain and HIF- $\alpha$  activation during hypoxia. Using mitochondria devoid p<sup>0</sup> cells (Mansfield et al. 2005; Bell et al. 2007; Schroedl et al. 2002), cells lacking cyt c (Mansfield et al. 2005) or knock-down of Rieske Fe-S protein (Bell et al. 2007) it has been shown, that hypoxic HIF-1 $\alpha$  and HIF-2 $\alpha$  protein stabilization was prevented. Similarly, knock-down of TFAM, resulting in

depletion of mtDNA and impairment of ETC subunits, impairs stabilization of HIF- $\alpha$  (Bell et al. 2007). All these studies suggested a direct relationship between mitochondrially generated ROS and HIF- $\alpha$  stabilization. Moreover, cells lacking cyt b (Bell et al. 2007) and complex I activity (Schroedl et al. 2002) both stabilize HIF- $\alpha$  in response to hypoxia, despite electron transport and respiration being incompetent, the ability of ROS production at complex III Q<sub>o</sub> site is retained. Q<sub>o</sub> site of complex III, has been proposed to be responsible for the increased hypoxic ROS production and consecutive HIF- $\alpha$  stabilization by inhibiting hydroxylation of HIF- $\alpha$  (Bell et al. 2007; Klimova and Chandel 2008). Indeed, ROS produced by complex III released into intermembrane space of mitochondria (Muller et al. 2004) may enter cytosol (Ježek and Hlavatá 2005) and affect cellular processes, e.g. by changing cytosolic redox-state.

Mechanism of how mitochondrial ROS influence PHD activity is mostly unresolved, possibly by combination of a posttranslational modification of the PHDs, such as phosphorylation and decreasing the availability of crucial cofactor Fe<sup>2+</sup> (oxidizing it to Fe<sup>3+</sup>) which is required for hydroxylation to occur (Bell et al. 2007; Klimova and Chandel 2008). Contrary to hypoxia, p<sup>0</sup> cells are able to stabilize HIF- $\alpha$  in anoxia. Inhibition of ROS acts on the PHD activity and HIF- $\alpha$  stabilization. HIF- $\alpha$  stabilization is prevented by mitochondrially-targeted antioxidant MitoQ (Bell et al. 2007), Glutathione S transferase addition decreased ROS and HIF in JunD<sup>-/-</sup> cells (Gerald et al. 2004). Antioxidant treatment was observed to diminish HIF-1 $\alpha$  expression and Myc-mediated tumorigenesis in mouse xenograft models (Gao et al. 2007). Herein, suppression of tumor growth by antioxidants was dependent on ability to promote HIF-1 $\alpha$  degradation, since tumors expressing stabilized form of HIF were not affected by antioxidants. Nevertheless, the role of mitochondria in these processes is yet to be investigated in details, since the sole dependence of ROS production on oxygen concentration for isolated mitochondria does not include any ROS burst region and it is simply hyperbolically declining (Hoffman and Brookes 2009).

- **Regulation of HIF by metabolites: pseudohypoxia**

The physiological function of HIF is to promote adaptation of cells to low oxygen by inducing glycolysis and promoting changes that lead to neovascularization. Stabilization of HIF- $\alpha$  occurs not only in response to low oxygen tension; a phenomenon termed “pseudohypoxia”, describes a high activity of HIF under normoxic conditions (Selak et al. 2005). Pseudohypoxia is a result of impaired HIF- $\alpha$  degradation, which can arise in response to various genetic alterations, such as VHL-tumor suppressor loss in renal carcinoma (Staller et al. 2003) and loss of mitochondrial tumor suppressors succinate dehydrogenase (SDH) and fumarate hydratase (FH); see (King et al. 2006), that lead to formation of pheochromocytoma, paraganglioma and leiomyoma, respectively. Since VHL loss

influences directly HIF- $\alpha$  degradation process, the defects caused by SDH and FH loss are more complex (metabolic signaling). Mutations in subunits B and D of SDH cause disintegration of SDH complex and loss of SDH enzymatic activity, which results in accumulation of succinate in mitochondrial matrix. Succinate which leaks out into cytosol then inhibits prolyl hydroxylation of HIF- $\alpha$  by product inhibition of cytosolic PHDs. SDH and FH deficient tumors were reported to have elevated levels of fumarate and succinate, HIF expression and high vascularity (*Pollard et al. 2005*). Inhibition of PHD by its product succinate leads to HIF- $\alpha$  stabilization and activation of HIF-pathway. Similarly, FH-deficiency results in accumulation of fumarate, which inhibits PDH owing to chemical similarity to succinate. This is a novel mechanism of cellular signalization, where certain metabolic intermediates act as “signal” transducers to influence distant cellular targets. Metabolic signaling includes other metabolites, such as pyruvate (*Lu et al. 2002*), which was reported to promote HIF- $\alpha$  stabilization independently of oxygen presence. Among other metabolites, lactate, fumarate, succinate and oxoglutarate are involved in metabolic signaling (*Bellance et al. 2009b; Koivunen et al. 2007*). HIF stabilization by metabolites can strengthen the HIF effect in hypoxia or maintain HIF expression level after hypoxic period in the tissue.

- **HIF-1 mediated changes**

HIF-1 transcription factor regulates expression of multiple genes (*Semenza 2007; Papandreou et al. 2006; Hu et al. 2003; Wigfield et al. 2008*) involved in energetic metabolism in response to HIF- $\alpha$  stabilization event. HIF-1 $\alpha$  and HIF-2 $\alpha$  regulate overlapping subset of genes; alternatively, genes that possess both HRE1 and HRE2 are differently regulated by HIF-1 and HIF-2. Generally, regulation is cell-type specific and depends upon extent of expression of particular HIF- $\alpha$  isoform (*Fukuda et al. 2007*). Expression of HIF in hypoxia mediates changes leading to angiogenesis in order to reoxygenate hypoxic tissue, which is a primary function of HIF. For instance, expression of VEGF and EPO governed by HIF expression has been shown to promote angiogenesis (*Rankin et al. 2008*). Suppression of HIF- $\alpha$  impairs cell survival under the hypoxia (*Welford et al. 2006*). HIF is considered to regulate overall fate of intracellular glucose, mainly connection to anabolic processes and switch between them. In following section, basic responses mediated by HIF in response to hypoxia contributing to phenotypic switch, namely glycolytic phenotype, will be summarized. Among other targets, anti-apoptotic protein BCL-xL has been described to be regulated in HIF-dependent manner (*Chen et al. 2009*). More targets of HIF are being reported continually.

- **Upregulation of glucose uptake and glycolytic pathway**

HIF stimulates in parallel the enzymes responsible for the glycolytic breakdown of intracellular glucose, such as hexokinase1 (HK1) and 2 (HK2), more important in hypoxia, (*Mathupala et al. 2001*), PFK-1 (or C and L , PFK-C, PFK-L), aldolase, enolase1 and glyceraldehyde-3-phosphate dehydrogenase (GAPDH). It has been reported that all 12 enzymes required for glycolysis are directly regulated by HIF so that the entire process is coordinately stimulated (*Iyer et al. 1998; Seagroves et al. 2001*).

- **Regulation of lactate dehydrogenase**

Typical feature of certain cancer cells is high lactate production, resulting in cytosolic and extracellular acidification. Such an adaptation is required in order to maintain sufficient NAD levels even if oxidative phosphorylation is attenuated. Activation of glycolysis provides sufficient ATP levels under the conditions of increased energetic demand in hypoxia or in highly proliferative tissues. Expression of LDH is controlled either by c-Myc (*Shim et al. 1997*) and HIF pathway (*Ebert and Bunn 1998*) and cAMP-related pathway (*Li et al. 2004*). Primarily, increase of LDH expression is an adaptation to low oxygen, but lactate formation is also a principal hallmark of Warburg effect. Overexpression of LDH has been reported in various tumors (*Forti et al. 2002*). It is not clear, whether the overexpression of LDH is a cause or consequence of downregulated respiration. Obviously, there is tight interconnection between glycolysis and oxidative phosphorylation, since LDH inhibition results in increased respiration (*Fantin et al. 2006*) and vice versa. Similarly, attenuation of mitochondrial respiration in the presence of LDH has an impact on mitochondrial membrane potential. Inactivation of respiratory chain causes, that mitochondrial membrane potential is concomitantly increased, as mitochondria of cells that rely solely on glycolytic ATP remain in state 4 (*Rossignol et al. 2004*). Elevated mitochondrial membrane potential is a common feature of various tumor cells (*Lum et al. 2007*). In contrast to normal cells, absence of LDH slows down a growth rate of tumor cells even under the normoxic conditions and impairs growth under hypoxia (*Fantin et al. 2006*). Block of proliferation is attributed to the inability of cancer cells to maintain ATP levels in the absence of LDH. Interestingly, oxidative metabolism is possible only in subset of tumors; some of cancer cells strictly require LDH presence (*Xie et al. 2009*). Tumor cells have elevated pyruvate-to-lactate conversion catalyzed by LDH and genetic alteration including PDH attenuation promotes shift in metabolic strategy towards anaerobic metabolism and supports aggressive phenotype of tumor in vivo. LDH-A form increases during mammary gland tumorigenesis (*Li et al. 2004*) and LDH activity is also elevated in breast tumors compared to normal mammary tissues (*Hilf et al. 1976*).

- **Regulation of pyruvate dehydrogenase**

Pyruvate is converted to acetyl-coenzyme A (Ac-CoA) by mitochondrial pyruvate dehydrogenase complex (PDH) and subsequently enters the TCA cycle. Reaction is irreversible and unique within the cell, therefore carefully controlled to maintain glucose and lipid homeostasis. PDH activity is regulated by products NADH and acetyl-CoA, which inhibit pyruvate decarboxylation and further reactions of PDH by acetylating of E2 subunit.

Additional regulatory mechanisms of PDH activity include phosphorylation/dephosphorylation of E1 subunit. Pyruvate dehydrogenase kinase (PDK), which is allosterically activated by acetylated (inactivated by product inhibition) E2 subunit in turn phosphorylates E1 subunit of PDH (*Patel and Korotchkina 2003*). Reactivation is accomplished by pyruvate dehydrogenase phosphatase (PDP). There are four isoenzymes of PDK and two isoenzymes of PDP present in mammalian tissues, with different tissue distribution, specific activity and sensitivity (*Patel and Korotchkina 2006*).

Active inhibition of oxidative metabolism seems to be a part of adaptation to hypoxia. PDK-1 expression level has been shown to be increased in response to HIF- $\alpha$  stabilization (*Kim et al. 2006a*) after hypoxia exposure and in VHL-deficient cells (*Papandreou et al. 2006b*). PDK-1 induced inactivation of PDH in hypoxia effectively decreases mitochondrial oxygen consumption (*Papandreou et al. 2006*). Inhibition of oxidation of pyruvate in hypoxia provides growth advantage, since it makes pyruvate available for LDH. Pyruvate to lactate conversion and glycolytic ATP production is therefore accelerated. PDK-1 inhibition results in increased cell-death in hypoxia in head and neck carcinoma (*McFate et al. 2008*) so that downregulation of respiration is a requirement for cell survival in hypoxia. It was also proposed that PDK-1 mediated attenuation of TCA cycle reduces ROS production in conditions when electron transport is ineffective due to the limited oxygen (*Kim et al. 2006a*) or to protect tumoral cells which are suddenly oxygenated by new blood vessel, from oxidative stress caused by oxidative burst after reoxygenation (*Wigfield et al. 2008*). To support this view, HIF activation in PHD<sup>-/-</sup> mouse (*Aragones et al. 2008*) causes reduction of mitochondrial respiration along with oxidative stress (PDK overexpressed, glycolysis increased). On the contrary, wild-type animals, unable to switch to anaerobic metabolism so fast, displayed increased oxidative damage of mitochondria. Further utilization of oxidative metabolism was not possible in cells derived of *wt* animals. Inhibition of respiration is considered to be necessary in hypoxic conditions, because when hypoxia is severe and sustained, mitochondria may be impaired by oxidative damage if HIF is not activated.

PDK-1 expression and PDH inhibition can significantly influence the level of metabolites in cells. Accordingly, it has to been reported that by inhibition of PDH, the ability of cells to generate sufficient cytosolic Ac-CoA is compromised. Reduction of TCA activity and rate of conversion of

pyruvate into Ac-CoA and further citrate generation suppress cells growth and proliferation. Indeed, inhibition of cell growth and proliferation has been observed upon HIF activation in normoxia in hematopoietic cells (*Lum et al. 2007*). This is the apparent contradiction in term of advantage of PDK-1 expression, considering negative effect on proliferation of cancer cells, even if PDK-1 expression was reported to support cell growth. The extent of PDH inhibition by HIF should be considered to evaluate consequences of PDH attenuation in respect to cell type and oxygen tension.

- **Interference with Myc pathway - regulation of mitochondrial biogenesis**

Myc protein is an essential transcription factor that regulates various cellular processes. Myc dimerizes with Max to form a functional transcription factor (*Cowling and Cole 2006*), and binds E-box element to direct genes involved in regulation of proliferation, glucose and energy metabolism, apoptosis and differentiation. Myc competes with Mad family members (e.g. Mxi1 protein) to form a dimer with Max and repress Myc-inducible genes (*Nilsson and Cleveland 2003*). Myc pathway promotes apoptosis induced by hypoxia or serum deprivation (*Brunelle et al. 2004*). Myc antagonist Mxi1 protein was shown to be highly increased in hypoxic cells (*Corn et al. 2005*) in HIF-1 $\alpha$ -dependent manner. On the contrary, c-Myc expression in hypoxia was downregulated completely. Downregulation of Myc expression during hypoxia gives Mxi better opportunity for interaction with Max and repression of Myc-regulated genes (*Corn et al. 2005; Zhang et al. 2007*), so in fact HIF regulates Myc function.

Interestingly, there are genes involved in glucose metabolism, which are regulated by both c-Myc pathway and HIF pathway, for example LDH-A, GLUT1 and (*Osthus et al. 2000*), which possess both Myc and HIF-responsive elements. The implication for coordinate regulation of glycolysis by these two transcription factors depends on whether we consider the metabolism of a normal cell versus a cancer cell. Normal cells are governed by mitogenic stimuli to switch to anaerobic metabolism. In normoxia, mitogenic stimuli induce transition to fast-proliferation state, where high glycolysis is required and glycolytic genes are upregulated in Myc-directed manner (*Corn et al. 2005*). Similarly, in normal cells exposed to hypoxia, HIF-1 dependent upregulation of glycolytic genes mediates an appropriate physiologic transition to glycolysis for ATP production. In hypoxia, even when Myc is downregulated, upregulation of glycolytic enzymes can still occur due to upregulation of HIF pathway. Hypoxia results in repression of c-Myc target genes except when they are also regulated by HIF pathway. Genes regulated solely by c-Myc pathway, are generally repressed under hypoxia unless there is also a regulation by HIF pathway. Coordination of regulation of glycolytic genes by c-Myc and HIF has been proposed to explain the observation that cancer cells preferentially utilize glycolysis versus oxidative phosphorylation to harness energy when oxygen is limited. Deregulation

of c-Myc and HIF in cancer cells results in activation of glucose transporters and glycolytic enzymes. Myc activity however is elevated in HIF-2 expressing tumors. Opposite effect of HIF-1 and HIF-2 on c-Myc activity and differential response to cell cycle regulation (*Gordan et al. 2008*) has been reported.

Importantly, since both HIF and Myc upregulate glucose transport and glycolysis, they have different functions in regulating mitochondrial metabolism. Mechanism of Myc downregulation of mitochondrial respiration and mitochondrial mass in HIF-dependent manner during hypoxia are reported (*Zhang et al. 2007*). Hypoxia-dependent Myc downregulation and Mxi-1 upregulation results in inhibition of PGC-1 $\beta$ . This consequently inhibits mitochondrial biogenesis when HIF expressed.

- **Regulation of OXPHOS proteins expression**

As mentioned previously, HIF regulates energy metabolism by enhancing glycolysis and inhibits pyruvate entering into the mitochondria. HIF also regulates oxidative metabolism at the level of OXPHOS enzyme, namely cytochrome-c oxidase (COX) synthesis. COX subunit 4 (COX4), is a regulatory subunit which binds ATP and causes allosteric inhibition of COX activity at high ATP/ADP ratios. In yeast cells, hypoxia activates expression of COX5a (yeast homologue of COX4). COX5b expression is repressed and COX5a transcription is activated at high O<sub>2</sub> concentrations, whereas at low O<sub>2</sub> concentrations, COX5a transcription is inactivated and COX5b transcription is de-repressed (*Semenza 2007*). Replacement of COX5a by COX5b results in increase of enzyme turnover rate and rate of intramolecular electron transfer of comparing to normoxic complex. First, the turnover rate of cytochrome c oxidase in cells that express Vb is higher than in cells that express Va. Second, the rates of intramolecular electron transfer are also higher in cells that express Vb (*Waterland et al. 1991*) (alterations of kinetic properties of COX and optimization of respiration according to oxygen availability).

COX4-2, but not COX4-1 isoform, is induced under hypoxia in HIF-dependent manner, since gene encoding COX4-2 contains HRE (*Fukuda et al. 2007*). COX4-1 is rapidly degraded in hypoxic conditions. Degradation of COX4-1 is probably promoted by mitochondrial protease LON, which is also induced by HIF. COX4-2 maintains respiratory rate in hypoxic condition in contrast to COX4-1. Expression of COX4-1 in hypoxic cells causes elevation of ROS production by respiratory chain. Therefore, a switch of the isoforms should optimize electron transport, ATP production, and ROS production according to oxygen availability (*Fukuda et al. 2007*), in concert with other hypoxic adaptations, such as PDK and LDH expression. Increased production of ROS in cells expressing COX4-1 may be relevant for *in vivo* situations, when blood flow into tumor is interrupted and oxygen

tension declines rapidly. In such cases, cells which are not yet adapted to hypoxia, thus expressing normoxic COX4 isoform, could be hypothetically responsible for ROS burst during primary hypoxic exposure, which may in turn improve HIF stabilization (*Klimova and Chandel 2008*).

Alterations of OXPHOS complexes biogenesis has been observed in renal carcinoma cells, which are VHL-deficient. VHL-deficiency results in constitutive HIF expression, which in turn causes processing of OXPHOS proteins (namely COX precursors), mtDNA (*Hervouet et al. 2005*) and stimulation of Mn-SOD expression (*Hervouet et al. 2008*). We can assume, that VHL-deficient cells undergo complex alteration in mitochondrial OXPHOS system and antioxidant defense to deal with potentially harmful effect of increased ROS production in hypoxia. Autoregulation between levels of HIF, ROS and OXPHOS subunit content may exist: ROS produced stabilize HIF, HIF downregulates OXPHOS and ROS, production decreases (*Hervouet et al. 2008*).

#### 2.3.2.1.4. AMPK pathway NFκB, mTOR participation in hypoxia

AMP-activated protein kinase (AMPK) is a cellular energy sensor since its activity is sensitive to AMP: ATP ratio and promotes catabolic processes while inhibiting anabolic metabolism (*Towler and Hardie 2007*). The O<sub>2</sub> limitation usually brings about an immediate ATP shortage, as the supply of O<sub>2</sub> to mitochondria drops. Recently it has been suggested that oxidative stress and not an increase in the AMP/ATP ratio is required for hypoxic activation of AMPK (*Emerling et al. 2009*). Full activation of AMPK requires specific phosphorylation within the activation loop of the catalytic domain of the α-subunit by upstream kinases such as the serine/threonine protein kinase LKB1. Hypoxia via a ROS-burst reportedly activated AMPK through LKB1 without an increase in the AMP/ATP ratio (*Emerling et al. 2009*). Likewise for HIF, mitochondrial origin of these ROS has been demonstrated by experiments, in which p<sup>0</sup> cells failed to activate AMPK during hypoxia but were able to upon addition of external H<sub>2</sub>O<sub>2</sub>. When activated, AMPK phosphorylates and inhibits acetyl-CoA carboxylase (ACC), the rate-limiting enzyme in fatty acid synthesis, catalyzing malonyl-CoA formation. The latter is a potent inhibitor of fatty acid oxidation, therefore, this is promoted, whereas lipogenesis is reduced. Likewise the 3-hydroxy-3-methylglutaryl CoA reductase is inhibited by AMPK, reducing cholesterol formation. Upon exercise AMPK elevates GLUT4 and consequently glucose uptake. AMPK upregulates glucose energy metabolism and transcriptional activity of HIF. Hypoxia-induced mitochondrial ROS have been also shown to enhance the DNA-binding of nuclear factor κB (NFκB, (*Chandel et al. 2000*)). This provides an alternative redox-dependent regulation of gene expression. Typically, activation of the NFκB pathway starts with phosphorylation of IκB at specific serine residues that targets its proteasome degradation. The consequent release of NFκB subunits allows their migration to the nucleus and binding to promoter/enhancer regions of target genes. An

alternative without I $\kappa$ B degradation upon its phosphorylation at tyrosine residues also plays a role. High hypoxia has been found to activate NF $\kappa$ B via phosphorylation at tyrosine residues but with I $\kappa$ B degradation (Koong *et al.* 1994). In HeLa cells it may proceed via activation of redox-regulated tyrosine kinase c-Src (Fan *et al.* 2002). A dual role of mitochondrial ROS than exists, at moderately elevated levels during hypoxia NF $\kappa$ B activation via c-Src promotes cell survival, whereas at high burst it led to cell death (Lluis *et al.* 2007).

#### 2.3.2.2. Oncogenes in metabolic reprogramming

Ongoing genetic characterization of human cancers reveals very complicated architecture of potential cancer promoters and tumor-suppressor genes which implies also a great variability of metabolic phenotypes. The diverse mechanisms of tumor induction have in common their influence on differentiation, cell cycle arrest, and apoptosis. Genomic instability as a force for new mutations causes checkpoint loss and disruption of cell-cycle controls and cellular metabolism (Halazonetis *et al.* 2008). Many molecular features of cancer cells including DNA mutations in oncogenes can increase the ratio of glycolysis to oxidative glucose metabolism as a secondary effect of oncogene activation. Combination of different transforming proteins showed a correlation between tumor aggressiveness, dependence on glycolytic energy production and decreased dependence on mitochondrial energy production (Ramanathan *et al.* 2005). Several general oncoproteins can influence energy substrate utilization by affecting cellular targets leading to metabolic changes that favor cancer cells to survival, apart of cellular proliferation control. In this chapter, I will summarize some of the main oncogenic pathways reported to contribute to metabolic remodeling.

- **PI<sub>3</sub>K/Akt pathway**

Alterations of Akt pathway have been reported in various malignancies (DeBerardinis *et al.* 2008), generally Akt pathway being augmented by various mechanism thus promoting cell survival of cancer cells. Akt expression has been reported to directly stimulate glucose uptake and induce aerobic glycolysis; moreover, maintenance of Akt activity was required for the rapid dissemination of malignancy of leukemic cell *in vivo* (Elstrom *et al.* 2004) thus promoting cancer progression apart of apoptosis resistance. With increased glycolysis, no increase of respiration was observed; however, accumulation of NADH was additional effect of limited ability of glycolytic pathway to reoxidize NADH. Although increased LDH expression is observed in highly glycolytic cells, NADH can accumulate, since glucose uptake is maintained in high excess of cellular demand. Besides, Akt stimulated metabolic changes make cells unable to survive in glucose-limiting conditions (Elstrom *et al.* 2004). Changes in NADH levels have been observed also in respiratory-deficient model (Pelicano

*et al. 2006*). Here, mitochondria dysfunction leads to the complex cellular redox changes that mediate inactivation of PTEN lipid phosphatase (a negative regulator of Akt), thus activate Akt. Akt activation and elevated glycolysis gives a growth advantage in normoxic as well as in hypoxic conditions. Inhibition of Akt pathway was reported to reduce glucose uptake, but does not influence glutamine metabolism (*Wise et al. 2008*). Among other targets of Akt, Akt/PI<sub>3</sub>K pathway has been reported as a regulator of HIF- $\alpha$  stabilization and function (*Zundel et al. 2000*), although HIF- $\alpha$  is not a direct target of Akt phosphorylation. AKT also stimulates fatty acid synthesis by increasing the activity of ATP citrate lyase (ACL), (*Hammerman et al. 2004*). In this way mitochondrial fatty acid oxidation is suppressed either by increased production of acetyl-CoA, the product of the ACL reaction; or by downregulating carnitine palmitoyl transferase 1A (*Buzzai et al. 2005*). As a result, parental cells can maintain their viability in the absence of glucose by oxidizing the fatty acids, while AKT-transformed cells lack this ability and undergo apoptosis.

- **p53 pathway**

p53 tumor suppressor protein is a common transcription factor of multicellular organisms known for its role to retain a stability of genome by preventing genome mutation. Additional cellular functions of p53 has been reported, e.g. cell cycle regulation, apoptosis regulation and, also, aerobic metabolism regulation. It has been shown, that oxygen consumption was affected in p53-deficient mice and subsequently in human cancer cells with p53 deficiency, as compared to non-deficient model (*Matoba et al. 2006*). Respiration deficiency underlies to SCO2 protein deregulation by p53 deficiency. p53 regulates level of SCO2, a protein required for proper assembly of cytochrome c oxidase, resulting in impaired COX-2 biogenesis, which is mitochondrial-encoded subunit. This alteration causes impairment of COX assembly and a shift towards anaerobic metabolism. Lactate synthesis was concomitantly increased, but ATP levels remained stable. Decreased COX activity and COX-2 synthesis has been confirmed by other study (*Zhou et al. 2003a*).

- **Myc pathway**

Myc deregulation has been described in multiple human cancers (*Nilsson and Cleveland 2003*). High levels of c-Myc overexpression can result in accumulation of significant DNA damage (*Ray et al. 2006*) interfering with p53 function (*Vafa et al. 2002*). Myc regulates broad spectrum of genes involved in cell cycle regulation, metabolism, mitochondrial function and regulation of apoptosis by transcription and posttranscriptional manner (*Cole and Cowling 2008*). Myc heterodimerizes with Max to form a functional transcription factor and MYC/Max dimers bind to E-box of specific target genes and stimulate transcription (*Cowling and Cole 2006*). Conversely, Myc-regulated genes are

repressed by Mxi/Max transcription complex. Deregulation of Myc expression is sufficient to promote cellular transformation and tumorigenesis, induced by genomic instability. Myc deregulation occurs as a result of point mutations, gene amplification, chromosomal translocations and other oncogenic events in gastric carcinoma (*Calcagno et al. 2008*).

Myc has been shown to influence genes involved in glucose metabolism by inducing expression of glycolytic enzymes (*Valera et al. 1995*) as a response to mitogenic or growth factor stimuli, which requires transition to glycolysis for rapid ATP production. Myc has been shown to be involved also in the glutamine dependence feature of certain tumours, leading to commit Myc-dependent apoptosis in a glutamine deficient ambient (*Yuneva et al. 2007*). Myc with deregulated expression has increases glutamine metabolism, and upregulated glutamine importers controlled by Myc (*Wise et al. 2008*). Herein, glutamine was necessary to maintain a viability and survival despite the abundance of glucose.

- **Ras**

Ras transformation has been reported to influence cellular targets linked to energy-production pathways, indicating that oncogenic K-ras induces a strong remodeling of metabolism during the transformation process. Correlations between oncogenic Ras and energy metabolism have been reported (*Vizan et al. 2005*). Depending of type of mutation, cells exhibited either increased glycolysis and lactate production, or high PPP flux with increased nucleic-acid synthesis and high TCA flux. Former phenotype enhanced resistance to apoptosis. In other study, K-ras transformation resulted in a stronger dependence from glycolysis for cell survival, reduced oxidative phosphorylation ability and a fragility towards glucose depletion compared to their immortalized, normal counterparts (*Chiaradonna et al. 2006*). Expression profiling revealed alteration of several genes encoding subunits of cytochrome-c oxidase. An increased glycolytic flux, down-regulated expression of several genes involved in fatty acid biosynthesis, unbalanced transcription of genes encoding subunits of the pyruvate dehydrogenase complex, subunits of respiratory complex II and IV as well as of ATP synthase was observed in Ras-transformed fibroblasts compared to their control cell line.

- **HER and regulation of fatty acids metabolism**

Metabolism of fatty acids seems to be a rather underestimated issue as compared to glucose metabolism in cancer cells. Tumor behaviour has been shown to be influenced by expression of fatty acid synthase (FASN) towards enhanced invasiveness and proliferation. Indeed, expression of FASN and de-novo lipogenesis has long been attributed to several cancer types (*Kuhajda et al. 1994*;

*Kuhajda 2000*). Interestingly, FASN overexpression causes transformation itself (*Vazquez-Martin et al. 2008*). Cellular inducers of FASN hyperactivity remain elusive, but it is established that FASN expression correlates with hypoxia, ROS production, and with HIF and PIP3/AKT pathways due to the PTEN inactivation, with increasing resistance to apoptosis in hypoxia (*Furuta et al. 2008; Menendez et al. 2004*). Consequently, de-novo lipogenesis is not only supporting cell growth but belongs to important signaling events. Moreover, tumor-associated FASN activity regulates intracellular signaling pathway associated with human endothelial receptor (HER) (*Menendez et al. 2004*). Importantly, FASN overexpression causes an immediate susceptibility of transformed cells to the FASN inhibitor, an inhibitor C75 (*Vazquez-Martin et al. 2008*). Thus cell die upon inhibitor addition. This is clearly explained by the ability of FASN to trigger expression and activity of tyrosine kinase receptor HER/neu receptor. In turn, HER activation further affects cell survival and provides a feedback regulation on expression of FASN (by SREBS activation) to support cell growth and control of proliferation by tyrosine kinases, etc. Tyrosine kinase receptor HER2/3 (also termed erbB-2) also initiates PIP3/AKT signaling. In conclusion, fatty acid synthesis is integrated with prosurvival signaling pathways in tumor cells. Note also, that NADPH synthesis by pentose phosphate shuttle and by cytoplasmic malic enzyme is required for fatty acid synthesis.

#### 2.3.2.3. Proliferation rate

To maintain tumorigenic potential, sustained high proliferation rate of cancer cells during invasive growth is necessary. Proliferation rate is, however, very demanding on biomass formation and requires appropriate metabolic adaptations to provide constant supply of proteins, lipids and de novo synthesis of purines and pyrimidines as well as ribose for nucleic acid synthesis to form new cells. In normal proliferating cells (embryogenesis, growth) signals that stimulate cell proliferation also participate in the reorganization of metabolic activity that enables proliferation. High rate of glucose uptake is often disproportional to low oxygen consumption rate in tumor cells. Glucose has at least two possible fates within the cell: it may be oxidized to produce cellular bioenergy or it may be converted into other macromolecules to support cellular biosynthesis. Extracellular signals may directly upregulate glucose utilization in order to meet energy demand and stimulate glucose-dependent macromolecular synthesis. Reports of metabolic studies of human glioblastoma cells indicate, that despite low respiration, constant pyruvate flux through PDH is maintained (*DeBerardinis et al. 2007*). Pyruvate, product of glucose metabolism, imported into mitochondria, is major precursor of Ac-CoA but also the citrate for FA synthesis, particularly phospholipids, essential for cell growth. In the same study, the role of glutamine metabolism was highlighted. By glutamine metabolism, NADPH pool is maintained for cellular biosynthetic pathways, and recovers low NADPH

production by PPP. Major contribution of glutaminolysis to lipid synthesis is production of oxaloacetate or malate (FIG 2-10), which replenish TCA cycle by cataplerotic reactions and along with glucose-derived Ac-CoA participate in citrate synthesis. Utilization of two distinct pathways, glycolysis and glutaminolysis, provides glioblastoma cells ability to generate biosynthetic precursors for multiple catabolic pathways, form biomass, reflected in growth advantage over non-transformed cells. New lipid biomass might be derived from the conversion of other macromolecules to lipids or from the utilization of pre-existing extracellular lipids. Proliferative cells as well as cancer cells, however, utilize preferably de-novo synthesis of FA (*Jackowski et al. 2000*). Accordingly, major cellular lipid precursor remained glucose over glutamine (*DeBerardinis et al. 2007*) based on detection of radioactive tracer.

Depression of respiration in hypoxic cells can be well explained by lack of substrate due to the pyruvate shunt towards fermentation (section 2.3.2.1.3.). These glucose-derived carbons, when incorporated into citrate, may either be oxidized via the TCA cycle or exported from mitochondria (cataplerotic flux). It was reported, that depression of respiration in proliferating cells in normoxia was caused by lack of substrate for OXPHOS due to the elevated citrate efflux from mitochondria (during glutaminolysis) to maintain high rate of FA synthesis (*DeBerardinis et al. 2007; Bauer et al. 2005*). In this case, reduction of respiration is secondary to metabolic activities needed for biosynthesis of proliferating cells. Once citrate exported of mitochondria, cytosolic citrate is processed by ATP citrate lyase (ACL) to produce cytosolic Ac-CoA and regenerate oxaloacetate. Cytosolic Ac-CoA is the requisite building block for all endogenous synthesis of acyl groups and sterols. ACL expression/inhibition likely regulate formation of cytosolic Ac-CoA, governs the direction of citrate towards oxidation by TCA cycle, and mitochondrial oxygen consumption (*Bauer et al. 2005*). Combination of glucose presence and ACL overexpression provides tumor cells an advantage to proliferate extensively (*Hatzivassiliou et al. 2005*). Upon interruption of its high glucose-to-lipid flux, factors in the *in vivo* tumor microenvironment may allow a tumor cell to initiate adaptive responses, such as differentiation, in order to maintain its survival and compensate for the growth rate. Disrupting citrate transport offers the possibility to treatment strategies (*Mashima et al. 2009*) by suppressing of proliferation rate of tumor cells.

Proliferation rate can be regulated in hypoxic conditions also by HIF, since expression of PDK-1 attenuated pyruvate entry to mitochondria by inhibiting of PDH activity. When expressed, PDK-1 suppresses the activity of PDH and limits the influx of pyruvate into the TCA cycle. As pyruvate entry into the TCA cycle is suppressed, there would be a concomitant decline in the production of citrate. At this point, the additional regulatory mechanism should be reminded. In growing cells, the citrate exported from mitochondria into the cytosol suppresses glycolysis at the level of PFK-1. This partial

suppression of PFK-1 may be adaptive for cell growth by allowing a greater amount of G6P to be diverted into nucleotide biosynthesis and glycosylation reactions. Therefore, HIF-1 $\alpha$  enhanced PDK-1 activity results in a decline in mitochondrial citrate production, resulting in a derepression of PFK-1 activity and a concomitant suppression of lipid synthesis (both by PPP- and citrate-related ways). By activated LDH that utilize pyruvate, HIF-1 $\alpha$  transcription reprograms the intracellular utilization of glucose from its use in lipid and nucleotide synthesis and redirects glucose almost exclusively into anaerobic glycolysis to support cellular NADH reoxidation. Deregulation of pyruvate entering to mitochondria, slows down the rate of FA synthesis, as reported for hematopoietic cells (*Lum et al. 2007*). However, considering variability of existing expression pattern of multiple enzymatic isoforms, this model remains one of many and may be specific for a particular cell type.

#### 2.3.2.4. Metabolism of glutamine in cancer cells, glucose deprivation

Although metabolism of cancer cells is strongly dependent on glucose, depletion of glucose can occur in solid tumors; therefore, cancer cells possess alternative metabolic adaptations to overcome glucose deprivation. Among these, utilization of fatty acids (FA) can be used as metabolic substrate, or alternatively, utilization of glutamine to support cancer growth. Since this thesis deal with glutamine metabolism, in this chapter I will shortly summarize basic principles of glutamine metabolism and glutamine utilization and its interference with glucose-utilizing pathways. Some tumor-derived cells have been reported to grow in glucose-free medium supplemented with amino acids (*Helmlinger et al. 2002*), which was a result of altered channeling of amino acids into metabolic pathways, namely glutamine, as compared to normal cells and tissues. In HeLa cells, although only 5% of metabolized glucose entering the TCA cycle, significant oxidative ATP production is maintained owing to glutamine metabolism (*Reitzer et al. 1979*). Glutaminolysis is the alternative pathway utilized to replenish TCA cycle and produce ATP by oxidative metabolism even in the presence of glucose (*Reitzer et al. 1979*). Elevated glutamine-dependent metabolism was observed in various types of tumors (*Matés et al.*), however, glutaminolysis is not universal for all cancers, and it might be as well induced as a consequence of oncogenic event, for instance Myc deregulation (*Wise et al. 2008*). Glutamine is gained from the extracellular space by glutamine transporters such as ASCT2 and SN2. Inside the cell, glutamine is deaminated to glutamate via glutaminase (GLS) or the transaminated to glutamate through the enzymes of nucleotide biosynthesis, following by the transamination of glutamate to  $\alpha$ -ketoglutarate ( $\alpha$ -KG) via transaminases such as alanine aminotransferase (ALT, see FIG 2-10).  $\alpha$ -KG is imported to mitochondria and enters the TCA cycle.

Glutamine which entered Krebs cycle (in form of KG) does not have to be metabolized completely, but readily exported of mitochondria as malate (FIG 2-10) and catalysed by the

cytoplasmic malic enzyme (ME) to pyruvate. This reaction results in NADPH production, largely induced along with glutaminolysis. Pyruvate formed by the reaction of malic enzyme (ME) contributes to the lactate production (*Reitzer et al. 1979; DeBerardinis et al. 2007*). Indeed, 60% of glutamine was observed to be metabolized to lactate in human glioblastoma cells (*DeBerardinis et al. 2007*). Alternatively, citrate efflux supports the FA synthesis. Bi-product of FA synthesis OAA is reduced to malate via cytosolic malate dehydrogenase and is imported to mitochondria via malate/ $\alpha$ -KG exchanger. Reaction of malate dehydrogenase is driven if excess NADH existing in cytoplasm (as occurs with high rate of aerobic glycolysis). Increased lipid metabolism, particularly phospholipids synthesis, was observed as a response to activation of glutaminolysis through transcriptional regulation of glutamine transporters and glutaminolytic enzymes induced by Myc oncogene (*Wise et al. 2008*).

If complete TCA takes place, malate imported to mitochondria can replenish TCA cycle. However, due to the increased activity of mitochondrial ME (*Moreno-Sánchez et al. 2009*), malate is preferably metabolized to pyruvate. Pyruvate along with glutamine can support full TCA cycle activity.

In case of glucose starvation, glutamine can fully compensate for missing glucose; i.e. activation of glutaminolysis and reduction of pyruvate metabolism in mitochondria prevents cell death caused by glucose limitation (*Mazurek et al. 2002*). Indeed, glutaminolysis can in fact compensate for cellular ATP, pyruvate, lactate and NADPH pool, normally supplied by glucose metabolism via PPP. Requirement for glutaminolysis is, however, aerobic conditions. Therefore, it is possible that some cells within tumor adapt to current substrate by reprogramming of energy metabolism according to the actual exogenous substrate. Furthermore, combination of substrate availability therefore notably influence metabolism of cancer cells. In case of Myc deregulation induced changes in glutamine metabolism, which in turn influence other processes involved in glucose metabolism (*Wise et al. 2008*). Myc, however, in this case caused complete dependency of cell growth and proliferation on glutamine in human glioma cells. According to *Reitzer*, glutaminolysis is dependent on character of present sugar. On contrary, deregulation of Myc and induction of glutamine metabolism influence also the fate of glucose, namely towards lactate production and not to mitochondrial oxidation. This apparent contradiction is not so contradicting considering genetic variability of tumor cells and fully depends on character of oncogenic transformation. These differences can appear even within one tumor, resulting in a heterogenous spatial organization of cells with different metabolic activity. Such hypothesis is supported by findings of metabolites gradients and metabolites concentrations differences within one tumor. Glucose presence enables proliferation in regions of high-glucose concentrations. Induction of glutaminolysis allows cancer cells to invade areas with low glucose. In human colon cancer cell lines, glutamine supplementation

stimulates proliferation, promotes a less differentiated phenotype and inhibits cell adhesion to solid matrix, changes expected for a more aggressive tumour behavior *in vivo* (Turowski et al. 1994).

#### 2.3.2.5. Reversal to fetal phenotype

Aerobic glycolysis can be considered to be a result of reprogramming of metabolic genes/enzymes to make cancer cells to function more like fetal cells and to enable a greater fraction of glucose metabolites to be incorporated into macromolecule synthesis rather than burned to CO<sub>2</sub>. Hypothesis of retrodifferentiation interprets increased glucose metabolism as a transition from normal to fetal-like energy metabolism during oncogenesis (Uriel 1976). For instance, during fetal development the hepatocytes derive most of its energy requirements from glycolysis producing large amounts of lactate. However, soon after birth, the increased availability of oxygen triggers a sharp reduction in the rates of glucose consumption (Cuezva et al. 2007). Similarly, (Taketa et al. 1988) express fetal isoforms of glycolytic genes. Recent studies indicate a new role of embryonic pyruvate kinase isoform M2 (PKM-2), a glycolytic enzyme that catalyzes the final, irreversible, step of glycolysis in carcinogenesis (Christofk et al. 2008a; Christofk et al. 2008b). These studies describe, how single exchange of enzymatic isoform influence metabolic phenotype of the cell. PKM-2 is a splice variant of PKM-1, expressed during embryonic development. Tumor tissues have been reported to express exclusively embryonic isoform (Taketa et al. 1988). Pyruvate kinase is allosterically activated by glycolytic intermediate FBP and PKM-2 was shown to be able to bind phosphorylated tyrosines (Christofk et al. 2008b). Interestingly, binding of tyrosine–phosphate catalyses release of FBP from PK and inhibition of enzyme and build-up of glucose intermediates. Regulation of pyruvate kinase by phosphotyrosine and FBP binding is specific for M2 isoform, whereas PKM-1 is constitutively active enzyme. PKM-1 expression results in reversal of Warburg effect (decreased lactate production and increased oxygen consumption) supported by PKM-2 expression, and dependency on oxidative phosphorylation for cell proliferation. PKM-2 expressing cells convert pyruvate preferentially to lactate whereas PKM-1 expressing cells metabolise pyruvate in the mitochondria. Presence of PKM-2 isoform provides ability to undergo a dynamic regulation both by substrate and tyrosine pathway and growth factor signal transduction. Expression of PKM-2 enables cells to distribute glucose metabolites into anabolic versus catabolic processes depending on the demands of rapidly growing cells (Christofk et al. 2008b).

More recently, concept of retrodifferentiation was challenged by the discovery of cancer initiating stem cells which might also explain the presence of embryonic features in tumors. Recent data has been provided to support the existence of so-called cancer stem cells in blood cell-derived cancers and solid tumors of the breast (Kakarala and Wicha 2008), colon (Lenz 2008), pancreas (Lee

*et al. 2008*), and skin (*Schatton et al. 2008*). Cancer stem cells may be responsible for self-renewal and tissue repair, resistance to apoptosis, and unlimited replication. Energy metabolism of cancer stem cells, however, remains to be explored.

## 2.4. MITOCHONDRIAL UNCOUPLING PROTEIN ISOFORMS

Among members of uncoupling protein subfamily, eight distinct isoforms can be recognized which form one branch of mitochondrial anion carrier gene family, containing 46 members in mammals (*Hanák and Jezek 2001; Ježek and Urbánková 2000*). In mammals, isoforms UCP1 to UCP5 are recognized and three other isoforms (originally termed PUMPn) exist in plants. The phylogenetically oldest seems to be the UCP4 isoform, the orthologues of which exist in *Dictyostelium discoideum* and *Caenorhabditis elegans* (*Hanák and Jezek 2001*). In mammals, the UCP2 isoform exhibits the widest expression pattern among all isoforms, while UCP3 is expressed typically in skeletal muscle and UCP3 (*Boss et al. 1997; Vidal-Puig et al. 1997*) and UCP4 typically in the brain (*Mao et al. 1999; Sanchis et al. 1998*), however, their expression in certain other tissues was not excluded. UCP1, originally ascribed exclusively to brown adipose tissue, has been reported recently in thymocytes (*Carroll et al. 2005; Adams et al. 2008a; Adams et al. 2008b*), pancreatic  $\beta$ -cells (*Sale et al. 2007*), thymus (*Carroll et al. 2005; Frontini et al. 2007; Carroll et al. 2004*), skin (*Mori et al. 2008*), and brain (*Jastroch et al. 2007*).

### 2.4.1. Uncoupling by uncoupling proteins

Although established mitochondrial transporters, transport substrates for UCPs are yet to be definitively recognized. Uncoupling proteins are transporters of anionic forms of fatty acids. Within the context of search for the substrate pattern, hydroperoxy fatty acids (FAs) derived from polyunsaturated FAs (PUFAs) are reported as just one series of the best transport substrates for UCP2. Indeed, hydroperoxy FAs have been confirmed by our group to induce protonophoric (uncoupling) ability in UCP2-containing proteoliposomes (*Jabůrek et al. 2004*), being transported by UCP2 in anionic forms. The widest anion substrate specificity has been found for the UCP1 isoform (*Ježek and Garlid 1990*). Also short-chain alkylsulfonates, as well as halide anions, typically chloride, and several small anions such as hypophosphate and physiologically relevant anions such as pyruvate and other ketocarboxylates are translocated in a uniport mode by UCP1. The question whether also UCP2 and other mammalian UCPs conduct chloride or pyruvate is still un-answered. Nevertheless, transport of these two and other small anions has been excluded for PUMP1 (*Costa and Vercesi 1996; Ježek et al. 1997*).

Similarly, the detail transport phenotype of UCPs still remains to be determined. Indeed, models of uncoupling for UCP2 have been developed (likewise for UCP1, (*Klingenberg and Echtay 2001; Garlid et al. 2000; Ježek et al. 1998; Skulachev 1991; Nedergaard and Cannon 2003*). Classical mitochondrial experiments as well as reconstitution studies suggest that all UCP isoforms are able to

mediate proton translocation across the lipid bilayer. Free FAs released from the triglycerides are considered as physiological activators of UCP1 function. However, there remains considerable controversy about the molecular mechanisms of this activation. Currently, two mechanisms are accepted: *i*) the fatty-acid cycling, or protonophore model (*Skulachev 1991; Garlid et al. 1996*) and *ii*) the proton buffering model (*Winkler and Klingenberg 1994*). Both hypotheses continue to be matter of debate and arguments have been made for and against both models.

In fatty acid cycling or protonophore model of fatty acid cycling model (FIG 2-11), the FA anions are regarded as true anionic transport substrates of UCPn. UCP translocates the anionic forms of FAs or alkylsulfonates from matrix side of the membrane to the intermembrane space which is driven by electric potential generated by electron transport. In the absence of a carrier, charged fatty-acid anions inside the matrix would not be able to cross the inner mitochondrial membrane. After protonation in the intermembrane space, FA returns (alkylsulfonates are unable) in a protonated form by flip-flop mechanism, hence carrying and subsequently releasing proton. Note, that such mechanism would act until all cycling substrates are removed from the membrane either by metabolism or being bound to sites with higher affinities, if exist (*Ježek et al. 1998*). Evidence supporting the fatty acid cycling model are derived from the experiments in which UCP1 was proved to transport alkylsulfonates ranging in alkyl chain length between C11 and C16. These molecules are considered as analogues of fatty acids which cannot be protonated at physiological pH and therefore exist only as an anionic form (*Ježek and Garlid 1990*). Alkylsulfonates were shown to be competitive inhibitors of UCP mediated Cl<sup>-</sup> transport (*Ježek and Garlid 1990*). UCP1, UCP2, UCP3, and PUMP1 have been reported to provide anion uniport of long-chain alkylsulfonates, univalent hydrophobic FA mimics unable to return in a protonated form through the lipid bilayer, and hence transport of alkylsulfonates is not accompanied by counter-directional H<sup>+</sup> uniport. The FA cycling model (*Skulachev 1991*) has also been supported by numerous reconstitution studies in liposomes (*Garlid et al. 2000; Ježek 1999; Jabůrek et al. 1999*) and black lipid membranes (*Urbánková et al. 2003; Beck et al. 2007*). It has been shown that transport of PUFAs is faster with UCP1 and UCP2 reconstituted to liposomes (*Žáčková et al. 2003*) as well as to BLM (*Beck et al. 2006; Beck et al. 2007*). Also hydroperoxy FAs derived from PUFAs during lipid peroxidation and liberated from phospholipids by phospholipase A2 have been confirmed as UCP2 anion transport substrates (*Jabůrek et al. 2004*), as well as nitrolinoleic acid.

The opposing models to FA cycling hypothesized (FIG 2-11) the existence of a pure proton-pathway for which FAs are enhancers of otherwise basal transport (*Klingenberg and Echtay 2001; Nedergaard and Cannon 2003*). According to this model, intermembrane fatty-acids insert their head groups into the proton transport pathway and provide buffering sites to assist proton

translocation via UCP1. Except of inserted fatty acids, proton transport pathway is formed by histidines and arginines resident in UCP1 structure. Among "enhancers", numerous other compounds have been suggested, such as 9-hydroxynonenal (HNE) and similar compounds (*Murphy et al. 2003*) originating from lipid peroxidation likewise hydroperoxy FAs (*Brand et al. 2004; Ježek and Hlavatá 2005*). The proton-buffering model is supported by the fact that fatty acid activation of UCP1 function is pH-dependent. There is a sharp increase across the IMM over pH range 7.0-8.0 (*Nicholls and Rial 1989*). The pH dependency may be an indication of the involvement of an amino acid side chain of UCP1 which was proposed in proton buffering model. Also mutagenesis experiments showed amino acids HIS145, HIS147 and ASP 27 to be necessary for fatty acids dependent transport (*Klingenberg and Huang 1999*), however these residues are not conserved among all UCP isoforms (*Ježek and Ježek 2003*).

A common prediction of both models (and several "mixed" transport models for UCPs (*Klingenberg and Echtay 2001; Nedergaard and Cannon 2003; Cannon et al. 2006*) is that compounds arising from lipid peroxidation may initiate function of UCP2, hence may activate UCP2-mediated uncoupling (*Jabůrek et al. 2004; Murphy et al. 2003*). Even if this uncoupling cannot reach a high extent (in terms of mitochondrial membrane potential,  $\Delta\Psi_m$  - rather a mere decrease of single units of mV is expected) due to a minute amounts of UCP2 expressed in tissues (*Ježek et al. 2004; Alán et al. 2009*), such a "mild uncoupling" possesses the ability to significantly attenuate mitochondrial production of superoxide on both Complex III (*Korshunov et al. 1997; Korshunov et al. 1998*) and Complex I (*Dlasková et al. 2008b; Dlasková et al. 2008a; Plecítá-Hlavatá et al. 2009*) sites. This ability led to suggestions of a feedback suppression of oxidative stress and particularly lipid peroxidation by its intermediates (*Jabůrek et al. 2004; Murphy et al. 2003*). Note, that according to the nature of the model for UCP2 transport mechanism (due to the considered transport substrates), distinct species might play a role in such a feedback mechanism. If, UCP2 is a pure protonophore and lacks the ability to translocate anions, certain "activating" species such as previously suggested HNE would serve a role in such a hypothetical feedback mechanism. HNE and the other reactive alkenals are near-terminal products of lipid peroxidation cascade and originate from the PUFA chains still covalently bound to the lipids (*Brand et al. 2004; Ježek and Hlavatá 2005*). Hence, their release is automatically ensured. In turn, according to the FA cycling hypothesis, cleaved-off, free PUFAs or hydroperoxy PUFAs (*Jabůrek et al. 2004*), represent the exclusive alternative.

#### 2.4.2. Possible physiological roles of mitochondrial uncoupling proteins UCP2 to 5

More than decade of studies did not answer the basic question of its function in mitochondria and its physiological roles, neither demonstrated in indisputable manner exemplar situations under which such roles might be executed. Scientists would hardly find more controversial field, where both mechanism as well as a physiological role were disputed for a studied protein. Controversy of uncoupling mechanism is accompanied by the explanation of their specific role in cell biology. The originally suggested functional roles were later disputed such as for attenuation of reactive oxygen species (ROS) formation (*Nedergaard and Cannon 2003; Cannon et al. 2006; Fislér and Warden 2006; Krauss et al. 2005; Mattiasson and Sullivan 2006*) since mild uncoupling is the principal regulator of oxidative stress (*Dlasková et al. 2008a; Plecítá-Hlavatá et al. 2009*), besides ROS protection has a wide implications to cell physiology and pathology. Among other physiologically acceptable roles of UCPS, regulation of glucose-stimulated insulin secretion (GSIS) (*Zhang et al. 2001; Joseph et al. 2004*), and regulation of mitochondrial Ca<sup>2+</sup> handling (*Trenker et al. 2007; Wu et al. 2009; Brookes et al. 2008*), chemoresistance of tumors (*Derdak et al. 2008*), neuroprotection (*Mattiasson and Sullivan 2006*), and atherosclerosis (*Blanc et al. 2003*) have been proposed.

##### 2.4.2.1. UCP2 and diabetes

ATP/ADP ratio is important factor for regulating insulin secretion from pancreatic  $\beta$ -cells. If this ratio is decreased by uncoupling of oxidative phosphorylation, the effect of glucose on insulin secretion is reduced. Therefore, UCP2 was suggested as a negative regulator of insulin secretion. This theory was first proven by adenoviral overexpression of UCP2 in insulin secreting cells and rat islets, which led to the decreased level of insulin secretion after treatment with glucose (*Chan et al. 1999*).

Zhang et al. (*Zhang et al. 2006*) showed that pancreatic islets of Langerhans from UCP2 knockout mice have increased insulin secretion in response to glucose and lower glucose blood level than control animals. Furthermore, the authors showed that the leptin-deficient *ob/ob* islets, in which insulin secretion is unresponsive to glucose, expressed much higher levels of UCP2 than control islets. The authors then crossed the *ob/ob* mice with the UCP2<sup>-/-</sup> mice and showed that the *ob/ob* mice lacking UCP2, although still severely obese, were partially rescued from the development of diabetes as a result of improved  $\beta$ -cell function. Thus these studies indicate that UCP2 may be a link between obesity,  $\beta$ -cell dysfunction, and type 2 diabetes. De Souza et al. (*De Souza et al. 2007*) examined effects of short-term treatment of animal models of type 2 diabetes mellitus with an antisense oligonucleotide RNA to UCP2. The treatment resulted in a significant improvement of hyperglycaemic syndrome. This effect was due to an improvement of insulin secretion, and also to improved peripheral insulin action.

#### 2.4.2.2. UCP2 and immunity response

As already mentioned, UCP2 is highly expressed in the cells of immune system and several studies confirmed important physiological role of UCP 2 in regulation of immunity response. Arsenijevic and co-workers (*Arsenijevic et al. 2000*) were the first to demonstrate it. They investigated the response to *T. gondii* infection in *Ucp2<sup>-/-</sup>* mice, and found that they are completely resistant to infection, in contrast with the high lethality observed in WT littermates. During this chronic infection *T. gondii* cysts were nearly three times more numerous in wild-type mice than in *UCP2<sup>-/-</sup>* mice. To explain this observation they isolated macrophages from wild-type and mutant mice and compared their ability to eliminate *T. gondii* *in vitro*. They found that macrophages isolated from *UCP2<sup>-/-</sup>* mice have 80% increased ROS production and greater toxoplasmacidal activity even *in vitro*. Therefore, they concluded that the ability of *UCP2<sup>-/-</sup>* mice to more efficiently resist to *T.gondii* infection is related to greater capacity of their macrophages to generate ROS.

The work was extended (*Rousset et al. 2006*) by the observation that UCP2 influences the early stage of immune response. During acute *Listeria monocytogenes* infection *UCP2<sup>-/-</sup>* mice had lower level of anti-inflammatory cytokine IL10. This cytokine mediates its anti-inflammatory effect by inhibiting pro-inflammatory cytokines production. Indeed, low level of IL10 at day 3 after infection resulted in higher level of pro-inflammatory cytokines IFN $\gamma$ , IL6, and IL1 $\beta$  and of the chemokine MCP1 at day 4 in *UCP2* ablated mice. This consequently led to significantly higher amount of recruited phagocytes in the spleen of *Ucp2<sup>-/-</sup>* mice and more efficient immune response. LPS is an endotoxin, which binds to the CD14/TLR4/MD2 receptor complex and thus promotes the secretion of pro-inflammatory cytokines in many cell types, but especially in macrophages. It was observed that treatment of isolated macrophages with LPS causes decrease of their UCP2 mRNA and protein level (*Arsenijevic et al. 2000*). Recently it was published that UCP2 downregulation after LPS treatment is mediated by MAPK family, namely p38 and JNK signalling pathways. In fact, the authors suggested a signal amplification loop, in which this downregulation of UCP2 protein leads to increased level of mitochondrial ROS production in macrophages which in turn intensifies MAPK signalling (*Emre et al. 2007*). Furthermore, it was observed that overexpression of UCP2 in macrophages cell line negatively regulates level of nitric oxide generation induced by LPS treatment. This would imply that UCP2 is involved in regulation of generation of bactericidal agents peroxynitrite, which derives by combination of superoxide and NO (*Kizaki et al. 2002*).

#### 2.4.2.3. UCP2 and atherosclerosis

Negative role of ROS in formation of atherosclerotic plaques is well established and the role of UCP2 was investigated (*Blanc et al. 2003*). They used *LDLR<sup>-/-</sup>* mice, which are prone to atherosclerosis

and destroyed their bone marrow by irradiation. Subsequently they performed bone marrow transplantation with wild type or UCP2<sup>-/-</sup> donors. After feeding the mice with atherogenic diet for 7 weeks they observed significant increase in atherosclerotic lesion size in the aortic sinus and thoracic aorta of UCP2<sup>-/-</sup> transplanted mice. Analysis of plaque composition revealed a significant increase in macrophage accumulation, apoptotic cell death, and also decrease in collagen content. Nitrotyrosine staining confirmed higher level of ROS in plaques from UCP2<sup>-/-</sup> transplanted mice. Previous observations are in agreement with work of Ryu (*Ryu et al. 2004*) who showed that THP1 monocytes with UCP2 overexpression had lower protein and mRNA levels of  $\beta 2$  integrins. Consequently, adhesion of these monocytes to TNF- $\alpha$ -stimulated human aortic endothelial cell (HAEC) monolayers and to plates coated with intercellular adhesion molecule-1 was reduced. UCP2 overexpression also inhibited cell spreading and actin polymerization in monocytes treated with TNF- $\alpha$  and monocyte chemoattractant protein-1 (MCP-1), and reduced MCP-1-induced transmigration of monocytes through HAEC monolayers.

#### 2.4.2.4. UCP2 and neuroprotection

Evidence is accumulating that UCP2 is also involved in neuroprotection. UCP2 prevents cell death in global cerebral ischemia (*Mattiasson and Sullivan 2006*). Following cerebral ischemia, the levels of glucose and oxygen rapidly reduce and thus also levels of ATP production by mitochondria are lowered. The main consequence of such energy deficit is a neuronal depolarization with postsynaptic release of glutamate. The binding of glutamate to its receptors on postsynaptic neurons induces entry of Ca<sup>2+</sup> into the cell. This activates a cascade of intracellular events leading to cell death. In mice overexpressing human UCP2, brain damage after cerebral ischemia was diminished after experimental stroke and traumatic brain injury, and neurological recovery was enhanced. In cultured cortical neurons, UCP2 reduced cell death and inhibited caspase-3 activation induced by oxygen and glucose deprivation. The authors proposed that UCP2 neuroprotective effect can be explained by lowering membrane potential, which is known to decrease the level of Ca accumulation in mitochondria. The accumulation of intramitochondrial Ca is generally associated with release of cytochrome c and other events leading to apoptosis or cell death.

#### **2.4.3. Minute protein amount expression of uncoupling proteins and its consequences**

Controversies in the research on UCPs cover all aspects including their putative function, i.e. doubts exist whether these proteins really uncouple mitochondria in vivo (*Cannon et al. 2006; Esteves and Brand 2005*) since protein have not been localized. Their physiological roles in tissues will be undoubtedly given by the extent of uncoupling they induce when activated (*Esteves and Brand 2005; Ježek et al. 2004*). The lack of consensus on UCP function, even after a decade of research since the

discovery of UCP2 and UCP3 isoforms, stems from the rather minute amounts expressed (as compared to UCP1) and imported into the inner membrane and from the lack of a clear understanding of isoform-specific tissue distribution. From a bioinformatics viewpoint, UCP1, UCP2, UCP3, UCP4, and UCP5 form a distinct subfamily within the gene family of mitochondrial anion carriers (*Hanák and Jezek 2001; Ježek and Urbánková 2000; Klingenspor et al. 2008*). The carrier most sequentially similar to UCPs is the oxoglutarate carrier, which, however, lacks the unique uncoupling protein signature sequences (*Hanák and Jezek 2001; Ježek and Urbánková 2000*). Functionally, in vivo uncoupling was demonstrated unequivocally for the first known member, UCP1, originally considered to be specific for brown adipose tissue (BAT), where it serves as the final molecular component of catabolic cascade of nonshivering thermogenesis (*Cannon et al. 2006*). However, UCP1 has also been detected in thymocytes (*Carroll et al. 2005; Adams et al. 2008a; Adams et al. 2008b*), where its thermogenic role is probably replaced by a regulatory role in apoptosis due to its ability to attenuate production of mitochondrial reactive oxygen species (ROS) (*Dlasková et al. 2006*). ROS facilitate apoptosis, and hence UCP1 activation would have a preventive effect on apoptosis whereas UCP1 inhibition would promote apoptosis. UCP1 was recently detected in skin (*Mori et al. 2008*), where it is proposed to function (as in thymocytes) as a suppressor of mitochondrial ROS production.

Attempts to derive physiological roles for distinct UCPs also have been based on their expression pattern in various tissues. Owing to their low expression levels (with the exception of UCP1 in BAT), their thermogenic function is rather excluded and as the most relevant function seems to be the attenuation of mitochondrial ROS production (*Affourtit et al. 2007; Arsenijevic et al. 2000; Cannon et al. 2006; Esteves and Brand 2005; Jabůrek et al. 2004; Ježek et al. 2004*). Indeed the mild uncoupling is able to attenuate both superoxide formation within the Complex III (*Ježek and Hlavatá 2005*) as well as the Complex I (*Dlasková et al. 2008a; Dlasková et al. 2008b*). The extent of such an "antioxidant" mechanism in vivo would depend not only on absolute UCP levels but also on the activation state of each UCP and the extent of inhibition by purine nucleotides (*Beck et al. 2007*). The absolute protein levels serve as a basic parameter for rough estimation of UCP functional relevance in a given tissue.

#### **2.4.4. Existing transcript quantifications for mitochondrial uncoupling proteins UCP2 to 5**

Determination of UCP expression patterns is difficult due to their extreme hydrophobicity and impossibility to raise antibodies, which would not cross-react with other UCPs (*Pecqueur et al. 2001; Hurtaud et al. 2007*) or with other members of anion carrier gene family. Hence, most studies have relied on methods quantifying UCP mRNA levels such as northern blotting and RT-PCR. Despite the translational down-regulation described for UCP2 (*Hurtaud et al. 2006; Pecqueur et al. 2001*) and

UCP5 (*Kim-Han et al. 2001*), or the translational up-regulation of UCPs (*Hurtaud et al. 2007*), the precise determination of transcript levels still provides a valuable information.

UCP2 is considered to be expressed ubiquitously in mammalian tissues (*Fleury et al. 1997; Gimeno et al. 1997; Lengacher et al. 2004*). In contrast, UCP3 mRNA has been detected in northern blots of human skeletal muscle and in rodent skeletal muscle, heart, and BAT originally (*Boss et al. 1997; Vidal-Puig et al. 1997*). The original reports for UCP5 and UCP4 mentioned their high expression in the central nervous system (*Mao et al. 1999; Sanchis et al. 1998*). Northern blotting also detected UCP5 mRNA in both mouse and human heart, kidney (*Kim-Han et al. 2001; Sanchis et al. 1998; Yu et al. 2000*) and skeletal muscle (*Lengacher et al. 2004; Sanchis et al. 1998; Yu et al. 2000*). These results were confirmed by UCP5 immunodetection (*Kim-Han et al. 2001*). However, Sanchis et al. (1998) found even wider distribution of UCP5 mRNA, in the rat, mouse, and human gut, lung, testis, uterus, spleen, and white and brown adipose tissue. Additional findings were reported for the human prostate, pancreas, adrenal medulla and cortex, thyroid gland and liver, as well as for the mouse liver (but not spleen), lung, and skeletal muscle (*Yu et al. 2000*). Using quantitative RT-PCR with TaqMan probes {Lengacher, 2004 #48} found not only UCP4 and UCP5 mRNA in the mouse brain cortex (together with a lower amount of UCP2 transcript), but also ~100 times lower levels of UCP3 and UCP1 mRNA. In BAT and skeletal muscle, *Lengacher et al. (2004)* also identified all five UCP mRNAs, with the UCP1 mRNA level in BAT being ~100-fold higher than all other isoforms, and with UCP3 mRNA level being at least 10-fold higher in skeletal muscle. It is unclear, however, whether the minute levels of UCP mRNAs become translated into mature proteins. If indeed they were translated, one must re-evaluate the molecular physiology of UCPs based on their tissue distribution in light of findings such as UCP1 mRNA in human pancreatic  $\beta$ -cells (*Sale et al. 2007*), UCP5 in endocrine cells (*Ho et al. 2005; Ho et al. 2006*), UCP4 mRNA in preadipocytes (*Zhang et al. 2006*), or of the emerging role of UCP4 and UCP5 in brain pathologies (*Liu et al. 2006; Chan et al. 2006; Nakase et al. 2007; Naudí et al. 2007*). Observed disparity between the abundance of certain mRNAs and their corresponding protein products has been attributed to both translational down-regulation (*Pecqueur et al. 2001; Hurtaud et al. 2006*) and up-regulation (*Hurtaud et al. 2007*).

### 3. METHODS

This thesis describes three different projects. Methods are therefore presented as three separated parts A, B, C corresponding to the particular project.

#### 3.1. METHODS A

##### 3.1.1. Cell cultures

HTB-126 cells (strain derived of the ductal carcinoma of the breast) and HTB-125 (control cell line, a normal fibroblast-like line from the same patient, from normal breast tissue peripheral to an infiltrating ductal carcinoma which was the source for HTB-126) were purchased from ATCC (FIG 3-1).

##### 3.1.1.1. Culturing conditions

HTB-126 cells were maintained in two principal cultivation conditions. "Glucose medium" (further in text designated as Glc medium) consisted of High Glucose Dulbecco's Modified Eagle Media (DMEM; *GIBCO*, No 11960) containing 25 mM glucose, supplemented with 10% fetal calf serum (*Hyclone*), 100 U/ml penicilin, 100 U/ml of streptomycin, 10 mM HEPES. Alternatively, we used the "galactose medium" (further in text designated as glucose-deprived or Gln/GAL medium) that consisted of DMEM deprived of glucose and pyruvate (*GIBCO*, No 11966), supplemented with 10 mM galactose, 4 mM glutamine, 10 mM HEPES, 1 mM sodium pyruvate, and 10% fetal calf serum - dialyzed (*Hyclone*, No SH30079). Medium of HTB-125 was supplemented with 30 ng/ml of mouse EGF. All cells were kept in 5% CO<sub>2</sub> at 37°C at air saturation.

##### 3.1.1.2. Hypoxic cultivation

For hypoxia experiments, HTB-126 cells were incubated in hypoxic workstation InVivo300 (*RUSKIN*) under 1% O<sub>2</sub>, 5% CO<sub>2</sub>, balanced with N<sub>2</sub> for desired time period.

##### 3.1.2. Cell proliferation

Cell proliferation studies were carried out by plating  $1 \times 10^5$  cells on 10 cm (diameter) dishes containing 20 ml of cultivation medium. In order to prevent substrate limitation, medium was replaced every 2-3 days. At daily intervals, cells were harvested by trypsinization and counted. Doubling time was calculated according to the formula:  $DT = 0,693 \times t / \ln(N/N_0)$  with  $t$  (elapsed time),  $N_0$  (starting number of cells),  $N$  (final number of cells).

### 3.1.3. Neutral red assay

The neutral red (NR) assay measures the ability of viable cells to incorporate and bind neutral red, a supravital dye. We used the neutral red assay to assess cell viability, as originally detailed in (Borenfreund and Puerner 1985). Cells were grown in 96 well-plates in various conditions including aglycemia and hypoxia. First, cells were incubated 3 hours at 37°C with neutral red solution (1/60 v/v of a 4 mg/ml neutral red solution in NaCl 9‰). After, a washing of the cells was performed with NaCl 9‰ and cell fixation was obtained by a rapid washing a formol-calcium solution (1 ml formaldehyde 40%, 10ml of 10% calcium-chloride and 89 ml distilled water). Then, cell permeabilization and intracellular membranes lysis was obtained with a solution of 50% ethanol and 1% acetic acid. This results in the extraction of neutral red from the cell and homogenization was performed by stirring the plate. Absorbance was measured in a multi-well scanning spectrophotometer (SAFAS MP96) at a wavelength of 540 nm with a reference set at 630 nm. Tests were done in quadruplicate and repeated three times. The results of neutral red uptake (viability) were expressed as percent value of the control (untreated cells) absorbance.

### 3.1.4. Microscopy

The morphology of the mitochondrial network was studied by fluorescence confocal microscopy using Mitotracker Green FM (*Molecular probes*). Excitation and emission maxima for Mitotracker Green are 490 and 516 nm, respectively. Staining was performed 20 minutes in 37°C using 200 nM of Mitotracker green FM. Microscopy was performed on FluoView laser scanning inverted microscope (*Nikon*). The reconstitution of three-dimensional images was performed using Imaris Software (*Bitplane*). Cells were grown in desired cultivation conditions on glass chamber (*Lab-Tek*) and series of images were taken from three different chambers. For image analysis, images were selected randomly and the analysis was performed using a double-blinded approach. The area of mitochondrial sections was determined using Scanview and ImageJ softwares. The total mitochondrial area was normalized to the nucleus area on each micrograph.

### 3.1.5. Lowry assay

For protein determination, Lowry assay was used. Samples were mixed with distilled water to the final volume of 200 µl. Calibration of protein content was performed using 1 mg/ml of bovine serum albumin (BSA) solution of 10, 20, 30, 40 and 50 µl mixed with distilled water to the final volume of 200 µl. Blank was 200 µl of distilled water.

Samples, blank and calibration were mixed with 200 µl of 1 N NaOH solution. 2 ml of Solution A (mixture of 100 ml of Na<sub>2</sub>CO<sub>3</sub> 20 g/l, 1 ml of tartrate KNa 20 g/l, 1 ml of CuSO<sub>4</sub> 10 g/l) was added to each sample and incubated for 10 minutes at room temperature. 100 µl of folin solution (*SIGMA*)

was added and incubated for 20 minutes at room temperature in dark. After incubation, OD<sub>700</sub> value was measured using spectrometer (SAFAS). Blank was subtracted from the value. The amount of protein in each sample was calculated relating to the standard curve.

### **3.1.6. ATP measurement**

Cellular ATP synthesis was carried out on whole-cell lysates according to Ouhabi et al. (*Ouhabi et al. 1998*). Cells were treated with oligomycin, 2-deoxyglucose (2-DG) and oxamic acid for 4 hours. Cell pellets were solubilized in lysis solution. For each collected sample, the quantity of ATP was measured using bioluminescence in a Luminoskan using the ATP monitoring reagent (ATP Bioluminescence Assay, *Roche*). Standardization was performed with known quantities of ATP provided with the kit (5, 10, 15, 20, 25 pmol) and measured in parallel. The rate of ATP synthesis was calculated using linear regression. Rates were expressed in pmol ATP/mg protein.

### **3.1.7. Western blotting**

#### **3.1.7.1. Sample preparation**

Following treatment of interest (hypoxia or normoxia), cells were washed with PBS and harvested by trypsinization (0.25% trypsin-EDTA). Cell pellet obtained after centrifugation (5 min at 500 RCF) was washed once with PBS (*GIBCO*) and redundant liquid was removed completely. Pellet was frozen overnight in -80 °C. Cells were lysed using 4 % lauryl-maltoside with protease inhibitors (0.5 mM phenylmethylsulfonyl fluoride, 10 mg/ml pepstatin, and 10 mg/ml leupeptin) for 1 hour or unless complete solubilized. Additionally, the lysate was sonicated.

Protein concentration in extracts was quantified by Lowry protein assay.

Samples were diluted in 2x SDS-PAGE sample buffer (20% glycerol, 4% SDS, 100 mM Tris pH 6.8, 0.002% bromophenol blue) and 2% β-mercaptoethanol, to the final concentration of 1 mg/ml and incubated 30 min at 55°C.

#### **3.1.7.2. Electrophoresis**

Whole cell extracts were resolved either in 12% acrylamide gel or gradient gels (for oxphos quantification followed) with a linear acrylamide concentration 10 - 20%, which gives optimal resolution of proteins between 10 and 100 kDa. Gradient gels were prepared in multicasting chamber (*Bio-Rad Mini-PROTEAN II*). Electrophoresis was performed in electrophoresis running buffer (25 mM Tris, 192 mM glycine, 0.1% SDS) at 150 V. Gels with separated proteins were washed in transfer buffer for 15 minutes right before transfer.

#### 3.1.7.3. Protein transfer and immunodetection

Transfer was performed in CAPS electroblotting transfer buffer (10 mM 3-[cyclohexylamino]-1-propane sulfonic acid pH 11 with NaOH; 10% methanol) to 0.45 µm polyvinylidene difluoride (PVDF) membranes for 2 hours at 100 mA. Membranes were blocked overnight in 5% non fat milk in PBS with 0.02 % azide.

Membranes were incubated with primary antibody incubation (MitoProfile Total OXPHOS Human Antibody Cocktail (*MitoSciences*) containing mixture of mouse monoclonal antibodies against Complex I subunit NDUFB8 (MS105), Complex II subunit 30 kDa (MS203), Complex III subunit Core 2 (MS304), Complex IV subunit II (MS405), and ATP synthase subunit alpha (MS507) as an optimized premixed cocktail) for 4 hours at room temperature. Primary antibodies incubation was followed by three washes (15 min) in phosphate buffered saline solution (PBS, 1.4 mM  $\text{KH}_2\text{PO}_4$ , 8 mM  $\text{Na}_2\text{HPO}_4$ , 140 mM NaCl, 2.7 mM KCl, pH 7.3) with 0.05% Tween-20. The membranes were incubated for 1 hour with horseradish peroxidase-conjugated goat anti-mouse or anti-rabbit secondary antibodies (*Bio-Rad*) diluted in 5% non-fat milk. After washing membrane twice in PBS-Tween and once in PBS, immunodetection was performed with horseradish peroxidase development solution (ECL Plus reagent, *GE Healthcare*).

The signal was quantified by densitometric analysis using ImageJ software (*NIH*).

#### 3.1.7.4. Western-blot detection of CIDEa

Cells were collected by scraping off in the growth medium to ensure the detached cells are not lost in the rinsing procedure. The cell suspension was centrifuged and the pellet was resuspended in 50 µl of the lysis buffer. Alternatively, isolated mitochondria were used. Following addition of SDS-PAGE sample buffer (50 µl) it was boiled for 5 min at 95°C. 20–30 µg of total protein/lane was run on 12% SDS-PAGE, blotted onto PVDF membrane and the CIDEa antigen was detected using rabbit primary antibody (*ProSci*). Horseradish peroxidase- conjugated secondary anti-rabbit antibody and Luminol reagent (*Santa Cruz Biotechnology*) were used for visualization. Alternatively, alkaline phosphatase conjugated secondary anti-rabbit antibody (*Sigma*) was used and visualization was performed using BCIP/NBT reagent.

### 3.1.8. Respirometry

#### 3.1.8.1. General use of oxygraph

Respirometry was performed using high-resolution respirometer OROBOROS OXYGRAPH -2K (OROBOROS). Respiration is measured in a glassy chamber which is sterilized with 70% ethanol for 30 min before every measurement. The chamber is calibrated for 2 ml volume. Service of the electrodes is performed when oxygen signal does not respond to rapid changes of oxygen, when the time constant is insufficient or flux signal is not stable. Anode cleaning is performed with  $\text{NH}_4$  solution (25%;  $2 \times 15$  min) and cathode cleaning with aluminium oxide powder provided by manufacturer. 1 M KCl solution is used as an electrolyte. Oxygen calibration of oxygen signal is performed as a two-point calibration of 100% (R1) and 0% air saturation (R0) of medium (FIG 3-2). Resulting air calibration is the  $\text{O}_2$  concentration at air saturation  $c_{\text{O}_2}$  [nmol/ml;  $\mu\text{M}$ ], calculated as a function of temperature, barometric pressure, and oxygen solubility factor of the medium. Typical local barometric pressure was 101.1 kPa and oxygen concentration at 37°C was 210 nmol/ml (using  $\text{O}_2$  solubility factor 1 for pure water).

#### 3.1.8.2. Instrumental background

Instrumental background experiment is performed routinely in order to subtract the influence of oxygen flux arising from oxygen consumption of the oxygen sensor at high oxygen range and minimum back-diffusion into the chamber at low oxygen range. Background is specific for specific set-up and the user.

Background experiment is performed in cultivation medium with oxygen sensor calibrated for R1 and R0 in closed oxygraph chamber with no sample at experimental conditions. In closed chamber, oxygen flux reflects oxygen consumption of polarographic oxygen sensor. Afterwards, gradual step-wise reduction of oxygen content in oxygraph chamber is performed by injection of  $\text{N}_2$  (FIG 3-3 A). Resulting flux reflects oxygen consumption specific for actual oxygen level (FIG 3-3 A, B). At progressively lower steps of oxygen level, the oxygen consumption by the sensor decreases linearly, and the effect of oxygen back-diffusion is finally apparent as a positive slope or negative flux. Usually 3 - 5 steps at various oxygen levels are performed. The linear instrumental background equation with slope,  $b^\circ$ , and intercept,  $a^\circ$ , is calculated ( $J_{\text{O}_2} = b^\circ \cdot c_{\text{O}_2} + a^\circ$ ; FIG 3-3 B). Values  $a^\circ$  and  $b^\circ$  are applied into the DatLab4 software (OROBOROS) and used for following experiments or DatLab2 analysis, where uncorrected flux is recalculated according to inserted values into the corrected flux (FIG 3-3 C). Background flux is subtracted at each point of the measurement.

### 3.1.8.3. Measurement of oxygen kinetics

Mitochondrial respiration is a hyperbolic function of oxygen pressure. Each respiratory system is characterized by specific kinetic properties that determine oxygen kinetics of respiratory system. To perform kinetic measurement, cellular respiration is measured throughout the entire oxygen scale. Cells in oxygraph chamber are left to consume oxygen completely and reach the anoxic state. It is high-resolution application. Cellular respiration is measured as a function of  $p_{O_2}$  in physiological conditions (DMEM).

Calibration of oxygen sensor for air saturation (R1) was performed in open oxygraph chamber after signal stabilization. Further, a stirrer test was performed in order to obtain an exponential time constant for subsequent oxygen signal deconvolution (time response correction of oxygen signal) during data analysis. Measurements were performed at 37°C with stirring rate 700 RPM. Datlab4 enables to get enough data points and provides sufficient time-resolution to acquire maximum of data points for oxygen kinetics evaluation. Data were recorded with the sampling interval of 1 s interval. Background calibration and oxygen signal deconvolution is required.

Cells were harvested by trypsinization and cellular pellet was resuspended in cultivation medium (DMEM) to the desired cellular concentration (typically in a range of  $0.5 - 1 \times 10^6$  cells/ml). After cells consume the oxygen completely and reach the anoxic state, zero calibration (R0) was performed. After anoxic state (approximately 5 min), oxygraph chamber was uncovered in order to reoxygenate cellular suspension and to check eventual changes in cell viability caused by anoxic transition. Respiration after reoxygenation step is supposed not to differ markedly from the initial respiration at the beginning of the experiment (FIG 3-4 A). Independence of respiration on oxygen in high range can be tested if  $N_2$  is applied in order to deplete oxygen in chamber in order to accelerate experiment. Repeated aerobic-anoxic transitions can be studied. Due to the time-dependent decrease of respiration and cell viability, initial respiration does not have to be reached.

Data were calculated using DatLab2 software (*OROBOROS*) as a routine function of Datlab software. Raw data were exported from DatLab4 (*OROBOROS*). During analysis, the raw signal is deconvoluted with the exponential time constant of the oxygen sensor and oxygen flux is corrected for instrumental background. Internal zero calibration is performed with DatLab 2 software following instructions. Oxygen solubility applied for DMEM was 9.5 ( $O_2$  solubility in DMEM [ $\mu M \times kPa^{-1}$ ]). As a result,  $P_{50}$ ,  $p_{O_2}$  value at which respiratory rate is half-maximal, and  $J_{max}$ , maximal flux, is calculated from the hyperbolic function (*Eq. 1*) fitted over the low-oxygen range of 0 – 1,1 kPa (FIG 3-4 B). Extension of  $p_{O_2}$  region for analysis leads to the distortion of hyperbolic relation and gives artificial data.

$$J_{O_2} = \frac{J_{\max} \times P_{O_2}}{P_{50} + P_{O_2}}$$

Eq.1.

#### 3.1.8.4. Respiratory rate and respiratory states of intact cells

For following assays, data recording interval was 2 s. Flux was corrected for background.

Respiratory states were monitored in intact or, alternatively, permeabilized cells (section 3.1.8.6.). Using the intact cells provides a convenient way to monitor respiration as occurs under the cell culture conditions. Respiration of intact cells is supported exclusively by endogenous substrates, provided by the cell culture medium. This allows us to compare the eventual changes of cell respiration to variations of cell growth. Cells were harvested by trypsinization, and cellular pellet was resuspended in respiration medium and cell number was determined using hemocytometer. Permeabilization of cell membrane is not required since all inhibitors used are membrane permeant. When measurement with intact cells followed, cells were resuspended in DMEM. Routine respiration of intact cells was determined after signal stabilization. Transition to state 4 was stimulated by addition of 4 mg/ml solution of oligomycin (2 µg/ml final). Subsequent FCCP titration (0.5 µM steps) stimulates flux to the maximum capacity. Optimal concentration for maximum uncoupling was 1.5 µM of FCCP. Rotenone addition (200 nM) indicates the impact of complex I and antimycin A (AntA, 2.5 µM) of complex II and delineate extra-mitochondrial oxidative reactions. Protocol was held in saturating oxygen conditions to avoid effect of oxygen limitation on respiration.

From obtained values, analysis of respiratory ratios followed. Calculation of respiratory states is a convenient way how to compare studied samples. The respiratory control ratio (RCR – ration of endogenous respiratory flux to oligomycine-inhibited flux) and the uncoupling ratio (UCR – ratio of uncoupled flux to endogenous respiration) were originally defined by Chance and Williams (*Chance and Williams 1956*) on isolated mitochondria. The RCR is *state 3* to *state 4* respiration, and the UCR is *uncoupled* to *state 3* respiration. These two bioenergetic indexes are useful, but they can not be strictly determined with intact cells, since the endogenous respiration is different than *state 3* as mitochondrial respiration is limited in situ by substrate delivery (including oxygen) and ADP content (while on isolated mitochondria both are given in excess). Thus, we prefer to use the term of cell coupling ratio instead of RCR to designate the ratio of the endogenous respiration over that determined in presence of oligomycin, and the term of cell uncoupling ratio instead of UCR for the ratio of the uncoupled respiration on intact cell to the endogenous respiration.

However, designation of RCR and UCR is the point of convenience and will be further utilized during results presentation and discussion until indicated otherwise.

#### 3.1.8.5. Cell permeabilization

Cells were harvested by trypsinization and resuspended in respiration medium (0.5 mM EGTA, 3 mM MgCl<sub>2</sub>·6H<sub>2</sub>O, 65 mM KCl, 20 mM taurine, 10 mM KH<sub>2</sub>PO<sub>4</sub>, 20 mM Hepes, 110 mM sucrose, 1 g/l BSA, pH 7.1) and cell number determined. Cell suspension was diluted preferably to the final concentration of  $1 \times 10^6$  cells/ml. After flux stabilization, rotenone, succinate (10 mM final) and ADP addition (4 mM final) followed. Optimal concentration of digitonin was determined by titration of digitonin (1 mg/ml solution in DMSO) with steps of 1 µg (FIG 3-5). At optimal concentration of digitonin, respiration increased. Optimal concentration of digitonin was for HTB-126 5-6 µg per  $10^6$  cells.

#### 3.1.8.6. Multiple substrate-inhibitor protocol with permeabilized cells

After flux stabilization (E), complex I substrates malate (2 mM final) and glutamate (10 mM final) were added. Digitonin addition followed, resulted in decrease of respiration due to the cell permeabilization (state 2 respiration). ADP (4 mM final) was added to stimulate state 3 respiration. Succinate addition (10 mM final) resulted in state 3 with convergent complex I and II input. Maximal respiratory capacity was induced by FCCP. Inhibition with rotenone and AntA followed to inhibit complex I and complex II respiration. RCR and UCR were determined as state 3 to state 4 respiration and uncoupled respiratory rate to state 3 respiration.

#### **3.1.9. Statistical analysis**

All the data presented in this study correspond to the mean value of N experiments  $\pm$  SD. Comparison of the data sets was performed with the Student's t test, using SigmaPlot (*Microsoft*). Two sets of data were considered statistically different when  $p < 0.05$ .

## 3.2. METHODS B

### 3.2.1. Experimental animals

For quantification of UCPs mRNA, rat and mouse tissues were used. We used Wistar rat (250 to 275 g) and mouse Balb/c (20-25 g) as controls, UCP2<sup>-/-</sup> mouse strain was kindly donated by prof. Lowell of Harvard University (*Zhang et al. 2001*). Animals were kept at 24 ± 1 °C with 12:12-h light-dark cycles and full access to water and food. Animals were starved 24 hours prior decapitation. After decapitation, respective organs were removed with sterile instruments, and stored in -70°C. Rats were obtained from animal house of Institute of Physiology. Mice were raised in animal house of IKEM institute (SEMED).

### 3.2.2. RNA preparation

#### 3.2.2.1. Total RNA isolation

To work with RNA, everything is sterilized twice by autoclaving. We used a standard phenol-chloroform extraction method of the RNA isolation (*Chomczynski and Sacchi 1987*). About 200 mg of frozen animal tissue was grind into the powder using liquid nitrogen. Powder was removed and dissolved in 2 ml of lysis buffer (4 M GITC, 25 mM sodium citrate, 0,5% N-lauroyl sarcosil, 0,7% 2-mercaptoetanol, pH 7) and 200 µl of 2 M sodium acetate, pH 4.3. Phenol-chloroform extraction followed; 1,8 ml of phenol solution (pH 8, equilibrated with Tris-HCl) and 600 µl of chloroform was added and mixed. Solution was incubated on ice for 10 minutes and centrifugated afterwards (10,000 × g for 10 minutes). During centrifugation, two phases formed. The upper fraction (water phase containing RNA) was detracted, put into sterile eppendorf tube and precipitated with 2 volumes of ethanol (98%) at -20°C for 1 hour, followed by centrifugation (20,000 × g for 20 minutes). Pellet was washed twice with 75% ethanol (centrifugation 20,000 × g for 15 minutes). Pellet was dried and resuspended in sterile water.

Total RNA of skeletal muscle and white adipose tissue were extracted using a Fibrous Tissue and Regular Midi RNeasy kit (*Qiagen*), respectively. This procedure includes on-column DNase treatment.

#### 3.2.2.2. DNase treatment

DNase treatment was applied to degrade potential contamination by genomic DNA during RNA isolation. Solution containing RNA was treated with RNase-free DNase (*Top-Bio*, Czech Republic) in 1× DNase buffer (5× DNase buffer consists of 100 mM Tris-HCl, 100 mM NaCl, 60 mM

MgCl<sub>2</sub>, 20 mM CaCl<sub>2</sub>, pH 7.6) in 37°C for 1 hour, following phenol-chloroform extraction as described in previous paragraph.

#### 3.2.2.3. mRNA isolation

mRNA was isolated from total RNA treated with DNase, using mRNA isolation kit (*Roche*) and Oligo(dT) 3'Bio-oligo(dT)<sub>20</sub> (*Metabion*, Czech Republic). To separate mRNA from other fractions of total RNA, magnetic particles covalently bound to tetrameric streptavidin were used. Biotin is bound to oligo-dT that hybridizes with polyA sequences of mRNA. Streptavidin interacts with biotin which allows specific separation of mRNA from the sample.

#### 3.2.2.4. Determination of RNA amount

Nucleic acid content in the RNA samples were quantified from their spectra with a subtracted light scattering contribution using an Agilent 8453E UV-VIS spectroscopy system and 200- $\mu$ l quartz cuvettes or using NanoDrop spectrophotometer ND-100. An mRNA sample was used for further analysis only when its purity was reflected by the A<sub>260</sub>/A<sub>280</sub> ratios of 1.7 to 1.9.

### **3.2.3. Quantitative real-time PCR**

Real-time PCR was performed on a LightCycler instrument (*Roche*) in LightCycler Capillaries. Data are recorded with LightCycles software. RNA content was quantified using the method termed second derivative maximum which determines the threshold cycle (crossing point, Ct) in which fluorescent signal in capillary extend the background fluorescence (starting the exponential phase of the amplification). Crossing point is inversely correlated to the quantity of mRNA in the reaction mix.

#### 3.2.3.1. Signal detection

Real-time PCR was performed using fluorescent hybridization probes specifically annealing to the target sequence of desired gene additionally to specific primers. First probe is modified on 3' terminus by fluorescein, the other probe, annealing in the first one's proximity is modified on 5' terminus by fluorescence marker – LC-Red 640 for UCPs and LC-Red 705 for GAPDH. 3' terminus of second probe is modified by phosphate. When the probes are in proximity, Forster's resonance energy transfer proceeds between the probes and indicates their correct annealing to the amplicon cDNA in each PCR cycle. Principle is described in FIG 3-6.

### 3.2.3.2. Design of LightCycler primers and hybridization probes

Sets of two primers and two fluorescent hybridization probes were designed as shown in the TAB for rat and mouse UCP2 (*Ruzicka et al. 2005*), UCP3, UCP4, and UCP5. A primer set for glyceraldehyde-3-phosphate dehydrogenase (GAPDH, reference house-keeping gene) as well as primer and probe synthesis was provided by TIB MOLBIOL (Berlin, Germany). Several essential criteria were kept for primer design in order to achieve the highest precision of mRNA quantification. Each PCR primer from a pair was designed to anneal to a separate exon (corresponding to the unspliced mRNA molecule or to the gene sequence, where exons are separated by a long intron). This arrangement avoids any quantification of potential contaminating genomic DNA. PCR primers and hybridization probes were designed to hybridize the most variant part of the UCP sequence (the 5'-most) where various UCP isoforms differ (*Ježek and Urbánková 2000*). For example, in the case of rat UCP2 the amplicon spans 349 base pairs (i.e. bp 136-485). A 1-3 bp gap was usually left between adjacent hybridization probes (TAB 3-1). We thus sacrificed to choose amplicons close to the 3' terminus, i.e. the way that also includes detection of mRNA that potentially could have been cut/damaged during isolation. In turn, our selected design for UCP3 and UCP5 covers all their splicing variants. This is impossible to achieve with amplicons close to the 3' terminus.

### 3.2.3.3. Quantification method

Absolute quantification approach was chosen to quantify UCPs RNA amount. This approach allows the precise determination of copy number per cell, total RNA concentration, or unit mass of tissue. It requires the construction of a standard curve for each individual amplicon to ensure accurate reverse transcription and PCR amplification profiles.

Calibrations were made by seven order of magnitude-spanning dilution series of the PCR-amplified amplicons (example is given in FIG 3-7 A, B), starting from an initial quantity of 10 ng per reaction. Calibration curve is calculated by plotting the threshold cycle against cycle number on a logarithmic scale (FIG 3-7 B). The calculated calibration slopes (TAB 3-1) approached the predicted theoretical slope of 3.3, meaning that if two starting mRNA samples differed in content by one order of magnitude then equivalent amplified levels would be achieved 3.3 cycles apart. This is equivalent to doubling the amplicon amount in each single cycle.

### 3.2.3.4. Performance of the real-time RT-PCR

Routinely, 20–80 ng mRNA was used for real-time RT-PCR on a LightCycler (*Roche*) with 0.5  $\mu$ M primers and 0.2  $\mu$ M hybridization probes. Reverse transcription step (30 min at 55°C) was

followed by the reverse transcriptase inactivation for 30 s at 95°C, and by 40 cycles of 2 s denaturation and annealing for 25 s at temperatures described in Table I, and elongation for 25 s at 72°C. The MgCl<sub>2</sub> content was optimized for each set of primers and probes (see TAB 3-1). Fluorescent value of emitted light is recorded during annealing step and represents the respective amount of the amplified product. The absolute mRNA amounts, in picograms, were calculated from crossing points of each run according to standard calibration curve specific for each amplicon.

A series of control experiments were performed for each sample. PCR product length was confirmed by electrophoresis on 1.5% agarose gels. To verify that the genomic DNA was not amplified and thus did not contribute to the quantification, the reverse transcription step was omitted in control runs; in such controls, no fluorescence was detected. The specificity of the primers and hybridization probes for mouse UCP2 was verified with the various tissue mRNA samples of UCP2<sup>-/-</sup> mice and no fluorescence was observed. Similarly, there was no cross-amplification between particular UCP isoforms when a PCR reaction was performed with a vector containing a cDNA for any other UCP isoform (rat and human UCP2, UCP4).

#### **3.2.4. Statistical analysis**

All the data presented in this study correspond to the mean value of N experiments ± SD. Comparison of the data sets was performed with the Student's t test, using SigmaPlot (*Microsoft*). Two sets of data were considered statistically different when  $p < 0.05$ .

### 3.3. METHODS C

#### 3.3.1. Cell cultures

In this project, cell lines for inducible protein expression were used, HeLa and 293-HEK cell lines stably expressing *tet*-repressor protein (pcDNA6/TR vector expressing *tet*-repressor) were purchased from Invitrogen.

Cells were cultured in the presence of antibiotic blasticidin (1 µg/ml) to maintain *tet*-repressor expression at 37°C in a humidified incubator with 5% CO<sub>2</sub> in the Eagle's minimum essential medium (EMEM, HeLa cells) or Dulbecco's modified eagle medium (DMEM, 293-HEK) supplemented with 2 mmol/l L-glutamine, 10% fetal calf serum, 100 IU/ml penicillin, and 100 µg/ml streptomycin. Alternatively, HEP-G2 cells stably expressing mitochondrial-targeted GFP (mt-RoGFP) were used. Transfections were performed using Lipofectamine 2000™ (*Invitrogen*) or Fugene (Roche) transfection reagents with estimated efficiency up to 50%. Following transfection, cells were allowed to stabilize for 24 h and then subjected to further treatments. For confocal microscopy, cells were cultured for 2 days on glass coverslips coated with poly-L-lysine.

#### 3.3.2. Expression plasmids preparation

ORF of human CIDEA (clone ID IOH22361) was purchased from *Invitrogen* cloned into the pENTR-221 vector. For inducible expression of native protein, ORF CIDEA from pENTR-221 was subcloned by LR recombination reaction of Gateway system (*Invitrogen*) into the expression (destination, DEST) vector pT-REX-DEST30 (FIG 3-8 A), giving rise to the pT-REX-DEST30-CIDEA. For fluorescent imaging, CIDEA was cloned into the destination vector pDEST-53, enabling N-terminal fusion with green fluorescent protein (GFP).

ORF CIDEA was further used for preparation of truncated CIDEA ORFs lacking either CIDE-C domain (designated as CIDEΔC) or CIDE-N domain (designated as CIDEΔN). CIDEΔC and CIDEΔN were prepared using multistep PCR method, consisting of two separate PCR reactions, as depicted in a FIG 3-9 with primers of TAB 3-2. PCR reactions were performed according to standard protocol with Pfu polymerase (*Fermentas*). Using attB primers of the Gateway system, PCR product were subcloned into pDONR-221 vector by BP recombination reaction, giving rise to pENTR221-CIDEΔC and pENTR221-CIDEΔN. In order to obtain its fusion with GFP, these clones were subcloned by LR-recombination reaction into the pDEST-53, thus expressing N-terminal GFP-tag. To prepare CIDEA tagged with red fluorescent protein (RFP), ORF CIDEA was amplified by PCR and subcloned into the pDsRed-Monomer-C1 (*Clontech*) using *XhoI* and *EcoRI* restriction sites with T4 DNA ligase (*USB*).

For native CIDEa expression with inducible expression, an ORF of human CIDEa in an entry vector pENTR221 (*Invitrogen*) has been transposed into a vector T-REx pDEST30 (*Invitrogen*) for a tetracycline-induced expression, obtaining pDEST30-CIDEa plasmid containing the CIDEa. The HeLa cell line and 293-HEK cell line overexpressing the *tet*-repressor (*Invitrogen*). When transfected with vector DNA bearing *tet*-responsive element within promoter region, expression does not take place due to the binding of *tet*-repressor protein. To unblock the expression, tetracycline was added to the final concentration of 1 µg/ml. Tetracycline binding causes dissociation of *tet*-repressor from promoter thus initiating the expression (FIG 3-8 B).

### **3.3.3. Confocal microscopy**

Confocal microscopy was used to visualize fluorescent conjugates of CIDEa. The inverted fluorescent microscope Olympus IX81 with FluoView FV1000 laser scanning unit was employed for single photon microscopy with an Argon laser (457 nm, 488, 515 nm, 30 mW total output) for excitation (Olympus). A pinhole unit (50–800 µm) was used to set confocal conditions. For most of the experiments, The confocal inverted fluorescent microscope Leica SP2 AOBS DMIRE2 HCFluo TCS 1-B (an objective PL APO 100×/1.40–0.70 oil) was used with an Argon laser (488 nm/20mW, 514 nm/20mW) for excitation of cells in a thermostable sample chamber set to 37°C, supplied from a CO<sub>2</sub> incubator, to mimic cultivation conditions. A pinhole 1 Airy unit was used to set confocal conditions.

Confocal microscopy was used for colocalization experiments of CIDEa with mitochondria or nucleus. To localize CIDEa to mitochondria, red fluorescent dye TMRE (Molecular Probes, 0.5 µM, excitation 546 nm and emission 574 nm) or Mitotracker Green (Molecular Probes, 200 nM, excitation 490 and emission 516 nm) were used. For GFP (DEST 53) excitation 478 nm and emission 707 nm was used, for RFP 557 nm excitation and 585 nm emission maxima were used. Obtained pictures were analyzed and managed using Leica LCS Lite software.

### **3.3.4. Initiation of apoptosis**

The pDEST30-CIDEa-transfected T-REx-HeLa cells were subjected to tetracycline (1 µg/ml) for defined time intervals, thus obtaining a time-course of induced CIDEa expression.

In experiments where apoptosis initiators were used, cells were subjected to tetracycline treatment for 8 h followed by 2 h incubations with following apoptosis initiators: a DNA topoisomerase I complex inhibitor camptothecin (2 µmol/l); a protonophore CCCP (2 µmol/l); a potassium ionophore valinomycin (2 µmol/l); and a calcium ionophore A23187 (2 µmol/l). Extent

of apoptosis was assayed using caspase-3 activity, TUNEL assay and cell death assay assessing cell morphology.

### **3.3.5. Preparation of subcellular fractions**

Minor modifications of previously described method (*Carcamo et al. 2002*) have been adapted. T-REx-HeLa cells were washed twice with 2 ml of ice-cold PBS and scraped into 1 ml of PBS. Suspension was centrifuged ( $1500 \times g$ , 5 min,  $4^{\circ}\text{C}$ ), the pellet was resuspended by gentle pipetting in 300  $\mu\text{l}$  of ice-cold buffer A (10 mmol/l HEPES, pH 7.9; 10 mmol/l KCl; 1.5 mmol/l  $\text{MgCl}_2$ ; 0.5 mmol/l DTT; 0.1% (v/v) NP-40), incubated for 10 min on ice, and centrifuged ( $5500 \times g$ , 10 min,  $4^{\circ}\text{C}$ ). Following collection of supernatant, which contains cytosolic and mitochondrial fraction, the pellet was vigorously resuspended by syringe/needle in 3 volumes of ice-cold buffer B (20 mmol/l HEPES, pH 7.9; 420 mmol/l NaCl; 0.2 mmol/l EDTA; 1.5 mmol/l  $\text{MgCl}_2$ ; 0.5 mmol/l DTT; 0.5 mmol/l PMSF; 25% (v/v) glycerol) and incubated for 30 min on ice. Following centrifugation ( $12,000 \times g$ , 20 min,  $4^{\circ}\text{C}$ ), the supernatant (nuclear extract) was collected. Both extracts were stored in  $-80^{\circ}\text{C}$  until further use. Protein content in extracts was determined by the Bradford method (*Bradford 1976*).

### **3.3.6. Izolation of mitochondria**

Cells were washed with PBS and harvested by trypsinization. Cellular pellet was homogenized using homogenizer. In ice-cold homogenization buffer (0.25 M sucrose, 5 mM HEPES, 0.1 mM EDTA, pH 7.2) with 0.1 % BSA. The homogenate was centrifuges at  $500 \times g$  for 10 minutes. The pellet was discartes and the supernatant was centrifuged at  $10,000 \times g$  for 10 minutes to obtain the mitochondrial pellet. The resulting pellet was washed and resuspended in homogenization buffer without BSA. Mitochondrial fraction was subjected to western-blotting.

### **3.3.7. Caspase-3 activity**

The PBS-washed cells were lysed in 50  $\mu\text{l}$  of ice-cold lysis buffer (50 mmol/l HEPES, pH 7.4; 0.5% Triton X-100, a protease inhibitor cocktail tablet, 5 mmol/l DTT;  $4^{\circ}\text{C}$ ; 15 min). The lysate was cleared by centrifugation ( $14,000 \times g$ ;  $4^{\circ}\text{C}$ ; 15 min) and the supernatant total protein determined by the Bradford method (*Bradford 1976*). The lysate was assayed in 20 mmol/l HEPES, pH 7.1, 2 mmol/l EDTA, 5 mmol/l DTT, containing a protease inhibitor cocktail tablet and caspase-3 fluorescent substrate (Ac-DEVD-AMC; 50  $\mu\text{mol/l}$ ) by incubation at  $37^{\circ}\text{C}$  for 60 min. Background fluorescence was subtracted, as obtained in parallel samples with a caspase-3 inhibitor (Ac-DEVD-CHO; 2  $\mu\text{mol/l}$ ). The fluorescence was measured at 380/450 nm using an LS 50 B spectrofluorometer (*Perkin-Elmer*).

### **3.3.8. Western-blot detection of CIDEa**

Cells were collected by scraping off in the growth medium to ensure the detached cells are not lost in the rinsing procedure. The cell suspension was centrifuged and the pellet was resuspended in 50 µl of the lysis buffer. Alternatively, isolated mitochondria were used. Following addition of SDS-PAGE sample buffer (50 µl) it was boiled for 5 min at 95°C. 20–30 µg of total protein/lane was run on 12% SDS-PAGE, blotted onto PVDF membrane and the CIDEa antigen was detected using rabbit primary antibody (*ProSci*). Horseradish peroxidase- conjugated secondary anti-rabbit antibody and Luminol reagent (*Santa Cruz Biotechnology*) were used for visualization. Alternatively, alkaline phosphatase conjugated secondary anti-rabbit antibody (*Sigma*) was used and visualization was performed using BCIP/NBT reagent.

### **3.3.9. *In situ* detection of apoptosis (TUNEL assay)**

Detection of apoptosis by TUNEL assay was performed as per manufacturer instructions (*Roche*). Samples were evaluated under fluorescent microscope Olympus IX70 (*Olympus*). TUNEL assay is widely used assay for detection of DNA fragmentation.

### **3.3.10. Immunocytochemistry**

Cells were fixed by adding ice cold methanol and the whole plate was placed overnight into a –20°C freezer. Upon thawing, cells were rinsed twice with PBS and permeabilized by incubating in 0.2% Triton TX-100/PBS (v/v) for 30 min at room temperature. Blocking was performed by incubation for 15 min at room temperature in 3% BSA/PBS (w/v) and was followed by incubation with anti-CIDEa primary antibody (*ProSci*) diluted 1 : 100 in 3% BSA/PBS (w/v) for 45 min at 37°C. After rinsing three times in PBS, cells were incubated for 30 min at room temperature in fluorescein-conjugated secondary anti-rabbit antibody (*Molecular Probes*) suspended in 3% BSA/PBS (w/v). Following three washes in PBS, the slides were mounted using fluorescent mounting medium (*Dako Cytomation*). Confocal microscope FluoView FV1000 (*Olympus*) was used for evaluation of the slides.

### **3.3.11. Cell death assay**

Slides for immunocytochemistry were also used for identifying apoptotic cells. Approximately 300 cells total and 100 CIDEa positive cells were counted in random fields of each slide under fluorescent/phase contrast microscope. Apoptotic cells were distinguished based on typical morphological alteration of adherent cells undergoing apoptosis including becoming rounded and condensed. Condensation of cells was also readily apparent after nuclear staining by Hoechst

33258 dye (MolecularProbes, excitation, emission 352 nm / 461 nm). Cell numbers were then used for estimation of apoptotic cell percentages.

#### **3.3.12. Quantitative RT-PCR**

Quantitative PCR was performed as described in Part B, using CIDEa specific primers and probes (TAB 3-2.).

#### **3.3.13. Statistical analysis**

All the data presented in this study correspond to the mean value of N experiments  $\pm$  SD. Comparison of the data sets was performed with the Student's t test, using SigmaPlot (*Microsoft*). Two sets of data were considered statistically different when  $p < 0.05$ .

## 4. RESULTS

### 4.1. GLUCOSE DEPRIVATION

Intention of this part of the work was to elucidate, how glucose limitation influences the overall metabolic behavior of selected breast cancer cell versus their normal, non-cancer counterparts originating from the same myoendothelial breast tissue. To address this, cell growth and viability were tested first and respiration assays subsequently to clarify the working hypotheses and derive the relevant mechanisms. Cells were grown in a high-glucose (25 mM) medium (Glc medium) or in an alternative medium deprived of glucose and containing glutamine as an energy source and galactose as a carbon source required for maintaining PPP cycle activity and nucleic acid synthesis (Gln/GAL medium). Note, that glutamine content was equal in both media. Such a modification of cultivation medium forces the cells in the Gln/GAL medium to use mitochondrial OXPHOS to generate ATP, and thereby allows us to manipulate with the energy metabolism of living cells. Thus, the ATP production of cells grown in Gln/GAL medium is strictly dependent on mitochondrial oxidative phosphorylation. The Gln/GAL medium supports the “respirative” phenotype, since galactose is a poorly fermentable sugar, so that glycolysis is restricted. In the Gln/GAL medium, the TCA cycle flux is supported by glutaminolysis (*Reitzer et al. 1979*). On the contrary, the Glc medium induces a “glycolytic” phenotype. Both fermentative and oxidative phenotypes can only be expressed to the extent specific to the particular cell type. Metabolic alterations induced by the cultivation medium have been described elsewhere (*Reitzer et al. 1979; Rossignol et al. 2004; Dlasková et al. 2008b*).

#### 4.1.1. Cell growth

To assess the differences in cell growth, breast cancer HTB-126 and myoendothelial HTB-125 cells (originating from the same tissue) were plated to 10 cm dishes at the cell density of  $10^5$  per plate in two distinct cultivation media; Glc and Gln/GAL. Cellular population was observed over a period of 10 days. During this time, confluency was reached only in case of HTB-126 cells in Glc medium at day 9. Doubling time of HTB-125 cells in Glc medium was  $34 \pm 1.5$  hours, and  $28 \pm 1.3$  hours for HTB-126 cells. Cultivations in the Gln/GAL medium resulted in augmentation of doubling time (slower growth) to  $47 \pm 2.1$  and  $39 \pm 1.1$  hours for HTB-125 and HTB-126 cells, respectively. No extensive acidification of the medium occurred (FIG 4-11), as typical for e.g. HeLa cells. Slight differences in cellular morphology were observed in HTB-126 cells upon Gln/GAL cultivation, i.e. cell clustering and lesser uniformity was observed as compared to the cells grown in the Glc medium (not shown).

#### **4.1.2. Cell viability upon mitochondrial inhibition**

Impact of mitochondrial inhibitors on cell viability of cancer HTB-126 cells was tested to illustrate better the effect of energy substrate exchange on their survival. Cells were plated on 96-well plates to the density of  $10^4$  per well. After 24 hours, the medium was replaced with media containing specific inhibitors of mitochondrial respiratory chain: rotenone for complex I, antimycin A for complex III and oligomycin for complex V (final concentrations are designated in FIG 4-1). Treatment continued for 8. Neutral red assay was performed to test the cellular viability.

Results are expressed as a ratio of neutral red uptake of the sample to the control sample grown with no inhibitor. Declining ratios indicate the loss of cell viability during the treatment. The aim was to ascertain: i) whether inhibition of mitochondria reflects in cell viability, and ii) to what extent mitochondrial energy producing pathway contributes to the cell survival in cancer cells. As shown at FIG 4-1 A, B, and C, there is a difference in responses of Glc and GAL cells when exposed to mitochondrial inhibitors. Cell viability, as expressed by neutral red uptake ratio, was significantly influenced by the presence of mitochondrial inhibitors in the Gln/GAL medium, while a little effect was observed in the Glc medium. This demonstrate that cancer cells verily utilize mitochondrial OXPHOS to produce ATP and maintain viability when glucose is absent in the medium.

#### 4.1.3. Respiration

- **Respiratory flux,  $J_{O_2}$**

To follow the functional adaptation of the mitochondrial oxidative phosphorylation of cells grown in glucose or glucose-deprived medium, a high-resolution respirometry was used. Respiration of intact cells was measured. The respiratory flux ( $J_{O_2}$ ) is the highest at the air saturation and declines to the low extent in the range above 2 kPa (0-10 % flux for HTB-126 GAL cells). Addition of succinate had no stimulatory effect on oxygen consumption indicating that cell membrane is intact. We have compared the respiratory flux values (routine respiration of intact cells supported by intrinsic substrates) measured i) in glucose medium (Glc), ii) after the glucose removal (instant replacement by Gln/GAL medium, Gal0), and iii) in cells adapted to the growth in the glucose-deprived medium (GAL 4, such adaptation occurs after 4 days of growth in the glucose deprived-medium). Cultivation under glucose-deprived conditions (minimum of 4 days) leads to a large increase in the respiratory flux (FIG 4-2 and 4-3 B) of cancer cells ( $90.7 \pm 4.8 \text{ pmol O}_2 \times \text{s}^{-1} \times 10^{-6}$  cells) compared to Glc cells ( $24 \pm 4.8 \text{ pmol O}_2 \times \text{s}^{-1} \times 10^{-6}$  cells). No significant increase was observed in non-cancer HTB-125 cells ( $41.4 \pm 1.6$  in Glc,  $49.9 \pm 4.4$  in the Gln/GAL medium, respectively).

The removal of glucose and its replacement by Gln/GAL medium (Gal0) led to a two-fold increase in cell respiration of cancer cells HTB-126 ( $40 \pm 4.8 \text{ pmol O}_2 \times \text{s}^{-1} \times 10^{-6}$  cells), whereas no significant change was observed in the non-cancer cells (FIG 4-2). The difference between Glc and GAL0 group might be a result of the inhibitory effect of glucose exerted on mitochondrial respiration. The increased respiratory flux of Gal0 group was attributed to the removal of Crabtree effect (more in section 4.4.).

- **$P_{50}$ ,  $J_{max}$**

A steep decline of oxygen consumption was observed below the oxygen pressure of 2 kPa. For cancer and control cells, we have determined the oxygen pressure at 50 % of maximum flux ( $P_{50}$ ), which gives a measure of the apparent cellular affinity to oxygen.  $P_{50}$  can be determined by high-resolution respirometry by plotting the flux value as a function of the  $p_{O_2}$  and fitting with a theoretical hyperbolic curve. The 1.1 kPa region was used to calculate  $P_{50}$  and the corresponding maximal flux -  $J_{max}$ . The calculated  $J_{max}$  is pertinent to the low oxygen range and is usually 5-10% lower than the flux observed at air saturation -  $J_{O_2}$ , indicating that oxygen saturation is nearly but not fully reached. Oxygen kinetics curves corresponding to the cell-specific flux are shown in FIG 4-3 A, B. The  $P_{50}$  values are shown in the histogram of FIG 4-4. They have revealed higher  $P_{50}$  values in the cancer cells, in comparison to the non-cancer cells. A slight decrease of  $P_{50}$  values observed in cells grown under high glucose as compared to the glucose-deprived medium (GAL4) indicated a

lower apparent affinity of the cellular respiratory system to oxygen. Besides characterization of the cellular response to hypoxia,  $P_{50}$  is an indicator of the activity of ETC, particularly COX turnover rate. Increase of  $P_{50}$  value of HTB-126 GAL4 group compared to HTB-126 Glc is associated with an increase of activity and turnover rate of the respiratory chain components upon sustained growth in glucose-limiting conditions. However, slight increase of  $P_{50}$  does not correspond to robust increase of respiratory rate (4-fold increase of GAL4 compared to Glc) that presumes large increase of  $P_{50}$ . Although the respiratory flux was significantly higher for the glucose-deprived cells,  $P_{50}$  values differed only by 10% ( $p < 0.05$ ), indicating higher, but still comparative metabolic state of both Glc and GAL4 groups.

Aside of the metabolic state, resulting  $P_{50}$  is a function of oxygen gradient that depends on cell size (diameter), regularity of the cellular shape, and possibly also on mitochondrial network arrangement and vicinity to the cell membrane. The effect of oxygen diffusion on mitochondrial respiration can be evaluated by comparing  $P_{50}$  values at different cell densities (FIG 4-5). By testing multiple cell densities, we also test the independence of the enzyme affinity from the enzyme concentration. In non-cancer HTB-125 Glc cells, the plot of  $P_{50}$  as a function of  $J_{max}$  indicates a constant value of  $P_{50}$  for a broad range of cell densities. Conversely, in cancer HTB-126 cells we observed an increase of  $P_{50}$  with increasing  $J_{max}$  (FIG 4-5). The resulting slopes (given in the figure legend) should provide an estimation of the diffusion effect. Increasing slope indicates increased influence of oxygen diffusion. Thus, it can be deduced that oxygen diffusion toward the mitochondrion varies between HTB-126 and HTB-125 cells. It remains to be understood how carcinogenesis introduced this difference.

- **Intact cells**

To investigate closely the nature of increased flux of cells growth in Gln/GAL medium, respiration with respiratory inhibitors was performed. To rule out the possibility that increase of respiration upon growth in glucose-deprived conditions is caused by uncoupling, quantification of coupling and uncoupling ratios were performed. The routine respiration consists of the mitochondrial oxygen consumption and the non-mitochondrial oxygen consumption (side oxidative reactions, these usually account for 4-15% in our system). The cellular endogenous flux (routine respiration, corresponding to the *in situ* state of mitochondrial respiration) is a result of oxidation of endogenous substrates (NADH and  $FADH_2$  derived from cellular catabolic reactions of glucose and lipids) by ETC. Routine respiration is a function of ATP demand and substrate availability, which could be considerably limited. Respiration is used to produce ATP at the level of the  $F_0F_1$ -ATPase, so that inhibition of by oligomycin leads to the reduction of respiration to the extent corresponding to the respiratory rate that is utilized for ATP synthesis. A significant part of

flux was inhibited by oligomycin both in cancer and control cells indicating high extent of respiratory capacity is controlled by ADP phosphorylation rate. Subsequently, RCR ratios of respiratory states were evaluated (FIG 4-6 A), as routine respiration expressed relatively to oligomycin-inhibited respiration. This ratio is a measure of flux dependence on phosphorylation rate – coupling of electron transport to ATP synthesis.

The uncoupled flux reflects the maximal capacity of the respiratory chain, which occurs without feedback control by the  $F_0F_1$ -ATPase (termed uncoupling). Uncoupling of respiration indicates the reserve capacity of ETC, or how close the system in routine state works to its upper limit (maximally uncoupled flux) as expressed by UCR (FIG 4-6 A). For instance, if the ADP level is elevated due to the increased energy demand, the routine flux increases and the UCR ratio declines nearer to 1. Alternatively, a decline of UCR can be caused by uncoupling. No cells tested exhibited routine respiration close to its fully uncoupled maximal flux, indicating the reserve capacity of respiratory chain both in control and cancer cells. Limitation of the endogenous flux comparing to maximal capacity may be caused by substrate flow into mitochondria, possibly along with ADP limitation.

Addition of rotenone gives us the estimation of the flux supported by complex I since complex II can still operate despite complex I inhibition. Antimycin A (AntA) inhibits the remaining electron flow through ETS and delineates mitochondrial respiration from the side cellular oxidative reactions (FIG 4-6 B). The routine respiration was generally inhibited completely by rotenone, indicating a strong contribution of complex I respiration to the absolute respiratory rate, while complex II does not participate on the electron transport of ETS (except for HTB-126 GAL cells, FIG). The difference between oligomycin and AntA-inhibited states is attributed to the leak respiration.

Quantification of components of the respiratory flux is shown in FIG 4-6 B. Bars shows, how individual elements of respiratory flux (leak, complex I and complex II respiration) are integrated and contribute to the final flux and ETC capacity.

- **Permeabilized cells**

This assay (described in section 3.1.8.6.) was used to decide, whether complex II was deficient in HTB-126 Glc cells or limited by substrate in intact cells. When measuring respiration of permeabilized cells, we could evaluate an impact of exogenous substrates on the mitochondrial respiration *in situ*; permeabilization allows maintaining mitochondrial network integrity and its interactions with the cytoskeleton, the Golgi system and the endoplasmic reticulum. Using permeabilized cells we can monitor the mitochondrial respiration by addition of specific substrates and inhibitors of the OXPHOS. This method is widely used for the diagnosis of

mitochondrial diseases (permeabilized muscle fibers). In permeabilized cells, flux of internal substrates is disconnected and respiration is entirely dependent on the exogenous substrates added. Contrary to the intact cells, where substrate availability may limit the respiratory flux, artificial substrates are added to the permeabilized cells in excess, thus stimulate maximal performance of the intermediate metabolism and associated mitochondrial respiration. Cells were permeabilized by digitonin, measurements have been performed in the respiratory medium, distinct from DMEM.

The assay is a modification of the one used for intact cells, as it is shown in FIG 4-7 A (grey line). First, the endogenous flux was monitored, followed by the addition of glutamate and malate, which, however, did not exert any influence on respiration of intact cells. Permeabilization by digitonin resulted in a decline of respiratory rate to the level corresponding to state 2 (substrate present, no ADP). After stabilization, ADP was added to stimulate state 3 respiration with complex I input (due to the presence of complex I – specific substrates glutamate and malate). Addition of succinate, surprisingly, activated complex II respiration, resulting in complex I+II respiration (quantified as a succinate control ratio, SCR, TAB 4-1). This indicates that complex II is functional and can participate in electron transport, when substrate is available contrary to intact HTB-126 Glc cells, where complex II activity has not been detected. Hence, lack of complex II respiration detected in intact cells means that little succinate or  $FADH_2$  is present in the intact cells. The addition of oligomycin resulted in transition to state 4 respiration (pseudo state 4 respiration since ADP is present). At this point we can calculate RCR as uncoupled flux to state 3 respiration (with complex I+II input). Data are presented in FIG 4-7 and TAB 4-1. The uncoupling of flux by uncoupler (FCCP) stimulates the flux to its maximal capacity. Interestingly, convergent complex I+II electron input stimulated respiration of HTB-126 Glc cells close to the maximum capacity of respiratory system (UCR 1.08 FIG). Hence, when considering the contribution of succinate on respiratory flux, the increase of state 3 respiration compared to endogenous respiration of intact cells (ratio 3/E), can be attributed to the complex II as indicated by succinate control ratio (SCR, TAB 4-1). These data show that complex II is not defective in HTB-126 Glc cells, but rather attenuated due to the lack of substrate.

In HTB-126 GAL cells, substrate combination resulted in the elevated state 3 respiration as compared to endogenous flux. However, UCR ratio was 1.7 (FIG 4-7, TAB 4-1). Under the conditions of unlimited substrate and ADP delivery, state 3 respiration does not meet its kinetic limits. Therefore, we can suggest that principal controlling factor of the state 3 respiratory rate of HTB-126 GAL cells is the rate of phosphorylation system (ATP synthase, the ADP/ATP carrier, and  $P_i$  carrier), but not substrate. Contribution of complex II respiration has been also elevated in HTB-126 GAL cells (SCR).

Increase of state 3 respiration of permeabilized cells related to routine respiration as occurs in intact cells with endogenous substrates is summarized in TAB 1 (ratio 3/E). This indicates that substrate flux is compromised in intact cells and respiratory complexes do not proceed at the maximum kinetic rate. Respiration of permeabilized cells revealed complex II inhibition under the standard cultivation conditions of cancer cells. Importantly, the existence of SCR (>1) clearly shows functionality of complex II. Participation of individual respiratory complexes to the overall respiratory flux is summarized in FIG 4-7 B and TAB 4-1.

#### **4.1.4. ATP synthesis**

ATP amount was measured in HTB-126 Glc cells in response to glycolytic inhibitor 2-deoxy glucose (2-DG), lactate dehydrogenase inhibitor (oxamate) and  $F_0F_1$ -ATPase inhibitor oligomycin. Results were expressed as pmols per mg of total cellular protein and subsequently related to control samples. FIG 4-8 shows, that inhibition of hexokinase disrupts the cellular ATP balance to higher extent than inhibition of LDH or mitochondrial ATP synthesis.

#### **4.1.5. Expression of OXPHOS proteins**

The expression levels of respiratory chain proteins (subunits of complex I, complex II and complex IV) was estimated by western blots of cell lysates prepared from HTB-125 and HTB-126 cells grown in glucose medium or glucose-deprived medium at least 4 days. An example of western blot is given (FIG 4-9 inset) and the results of the densitometric analysis are summarized in the histogram of FIG 4-9. The results were expressed as the ratios of the protein band densities measured in the glucose-deprived medium, to those obtained in the glucose medium (for the same content of cell lysate proteins). A value of 1 means no change in the expression level of complex I, II, and IV in the glucose deprived medium, while a value >1 indicates upregulation of expression. The results show an increase of protein expression with a mean factor of  $1.26 \pm 0.098$ ,  $1.88 \pm 0.48$ , and  $2.39 \pm 0.15$  for CI, CIV, and CII, respectively, in non-cancer cells grown in the absence of glucose. In cancer cells, this increase was more pronounced and the mean factor value was of  $1.28 \pm 0.01$ ,  $4.17 \pm 0.34$ , and  $5.97 \pm 1.70$  for CI, CIV, and CII, respectively.

Elevated respiratory rate along with induction of OXPHOS proteins expression shows that mitochondrial biogenesis is activated in the glucose-deprived medium.

## **4.2. HYPOXIA**

Additionally to glucose deprivation, we exposed cells to the low oxygen conditions (1% oxygen, 6 days). As for glucose deprivation, cell growth, respiration and OXPHOS composition were examined.

### **4.2.1. Cell viability under the hypoxia**

Cell viability was measured at hypoxia using the neutral red assay. Cancer and normal cell were plated to 96-well plates to the cell density of 10,000 (HTB-126) and 5,000 (HTB-125), respectively. Both cell types were grown in the Glc as well as Gln/GAL medium. After cells attached (8 hours), plates were moved to 1% oxygen or to normoxic condition as reference. Neutral red assay was performed after 24 hours and after 6 days, respectively. We expressed the results as the ratios of cell viabilities obtained in hypoxia to that measured at normoxia (FIG 4-10). A ratio of 1 means that viability is similar in hypoxia and normoxia; a ratio <1 indicates a loss of viability during hypoxia. This notion of viability must be clarified here, as the neutral red assay reflects the active uptake of neutral red inside the cell. Increase of neutral red uptake can be related to increased cell mass, but also be used as a metabolic index (*Nouette-Gaulain et al. 2009*). In the glucose medium, hypoxia induced a minute decrease (20 % reduction in cell viability) at day 1, and no change was observed after 6 days (8 %). Conversely, in cancer HTB-126 cells, hypoxia resulted in a large increase in the cell viability after 6 days (54 % increases). In the glucose-deprived medium, 6 days of hypoxia induced a significant decrease of cell viability (51 % reduction after 6 days) in HTB-125 non-cancer cells. The same phenomenon was observed in cancer cells, albeit to a dramatic extent. Indeed, 1 day of hypoxia induced a 43 % decrease in cell viability in the glucose-deprived medium, and after 6 days all the cells died. These observations suggest that 1% hypoxia exerts opposite effects on cancer cells viability, depending on the presence or the absence of glucose in the culture medium. They also reveal that cancer cells are more sensitive to hypoxia, as they undergo a larger metabolic remodeling in comparison with non-cancer cells.

### **4.2.2. Respiration**

The endogenous respiration of HTB-125 and HTB-126 cells grown in glucose or glucose-deprived medium was measured after 6 days in normoxia or 1% hypoxia. The respiratory flux of intact cells was determined FIG 4-11, as was the pH value of the cell culture medium. The results show that 1% hypoxia slightly increased cell respiration by 34 % for the HTB-125 cells grown in the Glc medium, and by 26 % in the glucose-deprived medium for control cells. Conversely, 1% hypoxia reduced mitochondrial respiration in cancer cells by 36 % in the glucose medium and by

23 % in the glucose-deprived medium. These results indicate that hypoxia stimulates cell respiration in non-cancer cells, independently of the culture medium, while it inhibits cell respiration in cancer cells. Again, this argues for a different sensitivity and a variable response of cell metabolism toward hypoxia in cancer cells versus the non-cancer counterpart. When  $P_{50}$  measured, there was an increase in  $P_{50}$  in HTB-126 Glc cells (1.3 in hypoxic as compared to 0.86 in normoxic cells), indicating decrease of mitochondrial performance in regulation. In term of affinity, increase of  $P_{50}$  means decrease of affinity to oxygen.  $P_{50}$  of HTB-126 GAL cells did not change.

#### **4.2.3. OXPHOS proteins expression under hypoxia**

Western blot of cell lysates of HTB-126 cells grown in 1% oxygen was compared to control samples (normoxia). As expected from the data of respiration, there was a profound decrease of subunits of complexes I, IV, and III (FIG 4-12). No significant change was observed for HTB-126 GAL cells exposed to hypoxia.

### **4.3. MITOCHONDRIAL NETWORK MORPHOLOGY**

Mitochondrial bioenergetic capacity is linked to the configuration of the mitochondrial network, so we analysed this feature in living HTB-125 and HTB-126 cells by confocal microscopy. Data are depicted in FIG 4-13. In non-cancer HTB-125 cells, neither the removal of glucose nor the limitation of oxygen availability caused changes of the mitochondrial network morphology and total area. Interestingly, the combination of glucose deprivation and 1% O<sub>2</sub> induced a wider spreading of this network, with a significant increase in the total organellar area (as compared to normoxic HTB-125 in glucose medium). In HTB-126 cancer cells these changes were more sensitive, as the sole removal of glucose triggered an increase in mitochondrial total area (1.51-fold). Yet, the combination of aglycemia and 1% O<sub>2</sub> hypoxia induced further changes (total mitochondrial area was increased by a factor of 1.91), comparable with what was observed in the non-cancer HTB-125 cells. In all conditions, the mitochondrial network remained in the tubular configuration and no excessive fragmentation was observed.

#### 4.4. CRABTREE EFFECT

A short-time effect of the presence of glucose on cell respiration was investigated in HTB-126 cancer cells. HTB-126 GAL cells possess the pronounced Crabtree effect (FIG 4-14 A, B). The effect of glucose addition or removal on respiratory rate and  $P_{50}$  of HTB-126 was evaluated.

Glucose addition (25 mM final) to the respiring HTB-126 GAL cells induced a rapid and pronounced (40%) decline of respiration in glucose-deprived cells (designated as GAL/Glc – FIG 4-15). Surprisingly, this rapid decline of respiratory rate had no effect on  $P_{50}$  (TAB 4-2). Likewise, removal of this Crabtree effect was reached when cells originally grown in the Glc medium were transferred to the Gln/GAL medium (this sample was designated as Glc/GAL). Such a shift results in a two-fold increase of cellular respiratory rate. In this group, glucose addition, again, could reduce the respiratory rate below original value (not shown).

According to results presented above, the cell specific uncoupled flux of HTB-126 Glc cells reached as high as  $38 \text{ pmol O}_2 \times \text{s}^{-1} \times 10^{-6} \text{ cells}$ , represented by the UCR of 1.64 (a 1.64-fold increase over the routine respiration). Glucose removal then stimulated respiration to the level comparable to the uncoupled flux of HTB-126 Glc cells.

To find out, whether removal of glucose stimulates respiration to the limits of maximal respiratory performance of HTB-126 Glc cells, titration by an uncoupler was performed. Surprisingly, the respiratory flux of HTB-126 Glc/GAL sample can be further stimulated by uncoupler, resulting in the UCR of 1.53. Enhancement of maximal capacity can be caused either by induced mitochondrial biogenesis or removal of present inhibition. Regarding the rapid experimental set-up and time scale, we definitely exclude involvement of biogenesis in this case. Rather, the ability to uncouple flux upon glucose removal suggests that electron transport and concomitant proton pumping was retarded when glucose was present. The removal of glucose withdraws this inhibition.

Conversely, the glucose addition causes a rapid transition to the low-respiration state (designated as a GAL/Glc sample group). Uncoupling of oxygen flux in the GAL/Glc group is possible albeit not to the original extent. The results of rapid transition exclude the bioogenesis process, hence the resulted effect must be fully regulated by metabolic alteration.

The data present in this section indicate an inhibition of electron transport through complexes I or II when glucose is present. The removal of glucose causes the extension of ETS capacity. The exact nature of this effect requires further investigations.

#### **4.5. ABSOLUTE QUANTIFICATIONS OF UCP2 TRANSCRIPTS**

We have confirmed the presence of UCP2 mRNA in all eight rat tissues studied (FIG 4-16). The absolute amount of UCP2 mRNA (in pg per 10 ng of total isolated mRNA) decreased in the order of spleen > heart > lung > WAT > brain > skeletal muscle > kidney > liver, spanning a 30-fold difference in UCP2 transcript content (FIG 4-16 A). Only in the rat spleen and lung were the UCP2 transcript levels of the same order of magnitude as the control GAPDH transcript levels (FIG 4-19). With the exception of the heart UCP2 mRNA, a similar pattern was found for mouse tissues (FIG 4-17 A). The heart UCP2 transcript level in mouse was up to 40-fold lower than in the mouse lung. In turn, the heart and lung UCP2 transcript levels were equivalent in the rat.

#### **4.6. ABSOLUTE QUANTIFICATIONS OF UCP3 TRANSCRIPTS**

As expected (*Boss et al. 1997; Vidal-Puig et al. 1997*), we detected the highest UCP3 mRNA levels in rat and mouse skeletal muscle and intermediate levels in mouse heart (FIG 4-17 B), the latter being of the same order of magnitude as the UCP2 lung transcript levels. In contrast to the very high UCP2 mRNA levels found in the rat heart, the UCP3 mRNA was much less abundant. The other UCP3 transcript levels reached only ~10–3 pg per 10 ng of total isolated mRNA with the exception of rat liver (~10–5) and rat kidney (not detectable, FIG 4-16 B). A similar pattern was found for mouse tissues, with the exception of higher levels of UCP3 transcript in the spleen and WAT (FIG 4-17 B).

#### **4.7. ABSOLUTE QUANTIFICATIONS OF UCP4 TRANSCRIPTS**

The absolute mRNA levels of the UCP4 isoform in rat tissues were generally among the lowest determined (FIG 4-16 C). There were by up to three orders of magnitude lower than the UCP2 mRNA levels. As expected (*Mao et al. 1999*), the maximum UCP4 mRNA level was in the brain, but still two orders of magnitude lower than the UCP2 mRNA level. In turn, UCP4 transcript abundance in the rat brain (similarly for UCP5, see below) was similar to that of UCP2 mRNA in the mouse lung (FIG 4-16 C vs. FIG 4-17 A). The mouse skeletal muscle UCP4 transcript level exceeded that of UCP2. Similarly, mouse WAT contained nearly equivalent levels (~0.05 pg per 10 ng of total isolated mRNA) of UCP2, UCP3, and UCP4 transcripts. The UCP4 transcript level was not increased in the brain of the UCP2<sup>-/-</sup> mice compared with wild-type mice (FIG 4-18).

#### **4.8. ABSOLUTE QUANTIFICATIONS OF UCP5 TRANSCRIPTS**

Similar to the rat UCP3 and UCP4 mRNAs, rat UCP5 mRNA was primarily expressed in a single tissue, namely brain. Whereas in the case of rat UCP3 such an apparent exclusivity was found in the skeletal muscle, in the case of rat UCP5 it was the brain (FIG 4-16 D). In other tissues the levels of UCP5 mRNA (~10–3 pg per 10 ng of total isolated mRNA) transcript levels of UCP5 were similar to the UCP3 levels. The rat UCP5 mRNA levels were still at least three-fold higher than those of UCP4. The tissue distribution of mouse UCP5 mRNA expression was somewhat more heterogeneous compared with the other UCPs, although UCP5 mRNA levels in brain were highest among the tested tissues (FIG 4-17 D). Notably, ~0.5 pg per 10 ng of total isolated mRNA was found for the UCP5 and UCP4 transcripts in the mouse brain, as well as for UCP2 mRNA in mouse lung and UCP3 mRNA in mouse skeletal muscle. The mouse heart UCP5 mRNA level was equivalent to that of UCP3. UCP5 mRNA in WAT and spleen was even more abundant than UCP3 mRNAs in these tissues and UCP2 mRNA in WAT. Although only at levels of ~0.05 pg per 10 ng of total isolated mRNA, UCP5 was the predominant isoform in the mouse liver and kidney. The UCP5 transcript was not elevated in the brain of UCP2<sup>-/-</sup> mice.

#### **4.9. QUANTIFICATION OF UCPS TRANSCRIPT LEVELS IN UCP2-NULL MICE TISSUES**

To test, if genetic deletion of UCP2 triggers compensatory expression of other UCPn isoform, expression pattern of UCPn isoform was quantified in lung, brain and liver. We have obtained no compensatory increase in transcript level of any isoform tested (FIG 4-18).

#### **4.10. QUANTIFICATION OF GAPDH**

GAPDH is extensively used as a housekeeping gene in number of studies. However, we have detected variable levels of GAPDH transcripts in tested tissues, among which skeletal muscle and heart were the tissues with the highest expression of GAPDH (FIG 4-19).

#### **4.11. QUANTIFICATION OF CIDEA TRANSCRIPT LEVEL IN RAT TISSUES**

Published quantification of CIDEa transcripts were usually based on Northern-blot analysis or by classical non-quantitative PCR method. In this work, basal level of CIDEa transcript were quantified by quantitative real-time PCR. We have analyzed WAT, heart, brain, kidney, spleen, liver, skeletal, muscle and lung tissue. The highest expression was reported in BAT (*Zhou et al. 2003; Inohara et al. 1998*), which was not analyzed in this work. The highest expression was found in WAT (FIG 4-20).

#### 4.12. CIDEA OVEREXPRESSION LEADS TO APOPTOSIS IN HELA CELLS

Previous studies on CIDE proteins stated that overexpression of the protein causes apoptosis (*Chen et al. 2000*). We have employed T-REx HeLa cells, a cell line stably expressing tetracycline repressor, transfected with pDEST30-CIDEa, which allows regulated and timed CIDEa expression under control of *tet* repressor binding element. First a time course of tetracycline incubation was studied. Time point 0 h clearly shows no expression of CIDEa (FIG 4-21 B), similarly to 293-HEK (FIG 4-21 A), indicated that expression of the protein is suppressed in the absence of tetracycline during the 24 h stabilization period post transfection.

We found that the maximum expression was reached at 12 h post tetracycline (1 µg/ml) addition (16 h for 293-HEK), but afterwards, the expression was declining. It may imply that overexpression of CIDEa induces apoptosis resulting in cell death, a fact corresponding with previous reports (*Chen et al. 2000*). The disappearance of CIDEa in the cell population suggests that the transfected cells die, whereas the non-transfected do not. In our case, the majority of transfected cells would perish between 12 and 24 h post-tetracycline addition. Such a short time required for the cells to die may reflect the amount of CIDEa plasmid used for transfection, also shown by others (*Inohara et al. 1998*), and sensitivity of the cells.

While caspase-3 activity varied throughout the time course (data not shown), the percentage CIDEa redistribution during apoptosis in HeLa cells 95 of TUNEL-positive cells displayed an apparent maximum at 8–12 h with both time points showing significantly higher percentage than time point 0 (FIG 4-22). Hence further experiments conducted used 8 h of tetracycline (1 µg/ml) treatment followed by 2 h in the presence of apoptosis initiators.

#### **4.13. CELLULAR DISTRIBUTION OF CIDEA UPON ITS OVEREXPRESSION**

CIDEb was shown to be localized in mitochondria when overexpressed in Chinese hamster ovary cells (*Chen et al. 2000*) and CIDEa in brown fat mitochondria (*Zhou et al. 2003*). Similarly, in this work we attempt to localize CIDEa protein into mitochondria by different approaches; by using fusion proteins with GFP or RFP tags or by immunohistochemistry.

RFP-fused CIDEa protein localization was examined in HeLa cells with mitochondrially-targeted Ro-GFP stable cells line (not shown). Similarly, GFP-fused CIDEa protein localized to mitochondria, as compared to TMRE-stained mitochondria of HEK-293 cells (FIG 4-23).

We also found that CIDEa was localized to mitochondria upon its tetracycline-regulated expression in HeLa cells. Immunocytochemistry of CIDEa-overexpressing T-REx HeLa cells shows both nuclear as well as extranuclear localization of CIDEa (FIG 4-26). Quantification of CIDEa-positive cells over four independent experiments (100 CIDEa-positive cells counted per experiment) yielded higher number of cells displaying either nuclear or mixed, i.e. nuclear as well as extranuclear, CIDEa localization in camptothecin- and valinomycin-treated cells, 50 and 80%, respectively, versus the DMSO-treated cells – 40% (FIG 4-27).

#### **4.14. ROLE OF CIDE-N AND CIDE-C DOMAIN IN SUBCELLULAR LOCALIZATION**

To investigate a role of so-called CIDE-domains in cellular localization of CIDEA protein, we tested cellular localization of CIDE $\Delta$ C and CIDE $\Delta$ N proteins fused with N-terminal GFP. Our results of our experiments clearly support a role of CIDE-C domain for mitochondrial localization of CIDEA protein. Since CIDE $\Delta$ N showed mitochondrial localization, CIDE $\Delta$ C protein conferred cytosolic localization, as shown in FIGs 4-24, 4-25.

#### **4.15. CIDEA REDISTRIBUTION IS ASSOCIATED WITH TREATMENT OF HELA CELLS WITH APOPTOSIS INDUCTORS**

CIDEa expressed under inducible repressor regulation appears to localize in both extranuclear and nuclear space as shown in confocal microscopy images (FIG 4-26, DMSO). Despite the plausibility of confocal images, we used CIDEa immunodetection in subcellular fractions of CIDEa-overexpressing T-REx HeLa cells to reveal the presence of the protein in general cytosolic, containing mitochondria, as well as nuclear fractions (FIG 4-27).

Valinomycin effect on CIDEa redistribution is more apparent than in the case of camptothecin and corresponds with the quantification of CIDEa-positive cells displaying at least some nuclear localization of CIDEa (vide supra). Heterogeneous cell population was present in our experiments with variable percentage of cells undergoing apoptosis (FIG 4-27).

Pretreatment of cells with pan caspase inhibitor z-VAD-fmk did not significantly alter the percentage of CIDEa positive cells displaying apoptotic morphology, i.e. cells displaying shrinkage and/or nuclear fragmentation, thus demonstrating the caspase-independence of the process (FIG 4-28). On the contrary, the percentage of CIDEa positive/apoptotic cells in samples treated with valinomycin was significantly higher than those treated with DMSO (78 vs. 40%) thus supporting the link between redistribution of CIDEa and apoptosis.

## 5. DISCUSSION

The first objective of my thesis was to analyse the impact of glucose deprivation and oxygen limitation, as occurs in most solid tumors, on the bioenergetic properties of cancer cells in comparison with non-cancer cells. It was the intention to determine the capacity and the functioning level of the mitochondrial oxidative phosphorylation in breast cancer cells. Then, we followed in investigation whether microenvironmental metabolic stresses (i.e glucose and/or oxygen limitation) could reshape this system to permit cell survival.

Few studies have performed in-depth analysis of mitochondrial bioenergetics in cancer cells, as they most typically measured the intracellular ATP levels or the mitochondrial content. Here we used high resolution respirometry to decipher the functioning of the oxidative phosphorylation system and we assessed the main bioenergetic parameters such as the respiratory flux, the coupling degree, the uncoupling ratio, the apparent affinity to oxygen or the contribution of each of the respiratory chain complexes to the overall flux of energy production. We combined measurements performed on intact cell and permeabilized cells to determine the control of respiration by substrate delivery. The cells were grown in different culture conditions to measure the impact of energy substrate type and availability on the remodeling of the metabolic machinery but also cell viability and mitochondrial network morphology. As recently proposed, the bioenergetics of tumors is variable, and the role of microenvironment was not thoroughly evaluated. Here we evaluated the combined impact of glucose deprivation and oxygen limitation as no study considered this problem from the bioenergetic perspective.

In the recent years, studies of carcinogenesis focused on the action of oncogenes, induction of DNA instability, regulation of signaling pathways and processes that lead to uncontrolled cell proliferation resulting in neoplastic transformation. However, an emerging role of metabolic remodeling and ROS signaling has arisen recently. According to several theories, metabolic remodeling that accompanies cancer progression possesses an equal impact on survival than initiators of carcinogenesis, or that it is even required for cancer cells to gain their neoplastic potential. In the pioneering work of Otto Warburg, the incapacity of a cell to perform mitochondrial respiration was considered as the initiating cause of cancer. This concept was strengthened by the discovery of cancers caused by mutations in mitochondrial energy proteins (SDH, FH), but it is also challenged by the discovery of cancers which utilize more mitochondrial OXPHOS rather than glycolysis to proliferate.

This latter proposal encouraged further exploration of energy metabolism of cancer cells and revealed a wide spectrum of metabolic activities within tumor types, differing by ratio of utilization of aerobic and anaerobic pathways for energy production. Aerobic glycolysis remains among most common phenotype of cultured cancer cells, but the importance of mitochondrial OXPHOS remains

underinvestigated in surgical pieces. Such aerobic glycolysis (i.e. glycolysis occurs but OXPHOS does not despite the presence of oxygen) remains unclear. Likewise, it is not known how mitochondria and the (dys)function of OXPHOS participate in the development of oncogenic transformation. To answer these question necessitate a rigorous analysis of the bioenergetic profiles of cancer cells and tumors.

Second, we also performed complete analysis of expression pattern of mitochondrial uncoupling proteins in rat and mouse tissues to clarify recent discrepancies about their tissue distribution. Providing this information, we can better evaluate yet incompletely understood physiological role of UCPs.

Further, we investigated a role of the CIDEa protein in apoptosis. According to the proposed model of CIDE participation in apoptosis, CIDE proteins bind to the DFF-45 protein which is an inhibitor of DFF-40 nuclease, thus activate apoptotic DNA fragmentation independently of apoptosis. We hypothesize that the significance of mitochondrial (*Inohara et al. 1998; Zhou et al. 2003*) location of CIDE proteins lies in being an inactive (non-apoptotic) position (*Valoušková et al. 2008*). CIDE proteins may even associate with yet unknown docking partners in the intermembrane space, thus strengthening the inactive position (vide infra). Our second hypothesis assumes that upon certain (again yet unknown) stimuli, relocation of CIDE from this “resting position” takes place in order to induce apoptosis (*Valoušková et al. 2008*). Migration of CIDEs from mitochondria to nucleus (or to cytosol) has not been reported until 2008, at least not for apoptosis induced by staurosporine or etoposide (*Chen et al. 2000*).

- **Glucose deprivation and its impact on energy metabolism**

In our work, we have shown, that OXPHOS composition, content and performance depends largely on substrate availability and cell type. As depicted in FIG 4-2, respiration of HTB-126 cells grown under standard high-glucose conditions is four-times lower than after the adaptation to Gln/GAL medium, short of glucose. Despite a wide belief of the mitochondrial aberration in cancer cells, we have demonstrated that mitochondrial respiration is intact and fully competent in HTB-126 cells. Cancer and normal cells void of glucose are able to maintain cell proliferation under the normoxic conditions albeit with considerable loss of proliferation rate. Under the high-glucose conditions, HTB-126 cells exhibit a low-respiration state and mostly glycolytic ATP production (FIG 4-8); this phenomenon is normally described as the Warburg effect. A four-fold increase of respiration in Gln/Gal medium can be ascribed to several factors. Compared to the Glc medium, the coupling ratio in the Gln/GAL medium was preserved, therefore, we can exclude the possibility that uncoupling would be responsible for this increase of respiratory rate. If the increase of respiration was caused by an extensive uncoupling, the coupling ratio would be proportionally decreased.

Moreover,  $P_{50}$  is sensitive to uncoupling, so transition into uncoupled state probably does not occur, since  $P_{50}$  remains constant. On the contrary, respiratory system seems to retain its qualitative properties, as assumed from UCR and RCR ratios of intact cells, which remained within the similar range. In the Gln/GAL medium increase of  $P_{50}$  can be attributed to the overall turnover of ETS activity due to the impact of complex II activity (FIG 4-6 B).

Next, we have investigated why the respiration is low in the HTB-126 Glc cells. We can only predict that sustained glucose presence possesses a stimulatory effect on glucose metabolism and/or inhibitory effect on oxidative metabolism. We assumed, that glucose could supports the cells growth aside of ATP production. In order to support also the cell growth, FA synthesis should be enhanced to support membrane synthesis. The major precursor of FA synthesis is citrate, synthesized in TCA cycle. TCA cycle does not have to be necessarily intact (*Owen et al. 2002*). It has been frequently recognized that truncation of TCA cycle might occur in number of cell types and serves to synthesize number of metabolic precursors for anabolic processes (cataplerotic flux). When glucose serves as a chief energy substrate, remaining carbons that are not deviated to lactate synthesis, enter a truncated TCA cycle where citrate is preferentially extruded to the cytosol and feeds the fatty acids and sterol synthesis. The citrate extrusion from mitochondria would explain the low respiratory flux of HTB-126 Glc cells with the exclusive complex I electron input (FIG 4-6 B). Such organization of metabolic pathways and metabolite sorting would theoretically support the high cell growth rate of cancer cells grown in high-glucose medium.

In intact cells, complex II activity has not been detected. This may be caused either by complex II deficiency or substrate limitation. Experiments with permeabilized cells gave us a better picture about functioning and organization of mitochondrial respiration of cancer HTB-126 cells. We have concluded that the substrate flux through TCA cycle is probably compromised in intact cells with regard to the succinate-related respiration in permeabilized cells (FIG 4-7 B). Complex II respiration does not occur in intact cells despite the presence of sufficient amount of complex II subunits, obvious complex II functionality with succinate and sufficient substrate levels in culturing medium (glutamine). Therefore, we support the statement that complex II is limited by substrate at the level of TCA cycle in HTB-126 Glc cells. This phenomenon can be explained on the basis of cell-growth support, as reported previously (*DeBerardinis et al. 2007*). In this case, metabolites of TCA cycle are rather utilized as anabolic precursors of FA rather than for completion of TCA cycle. Thus the citrate efflux of mitochondria would depress the substrate flow through succinate-dehydrogenase complex and explain the absent flux through complex II (FIG 5-1).

The cells growing in Gln/GAL medium were considered to undergo glutaminolysis in order to support the cell growth utilizing mitochondrial OXPHOS. In attempts to confirm this, we have revealed that glutaminolysis likely support other cellular processes. The Gln/GAL medium provides a

source of glutamine, a major oxidizable substrate of tumor cells. It is deaminated to glutamate through a phosphate-dependent glutaminase. Glutamate is preferentially transaminated to  $\alpha$ -ketoglutarate that enters the TCA cycle afterwards. Even if glutamine is not oxidized completely, before extrusion from TCA cycle towards anabolic processes, it has to be metabolized to malate and pass the succinate-dehydrogenase complex. Therefore, in any case glutaminolysis must support complex II respiration. However, in HTB-126 GAL cells, complex II participated on the respiratory flux by a minor part. NADH reoxidation was detected as complex I respiration represents the major part of respiratory activity of HTB-126 GAL intact cells. NADH production in TCA cycle cannot operate without a source of Ac-CoA. Pyruvate as a precursor of Ac-CoA can be gained from culturing media, and synthesized by cytoplasmic or mitochondrial malic enzyme from malate (FIG 5-2).

Decreased proliferation rate can be subscribed to glutamine distribution among the ATP producing and the anabolic pathways. We suggest a dual role of glutamine in the glucose-free medium; being an energy source and also a metabolic precursor of synthetic pathways. Similarly to HTB-126 Glc cells, permeabilization of HTB-126 GAL cells revealed a strong limitation of complex II respiration in intact cells. Succinate as a respiratory substrate supports the complex II respiration to the higher extent than intrinsic substrates in intact cells (FIG 4-7).

Furthermore, preferential utilization of glucose over glutamine has been revealed in cancer cells. The Gln/GAL medium is widely used to stimulate cells to maximal OXPHOS performance, designated as the OXPHOS phenotype. Dependency of glucose-deprived cancer cells on OXPHOS has been demonstrated by the elevated sensitivity to mitochondrial inhibitors and by viability tests (FIG 4-1). In this study, however, we indicate the Gln/GAL medium as a “glucose-deprived” medium, since glucose and galactose are the only variable components of culturing media; the other components including pyruvate and glutamine remain constant. Glutaminolysis can, therefore, occur under both conditions (i.e. Glc and Gln/GAL medium) and cells could theoretically use oxidative metabolism to produce ATP both in Gln/GAL or Glc medium. Instead, breast cancer HTB-126 cells clearly prefer glucose to glutamine as an energy substrate when glucose is present, as indicated by the low respiratory flux of HTB-126 Glc cells. Indeed, HTB-126 cells do not exhibit any complex II-dependent respiration. We hypothesized, that presence of glucose has an inhibitory effect on respiration additionally to being a preferred energy source and FA precursor. Such an effect has already been described as Crabtree effect. This is demonstrated by an immediate increase of respiration upon removal of glucose medium and its replacement by Gln/GAL medium (FIG 4-14). In this case, we have obtained a 40% increase of respiratory rate due to the glucose removal. This 40% can be attributed to the removal of Crabtree effect. The remaining increase of respiration is attributed to more general adaptation that cells undergo in order to survive glucose deprivation. This adaptation

occurs, however, on the expense of cell growth rate, which is considerably retarded under the glucose-limiting conditions.

The Crabtree effect occurs in cancer and fast proliferating cells and is defined as the inhibition of respiration by the added glucose. During our experiments, glucose was either added, or removed by exchange of medium. To date, mechanism of Crabtree effect remains unresolved. A single mechanism has been set to explain cause of Crabtree effect in yeast, since a FBP overproduction upon glucose addition further inhibits complex I directly or indirectly (*Diaz-Ruiz et al. 2008*). It is not known, whether Crabtree effect and glycolytic cancer cells (observed in a Warburg effect) utilize the same enzyme isoforms and/or pathways.

The effective proof that the respiration and/or substrate flow to the mitochondria is inhibited has not yet been given. In this thesis it has been shown, that glucose presence significantly decreases the respiratory flux and depresses a respiratory capacity of the respiratory system. We suggest that molecular inhibition of individual respiratory complexes probably occurs. Two arguments are given to support this view. *i)* If a decrease of respiration was caused by the decreased substrate influx to the respiratory chain, maximum respiratory capacity (measured as uncoupled flux) would remain unchanged and corresponding UCR ratio would decrease concomitantly. Physical inhibition of electron transport and proton pumping could compromise maximum capacity of respiratory chain along with inhibition of routine flux. Similarly, when glucose was removed, we have obtained the increased respiratory flux, that exceeds former ETS capacity. In addition, further uncoupling is possible, indicating, that the previous inhibition was removed by glucose removal. *ii)* A decrease or increase of respiratory flux should be accompanied with concomitant decrease or increase of cellular  $P_{50}$ . We can predict that inhibition of components of ETS, including cytochrome-c oxidase population, occurs during glucose presence.  $P_{50}$  should be increased with increased enzymes turnover, but, instead, we can speculate about repression and derepression of respiratory enzymes and cytochrome-c oxidase. In other words,  $P_{50}$  obtained for HTB-126 Glc cells was higher because of the repression of enzymes of ETC but should have been lower. Of course, this hypothesis remains to be explored in more details.

Note that the control cells do not exhibit the Crabtree effect. For them, the respiratory flux and  $P_{50}$  does not change upon manipulation of glucose levels. Consequently, we can speculate about other cellular mechanism contributing to the observed Crabtree effect. Even if HTB-126 cells exhibit an intermediary phenotype with the respect to aerobic glycolysis and OXPHOS utilization and dependence on ATP production, they still exhibit a strong Crabtree effect. Because of this and since the definition of Crabtree effect is not so strict when we consider it occurs also in fast-growing normal cells. It is often demonstrated along with the Warburg effect, so we can take into account enzymatic pattern of cancer cells.

However, elevated respiratory capacity of HTB-126 GAL cells cannot be only attributed to removal of glucose inhibitory effect. The difference of respiratory capacity between of Glc and Gal0 group is attributed to removal of glucose inhibitory effect, since increased flux of GAL4 as compared to Gal0 group must have other origin. We proposed, that mitochondrial biogenesis was induced during adaptation to glucose starvation based on the elevated OXPHOS protein levels. Despite complex alterations of metabolic pattern upon shortage of glucose, the kinetic properties of respiratory chain, as reflected by  $P_{50}$ , remained within a comparable range. Normally, increased respiratory flux caused by increase of metabolic activity results in increased activity of respiratory complexes. Kinetic functioning of respiratory chain dependent on oxygen is described by  $P_{50}$ , which also expresses behavior of the system under hypoxic conditions occurring during aerobic-anoxic transition. Each point of the measurement actually represents the steady-state at the respective oxygen level, which would occur if cells were exposed to that particular oxygen level.  $P_{50}$  is not a constant value, but culminates with functional respiratory chain alterations. A basic example is the transition from state 2 to state 3 by ADP stimulation that causes increase of the respiratory flux as well as  $P_{50}$ .  $P_{50}$  value is directly dependent on turnover rate of enzymes of respiratory chain, mostly cytochrome-c oxidase. Excess capacity of cytochrome-c oxidase causes that the enzyme works far from its kinetic limits. Owing to the excess capacity, COX turnover rate is low even at the maximum aerobic performance and COX can therefore effectively regulate affinity to oxygen by flexibly regulating turnover rate. Increase of respiratory flux presumes increased metabolite influx into the mitochondria and increase of electron input of respiratory system in our conditions. Although respiration of HTB-126 GAL cells multiplied compared to HTB-126 Glc cells, the  $P_{50}$  values remained within a narrow range. This suggests that system works under similar kinetic conditions and that COX acts at a comparable turnover rate. Since the kinetic data predicate the increased quantity, we suggest that stimulation of biogenesis occurs as an adaptative response to the glucose removal in breast cancer cells. Increase of respiratory activity is basically attributed to elevated mitochondrial mass and enrichment of OXPHOS proteins. As a result, respiratory rate increases. In our system, biogenesis results in multiplying of mitochondria content with similar qualitative properties as such as  $P_{50}$ , RCR and UCR, indicating comparable fluxes through COX. Indeed, we have detected increase of OXPHOS proteins levels quantified by western-blot.

Taken together, regulation of respiratory flux of HTB-126 is multifactorial. Respiration can be inhibited by presence of glucose, substrate administration among respiratory and biosynthetic pathways and the level of mitochondrial biogenesis.

- **Hypoxia and its impact on energy metabolism**

Investigations of hypoxic adaptations have shown that cancer cells downregulate mitochondrial OXPHOS. In general, the neoplastic potential of cancer cells depends on high growth rates compared to the tissue of origin. We have followed how cell-type specific differences along with substrate-specific differences influence a cell growth. Cell proliferation under normoxia is not dependent on the presence of glucose, although glucose medium markedly improved the cell growth rate of both cancer and control cells (FIG 4-10). The role of mitochondria in survival of hypoxia remains questionable. The interesting difference between the control and cancer cells has arisen when viability tests were performed. We hypothesized, that compromised mitochondrial oxidative metabolism under hypoxia has an impact on the viability of cancer cells in 1% oxygen. Cancer cells in glucose medium are able to outgrow their normoxic counterparts in the same time scale. Since under normoxia, contact inhibition between cells is maintained, hypoxia resulted in stacking of cells.

Decreased respiration is reported after hypoxic exposure (2.3.2.1.2.). Decrease of respiration arises from expression changes which subsequently result in restriction of pyruvate influx into the mitochondria (*Kim et al. 2006a; Papandreou et al. 2006*). Observed acidification of medium indicates an increase of lactate-dehydrogenase activity, which is typically accompanied by the decrease of respiratory rate by channeling of pyruvate towards fermentative metabolism. Increased rate of glycolysis is plausible under these conditions considering increased growth of cancer cells in glucose and excessive medium acidification. Biogenesis of mitochondria has been reported to be affected in hypoxic cells, which usually originates from gene expression pattern dependent on HIF activation (*Zhang et al. 2007*). We have observed pronounced decrease of OXPHOS proteins in HTB-126 Glc by WB (FIG 4-12). Induction of mitochondrial degradation probably occurs as there was no substrate influx to the mitochondria. As a consequence, suppression of mitochondrial biogenesis can be induced. On the other side, both control cell types were able to survive hypoxic exposure, with decreased viability by 20%.

When glucose was missing, cancer HTB-126 GAL cells were unable to survive under hypoxic conditions. This is interesting difference, which seems trivial at the first sight. Mitochondrial respiration, mitochondrial P<sub>50</sub> and OXPHOS proteins content and did not change after hypoxia exposure. All data predicts that the decrease of mt biogenesis did not occur. Control cells under the same conditions were able to survive hypoxic conditions, only at the expense of decrease viability by 20%. These results are important in the context of mitochondrial biogenesis induction in numerous pathophysiological states where oxygen limitation triggers the up-regulation of OXPHOS. This compensatory adaptative response of normal tissues was described in physiological conditions of hypoxia, such as exercise training or high altitude (*Dufour et al. 2006; Essop 2007*). Moreover, it was reported, that during hypoxia, ADP/O ratio increases so that mitochondrial oxidative

phosphorylation works more efficiently (*Gnaiger et al. 2000*). Another possibility to overcome hypoxia is to rearrange mitochondrial composition to increase affinity to oxygen. This, however, we cannot confirm since  $P_{50}$  changes of HTB-125 GAL in response to hypoxia were not observed.

The  $P_{50}$  analysis revealed a decreased affinity of HTB-126 Glc cells to oxygen, which, along with extremely low flux indicates a strong impact of oxygen on respiration and decreased control by non-oxygen related factors, such as ADP. Increased sensitivity to oxygen would cause inhibition of respiration during incubation at 1% oxygen and inhibition of utilization of oxidative metabolism completely. Adaptations to hypoxia are well known under pathological conditions (cancer), such as channeling of substrates towards fermentative pathways and compromised mitochondrial metabolism. Decreased affinity to oxygen would be the next consequence and outcome of cellular adaptation to hypoxia. We have also observed a decrease of mitochondrial content by microscopy and western-blot. In cancer cells, inhibited biogenesis pathways in hypoxia have been reported previously (*Zhang et al. 2007*) and we support the respective hypothesis predicting these changes to occur. On contrary, no decrease of OXPHOS components has been observed in glucose-deprived medium. It remains to be determined, if HIF stabilization was affected due to the lack of glucose. Similarly, it is to be understood if mitochondrial degradation is the crucial step in hypoxic adaptations of cancer cells along with induction of glycolysis. In this case, suppression of mitochondrial degradation could be the crucial deficit for survival of cancer cells in 1% oxygen.

In conclusion, we hypothesize, that inhibition of biogenesis might be of equal importance in survival of hypoxia than induction of glycolysis in cancer cells. Cancer cells deprived of glucose can not survive hypoxic exposure, since inhibition of respiration is infeasible upon glucose deprivation. Mitochondria of HTB-126 GAL cells are not aberrant in glucose limiting conditions, but not able to provide energy to maintain cell growth under the hypoxia. However, what seem disadvantageous for under certain conditions can possibly be advantageous for cancer cells under different condition beyond the scope of this study, such as invasion to the glucose-limiting areas. Under our experimental conditions, glucose deficiency seems to be superior to oxygen deprivation.

- **Novel findings of presence of a wider pattern of UCPn isoforms in studied tissues**

Historically, UCP2 has been presented as a protein with wide expression pattern throughout the body tissues, since UCP3, UCP4 and UCP5 exhibited more specific expression pattern. This work has revealed wider expression of UCP5 isoform among studied tissues.

The advantage of quantitative real-time PCR with properly designed primers and probes lies in the unsurpassed selectivity and resolution that are not achievable by northern blotting or “chip screening”. Thus we provide reference data for the four UCP isoform transcript levels that span four to five orders of magnitude. The major question remains how the translation machinery deals with

transcripts of such varying and distinct abundance. Is the resulting translation only 10,000-fold less frequent when the transcript is of  $10^{-4}$  relative abundance? Alternatively, is there a threshold under which translation is nil for a very-low-abundance transcript? One could also speculate on the existence of a mechanism that upregulates the translation of low-abundance transcripts. Indeed, the observed disparity between the abundance of certain mRNAs and their corresponding protein products has been attributed to both translational down-regulation (*Pecqueur et al. 2001; Hurtaud et al. 2006*) and up-regulation (*Hurtaud et al. 2007*).

We have chosen a reference unit that is quite versatile and has practical implications, namely the unit of picograms of a given transcript per 10 ng of total isolated mRNA. One unit is close to the expected average transcription of 10,000 genes if all genes were transcribed equivalently. Only the level of the UCP2 transcript in the rat spleen approached one such unit. The selected reference gene, GAPDH, was transcribed in different tissues at levels between 1 and 10 pg per 10 ng of total isolated mRNA, corresponding to 0.01% to 0.1% of average gene representation (mRNA abundance). The finding that UCP2 transcript abundance was highest in the spleen points to important physiological role of UCP2 in macrophages (*Arsenijevic et al. 2000; Giardina et al. 2008*) and other white blood cell types, resident in the spleen. Similarly, the second highest UCP2 transcript amount, found in the rat and mouse lung, may reflect its predominating expression in the alveolar macrophages.

Attempting at least to find the order of magnitude proportionality between the measured levels of UCP mRNAs and their corresponding protein products, we can compare data for mouse spleen. These data show that UCP2 accounts for ~0.03% of all mitochondrial proteins (*Pecqueur et al. 2001*). Compare this to our finding of 0.002% for UCP2 transcript abundance (FIG 4-17 A). Considering on average 10,000 transcribed genes as 100%, these data would match only, if approximately each tenth transcribed protein in general was mitochondrial. The reported mouse lung UCP2 protein level (~0.002 % of rat mitochondrial proteins, *Pecqueur et al. 2001*) seems to correlate with a rather high estimated transcript abundance of 0.004% (FIG 4-17 A). Also, our [ $^3\text{H}$ ]GTP binding study reflecting UCP2 protein amounts (*Žáčková et al. 2003*) correlated better with the rat UCP2 transcript quantification (FIG 4-16 A), indicating rather high amounts of UCP2 protein in rat lung mitochondria, and 10-fold lower levels in rat liver mitochondria (*Žáčková et al. 2003*). However, specific quantification of UCP protein level and to distinct the specific isoform with an antibody is impossible to our knowledge. Indeed, the UCP2 mRNA was one order of magnitude greater in lung than in liver (FIG 4-16 A).

The results presented clearly show that the tissue-specific expression pattern of individual isoforms is quite distinct between rat and mouse and that the levels of mouse UCP4 and UCP5 transcripts, previously considered to be very low, are in fact quite high. The question, what

transcript amount tells us about the protein level and if the low transcription of UCPs isoforms really results in translation and maturation of the mitochondrial protein, is a matter of debate. The finding that numerous tissues express more than one UCP isoform sheds new light on previous studies in mice in which one isoform, UCP2 or UCP3, was ablated. Their reported interpretations might be yet inconclusive due to the possible expression of other UCP isoforms, if one considers the possibility of functional redundancy among UCPs. However, in attempt to see any compensatory increase of other UCP isoform after UCP2 ablation, no difference has been found (FIG 4-18).

Regarding the GAPDH quantification, large differences in transcript levels has been detected both in rat and mouse tissues. This supports numerous notions, that one should be careful when interpreting data normalized to GAPDH levels. GAPDH varies with various stimuli, such as carcinogenesis, for review see (*Bustin 2000*). In this study, however, GAPDH was used only as a reference gene.

- **Possible consequences of the presence of several UCPn isoforms in organs and tissues**

With the precision of calibrated real-time RT-PCR, we can claim that when no amplification proceeds within a sample there is definitively no transcript present, unless it exists in the range of attograms per 10 ng of total isolated mRNA. With such sensitivity, we identified UCP5 and UCP4 transcripts in all tested rat tissues, and we confirmed previous findings of UCP5 mRNA in mouse liver, lung, kidney, and spleen (*Sanchis et al. 1998*), heart (*Kim-Han et al. 2001; Sanchis et al. 1998; Yu et al. 2000*), and skeletal muscle (*Lengacher et al. 2004; Sanchis et al. 1998; Yu et al. 2000*). In the mouse these transcripts levels were very high (0.1 pg per 10 ng of total isolated mRNA, FIG 4-17 D). Also surprising was the rather high UCP4 mRNA level in mouse skeletal muscle (up to 0.1 pg per 10 ng of total isolated mRNA), being only five times lower than the UCP4 transcript level in mouse brain (4-17 D).

Patterns of the four studied UCP isoforms are remarkable for the heart and brain. In the rat heart, UCP2 mRNA was present at up to 0.5 units (i.e. pg per 10 ng of total isolated mRNA, the second highest level measured in our tissue set), exceeding by the two to three orders of magnitude the levels of UCP3, UCP4, and UCP5 transcripts. In turn, among mouse UCP mRNAs, UCP3 and UCP5 mRNAs were the most abundant and nearly equivalent, whereas UCP2 mRNA was 10-fold less abundant. For reason unknown, UCP2 seems to have been phylogenetically selected for its role in the rat heart, and likewise for UCP3 and UCP5 in the mouse heart. This finding puts into context the previous striking reports demonstrating the importance of UCP2 function in the rat heart (*Bo et al. 2008; McLeod et al. 2005*).

In the rat brain, the predominant rat UCP2 transcript and roughly half-abundant UCP5 transcript exceeded 10-fold the UCP4 mRNA levels, whereas, on the contrary, in the mouse brain the UCP4 transcript and the equally abundant UCP5 transcript outnumbered UCP2 mRNA by 10-fold. In conclusion, the tissue distribution of UCP isoform mRNAs differs between rat and mouse. As such, researchers must heed caution when extrapolating the findings/conclusions for one of these rodent species onto the other and when reporting on studies of single-gene knockout mice.

- **CIDEa protein redistribution**

The aim of this work was to elucidate cellular function of CIDEA protein, its possible migration between cellular compartments and organelles and thus attempted to determine its function in apoptosis. Our presumption raised from published data of possible pro-apoptotic function of CIDEa protein, which possess the sequence relation to DFF (*Inohara et al. 1998*). Proposed model suggests that homologous domain of CIDEa protein binds domains of DFF45 thus liberating DFF40 to execute apoptosis. Prerequisite of this model is localization of CIDE proteins into the cytosolic or nuclear fraction. Since it remains to be determined, if assembling of DFF proceed in cytosol or nucleus, and thus action of CIDE proteins in cytosolic or nuclear fraction is elusive.

Here, we determined mitochondrial localization of CIDEa protein overexpressed in cultured cells and nuclear redistribution upon apoptosis induction. However, the final proof that CIDE binds to the homologous domain on DFF45 hence opposing its inhibitory effect on the DFF40 nuclease, which subsequently cleaves DNA, is still missing. Owing to its mitochondrial and nuclear localization, and interaction with mitochondrial UCP1, CIDEA may serve as a sensor of energy production in mitochondria and after the signal, overcome caspases to induce apoptosis independently of caspases cleavage. However, it seems that this is not the case.

Our findings of CIDEa redistribution during incumbent apoptosis, induced either by CIDEa overexpression or in synergy with other apoptotic initiators, make the model, in which the DFF45/DFF40 complex enters the nucleus and CIDEa has to migrate therein to initiate its dissociation, more plausible. This model is also supported by the finding that the whole DFF45/DFF40 complex is imported more readily into the nucleus than its components separated (*Neimanis et al. 2007*). If CIDEa could disrupt the complex in the cytosol, migration of the free DFF40 nuclease into the nucleus might not be as intense. We found that migration of CIDEa into the nucleus is more apparent during apoptosis initiation by camptothecin and valinomycin and is independent of caspase activity. Hence, in some cell types (*Gummesson et al. 2007*), CIDEa may constitute another mitochondria-mediated apoptotic pathway alternative to others well-known, e.g. cytochrome c release (*Garrido et al. 2006*). Exact pathway leading to CIDEa redistribution is unclear; however, we perceive the different mode of action for each stimulus as the culprit for more

pronounced redistribution of CIDEa after valinomycin treatment (FIGs 4-26 and 4-27 ). Main target of camptothecin, DNA- topoisomerase I complex, is clearly located in the nucleus. Result of the interaction, i.e. DNA strand breaks, could lead to release of mitochondrial proteins, including CIDEa, only via indirect means and after nuclear signaling to mitochondria. On the other hand, valinomycin is a potassium uniporter that causes collapse of mitochondrial membrane potential and its whole transformation into  $\Delta\text{pH}$  (Dlasková *et al.* 2008b), hence it likely triggers release of mitochondrial proteins as a result of mitochondrial network transformation.

Pro-apoptotic proteins Bax and Bak were shown to be involved in normal as well as apoptotic mitochondrial morphogenesis (Karbowski *et al.* 2006). But we think that role of CIDEa in apoptosis resembles that of cytochrome c rather than that of Bax/Bak. Previously, the overexpression of CIDEb in COS-1 cells was linked to apoptosis and those studies supported the pro-apoptotic role of the protein (Chen *et al.* 2000). Our data agree with the pro-apoptotic role of CIDEa, if present in high amounts in HeLa cells, where expression of native CIDEa is absent. In contrast, induction of CIDEa in mouse liver (Viswakarma *et al.* 2007) or brown fat (Liang *et al.* 2003; Zhou *et al.* 2003b) was not accompanied by an increase in apoptosis. This can be explained by the existence of a hypothetical co-factor of mitochondrial origin present in certain cell types and capable of preventing CIDEa-dependent apoptosis, suggesting regulation of CIDEa export from mitochondria. A co-factor could be a protein binding CIDEa. Previously, CIDEa was reported to interact with mitochondrial uncoupling protein UCP1 present nearly exclusively in brown adipose tissue, a tissue in which CIDEa did not induce apoptosis (Zhou *et al.* 2003b). Our attempts to verify the proposed interaction between CIDEa and UCP1 using surface plasmon resonance spectroscopy are so far inconclusive (Ježek and co-workers, unpublished data). Similarly, we do not have any evidence that CIDEa may interact with UCP1 homolog, UCP2, despite the presence of UCP2 in HeLa cells (Valoušková and co-workers, unpublished results). Nevertheless, our data (FIG C-26) support the mitochondrial origin of the postulated co-factor, since overexpressed CIDEa was found to be predominantly localized in mitochondria (Zhou *et al.* 2003b), similarly to its homolog CIDEb (Chen *et al.* 2000; Liang *et al.* 2003) or CIDE3 (Liang *et al.* 2003). Mitochondrial localization of CIDE proteins may thus serve as sequestering of potentially dangerous proteins much like others previously demonstrated (Kim *et al.* 2006b) that would otherwise put cells into peril of an unavoidable apoptosis.

Release of CIDEs from mitochondria and their migration to the nucleus would be then linked to apoptosis. The “resting position” would be represented by CIDE association with the postulated co-factor. Mechanisms of CIDE release from their supposed location within an intermembrane space of mitochondria are unknown, but hitching a ride on small mitochondrial “rafts” as proposed by Skulachev (Skulachev *et al.* 2004) and hypothesized for ganglioside GD3 (Garofalo *et al.* 2007) is possible. Certain stimulus must exist that causes CIDE to be exported out of mitochondria. Stimulus

may be represented by binding to another regulatory protein exhibiting higher affinity than a docking site, by glycosylation (de-glycosylation), by phosphorylation (de-phosphorylation), by redox regulations, etc.

One can also speculate that CIDE export across the outer mitochondrial membrane may be accomplished by transport through multimers of Bax/Bak or through voltage-dependent anion channel complexes with ceramide, a mechanism either similar or distinct from the ways used by other pro-apoptotic messengers such as cytochrome c, apoptosis-inducing factor, or endonuclease G (*Kim et al. 2006b*). Alternatively (similar to cytochrome c release), relocation of CIDE from mitochondria to cytosol may happen during frequent fission events in concert with participation of pro-fission proteins, such as DRP1, or inhibition of pro-fusion proteins, such as OPA1. OPA1 cleavage to an inactive form induced by potential collapse has been reported to explain an uncoupler-mediated mitochondrial fission, however we have shown that decreasing oxidative phosphorylation is required for initiation of fission (*Plecitá-Hlavatá et al. 2008*).

The CIDE transfer into the nucleus should have serious consequences. It would represent important feedback information signaling of e.g. energetic status towards modulation or even execution of apoptosis. As we demonstrated, the CIDE pathway is caspase-independent.

## 6. CONCLUSIONS

1. Cancer cells exhibit low respiratory flux in the presence of glucose. Glucose deprivation resulted in elevated respiration. In this thesis, I proposed that three distinct mechanisms regulate mitochondrial respiration of cancer cells: *i*) glucose inhibition, *ii*) substrate flux at the level of TCA cycle, *iii*) level of mitochondrial mass.
2. Crabtree effect exists in breast cancer cells. In this study it was clearly shown, that glucose presence possesses the inhibitory effect on the mitochondrial respiration. Therefore, Crabtree effect can be interpreted as an active inhibition of respiration by glucose at the level of mitochondrial respiratory enzymes.
3. Survival of oxygen limitation of breast cancer cells is dependent on glucose presence. Further, lack of glucose inhibits the downregulation of mitochondrial biogenesis under hypoxia.
4. Individual UCP isoform mRNA levels varied by up to four orders of magnitude in rat and mouse tissues.
5. UCP2 mRNA content is relatively high (0.4 to 0.8 pg per 10 ng of total mRNA) in rat spleen, rat and mouse lung, and rat heart.
6. Levels of the same order of magnitude were found for UCP3 mRNA in rat and mouse skeletal muscle, for UCP4 and UCP5 mRNA in mouse brain, and for UCP2 and UCP5 mRNA in mouse white adipose tissue.
7. Significant differences in pattern were found for rat vs. mouse tissues, such as the dominance of UCP3/UCP5 vs. UCP2 transcript in mouse heart and vice versa in rat heart; or UCP2 (UCP5) dominance in rat brain contrary to 10-fold higher UCP4 and UCP5 dominance in mouse brain.
8. We have confirmed mitochondrial localization of CIDEa and the role of CIDE-C domain in mitochondrial localization.
9. We observed redistribution, enhanced upon treatment with camptothecin or valinomycin, of CIDEa from mitochondria to nucleus.
10. We hypothesize that CIDEa is sequestered in mitochondria while transfer of this protein from mitochondria into the nucleus intensifies or even initiates apoptosis.

## 7. SUMMARY

Non-canonical bioenergetics concerns with those physiological and pathophysiological situations under which ATP synthesis is suppressed. This thesis brings an outcome of three types of studies within the field of the non-canonical bioenergetics, investigating specific bioenergetic phenotypes of cancer cells, on one hand; and a role of mitochondrial uncoupling proteins as deduced from their transcript distribution in various tissues and organs; plus a role of a novel and likely pro-apoptotic factor CIDEa in mitochondria.

Cancer cells generally present abnormal bioenergetic properties including an elevated glucose uptake, a high glycolysis and a poorly efficient oxidative phosphorylation system. However, the determinants of cancer cells metabolic reprogramming remain unknown. The main question in this project was how environmental conditions *in vivo* can influence functioning of mitochondrial OXPHOS, because details of mitochondrial bioenergetics of cancer cells is poorly documented. We have combined two conditions, namely glucose and oxygen deprivation, to measure their potential interaction. We examined the impact of glucose deprivation and oxygen deprivation on cell survival, overall bioenergetics and OXPHOS protein expression. As a model, we have chosen a human breast carcinoma (HTB-126) and appropriate control (HTB-125) cultured cells, as large fraction of breast malignancies exhibit hypoxic tumor regions with low oxygen concentrations and poor glucose delivery. The results demonstrate that glucose presence or absence largely influence functioning of mitochondrial oxidative phosphorylation. The level of mitochondrial respiration capacity is regulated by glucose; by Crabtree effect, by energy substrate channeling towards anabolic pathways that support cell growth and by mitochondrial biogenesis pathways. Both oxygen deprivation and glucose deprivation can remodel the OXPHOS system, albeit in opposite directions. As an adaptive response to hypoxia, glucose inhibits mitochondrial oxidative phosphorylation to the larger extent than in normoxia. We concluded that the energy profile of cancer cells can be determined by specific balance between two main environmental stresses, glucose and oxygen deprivation. Thus, variability of intratumoral environment might explain the variability of cancer cells' bioenergetic profile.

Mitochondrial uncoupling proteins are proteins of inner mitochondrial membrane that uncouple respiration from ATP synthesis by their protonophoric activity. Originally determined tissue distribution seems to be invalid, since novel findings show that UCP1 is not restricted exclusively to brown fat and that originally considered brain-specific isoforms UCP4 and UCP5 might have wider tissue distribution. Hence, in second part of this thesis, I discuss consequences of findings of UCPn transcripts in the studied mouse and rat tissues. We have shown that mRNA of UCPn varies up to four orders of magnitude in rat and mouse tissues with highest expression in rat spleen, rat and mouse lung, and rat heart. Levels of the same order of magnitude were found for UCP3 mRNA in rat

and mouse skeletal muscle, for UCP4 and UCP5 mRNA in mouse brain, and for UCP2 and UCP5 mRNA in mouse white adipose tissue. Further, we have shown that expression pattern of UCPn varies between animal species, rat versus mouse, such as the dominance of UCP3/UCP5 vs. UCP2 transcript in mouse heart and vice versa in rat heart; or UCP2 (UCP5) dominance in rat brain contrary to 10-fold higher UCP4 and UCP5 dominance in mouse brain.

Side pathways of apoptosis were revealed recently, namely those including proteins with homology to nuclease DFF responsible for apoptotic DNA cleavage, CIDE. Migration of CIDEs from mitochondria to nucleus (or to cytosol) has not been reported until 2008, except for cases with staurosporine or etoposide. We have shown for the first time that under conditions of spontaneous apoptosis due to CIDEa overexpression in HeLa cells, adapted for a tetracycline-inducible CIDEa expression, a portion of mitochondria-localized CIDEa molecules migrates to cytosol or nucleus.

## 8. REFERENCES

- Adams, A. E., Carroll, A. M., Fallon, P. G. & Porter, R. K. (2008a). Mitochondrial uncoupling protein 1 expression in thymocytes. *Biochimica et Biophysica Acta (BBA) - Bioenergetics*, *1777*, 772-776.
- Adams, A. E., Hanrahan, O., Nolan, D. N., Voorheis, H. P., Fallon, P. & Porter, R. K. (2008b). Images of mitochondrial UCP 1 in mouse thymocytes using confocal microscopy. *Biochimica et Biophysica Acta (BBA) - Bioenergetics*, *1777*, 115-117.
- Affourtit, C., Crichton, P., Parker, N. & Brand, M. (2007). Novel uncoupling proteins. *Novartis Found Symp*, *287*, 70-80.
- Alán, L., Smolková, K., Kronusová, E., Šantorová, J. & Ježek, P. (2009). Absolute levels of transcripts for mitochondrial uncoupling proteins UCP2, UCP3, UCP4, and UCP5 show different patterns in rat and mice tissues. *Journal of Bioenergetics and Biomembranes*, *41*, 71-78.
- Alirol, E. & Martinou, J. C. (2006). Mitochondria and cancer: is there a morphological connection? *Oncogene*, *25*, 4706-4716.
- Aragones, J., Schneider, M., Van Geyte, K., Fraisl, P., Dresselaers, T., Mazzone, M., Dirx, R., Zacchigna, S., Lemieux, H., Jeoung, N. H., Lambrechts, D., Bishop, T., Lafuste, P., Diez-Juan, A., Harten, S. K., Van Noten, P., De Bock, K., Willam, C., Tjwa, M., Grosfeld, A., Navet, R., Moons, L., Vandendriessche, T., Deroose, C., Wijeyekoon, B., Nuyts, J., Jordan, B., Silasi-Mansat, R., Lupu, F., Dewerchin, M., Pugh, C., Salmon, P., Mortelmans, L., Gallez, B., Gorus, F., Buyse, J., Sluse, F., Harris, R. A., Gnaiger, E., Hespel, P., Van Hecke, P., Schuit, F., Van Veldhoven, P., Ratcliffe, P., Baes, M., Maxwell, P. & Carmeliet, P. (2008). Deficiency or inhibition of oxygen sensor Phd1 induces hypoxia tolerance by reprogramming basal metabolism. *Nat Genet*, *40*, 170-180.
- Arsenijevic, D., Onuma, H., Pecqueur, C., Raimbault, S., Manning, B., Miroux, B., Couplan, E., Alves-Guerra, M., Gubern, M., Surwit, R., Bouillaud, F., Richard, D., Collins, S. & Ricquier, D. (2000). Disruption of the uncoupling protein 2 gene in mice reveals a role in immunity and reactive oxygen species production. *Nat Genet*, *26*, 435-439.
- Auer, F., Röper, B., Scheich, D., Molls, M., Eiermann, W. & Raab, G. (2007). Technical Improvement of pO<sub>2</sub> Measurements in Breast Cancer. *Strahlentherapie und Onkologie*, *183*, 265-270.
- Baker, M. J., Frazier, A. E., Gulbis, J. M. & Ryan, M. T. (2007). Mitochondrial protein-import machinery: correlating structure with function. *Trends in Cell Biology*, *17*, 456-464.
- Baudelet, C. & Gallez, B. (2002). How does blood oxygen level-dependent (BOLD) contrast correlate with oxygen partial pressure (p<sub>O<sub>2</sub></sub>) inside tumors? *Magnetic Resonance in Medicine*, *48*, 980-986.
- Bauer, D. E., Hatzivassiliou, G., Zhao, F., Andreadis, C. & Thompson, C. B. (2005). ATP citrate lyase is an important component of cell growth and transformation. *Oncogene*, *24*, 6314-6322.
- Bayascas, J. R., Yuste, V. J., Solé, C., Sánchez-López, I., Segura, M. F., Perera, R. & Comella, J. X. (2004). Characterization of splice variants of human caspase-activated DNase with CIDE-N structure and function. *FEBS Letters*, *566*, 234-240.
- Beck, V., Jaburek, M., Breen, E. P., Porter, R. K., Jezek, P. & Pohl, E. E. (2006). A new automated technique for the reconstitution of hydrophobic proteins into planar bilayer membranes. Studies of human recombinant uncoupling protein 1. *Biochimica et Biophysica Acta (BBA) - Bioenergetics*, *1757*, 474-479.
- Beck, V., Jaburek, M., Demina, T., Rupprecht, A., Porter, R. K., Jezek, P. & Pohl, E. E. (2007). Polyunsaturated fatty acids activate human uncoupling proteins 1 and 2 in planar lipid bilayers. *FASEB J.*, *21*, 1137-1144.
- Bell, E. L., Klimova, T. A., Eisenbart, J., Moraes, C. T., Murphy, M. P., Budinger, G. R. S. & Chandel, N. S. (2007). The Qo site of the mitochondrial complex III is required for the transduction of hypoxic signaling via reactive oxygen species production. *J. Cell Biol.*, *177*, 1029-1036.
- Bellance, N., Benard, G., Furt, F., Begueret, H., Smolková, K., Passerieux, E., Delage, J., Baste, J., Moreau, P. & Rossignol, R. (2009a). Bioenergetics of lung tumors: Alteration of mitochondrial biogenesis and respiratory capacity. *Int J Biochem Cell Biol*, *In press*.
- Bellance, N., Lestienne, P. & Rossignol, R. (2009b). Mitochondria: from bioenergetics to the metabolic regulation of carcinogenesis *Frontiers in Bioscience*, *14*, 4015-4034.
- Benard, G., Bellance, N., James, D., Parrone, P., Fernandez, H., Letellier, T. & Rossignol, R. (2007). Mitochondrial bioenergetics and structural network organization. *J Cell Sci*, *120*, 838-848.
- Benard, G. & Rossignol, R. (2008). Ultrastructure of the Mitochondrion and Its Bearing on Function and Bioenergetics. *Antioxidants & Redox Signaling*, *10*, 1313.
- Bentzen, L., Keiding, S., Nordmark, M., Falborg, L., Hansen, S. B., Keller, J., Nielsen, O. S. & Overgaard, J. (2003). Tumour oxygenation assessed by 18F-fluoromisonidazole PET and polarographic needle electrodes in human soft tissue tumours. *Radiotherapy and Oncology*, *67*, 339-344.
- Beppu, T., Kamada, K., Yoshida, Y., Arai, H., Ogasawara, K. & Ogawa, A. (2002). Change of Oxygen Pressure in Glioblastoma Tissue Under Various Conditions. *Journal of Neuro-Oncology*, *58*, 47-52.
- Blanc, J., Alves-Guerra, M. C., Esposito, B., Rousset, S., Gourdy, P., Ricquier, D., Tedgui, A., Miroux, B. & Mallat, Z. (2003). Protective Role of Uncoupling Protein 2 in Atherosclerosis. *Circulation*, *107*, 388-390.
- Bo, H., Jiang, N., Ma, G., Qu, J., Zhang, G., Cao, D., Wen, L., Liu, S., Ji, L. L. & Zhang, Y. (2008). Regulation of mitochondrial uncoupling respiration during exercise in rat heart: Role of reactive oxygen species (ROS) and uncoupling protein 2. *Free Radical Biology and Medicine*, *44*, 1373-1381.
- Bogenhagen, D. F., Rousseau, D. & Burke, S. (2008). The Layered Structure of Human Mitochondrial DNA Nucleoids. *J. Biol. Chem.*, *283*, 3665-3675.

- Borenfreund, E. & Puerner, J. (1985). Toxicity determined in vitro by morphological alterations and neutral red absorption. *Toxicol Lett.*, *24*, 119-124.
- Boss, O., Samec, S., Paoloni-Giacobino, A., Rossier, C., Dulloo, A., Seydoux, J., Muzzin, P. & Giacobino, J.-P. (1997). Uncoupling protein-3: a new member of the mitochondrial carrier family with tissue-specific expression. *FEBS Letters*, *408*, 39-42.
- Bradford, M. M. (1976). A rapid and sensitive method for the quantitation of microgram quantities of protein utilizing the principle of protein-dye binding. *Anal Biochem.*, *72*, 248-254.
- Brand, M. D., Affourtit, C., Esteves, T. C., Green, K., Lambert, A. J., Miwa, S., Pakay, J. L. & Parker, N. (2004). Mitochondrial superoxide: production, biological effects, and activation of uncoupling proteins. *Free Radical Biology and Medicine*, *37*, 755-767.
- Brandon, M., Baldi, P. & Wallace, D. C. (2006). Mitochondrial mutations in cancer. *Oncogene*, *25*, 4647-4662.
- Brizel, D. M., Scully, S. P., Harrelson, J. M., Layfield, L. J., Bean, J. M., Prosnitz, L. R. & Dewhirst, M. W. (1996). Tumor Oxygenation Predicts for the Likelihood of Distant Metastases in Human Soft Tissue Sarcoma. *Cancer Res*, *56*, 941-943.
- Brizel, D. M., Sibley, G. S., Prosnitz, L. R., Scher, R. L. & Dewhirst, M. W. (1997). Tumor hypoxia adversely affects the prognosis of carcinoma of the head and neck. *International Journal of Radiation Oncology\*Biophysics\*Physics*, *38*, 285-289.
- Brookes, P. S., Parker, N., Buckingham, J. A., Vidal-Puig, A., Halestrap, A. P., Gunter, T. E., Nicholls, D. G., Bernardi, P., Lemasters, J. J. & Brand, M. D. (2008). UCPs unlikely calcium porters. *Nat Cell Biol*, *10*, 1235-1237.
- Brunelle, J. K., Santore, M. T., Budinger, G. R. S., Tang, Y., Barrett, T. A., Zong, W.-X., Kandel, E., Keith, B., Simon, M. C., Thompson, C. B., Hay, N. & Chandel, N. S. (2004). c-Myc Sensitization to Oxygen Deprivation-induced Cell Death Is Dependent on Bax/Bak, but Is Independent of p53 and Hypoxia-inducible Factor-1. *J. Biol. Chem.*, *279*, 4305-4312.
- Burd, R., Wachsberger, P. R., Biaglow, J. E., Wahl, M. L., Lee, I. & Leeper, D. B. (2001). Absence of Crabtree Effect in Human Melanoma Cells Adapted to Growth at Low pH: Reversal by Respiratory Inhibitors. *Cancer Res*, *61*, 5630-5635.
- Bustin, S. (2000). Absolute quantification of mRNA using real-time reverse transcription polymerase chain reaction assays. *J Mol Endocrinol*, *25*, 169-193.
- Buzzai, M., Bauer, D. E., Jones, R. G., DeBerardinis, R. J., Hatzivassiliou, G., Elstrom, R. L. & Thompson, C. B. (2005). The glucose dependence of Akt-transformed cells can be reversed by pharmacologic activation of fatty acid [beta]-oxidation. *Oncogene*, *24*, 4165-4173.
- Cairns, R. A., Kalliomaki, T. & Hill, R. P. (2001). Acute (Cyclic) Hypoxia Enhances Spontaneous Metastasis of KHT Murine Tumors. *Cancer Res*, *61*, 8903-8908.
- Calcagno, D. Q., Leal, M. F., Assumpção, P. P., Cardoso Smith, M. d. A. & Rodríguez, B. R. (2008). MYC and gastric adenocarcinoma carcinogenesis. *World J Gastroenterol*, *14*, 5962-5968.
- Cannon, B., Shabalina, I. G., Kramarova, T. V., Petrovic, N. & Nedergaard, J. (2006). Uncoupling proteins: A role in protection against reactive oxygen species--or not? *Biochimica et Biophysica Acta (BBA) - Bioenergetics*, *1757*, 449-458.
- Carcamo, J. M., Pedraza, A., Borquez-Ojeda, O. & Golde, D. W. (2002). Vitamin C Suppresses TNF $\alpha$ -Induced NF $\kappa$ B Activation by Inhibiting I $\kappa$ B $\alpha$  Phosphorylation *Biochemistry*, *41*, 12995-13002.
- Cardenas-Navia, L. I., Yu, D., Braun, R. D., Brizel, D. M., Secomb, T. W. & Dewhirst, M. W. (2004). Tumor-dependent Kinetics of Partial Pressure of Oxygen Fluctuations during Air and Oxygen Breathing. *Cancer Res*, *64*, 6010-6017.
- Carroll, A. M., Haines, L. R., Pearson, T. W., Brennan, C., Breen, E. P. & Porter, R. K. (2004). Immunodetection of UCP1 in rat thymocytes. *J Biochem. Soc. Trans*, *32*, 1066-1067.
- Carroll, A. M., Haines, L. R., Pearson, T. W., Fallon, P. G., Walsh, C. M., Brennan, C. M., Breen, E. P. & Porter, R. K. (2005). Identification of a Functioning Mitochondrial Uncoupling Protein 1 in Thymus. *J. Biol. Chem.*, *280*, 15534-15543.
- Clay Montier, L. L., Deng, J. J. & Bai, Y. (2009). Number matters: control of mammalian mitochondrial DNA copy number. *Journal of Genetics and Genomics*, *36*, 125-131.
- Cole, M. D. & Cowling, V. H. (2008). Transcription-independent functions of MYC: regulation of translation and DNA replication. *Nat Rev Mol Cell Biol*, *9*, 810-815.
- Collingridge, D. R., Piepmeier, J. M., Rockwell, S. & Knisely, J. P. S. (1999). Polarographic measurements of oxygen tension in human glioma and surrounding peritumoural brain tissue. *Radiotherapy and Oncology*, *53*, 127-131.
- Corn, P. G., Ricci, M. S., Scata, K. A., Arsham, A. M., Simon, M. C., Dicker, D. T. & El-Deiry, W. S. (2005). Mxi1 is Induced by Hypoxia in a HIF-1-Dependent Manner and Protects Cells from c-Myc-Induced Apoptosis. *Cancer Biology & Therapy*, *4*, 1285-1294.
- Costa, A. D. T. & Vercesi, A. E. (1996). Evidence for Anion-translocating Plant Uncoupling Mitochondrial Protein in Potato Mitochondria. *J. Biol. Chem.*, *271*, 32743-32748.
- Cowling, V. H. & Cole, M. D. (2006). Mechanism of transcriptional activation by the Myc oncoproteins. *Seminars in Cancer Biology*, *16*, 242-252.
- Cuezva, J., Sánchez-Aragó, M., Sala, S., Blanco-Rivero, A. & Ortega, Á. (2007). A message emerging from development: the repression of mitochondrial  $\beta$ -F1-ATPase expression in cancer. *Journal of Bioenergetics and Biomembranes*, *39*, 259-265.
- Cuezva, J. M., Krajewska, M., de Heredia, M. L., Krajewski, S., Santamaria, G., Kim, H., Zapata, J. M., Marusawa, H., Chamorro, M. & Reed, J. C. (2002). The Bioenergetic Signature of Cancer: A Marker of Tumor Progression. *Cancer Res*, *62*, 6674-6681.

- De Souza, C. T., Araujo, E. P., Stoppiglia, L. F., Pauli, J. R., Ropelle, E., Rocco, S. A., Marin, R. M., Franchini, K. G., Carneiro, J. B., Saad, M. J., Boschero, A. C., Carneiro, E. M. & Velloso, L. A. (2007). Inhibition of UCP2 expression reverses diet-induced diabetes mellitus by effects on both insulin secretion and action. *FASEB J.*, *21*, 1153-1163.
- DeBerardinis, R. J., Lum, J. J., Hatzivassiliou, G. & Thompson, C. B. (2008). The Biology of Cancer: Metabolic Reprogramming Fuels Cell Growth and Proliferation. *Cell Metabolism*, *7*, 11-20.
- DeBerardinis, R. J., Mancuso, A., Daikhin, E., Nissim, I., Yudkoff, M., Wehrli, S. & Thompson, C. B. (2007). Beyond aerobic glycolysis: Transformed cells can engage in glutamine metabolism that exceeds the requirement for protein and nucleotide synthesis. *Proceedings of the National Academy of Sciences*, *104*, 19345-19350.
- Derdak, Z., Mark, N. M., Beldi, G., Robson, S. C., Wands, J. R. & Baffy, G. (2008). The Mitochondrial Uncoupling Protein-2 Promotes Chemoresistance in Cancer Cells. *Cancer Res*, *68*, 2813-2819.
- Dewhirst, M. W., Braun, R. D. & Lanzen, J. L. (1998). Temporal changes in pO<sub>2</sub> of R3230Ac tumors in fischer-344 rats. *International Journal of Radiation Oncology\*Biophysics*, *42*, 723-726.
- Diaz-Ruiz, R., Averet, N., Araiza, D., Pinson, B., Uribe-Carvajal, S., Devin, A. & Rigoulet, M. (2008). Mitochondrial Oxidative Phosphorylation Is Regulated by Fructose 1,6-Bisphosphate: A POSSIBLE ROLE IN CRABTREE EFFECT INDUCTION? *J. Biol. Chem.*, *283*, 26948-26955.
- Dlasková, A., Hlavatá, L., Jezek, J. & Jezek, P. (2008a). Mitochondrial Complex I superoxide production is attenuated by uncoupling. *The International Journal of Biochemistry & Cell Biology*, *40*, 2098-2109.
- Dlasková, A., Hlavatá, L. & Jezek, P. (2008b). Oxidative stress caused by blocking of mitochondrial Complex I H<sup>+</sup> pumping as a link in aging/disease vicious cycle. *The International Journal of Biochemistry & Cell Biology*, *40*, 1792-1805.
- Dlasková, A., Spacek, T., Skobisová, E., Santorová, J. & Jezek, P. (2006). Certain aspects of uncoupling due to mitochondrial uncoupling proteins in vitro and in vivo. *Biochimica et Biophysica Acta (BBA) - Bioenergetics*, *1757*, 467-473.
- Dufour, S. P., Ponsot, E., Zoll, J., Doutreleau, S., Lonsdorfer-Wolf, E., Geny, B., Lampert, E., Fluck, M., Hoppeler, H., Billat, V., Mettauer, B., Richard, R. & Lonsdorfer, J. (2006). Exercise training in normobaric hypoxia in endurance runners. I. Improvement in aerobic performance capacity. *J Appl Physiol*, *100*, 1238-1248.
- Ebert, B. L. & Bunn, H. F. (1998). Regulation of Transcription by Hypoxia Requires a Multiprotein Complex That Includes Hypoxia-Inducible Factor 1, an Adjacent Transcription Factor, and p300/CREB Binding Protein. *Mol. Cell. Biol.*, *18*, 4089-4096.
- Ekstrand, M. I., Falkenberg, M., Rantanen, A., Park, C. B., Gaspari, M., Hultenby, K., Rustin, P., Gustafsson, C. M. & Larsson, N.-G. (2004). Mitochondrial transcription factor A regulates mtDNA copy number in mammals. *Hum. Mol. Genet.*, *13*, 935-944.
- Elstrom, R. L., Bauer, D. E., Buzzai, M., Karnauskas, R., Harris, M. H., Plas, D. R., Zhuang, H., Cinalli, R. M., Alavi, A., Rudin, C. M. & Thompson, C. B. (2004). Akt Stimulates Aerobic Glycolysis in Cancer Cells. *Cancer Res*, *64*, 3892-3899.
- Emerling, B. M., Weinberg, F., Snyder, C., Burgess, Z., Mutlu, G. M., Viollet, B., Budinger, G. R. S. & Chandel, N. S. (2009). Hypoxic activation of AMPK is dependent on mitochondrial ROS but independent of an increase in AMP/ATP ratio. *Free Radical Biology and Medicine*, *46*, 1386-1391.
- Emre, Y., Hurtaud, C., Nübel, T., Criscuolo, F., Ricquier, D. & Cassard-doulicier, A.-M. (2007). Mitochondria contribute to LPS-induced MAPK activation via uncoupling protein UCP2 in macrophages *Biochem J*, *402*, 271-278.
- Erdtmann, L., Franck, N., Lerat, H., Le Seyec, J., Gilot, D., Cannie, I., Gripon, P., Hibner, U. & Guguen-Guillouzo, C. (2003). The Hepatitis C Virus NS2 Protein Is an Inhibitor of CIDE-B-induced Apoptosis. *J. Biol. Chem.*, *278*, 18256-18264.
- Erickson, K., Braun, R. D., Yu, D., Lanzen, J., Wilson, D., Brizel, D. M., Secomb, T. W., Biaglow, J. E. & Dewhirst, M. W. (2003). Effect of Longitudinal Oxygen Gradients on Effectiveness of Manipulation of Tumor Oxygenation. *Cancer Res*, *63*, 4705-4712.
- Essop, M. F. (2007). Cardiac metabolic adaptations in response to chronic hypoxia. *J Physiol.*, *584*, 715-726.
- Esteves, T. C. & Brand, M. D. (2005). The reactions catalysed by the mitochondrial uncoupling proteins UCP2 and UCP3. *Biochimica et Biophysica Acta (BBA) - Bioenergetics*, *1709*, 35-44.
- Fan, C., Li, Q., Ross, D. & Engelhardt, J. F. (2002). Tyrosine phosphorylation of IκBα activates NF-κB through a redox-regulated and c-Src-dependent mechanism following hypoxia/reoxygenation. *J. Biol. Chem.*, *M206718200*.
- Fantin, V. R., St-Pierre, J. & Leder, P. (2006). Attenuation of LDH-A expression uncovers a link between glycolysis, mitochondrial physiology, and tumor maintenance. *Cancer Cell*, *9*, 425-434.
- Feige, J. N. & Auwerx, J. (2007). Transcriptional coregulators in the control of energy homeostasis. *Trends in Cell Biology*, *17*, 292-301.
- Fernandez-Silva, P., Enriquez, J. & Montoya, J. (2003). Replication and transcription of mammalian mitochondrial DNA. *Experimental Physiology*, *88*, 41-56.
- Finocchietto, P., Barreyro, F., Holod, S., Peralta, J., Franco, M. a. C., MÃ©ndez, C., Converso, D. P., EstÃ©vez, A., Carreras, M. C. & Poderoso, J. J. (2008). Control of Muscle Mitochondria by Insulin Entails Activation of Akt2-mtNOS Pathway: Implications for the Metabolic Syndrome. *PLoS ONE*, *3*, e1749.
- Fisler, J. & Warden, C. (2006). Uncoupling proteins, dietary fat and the metabolic syndrome. *Nutrition & Metabolism*, *3*, 38.
- Fleury, C., Neverova, M., Collins, S., Raimbault, S., Champigny, O., Levi-Meyrueis, C., Bouillaud, F., Seldin, M. F., Surwit, R. S., Ricquier, D. & Warden, C. H. (1997). Uncoupling protein-2: a novel gene linked to obesity and hyperinsulinemia. *Nat Genet*, *15*, 269-272.
- Forti, S., Scanlan, M. J., Invernizzi, A., Castiglioni, F., Pupa, S., Agresti, R., Fontanelli, R., Morelli, D., Old, L. J., Pupa, S. M. & Ménard, S. (2002). Identification of Breast Cancer-Restricted Antigens by Antibody Screening of SKBR3 cDNA Library Using a Preselected Patient's Serum. *Breast Cancer Research and Treatment*, *73*, 245-256.

- Frontini, A., Rousset, S., Cassard-Doulcier, A.-M., Zingaretti, C., Ricquier, D. & Cinti, S. (2007). Thymus Uncoupling Protein 1 Is Exclusive to Typical Brown Adipocytes and Is Not Found in Thymocytes. *J. Histochem. Cytochem.*, *55*, 183-189.
- Fukuda, R., Zhang, H., Kim, J.-w., Shimoda, L., Dang, C. V. & Semenza, Gregg L. (2007). HIF-1 Regulates Cytochrome Oxidase Subunits to Optimize Efficiency of Respiration in Hypoxic Cells. *Cell*, *129*, 111-122.
- Furuta, E., Pai, S. K., Zhan, R., Bandyopadhyay, S., Watabe, M., Mo, Y.-Y., Hirota, S., Hosobe, S., Tsukada, T., Miura, K., Kamada, S., Saito, K., Iizumi, M., Liu, W., Ericsson, J. & Watabe, K. (2008). Fatty Acid Synthase Gene Is Up-regulated by Hypoxia via Activation of Akt and Sterol Regulatory Element Binding Protein-1. *Cancer Res*, *68*, 1003-1011.
- Gao, P., Zhang, H., Dinavahi, R., Li, F., Xiang, Y., Raman, V., Bhujwala, Z. M., Felsher, D. W., Cheng, L., Pevsner, J., Lee, L. A., Semenza, G. L. & Dang, C. V. (2007). HIF-Dependent Antitumorigenic Effect of Antioxidants In Vivo. *Cancer Cell*, *12*, 230-238.
- Garlid, K. D., Jaburek, M., Jezek, P. & Varecha, M. (2000). How do uncoupling proteins uncouple? *Biochimica et Biophysica Acta (BBA) - Bioenergetics*, *1459*, 383-389.
- Garlid, K. D., Orosz, D. E., Modrianský, M., Vassanelli, S. & Jezek, P. (1996). On the Mechanism of Fatty Acid-induced Proton Transport by Mitochondrial Uncoupling Protein. *J. Biol. Chem.*, *271*, 2615-2620.
- Garofalo, T., Tinari, A., Matarrese, P., Giammaroli, A. M., Manganelli, V., Ciarlo, L., Misasi, R., Sorice, M. & Malorni, W. (2007). Do mitochondria act as "cargo boats" in the journey of GD3 to the nucleus during apoptosis? *FEBS Letters*, *581*, 3899-3903.
- Garrido, C., Galluzzi, L., Brunet, M., Puig, P. E., Didelot, C. & Kroemer, G. (2006). Mechanisms of cytochrome c release from mitochondria. *Cell Death Differ*, *13*, 1423-1433.
- Garrido, N., Griparic, L., Jokitalo, E., Wartiovaara, J., van der Blik, A. M. & Spelbrink, J. N. (2003). Composition and Dynamics of Human Mitochondrial Nucleoids. *Mol. Biol. Cell*, *14*, 1583-1596.
- Gatenby, R. A., Smallbone, K., Maini, P. K., Rose, F., Averill, J., Nagle, R. B., Worrall, L. & Gillies, R. J. (2007). Cellular adaptations to hypoxia and acidosis during somatic evolution of breast cancer. *Br J Cancer*, *97*, 646-653.
- Gerald, D., Berra, E., Frapart, Y. M., Chan, D. A., Giaccia, A. J., Mansuy, D., Pouyssegur, J., Yaniv, M. & Mechta-Grigoriou, F. (2004). JunD Reduces Tumor Angiogenesis by Protecting Cells from Oxidative Stress. *Cell*, *118*, 781-794.
- Giardina, T. M., Steer, J. H., Lo, S. Z. Y. & Joyce, D. A. (2008). Uncoupling protein-2 accumulates rapidly in the inner mitochondrial membrane during mitochondrial reactive oxygen stress in macrophages. *Biochimica et Biophysica Acta (BBA) - Bioenergetics*, *1777*, 118-129.
- Gilkerson, R. W., Schon, E. A., Hernandez, E. & Davidson, M. M. (2008). Mitochondrial nucleoids maintain genetic autonomy but allow for functional complementation. *J. Cell Biol.*, *181*, 1117-1128.
- Jimeno, R., Dembski, M., Weng, X., Shyjan, A., Jimeno, C., Iris, F., Ellis, S., Woolf, E. & Tartaglia, L. (1997). Cloning and characterization of an uncoupling protein homolog. A potential molecular mediator of human thermogenesis. *Diabetes*, *46*, 900-906.
- Gnaiger, E., Månsson, G. & Hand, S. C. (2000). High phosphorylation efficiency and depression of uncoupled respiration in mitochondria under hypoxia. *Proceedings of the National Academy of Sciences of the United States of America*, *97*, 11080-11085.
- Gnaiger, E., Steinlechner-Maran, R., Méndez, G., Eberl, T. & Margreiter, R. (1995). Control of mitochondrial and cellular respiration by oxygen. *Journal of Bioenergetics and Biomembranes*, *27*, 583-596.
- Gordan, J. D., Lal, P., Dondeti, V. R., Letrero, R., Parekh, K. N., Oquendo, C. E., Greenberg, R. A., Flaherty, K. T., Rathmell, W. K., Keith, B., Simon, M. C. & Nathanson, K. L. (2008). HIF-1 $\alpha$  Effects on c-Myc Distinguish Two Subtypes of Sporadic VHL-Deficient Clear Cell Renal Carcinoma. *Cancer Cell*, *14*, 435-446.
- Gummesson, A., Jernas, M., Svensson, P.-A., Larsson, I., Glad, C. A. M., Schele, E., Gripeteg, L., Sjöholm, K., Lystig, T. C., Sjöström, L., Carlsson, B., Fagerberg, B. & Carlsson, L. M. S. (2007). Relations of Adipose Tissue CIDEA Gene Expression to Basal Metabolic Rate, Energy Restriction, and Obesity: Population-Based and Dietary Intervention Studies. *J Clin Endocrinol Metab*, *92*, 4759-4765.
- Guppy, M., Greiner, E. & Brand, K. (1993). The role of the Crabtree effect and an endogenous fuel in the energy metabolism of resting and proliferating thymocytes. *European Journal of Biochemistry*, *212*, 95-99.
- Guppy, M., Leedman, P., Zu, X. & Russell, V. (2002). Contribution by different fuels and metabolic pathways to the total ATP turnover of proliferating MCF-7 breast cancer cells. *Biochem. J.*, *364*, 309-315.
- Halazonetis, T. D., Gorgoulis, V. G. & Bartek, J. (2008). An Oncogene-Induced DNA Damage Model for Cancer Development. *Science*, *319*, 1352-1355.
- Halestrap, A. (2005). Biochemistry: A pore way to die. *Nature*, *434*, 578-579.
- Hammerman, P. S., Fox, C. J. & Thompson, C. B. (2004). Beginnings of a signal-transduction pathway for bioenergetic control of cell survival. *Trends in Biochemical Sciences*, *29*, 586-592.
- Hanák, P. & Jezek, P. (2001). Mitochondrial uncoupling proteins and phylogenesis - UCP4 as the ancestral uncoupling protein. *FEBS Letters*, *495*, 137-141.
- Hänze, J., Eul, B. G., Savai, R., Krick, S., Goyal, P., Grimminger, F., Seeger, W. & Rose, F. (2003). RNA interference for HIF-1 $\alpha$  inhibits its downstream signalling and affects cellular proliferation. *Biochemical and Biophysical Research Communications*, *312*, 571-577.
- Hatzivassiliou, G., Zhao, F., Bauer, D. E., Andreadis, C., Shaw, A. N., Dhanak, D., Hingorani, S. R., Tuveson, D. A. & Thompson, C. B. (2005). ATP citrate lyase inhibition can suppress tumor cell growth. *Cancer Cell*, *8*, 311-321.
- He, J., Mao, C.-C., Reyes, A., Sembongi, H., Di Re, M., Granycome, C., Clippingdale, A. B., Fearnley, I. M., Harbour, M., Robinson, A. J., Reichelt, S., Spelbrink, J. N., Walker, J. E. & Holt, I. J. (2007). The AAA+ protein ATAD3 has

- displacement loop binding properties and is involved in mitochondrial nucleoid organization. *J. Cell Biol.*, *176*, 141-146.
- Helmlinger, G., Sckell, A., Dellian, M., Forbes, N. S. & Jain, R. K. (2002). Acid Production in Glycolysis-impaired Tumors Provides New Insights into Tumor Metabolism. *Clin Cancer Res*, *8*, 1284-1291.
- Hervouet, E., Cizkova, A., Demont, J., Vojtiskova, A., Pecina, P., Franssen-van Hal, N. L. W., Keijer, J., Simonnet, H., Ivanek, R., Kmoch, S., Godinot, C. & Houstek, J. (2008). HIF and reactive oxygen species regulate oxidative phosphorylation in cancer. *Carcinogenesis*, *29*, 1528-1537.
- Hervouet, E., Demont, J., Pecina, P., Vojtiskova, A., Houstek, J., Simonnet, H. & Godinot, C. (2005). A new role for the von Hippel-Lindau tumor suppressor protein: stimulation of mitochondrial oxidative phosphorylation complex biogenesis. *Carcinogenesis*, *26*, 531-539.
- Hilf, R., Rector, W. D. & Orlando, R. A. (1976). Multiple molecular forms of lactate dehydrogenase and glucose 6-phosphate dehydrogenase in normal and abnormal human breast tissues. *Cancer*, *37*, 1825-1830.
- Ho, P. W.-L., Chan, D. Y.-L., Kwok, K. H.-H., Chu, A. C.-Y., Ho, J. W.-M., Kung, M. H.-W., Ramsden, D. B. & Ho, S.-L. (2005). Methyl-4-phenylpyridinium ion modulates expression of mitochondrial uncoupling proteins 2, 4, and 5 in catecholaminergic (SK-N-SH) cells. *Journal of Neuroscience Research*, *81*, 261-268.
- Ho, P. W.-L., Chu, A. C.-Y., Kwok, K. H.-H., Kung, M. H.-W., Ramsden, D. B. & Ho, S.-L. (2006). Knockdown of uncoupling protein-5 in neuronal SH-SY5Y cells: Effects on MPP<sup>+</sup>-induced mitochondrial membrane depolarization, ATP deficiency, and oxidative cytotoxicity. *Journal of Neuroscience Research*, *84*, 1358-1366.
- Hockel, M., Schlenger, K., Aral, B., Mitze, M., Schaffer, U. & Vaupel, P. (1996). Association between Tumor Hypoxia and Malignant Progression in Advanced Cancer of the Uterine Cervix. *Cancer Res*, *56*, 4509-4515.
- Hockel, M., Schlenger, K., Hockel, S. & Vaupel, P. (1999). Hypoxic Cervical Cancers with Low Apoptotic Index Are Highly Aggressive. *Cancer Res*, *59*, 4525-4528.
- Hohenberger, P., Felgner, C., Haensch, W. & Schlag, P. M. (1998). Tumor oxygenation correlates with molecular growth determinants in breast cancer. *Breast Cancer Research and Treatment*, *48*, 97-106.
- Hu, C.-J., Wang, L.-Y., Chodosh, L. A., Keith, B. & Simon, M. C. (2003). Differential Roles of Hypoxia-Inducible Factor 1{alpha} (HIF-1{alpha}) and HIF-2{alpha} in Hypoxic Gene Regulation. *Mol. Cell. Biol.*, *23*, 9361-9374.
- Hurtaud, C., Gelly, C., Bouillaud, F. & Lévi-Meyrueis, C. (2006). Translation control of UCP2 synthesis by the upstream open reading frame. *Cellular and Molecular Life Sciences*, *63*, 1780-1789.
- Hurtaud, C., Gelly, C., Chen, Z., Lévi-Meyrueis, C. & Bouillaud, F. (2007). Glutamine stimulates translation of uncoupling protein 2mRNA. *Cellular and Molecular Life Sciences*, *64*, 1853-1860.
- Chan, C. B., MacDonald, P. E., Saleh, M. C., Johns, D. C., MarbÅ n, E. & Wheeler, M. B. (1999). Overexpression of uncoupling protein 2 inhibits glucose-stimulated insulin secretion from rat islets. *Diabetes*, *48*, 1482-1486.
- Chan, S. L., Liu, D., Kyriazis, G. A., Bagsiyao, P., Ouyang, X. & Mattson, M. P. (2006). Mitochondrial Uncoupling Protein-4 Regulates Calcium Homeostasis and Sensitivity to Store Depletion-induced Apoptosis in Neural Cells. *J. Biol. Chem.*, *281*, 37391-37403.
- Chance, B. (1965). Reaction of Oxygen with the Respiratory Chain in Cells and Tissues. *J Gen Physiol*, *49*, 163-188.
- Chance, B. & Williams, G. R. (1956). The respiratory chain and oxidative phosphorylation. *Adv Enzymol Relat Subj Biochem*, *17*, 65-134.
- Chandel, N. S., Trzyna, W. C., McClintock, D. S. & Schumacker, P. T. (2000). Role of Oxidants in NF- $\kappa$ B Activation and TNF- $\alpha$  Gene Transcription Induced by Hypoxia and Endotoxin. *J Immunol*, *165*, 1013-1021.
- Chatterjee, A., Mambo, E. & Sidransky, D. (2006). Mitochondrial DNA mutations in human cancer. *Oncogene*, *25*, 4663-4674.
- Chen, N., Chen, X., Huang, R., Zeng, H., Gong, J., Meng, W., Lu, Y., Zhao, F., Wang, L. & Zhou, Q. (2009). BCL-xL Is a Target Gene Regulated by Hypoxia-inducible Factor-1{alpha}. *J. Biol. Chem.*, *284*, 10004-10012.
- Chen, Z., Guo, K., Toh, S. Y., Zhou, Z. & Li, P. (2000). Mitochondria Localization and Dimerization Are Required for CIDE-B to Induce Apoptosis. *J. Biol. Chem.*, *275*, 22619-22622.
- Cheng, W.-C., Leach, K. M. & Hardwick, J. M. (2008). Mitochondrial death pathways in yeast and mammalian cells. *Biochimica et Biophysica Acta (BBA) - Molecular Cell Research*, *1783*, 1272-1279.
- Cheng, W. C., Berman, S. B., Ivanovska, I., Jonas, E. A., Lee, S. J., Chen, Y., Kaczmarek, L. K., Pineda, F. & Hardwick, J. M. (2006). Mitochondrial factors with dual roles in death and survival. *Oncogene*, *25*, 4697-4705.
- Chiaradonna, F., Gaglio, D., Vanoni, M. & Alberghina, L. (2006). Expression of transforming K-Ras oncogene affects mitochondrial function and morphology in mouse fibroblasts. *Biochimica et Biophysica Acta (BBA) - Bioenergetics*, *1757*, 1338-1356.
- Chomczynski, P. & Sacchi, N. (1987). Single-step method of RNA isolation by acid guanidinium thiocyanate-phenol-chloroform extraction. *Analytical Biochemistry*, *162*, 156-159.
- Christofk, H. R., Vander Heiden, M. G., Harris, M. H., Ramanathan, A., Gerszten, R. E., Wei, R., Fleming, M. D., Schreiber, S. L. & Cantley, L. C. (2008a). The M2 splice isoform of pyruvate kinase is important for cancer metabolism and tumour growth. *Nature*, *452*, 230-233.
- Christofk, H. R., Vander Heiden, M. G., Wu, N., Asara, J. M. & Cantley, L. C. (2008b). Pyruvate kinase M2 is a phosphotyrosine-binding protein. *Nature*, *452*, 181-186.
- Iborra, F., Kimura, H. & Cook, P. (2004). The functional organization of mitochondrial genomes in human cells. *BMC Biology*, *2*, 9.
- Inohara, N., Koseki, T., Chen, S., Benedict, M. A. & Nunez, G. (1999). Identification of Regulatory and Catalytic Domains in the Apoptosis Nuclease DFF40/CAD. *J. Biol. Chem.*, *274*, 270-274.

- Inohara, N., Koseki, T., Chen, S., Wu, X. & Núñez, G. (1998). CIDE, a novel family of cell death activators with homology to the 45 kDa subunit of the DNA fragmentation factor. *EMBO J*, *17*, 2526-2533.
- Ishikawa, K., Hashizume, O., Koshikawa, N., Fukuda, S., Nakada, K., Takenaga, K. & Hayashi, J.-I. (2008a). Enhanced glycolysis induced by mtDNA mutations does not regulate metastasis. *FEBS Letters*, *582*, 3525-3530.
- Ishikawa, K., Takenaga, K., Akimoto, M., Koshikawa, N., Yamaguchi, A., Imanishi, H., Nakada, K., Honma, Y. & Hayashi, J.-I. (2008b). ROS-Generating Mitochondrial DNA Mutations Can Regulate Tumor Cell Metastasis. *Science*, *320*, 661-664.
- Isidoro, A., Martinez, M., Fernandez, P. L., Ortega, A. D., Santamaría, G., Chamorro, M., Reed, J. C. & Cuezva, J. M. (2004). Alteration of the bioenergetic phenotype of mitochondria is a hallmark of breast, gastric, lung and oesophageal cancer. *Biochem. J.*, *378*, 17-20.
- Iwahana, H., Yakymovych, I., Dubrovskaya, A., Hellman, U. & Souchelnytskyi, S. (2006). Glycoproteome profiling of transforming growth factor-beta (TGFbeta) signaling: Nonglycosylated cell death-inducing DFF-like effector A inhibits TGFbeta1-dependent apoptosis. *PROTEOMICS*, *6*, 6168-6180.
- Iyer, N. V., Kotch, L. E., Agani, F., Leung, S. W., Laughner, E., Wenger, R. H., Gassmann, M., Gearhart, J. D., Lawler, A. M., Yu, A. Y. & Semenza, G. L. (1998). Cellular and developmental control of O<sub>2</sub> homeostasis by hypoxia-inducible factor-1. *Genes & Development*, *12*, 149-162.
- Jabůrek, M., Miyamoto, S., Di Mascio, P., Garlid, K. D. & Jezek, P. (2004). Hydroperoxy Fatty Acid Cycling Mediated by Mitochondrial Uncoupling Protein UCP2. *J. Biol. Chem.*, *279*, 53097-53102.
- Jabůrek, M., Varecha, M., Gimeno, R. E., Dembski, M., Jezek, P., Zhang, M., Burn, P., Tartaglia, L. A. & Garlid, K. D. (1999). Transport Function and Regulation of Mitochondrial Uncoupling Proteins 2 and 3. *J. Biol. Chem.*, *274*, 26003-26007.
- Jackowski, S., Wang, J. & Baburina, I. (2000). Activity of the phosphatidylcholine biosynthetic pathway modulates the distribution of fatty acids into glycerolipids in proliferating cells. *Biochimica et Biophysica Acta (BBA) - Molecular and Cell Biology of Lipids*, *1483*, 301-315.
- Jastroch, M., Buckingham, J., Helwig, M., Klingenspor, M. & Brand, M. (2007). Functional characterisation of UCP1 in the common carp: uncoupling activity in liver mitochondria and cold-induced expression in the brain. *Journal of Comparative Physiology B: Biochemical, Systemic, and Environmental Physiology*, *177*, 743-752.
- Ježek, P. (1999). Fatty Acid Interaction with Mitochondrial Uncoupling Proteins. *Journal of Bioenergetics and Biomembranes*, *31*, 457-466.
- Ježek, P., Costa, A. D. T. & Vercesi, A. E. (1997). Reconstituted Plant Uncoupling Mitochondrial Protein Allows for Proton Translocation via Fatty Acid Cycling Mechanism. *J. Biol. Chem.*, *272*, 24272-24278.
- Ježek, P., Engstová, H., Žáčková, M., Vercesi, A. E., Costa, A. D. T., Arruda, P. & Garlid, K. D. (1998). Fatty acid cycling mechanism and mitochondrial uncoupling proteins. *Biochim. Biophys. Acta*, *1365*, 319-327.
- Ježek, P. & Garlid, K. (1990). New substrates and competitive inhibitors of the Cl<sup>-</sup> translocating pathway of the uncoupling protein of brown adipose tissue mitochondria. *J. Biol. Chem.*, *265*, 19303-19311.
- Ježek, P. & Hlavatá, L. (2005). Mitochondria in homeostasis of reactive oxygen species in cell, tissues, and organism. *The International Journal of Biochemistry & Cell Biology*, *37*, 2478-2503.
- Ježek, P. & Ježek, J. (2003). Sequence anatomy of mitochondrial anion carriers. *FEBS Letters*, *534*, 15-25.
- Ježek, P. & Plecítá-Hlavatá, L. (2009). Mitochondrial reticulum network dynamics in relation to oxidative stress, redox regulation, and hypoxia. *International Journal of Biochemistry and Cell Biology*.
- Ježek, P. & Urbánková, E. (2000). Specific Sequence Motifs of Mitochondrial Uncoupling Proteins. *IUBMB Life*, *49*, 63-70.
- Ježek, P., Žáčková, M., Růžička, M., Škobisová, E. & Jabůrek, M. (2004). Mitochondrial uncoupling proteins - facts and fantasies. *Physiol Res*, *53*, S199-S211.
- Johan, B., Johannes, H. A. M. K. & Albert, J. v. d. K. (2003). Tumor hypoxia at the micro-regional level: clinical relevance and predictive value of exogenous and endogenous hypoxic cell markers. *Radiotherapy and oncology : journal of the European Society for Therapeutic Radiology and Oncology*, *67*, 3-15.
- Joseph, J. W., Koshkin, V., Saleh, M. C., Sivitz, W. I., Zhang, C.-Y., Lowell, B. B., Chan, C. B. & Wheeler, M. B. (2004). Free Fatty Acid-induced {beta}-Cell Defects Are Dependent on Uncoupling Protein 2 Expression. *J. Biol. Chem.*, *279*, 51049-51056.
- Kakarala, M. & Wicha, M. S. (2008). Implications of the Cancer Stem-Cell Hypothesis for Breast Cancer Prevention and Therapy. *J Clin Oncol*, *26*, 2813-2820.
- Karbowski, M., Norris, K. L., Cleland, M. M., Jeong, S.-Y. & Youle, R. J. (2006). Role of Bax and Bak in mitochondrial morphogenesis. *Nature*, *443*, 658-662.
- Kayama, T., Yoshimoto, T., Fujimoto, S. & Sakurai, Y. (1991). Intratumoral oxygen pressure in malignant brain tumor. *J Neurosurg.*, *64*, 55-59.
- Kim-Han, J. S., Reichert, S. A., Quick, K. L. & Ugan, L. L. (2001). BMCP1: a mitochondrial uncoupling protein in neurons which regulates mitochondrial function and oxidant production. *Journal of Neurochemistry*, *79*, 658-668.
- Kim, J.-W., Tchernyshyov, I., Semenza, G. L. & Dang, C. V. (2006a). HIF-1-mediated expression of pyruvate dehydrogenase kinase: A metabolic switch required for cellular adaptation to hypoxia. *Cell Metabolism*, *3*, 177-185.
- Kim, R., Emi, M. & Tanabe, K. (2006b). Role of mitochondria as the gardens of cell death. *Cancer Chemotherapy and Pharmacology*, *57*, 545-553.
- King, A., Selak, M. A. & Gottlieb, E. (2006). Succinate dehydrogenase and fumarate hydratase: linking mitochondrial dysfunction and cancer. *Oncogene*, *25*, 4675-4682.

- Kizaki, T., Suzuki, K., Hitomi, Y., Taniguchi, N., Saitoh, D., Watanabe, K., Onoé, K., Day, N. K., Good, R. A. & Ohno, H. (2002). Uncoupling protein 2 plays an important role in nitric oxide production of lipopolysaccharide-stimulated macrophages. *Proceedings of the National Academy of Sciences of the United States of America*, *99*, 9392-9397.
- Klimova, T. & Chandel, N. S. (2008). Mitochondrial complex III regulates hypoxic activation of HIF. *Cell Death Differ*, *15*, 660-666.
- Klingenberg, M. & Echtay, K. S. (2001). Uncoupling proteins: the issues from a biochemist point of view. *Biochimica et Biophysica Acta (BBA) - Bioenergetics*, *1504*, 128-143.
- Klingenberg, M. & Huang, S.-G. (1999). Structure and function of the uncoupling protein from brown adipose tissue. *Biochimica et Biophysica Acta (BBA) - Biomembranes*, *1415*, 271-296.
- Klingenspor, M., Fromme, T., Hughes Jr, D. A., Manzke, L., Polymeropoulos, E., Riemann, T., Trzcionka, M., Hirschberg, V. & Jastroch, M. (2008). An ancient look at UCP1. *Biochimica et Biophysica Acta (BBA) - Bioenergetics*, *1777*, 637-641.
- Koivunen, P., Hirsila, M., Remes, A. M., Hassinen, I. E., Kivirikko, K. I. & Myllyharju, J. (2007). Inhibition of Hypoxia-inducible Factor (HIF) Hydroxylases by Citric Acid Cycle Intermediates: POSSIBLE LINKS BETWEEN CELL METABOLISM AND STABILIZATION OF HIF. *J. Biol. Chem.*, *282*, 4524-4532.
- Koong, A. C., Chen, E. Y. & Giaccia, A. J. (1994). Hypoxia Causes the Activation of Nuclear Factor {kappa}B through the Phosphorylation of I{kappa}B{alpha} on Tyrosine Residues. *Cancer Res*, *54*, 1425-1430.
- Koong, A. C., Mehta, V. K., Le, Q. T., Fisher, G. A., Terris, D. J., Brown, J. M., Bastidas, A. J. & Vierra, M. (2000). Pancreatic tumors show high levels of hypoxia. *International Journal of Radiation Oncology\*Biophysics*, *48*, 919-922.
- Korshunov, S. S., Korkina, O. V., Ruuge, E. K., Skulachev, V. P. & Starkov, A. A. (1998). Fatty acids as natural uncouplers preventing generation of and H<sub>2</sub>O<sub>2</sub> by mitochondria in the resting state. *FEBS Letters*, *435*, 215-218.
- Korshunov, S. S., Skulachev, V. P. & Starkov, A. A. (1997). High protonic potential actuates a mechanism of production of reactive oxygen species in mitochondria. *FEBS Letters*, *416*, 15-18.
- Krauss, S., Zhang, C.-Y. & Lowell, B. B. (2005). The mitochondrial uncoupling-protein homologues. *Nat Rev Mol Cell Biol*, *6*, 248-261.
- Kuhajda, F., Jenner, K., Wood, F., Hennigar, R., Jacobs, L., Dick, J. & Pasternack, R. (1994). Fatty acid synthesis: a potential selective target for antineoplastic therapy. *Proc Natl Acad Sci*, *91*, 6379-6383.
- Kuhajda, F. P. (2000). Fatty-acid synthase and human cancer: new perspectives on its role in tumor biology. *Nutrition*, *16*, 202-208.
- Lando, D., Peet, D. J., Whelan, D. A., Gorman, J. J. & Whitelaw, M. L. (2002). Asparagine Hydroxylation of the HIF Transactivation Domain: A Hypoxic Switch. *Science*, *295*, 858-861.
- Lartigau, E., Randrianarivelo, H., Avril, M., Margulis, A., Spatz, A., Eschwège, F. & Guichard, M. (1997). Intratumoral oxygen tension in metastatic melanoma. *Melanoma Res.*, *7*, 400-406.
- Lee, C. J., Dosch, J. & Simeone, D. M. (2008). Pancreatic Cancer Stem Cells. *J Clin Oncol*, *26*, 2806-2812.
- Legros, F., Malka, F., Frachon, P., Lombes, A. & Rojo, M. (2004). Organization and dynamics of human mitochondrial DNA. *J Cell Sci*, *117*, 2653-2662.
- Lechardeur, D., Dougaparsad, S., Nemes, C. & Lukacs, G. L. (2005). Oligomerization State of the DNA Fragmentation Factor in Normal and Apoptotic Cells. *J. Biol. Chem.*, *280*, 40216-40225.
- Lechardeur, D., Drzymala, L., Sharma, M., Zylka, D., Kinach, R., Pacia, J., Hicks, C., Usmani, N., Rommens, J. M. & Lukacs, G. L. (2000). Determinants of the Nuclear Localization of the Heterodimeric DNA Fragmentation Factor (ICAD/CAD). *J. Cell Biol.*, *150*, 321-334.
- Lengacher, S., Magistretti, P. & Pellerin, L. (2004). Quantitative rt-PCR analysis of uncoupling protein isoforms in mouse brain cortex: methodological optimization and comparison of expression with brown adipose tissue and skeletal muscle. *J Cereb Blood Flow Metab*, *24*, 780-788.
- Lenz, H.-J. (2008). Colon Cancer Stem Cells: A New Target In the War Against Cancer. *Gastrointest Cancer Res*, *2*, 203-204.
- Li, X., Qin, C., Burghardt, R. & Safe, S. (2004). Hormonal regulation of lactate dehydrogenase-A through activation of protein kinase C pathways in MCF-7 breast cancer cells. *Biochemical and Biophysical Research Communications*, *320*, 625-634.
- Liang, L., Zhao, M., Xu, Z., Yokoyama, K. K. & Li, T. (2003). Molecular cloning and characterization of CIDE-3, a novel member of the cell-death-inducing DNA-fragmentation-factor (DFF45)-like effector family. *Biochem. J.*, *370*, 195-203.
- Lindholm, D., Eriksson, O. & Korhonen, L. (2004). Mitochondrial proteins in neuronal degeneration. *Biochemical and Biophysical Research Communications*, *321*, 753-758.
- Liu, D., Chan, S., de Souza-Pinto, N., Slevin, J., Wersto, R., Zhan, M., Mustafa, K., de Cabo, R. & Mattson, M. (2006). Mitochondrial UCP4 mediates an adaptive shift in energy metabolism and increases the resistance of neurons to metabolic and oxidative stress. *NeuroMolecular Medicine*, *8*, 389-413.
- Lluis, J. M., Buricchi, F., Chiarugi, P., Morales, A. & Fernandez-Checa, J. C. (2007). Dual Role of Mitochondrial Reactive Oxygen Species in Hypoxia Signaling: Activation of Nuclear Factor- $\kappa$ B via c-SRC and Oxidant-Dependent Cell Death. *Cancer Res*, *67*, 7368-7377.
- Lopez-Rios, F., Sanchez-Arago, M., Garcia-Garcia, E., Ortega, A. D., Berrendero, J. R., Pozo-Rodriguez, F., Lopez-Encuentra, A., Ballestin, C. & Cuezva, J. M. (2007). Loss of the Mitochondrial Bioenergetic Capacity Underlies the Glucose Avidity of Carcinomas. *Cancer Res*, *67*, 9013-9017.
- Lu, H., Forbes, R. A. & Verma, A. (2002). Hypoxia-inducible Factor 1 Activation by Aerobic Glycolysis Implicates the Warburg Effect in Carcinogenesis. *J. Biol. Chem.*, *277*, 23111-23115.

- Lugovskoy, A. A., Zhou, P., Chou, J. J., McCarty, J. S., Li, P. & Wagner, G. (1999). Solution Structure of the CIDE-N Domain of CIDE-B and a Model for CIDE-N/CIDE-N Interactions in the DNA Fragmentation Pathway of Apoptosis. *Cell*, *99*, 747-755.
- Lum, J. J., Bui, T., Gruber, M., Gordan, J. D., DeBerardinis, R. J., Covelto, K. L., Simon, M. C. & Thompson, C. B. (2007). The transcription factor HIF-1 $\alpha$  plays a critical role in the growth factor-dependent regulation of both aerobic and anaerobic glycolysis. *Genes and Development*, *21*, 1037-1049
- Lyng, H., Sundf r, K. & Rofstad, E. K. (1997). Oxygen tension in human tumours measured with polarographic needle electrodes and its relationship to vascular density, necrosis and hypoxia. *Radiotherapy and Oncology*, *44*, 163-169.
- Maltepe, E., Schmidt, J. V., Baunoch, D., Bradfield, C. A. & Celeste, S. M. (1997). Abnormal angiogenesis and responses to glucose and oxygen deprivation in mice lacking the protein ARNT. *Nature*, *386*, 403 - 407.
- Mambo, E., Chatterjee, A., Xing, M., Tallini, G., Haugen, B. R., Yeung, S.-C. J., Sukumar, S. & Sidransky, D. (2005). Tumor-specific changes in mtDNA content in human cancer. *International Journal of Cancer*, *116*, 920-924.
- Mankoff, D. A., Eary, J. F., Link, J. M., Muzi, M., Rajendran, J. G., Spence, A. M. & Krohn, K. A. (2007). Tumor-Specific Positron Emission Tomography Imaging in Patients: [18F] Fluorodeoxyglucose and Beyond. *Clin Cancer Res*, *13*, 3460-3469.
- Mannella, C. A. (2006). Structure and dynamics of the mitochondrial inner membrane cristae. *Biochimica et Biophysica Acta (BBA) - Molecular Cell Research*, *1763*, 542-548.
- Mansfield, K. D., Guzy, R. D., Pan, Y., Young, R. M., Cash, T. P., Schumacker, P. T. & Simon, M. C. (2005). Mitochondrial dysfunction resulting from loss of cytochrome c impairs cellular oxygen sensing and hypoxic HIF-[alpha] activation. *Cell Metabolism*, *1*, 393-399.
- Mao, W., Yu, X. X., Zhong, A., Li, W., Brush, J., Sherwood, S. W., Adams, S. H. & Pan, G. (1999). UCP4, a novel brain-specific mitochondrial protein that reduces membrane potential in mammalian cells. *FEBS Letters*, *443*, 326-330.
- Margineantu, D. H., Gregory Cox, W., Sundell, L., Sherwood, S. W., Beechem, J. M. & Capaldi, R. A. (2002). Cell cycle dependent morphology changes and associated mitochondrial DNA redistribution in mitochondria of human cell lines. *Mitochondrion*, *1*, 425-435.
- Mashima, T., Seimiya, H. & Tsuruo, T. (2009). De novo fatty-acid synthesis and related pathways as molecular targets for cancer therapy. *Br J Cancer*, *100*, 1369-1372.
- Mat s, J. M., Segura, J. A., Campos-Sandoval, J. A., Lobo, C., Alonso, L., Alonso, F. J. & M rquez, J. (2009). Glutamine homeostasis and mitochondrial dynamics. *The International Journal of Biochemistry & Cell Biology, In Press, Corrected Proof*.
- Mathupala, S. P., Rempel, A. & Pedersen, P. L. (2001). Glucose Catabolism in Cancer Cells. IDENTIFICATION AND CHARACTERIZATION OF A MARKED ACTIVATION RESPONSE OF THE TYPE II HEXOKINASE GENE TO HYPOXIC CONDITIONS. *J. Biol. Chem.*, *276*, 43407-43412.
- Matoba, S., Kang, J.-G., Patino, W. D., Wragg, A., Boehm, M., Gavrilova, O., Hurley, P. J., Bunz, F. & Hwang, P. M. (2006). p53 Regulates Mitochondrial Respiration. *Science*, *312*, 1650-1653.
- Mattiasson, G. & Sullivan, P. G. (2006). The Emerging Functions of UCP2 in Health, Disease, and Therapeutics. *Antioxidants & Redox Signaling*, *8*, 1-38.
- Mayer, A., Hockel, M., Wree, A., Leo, C., Horn, L.-C. & Vaupel, P. (2008). Lack of Hypoxic Response in Uterine Leiomyomas despite Severe Tissue Hypoxia. *Cancer Res*, *68*, 4719-4726.
- Mazurek, S., Grimm, H., Boschek, C. B., Vaupel, P. & Eigenbrodt, E. (2002). Pyruvate kinase type M2: a crossroad in the tumor metabolome. *British Journal of Nutrition*, *87*, S23-S29.
- McFate, T., Mohyeldin, A., Lu, H., Thakar, J., Henriques, J., Halim, N. D., Wu, H., Schell, M. J., Tsang, T. M., Teahan, O., Zhou, S., Califano, J. A., Jeoung, N. H., Harris, R. A. & Verma, A. (2008). Pyruvate Dehydrogenase Complex Activity Controls Metabolic and Malignant Phenotype in Cancer Cells. *J. Biol. Chem.*, *283*, 22700-22708.
- McLeod, C. J., Aziz, A., Hoyt, R. F., Jr., McCoy, J. P., Jr. & Sack, M. N. (2005). Uncoupling Proteins 2 and 3 Function in Concert to Augment Tolerance to Cardiac Ischemia. *J. Biol. Chem.*, *280*, 33470-33476.
- Melo, R. F., Stevan, F. R., Campello, A. P., Carnieri, E. G. S. & Martinelli De Oliveira, M. B. (1998). Occurrence of the Crabtree effect in HeLa cells. *Cell Biochemistry and Function*, *16*, 99-105.
- Menendez, J. A., Vellon, L., Mehmi, I., Oza, B. P., Ropero, S., Colomer, R. & Lupu, R. (2004). Inhibition of fatty acid synthase (FAS) suppresses HER2/neu (erbB-2) oncogene overexpression in cancer cells. *Proceedings of the National Academy of Sciences of the United States of America*, *101*, 10715-10720.
- Moreno-S nchez, R., Rodr guez-Enr quez, S., Mar n-Hern ndez, A. & Saavedra, E. (2007). Energy metabolism in tumor cells. *FEBS Journal*, *274*, 1393-1418.
- Moreno-S nchez, R., Rodr guez-Enr quez, S., Saavedra, E., Mar n-Hern ndez, A. & Callardo-P rez, J. C. (2009). The bioenergetics of cancer: Is glycolysis the main ATP supplier in all tumor cells? *BioFactors*, *35*, 209-225.
- Mori, S., Yoshizuka, N., Takizawa, M., Takema, Y., Murase, T., Tokimitsu, I. & Saito, M. (2008). Expression of Uncoupling Proteins in Human Skin and Skin-Derived Cells. *J Invest Dermatol*, *128*, 1894-1900.
- Muller, F. L., Liu, Y. & Van Remmen, H. (2004). Complex III Releases Superoxide to Both Sides of the Inner Mitochondrial Membrane. *J. Biol. Chem.*, *279*, 49064-49073.
- Murphy, M. P., Echtay, K. S., Blaikie, F. H., Asin-Cayuela, J., Cocheme, H. M., Green, K., Buckingham, J. A., Taylor, E. R., Hurrell, F., Hughes, G., Miwa, S., Cooper, C. E., Svistunenko, D. A., Smith, R. A. J. & Brand, M. D. (2003). Superoxide Activates Uncoupling Proteins by Generating Carbon-centered Radicals and Initiating Lipid

- Peroxidation: STUDIES USING A MITOCHONDRIA-TARGETED SPIN TRAP DERIVED FROM  $\alpha$ -PHENYL-N-tert-BUTYLNITRONE. *J. Biol. Chem.*, 278, 48534-48545.
- Nakase, T., Yoshida, Y. & Nagata, K. (2007). Amplified expression of uncoupling proteins in human brain ischemic lesions. *Neuropathology*, 27, 442-447.
- Nakashima, R. A., Paggi, M. G. & Pedersen, P. L. (1984). Contributions of Glycolysis and Oxidative Phosphorylation to Adenosine 5'-Triphosphate Production in AS-30D Hepatoma Cells. *Cancer Res*, 44, 5702-5706.
- Nakata, B., Nishimura, S., Ishikawa, T., Ohira, M., Nishino, H., Kawabe, J., Ochi, H. & Hirakawa, K. (2001). Prognostic predictive value of 18F-fluorodeoxyglucose positron emission tomography for patients with pancreatic cancer. *Int J Oncol*, 19, 53-58.
- Naudí, A., Caro, P., Jové, M., Gómez, J., Boada, J., Ayala, V., Portero-Otín, M., Barja, G. & Pamplona, R. (2007). Methionine Restriction Decreases Endogenous Oxidative Molecular Damage and Increases Mitochondrial Biogenesis and Uncoupling Protein 4 in Rat Brain. *Rejuvenation Research*, 10, 473-484.
- Nedergaard, J. & Cannon, B. (2003). The 'novel' 'uncoupling' proteins UCP2 and UCP3: what do they really do? Pros and cons for suggested functions. *Experimental Physiology*, 88, 65-84.
- Neimanis, S., Albig, W., Doenecke, D. & Kahle, J. (2007). Sequence Elements in Both Subunits of the DNA Fragmentation Factor Are Essential for Its Nuclear Transport. *J. Biol. Chem.*, 282, 35821-35830.
- Nicholls, D. & Rial, E. (1989). Measurement of proton leakage across mitochondrial inner membranes and its relation to protonmotive force. *Meth Enzym*, 174, 85-94.
- Nilsson, J. A. & Cleveland, J. L. (2003). Myc pathways provoking cell suicide and cancer. *Oncogene*, 22, 9007-9021.
- Nordmark, M., Alsner, J., Keller, J., Nielsen, O. S., Jensen, O. M., Horsman, M. R. & Overgaard, J. (2001). Hypoxia in human soft tissue sarcomas: Adverse impact on survival and no association with p53 mutations. *Br J Cancer*, 84, 1070-1075.
- Nordmark, M., Eriksen, J. G., Gebiski, V., Alsner, J., Horsman, M. R. & Overgaard, J. (2007). Differential risk assessments from five hypoxia specific assays: The basis for biologically adapted individualized radiotherapy in advanced head and neck cancer patients. *Radiotherapy and Oncology*, 83, 389-397.
- Nordmark, M., Hřyer, M., Keller, J., Nielsen, O. S., Jensen, O. M. & Overgaard, J. (1996). The relationship between tumor oxygenation and cell proliferation in human soft tissue sarcomas. *International Journal of Radiation Oncology\*Biophysics*, 35, 701-708.
- Nouette-Gaulain, K., Bellance, N., Prévost, B., Passerieux, E., Pertuiset, C., Galbes, O., Smolkova, K., Masson, F., Miraux, S., Delage, J., Letellier, T., Rossignol, R., Capdevila, X. & Sztark, F. (2009). Erythropoietin protects against local anesthetic myotoxicity during continuous regional analgesia. *Anesthesiology*, 110, 648-659.
- Osthus, R. C., Shim, H., Kim, S., Li, Q., Reddy, R., Mukherjee, M., Xu, Y., Wonsey, D., Lee, L. A. & Dang, C. V. (2000). Deregulation of Glucose Transporter 1 and Glycolytic Gene Expression by c-Myc. *J. Biol. Chem.*, 275, 21797-21800.
- Ouhabi, R., Boue-Grabot, M. & Mazat, J.-P. (1998). Mitochondrial ATP Synthesis in Permeabilized Cells: Assessment of the ATP/O Values in Situ. *Analytical Biochemistry*, 263, 169-175.
- Owen, O. E., Kalhan, S. C. & Hanson, R. W. (2002). The Key Role of Anaplerosis and Cataplerosis for Citric Acid Cycle Function. *J. Biol. Chem.*, 277, 30409-30412.
- Papandreou, I., Cairns, R., Fontana, L., Lim, A. & Denko, N. (2006). HIF-1 mediates adaptation to hypoxia by actively downregulating mitochondrial oxygen consumption. *Cell Metabolism*, 3, 187 - 197.
- Patel, M. S. & Korotchkina, L. G. (2003). The biochemistry of the pyruvate dehydrogenase complex. *Biochemistry and Molecular Biology Education*, 31, 5-15.
- Patel, M. S. & Korotchkina, L. G. (2006). Regulation of the pyruvate dehydrogenase complex. *Biochem. Soc. Trans.*, 34, 217-222.
- Pecqueur, C., Alves-Guerra, M.-C., Gelly, C., Levi-Meyrueis, C., Couplan, E., Collins, S., Ricquier, D., Bouillaud, F. & Miroux, B. (2001). Uncoupling Protein 2, in Vivo Distribution, Induction upon Oxidative Stress, and Evidence for Translational Regulation. *J. Biol. Chem.*, 276, 8705-8712.
- Pelicano, H., Xu, R.-h., Du, M., Feng, L., Sasaki, R., Carew, J. S., Hu, Y., Ramdas, L., Hu, L., Keating, M. J., Zhang, W., Plunkett, W. & Huang, P. (2006). Mitochondrial respiration defects in cancer cells cause activation of Akt survival pathway through a redox-mediated mechanism. *J. Cell Biol.*, 175, 913-923.
- Pfeiffer, T., Schuster, S. & Bonhoeffer, S. (2001). Cooperation and Competition in the Evolution of ATP-Producing Pathways. *Science*, 292, 504-507.
- Plecitá-Hlavatá, L., Jezek, J. & Jezek, P. (2009). Pro-oxidant mitochondrial matrix-targeted ubiquinone MitoQ10 acts as anti-oxidant at retarded electron transport or proton pumping within Complex I. *The International Journal of Biochemistry & Cell Biology*, 41, 1697-1707.
- Plecitá-Hlavatá, L., Lessard, M., Santorová, J., Bewersdorf, J. & Jezek, P. (2008). Mitochondrial oxidative phosphorylation and energetic status are reflected by morphology of mitochondrial network in INS-1E and HEP-G2 cells viewed by 4Pi microscopy. *Biochimica et Biophysica Acta (BBA) - Bioenergetics*, 1777, 834-846.
- Pollard, P. J., Briere, J. J., Alam, N. A., Barwell, J., Barclay, E., Wortham, N. C., Hunt, T., Mitchell, M., Olpin, S., Moat, S. J., Hargreaves, I. P., Heales, S. J., Chung, Y. L., Griffiths, J. R., Dagleish, A., McGrath, J. A., Gleeson, M. J., Hodgson, S. V., Poulosom, R., Rustin, P. & Tomlinson, I. P. M. (2005). Accumulation of Krebs cycle intermediates and over-expression of HIF1 $\alpha$  in tumours which result from germline FH and SDH mutations. *Hum. Mol. Genet.*, 14, 2231-2239.

- Ramanathan, A., Wang, C. & Schreiber, S. L. (2005). Perturbational profiling of a cell-line model of tumorigenesis by using metabolic measurements. *Proceedings of the National Academy of Sciences of the United States of America*, *102*, 5992-5997.
- Rankin, E. B., Rha, J., Unger, T. L., Wu, C. H., Shutt, H. P., Johnson, R. S., Simon, M. C., Keith, B. & Haase, V. H. (2008). Hypoxia-inducible factor-2 regulates vascular tumorigenesis in mice. *Oncogene*, *27*, 5354-5358.
- Ray, S., Atkuri, K. R., Deb-Basu, D., Adler, A. S., Chang, H. Y., Herzenberg, L. A. & Felsner, D. W. (2006). MYC Can Induce DNA Breaks In vivo and In vitro Independent of Reactive Oxygen Species. *Cancer Res*, *66*, 6598-6605.
- Reitzer, L. J., Wice, B. M. & Kennell, D. (1979). Evidence that glutamine, not sugar, is the major energy source for cultured HeLa cells. *J. Biol. Chem.*, *254*, 2669-2676.
- Rijken, P. F. J. W., Bernsen, H. J. J. A., Peters, J. P. W., Hodgkiss, R. J., Raleigh, J. A. & van der Kogel, A. J. (2000). Spatial relationship between hypoxia and the (perfused) vascular network in a human glioma xenograft: a quantitative multi-parameter analysis. *International Journal of Radiation Oncology\*Biological\*Physics*, *48*, 571-582.
- Rodríguez-Enríquez, S., Juárez, O., Rodríguez-Zavala, J. S. & Moreno-Sánchez, R. (2001). Multisite control of the Crabtree effect in ascites hepatoma cells. *European Journal of Biochemistry*, *268*, 2512-2519.
- Rodríguez-Enríquez, S., Vital-González, P. A., Flores-Rodríguez, F. L., Marín-Hernández, A., Ruiz-Azuara, L. & Moreno-Sánchez, R. (2006). Control of cellular proliferation by modulation of oxidative phosphorylation in human and rodent fast-growing tumor cells. *Toxicology and Applied Pharmacology*, *215*, 208-217.
- Rofstad, E. K., Mathiesen, B., Henriksen, K., Kindem, K. & Galappathi, K. (2005). The Tumor Bed Effect: Increased Metastatic Dissemination from Hypoxia-Induced Up-regulation of Metastasis-Promoting Gene Products. *Cancer Res*, *65*, 2387-2396.
- Rofstad, E. K., Sundfor, K., Lyng, H. & Trope, C. G. (2000). Hypoxia-induced treatment failure in advanced squamous cell carcinoma of the uterine cervix is primarily due to hypoxia-induced radiation resistance rather than hypoxia-induced metastasis. *Br J Cancer*, *83*, 354-359.
- Rosignol, R., Gilkerson, R., Aggeler, R., Yamagata, K., Remington, S. J. & Capaldi, R. A. (2004). Energy Substrate Modulates Mitochondrial Structure and Oxidative Capacity in Cancer Cells. *Cancer Res*, *64*, 985-993.
- Rousset, S., Emre, Y., Join-Lambert, O., Hurtaud, C., Ricquier, D. & Cassard-Doulcier, A.-M. (2006). The uncoupling protein 2 modulates the cytokine balance in innate immunity. *Cytokine*, *35*, 135-142.
- Rudat, V., Vanselow, B., Wollensack, P., Bettscheider, C., Osman-Ahmet, S., Eble, M. J. & Dietz, A. (2000). Repeatability and prognostic impact of the pretreatment pO<sub>2</sub> histography in patients with advanced head and neck cancer. *Radiotherapy and Oncology*, *57*, 31-37.
- Ruzicka, M., Skobisová, E., Dlasková, A., Santorová, J., Smolková, K., Spacek, T., Zäcková, M., Modrianský, M. & Jezek, P. (2005). Recruitment of mitochondrial uncoupling protein UCP2 after lipopolysaccharide induction. *The International Journal of Biochemistry & Cell Biology*, *37*, 809-821.
- Ryu, J.-W., Hong, K. H., Maeng, J. H., Kim, J.-B., Ko, J., Park, J. Y., Lee, K.-U., Hong, M. K., Park, S. W., Kim, Y. H. & Han, K. H. (2004). Overexpression of Uncoupling Protein 2 in THP1 Monocytes Inhibits  $\beta_2$  Integrin-Mediated Firm Adhesion and Transendothelial Migration. *Arterioscler Thromb Vasc Biol*, *24*, 864-870.
- Sakai, H., Suzuki, T., Maeda, M., Takahashi, Y., Horikawa, N., Minamimura, T., Tsukada, K. & Takeguchi, N. (2004). Up-regulation of Na<sup>+</sup>,K<sup>+</sup>-ATPase [alpha]3-isoform and down-regulation of the [alpha]1-isoform in human colorectal cancer. *FEBS Letters*, *563*, 151-154.
- Sale, M., Hsu, F.-C., Palmer, N., Gordon, C., Keene, K., Borgerink, H., Sharma, A., Bergman, R., Taylor, K., Saad, M. & Norris, J. (2007). The uncoupling protein 1 gene, UCP1, is expressed in mammalian islet cells and associated with acute insulin response to glucose in African American families from the IRAS Family Study. *BMC Endocrine Disorders*, *7*, 1.
- Salvi, M., Brunati, A. M. & Toninello, A. (2005). Tyrosine phosphorylation in mitochondria: A new frontier in mitochondrial signaling. *Free Radical Biology and Medicine*, *38*, 1267-1277.
- Sanchis, D., Fleury, C., Chomiki, N., Goubern, M., Huang, Q., Neverova, M., Gregoire, F., Easlick, J., Raimbault, S., Levi-Meyrueis, C., Miroux, B., Collins, S., Seldin, M., Richard, D., Warden, C., Bouillaud, F. & Ricquier, D. (1998). BMCP1, a Novel Mitochondrial Carrier with High Expression in the Central Nervous System of Humans and Rodents, and Respiration Uncoupling Activity in Recombinant Yeast. *J. Biol. Chem.*, *273*, 34611-34615.
- Scarpulla, R. C. (2008). Transcriptional Paradigms in Mammalian Mitochondrial Biogenesis and Function. *Physiol. Rev.*, *88*, 611-638.
- Seagroves, T. N., Ryan, H. E., Lu, H., Wouters, B. G., Knapp, M., Thibault, P., Laderoute, K. & Johnson, R. S. (2001). Transcription Factor HIF-1 Is a Necessary Mediator of the Pasteur Effect in Mammalian Cells. *Mol. Cell. Biol.*, *21*, 3436-3444.
- Selak, M. A., Armour, S. M., MacKenzie, E. D., Boulahbel, H., Watson, D. G., Mansfield, K. D., Pan, Y., Simon, M. C., Thompson, C. B. & Gottlieb, E. (2005). Succinate links TCA cycle dysfunction to oncogenesis by inhibiting HIF- $\alpha$  prolyl hydroxylase. *Cancer Cell*, *7*, 77-85.
- Semenza, G. (2002). Signal transduction to hypoxia-inducible factor 1. *Biochem Pharmacol*, *64*, 993 - 998.
- Semenza, G. L. (2007). Oxygen-dependent regulation of mitochondrial respiration by hypoxia-inducible factor 1. *Biochem J*, *405*, 1-9.
- Shim, H., Dolde, C., Lewis, B. C., Wu, C.-S., Dang, G., Jungmann, R. A., Dalla-Favera, R. & Dang, C. V. (1997). c-Myc transactivation of LDH-A: Implications for tumor metabolism and growth. *Proceedings of the National Academy of Sciences of the United States of America*, *94*, 6658-6663.

- Shin, Y.-K., Yoo, B. C., Chang, H. J., Jeon, E., Hong, S.-H., Jung, M.-S., Lim, S.-J. & Park, J.-G. (2005). Down-regulation of Mitochondrial F1F0-ATP Synthase in Human Colon Cancer Cells with Induced 5-Fluorouracil Resistance. *Cancer Res*, *65*, 3162-3170.
- Schatton, T., Murphy, G. F., Frank, N. Y., Yamaura, K., Waaga-Gasser, A. M., Gasser, M., Zhan, Q., Jordan, S., Duncan, L. M., Weishaupt, C., Fuhlbrigge, R. C., Kupper, T. S., Sayegh, M. H. & Frank, M. H. (2008). Identification of cells initiating human melanomas. *Nature*, *451*, 345-349.
- Schroedel, C., McClintock, D. S., Budinger, G. R. S. & Chandel, N. S. (2002). Hypoxic but not anoxic stabilization of HIF-1alpha requires mitochondrial reactive oxygen species. *Am J Physiol Lung Cell Mol Physiol*, *283*, L922-931.
- Simonnet, H., Alazard, N., Pfeiffer, K., Gallou, C., Beroud, C., Demont, J., Bouvier, R., Schagger, H. & Godinot, C. (2002). Low mitochondrial respiratory chain content correlates with tumor aggressiveness in renal cell carcinoma. *Carcinogenesis*, *23*, 759-768.
- Skulachev, V., Bakeeva, L., Chernyak, B., Domnina, L., Minin, A., Pletjushkina, O., Saprunova, V., Skulachev, I., Tsyplenkova, V., Vasiliev, J., Yaguzhinsky, L. & Zorov, D. (2004). Thread-grain transition of mitochondrial reticulum as a step of mitoptosis and apoptosis. *Molecular and Cellular Biochemistry*, *256-257*, 341-358.
- Skulachev, V. P. (1991). Fatty acid circuit as a physiological mechanism of uncoupling of oxidative phosphorylation. *FEBS Letters*, *294*, 158-162.
- Snyder, S. A., Lanzen, J. L., Braun, R. D., Rosner, G., Secomb, T. W., Biaglow, J., Brizel, D. M. & Dewhirst, M. W. (2001). Simultaneous administration of glucose and hyperoxic gas achieves greater improvement in tumor oxygenation than hyperoxic gas alone. *International Journal of Radiation Oncology\*Biophysics*, *51*, 494-506.
- Stadler, P., Becker, A., Jürgen Feldmann, H., Hänsgen, G., Dunst, J., Würschmidt, F. & Molls, M. (1999). Influence of the hypoxic subvolume on the survival of patients with head and neck cancer. *International Journal of Radiation Oncology\*Biophysics*, *44*, 749-754.
- Staller, P., Sulitkova, J., Lisztwan, J., Moch, H., Oakeley, E. J. & Krek, W. (2003). Chemokine receptor CXCR4 downregulated by von Hippel-Lindau tumour suppressor pVHL. *Nature*, *425*, 307-311.
- Subarsky, P. & Hill, R. (2003). The hypoxic tumour microenvironment and metastatic progression. *Clinical and Experimental Metastasis*, *20*, 237-250.
- Subarsky, P. & Hill, R. (2008). Graded hypoxia modulates the invasive potential of HT1080 fibrosarcoma and MDA MB231 carcinoma cells. *Clinical and Experimental Metastasis*, *25*, 253-264.
- Sundfor, K., Lyng, H., Kongsgard, U., Tropé, C. & Rofstad, E. K. (1997). Polarographic Measurement of pO<sub>2</sub> in Cervix Carcinoma. *Gynecologic Oncology*, *64*, 230-236.
- Taketa, K., Shimamura, J., Ueda, M., Shimada, Y. & Kosaka, K. (1988). Profiles of Carbohydrate-metabolizing Enzymes in Human Hepatocellular Carcinomas and Preneoplastic Livers. *Cancer Res*, *48*, 467-474.
- Towler, M. C. & Hardie, D. G. (2007). AMP-Activated Protein Kinase in Metabolic Control and Insulin Signaling. *Circ Res*, *100*, 328-341.
- Trenker, M., Malli, R., Fertschaj, I., Levak-Frank, S. & Graier, W. F. (2007). Uncoupling proteins 2 and 3 are fundamental for mitochondrial Ca<sup>2+</sup> uniport. *Nat Cell Biol*, *9*, 445-452.
- Turowski, G. A., Rashid, Z., Hong, F., Madri, J. A. & Basson, M. D. (1994). Glutamine Modulates Phenotype and Stimulates Proliferation in Human Colon Cancer Cell Lines. *Cancer Res*, *54*, 5974-5980.
- Twig, G., Hyde, B. & Shirihai, O. S. (2008). Mitochondrial fusion, fission and autophagy as a quality control axis: The bioenergetic view. *Biochimica et Biophysica Acta (BBA) - Bioenergetics*, *1777*, 1092-1097.
- Urbánková, E., Voltchenko, A., Pohl, P., Jezek, P. & Pohl, E. E. (2003). Transport Kinetics of Uncoupling Proteins: ANALYSIS OF UCP1 RECONSTITUTED IN PLANAR LIPID BILAYERS. *J. Biol. Chem.*, *278*, 32497-32500.
- Uriel, J. (1976). Cancer, Retrodifferentiation, and the Myth of Faust. *Cancer Res*, *36*, 4269-4275.
- Vafa, O., Wade, M., Kern, S., Beeche, M., Pandita, T. K., Hampton, G. M. & Wahl, G. M. (2002). c-Myc Can Induce DNA Damage, Increase Reactive Oxygen Species, and Mitigate p53 Function: A Mechanism for Oncogene-Induced Genetic Instability. *Molecular Cell*, *9*, 1031-1044.
- Valera, A., Pujol, A., Gregori, X., Riu, E., Visa, J. & Bosch, F. (1995). Evidence from transgenic mice that myc regulates hepatic glycolysis. *FASEB J.*, *9*, 1067-1078.
- Valoušková, E., Smolková, K., Šantorová, J., Ježek, P. & Modrianský, M. (2008). Redistribution of cell death-inducing DNA fragmentation factor-like effector-a (CIDEa) from mitochondria to nucleus is associated with apoptosis in HeLa cells. *General Physiology and Biophysics*, *27*, 92-100.
- Vařecha, M., Amrichová, J., Zimmermann, M., Ulman, V., Lukášová, E. & Kozubek, M. (2007). Bioinformatic and image analyses of the cellular localization of the apoptotic proteins endonuclease G, AIF, and AMID during apoptosis in human cells. *Apoptosis*, *12*, 1155-1171.
- Vaupel, P., Hockel, M. & Mayer, A. (2007). Detection and Characterization of Tumor Hypoxia Using pO<sub>2</sub> Histograms. *Antioxidants & Redox Signaling*, *9*, 1221-1236.
- Vaupel, P., Mayer, A., Briest, S. & Hockel, M. (2003). Oxygenation Gain Factor: A Novel Parameter Characterizing the Association between Hemoglobin Level and the Oxygenation Status of Breast Cancers. *Cancer Res*, *63*, 7634-7637.
- Vaupel, P., Mayer, A. & Höckel, M. (2006). Impact of Hemoglobin Levels on Tumor Oxygenation: the Higher, the Better? *Strahlentherapie und Onkologie*, *182*, 63-71.
- Vazquez-Martin, A., Colomer, R., Brunet, J., Lupu, R. & Menendez, J. A. (2008). Overexpression of fatty acid synthase gene activates HER1/HER2 tyrosine kinase receptors in human breast epithelial cells. *Cell Proliferation*, *41*, 59-85.

- Ventura-Clapier, R., Garnier, A. & Veksler, V. (2008). Transcriptional control of mitochondrial biogenesis: the central role of PGC-1 $\alpha$ . *Cardiovasc Res*, *79*, 208-217.
- Vidal-Puig, A., Solanes, G., Grujic, D., Flier, J. S. & Lowell, B. B. (1997). UCP3: An Uncoupling Protein Homologue Expressed Preferentially and Abundantly in Skeletal Muscle and Brown Adipose Tissue. *Biochemical and Biophysical Research Communications*, *235*, 79-82.
- Viswakarma, N., Yu, S., Naik, S., Kashireddy, P., Matsumoto, K., Sarkar, J., Surapureddy, S., Jia, Y., Rao, M. S. & Reddy, J. K. (2007). Transcriptional Regulation of Cidea, Mitochondrial Cell Death-inducing DNA Fragmentation Factor  $\alpha$ -Like Effector A, in Mouse Liver by Peroxisome Proliferator-activated Receptor  $\alpha$  and  $\gamma$ . *J. Biol. Chem.*, *282*, 18613-18624.
- Vizan, P., Boros, L. G., Figueras, A., Capella, G., Mangues, R., Bassilian, S., Lim, S., Lee, W.-N. P. & Cascante, M. (2005). K-ras Codon-Specific Mutations Produce Distinctive Metabolic Phenotypes in Human Fibroblasts. *Cancer Res*, *65*, 5512-5515.
- Warburg, O. (1956). On the origin of cancer cells. *Science*, *123*, 309 - 314.
- Waterland, R., Basu, A., Chance, B. & Poyton, R. (1991). The isoforms of yeast cytochrome c oxidase subunit V alter the in vivo kinetic properties of the holoenzyme. *J. Biol. Chem.*, *266*, 4180-4186.
- Watkins, G., Douglas-Jones, A., Mansel, R. & Jiang, W. (2004). The localisation and reduction of nuclear staining of PPAR $\gamma$  and PGC-1 in human breast cancer. *Oncol Rep*, *12*, 483-488.
- Welford, S. M., Bedogni, B., Gradin, K., Poellinger, L., Broome Powell, M. & Giaccia, A. J. (2006). HIF1 $\alpha$  delays premature senescence through the activation of MIF. *Genes & Development*, *20*, 3366-3371.
- Wigfield, S. M., Winter, S. C., Giatromanolaki, A., Taylor, J., Koukourakis, M. L. & Harris, A. L. (2008). PDK-1 regulates lactate production in hypoxia and is associated with poor prognosis in head and neck squamous cancer. *Br J Cancer*, *98*, 1975-1984.
- Winkler, E. & Klingenberg, M. (1994). Effect of fatty acids on H<sup>+</sup> transport activity of the reconstituted uncoupling protein. *J. Biol. Chem.*, *269*, 2508-2515.
- Wise, D. R., DeBerardinis, R. J., Mancuso, A., Sayed, N., Zhang, X.-Y., Pfeiffer, H. K., Nissim, I., Daikhin, E., Yudkoff, M., McMahon, S. B. & Thompson, C. B. (2008). Myc regulates a transcriptional program that stimulates mitochondrial glutaminolysis and leads to glutamine addiction. *Proceedings of the National Academy of Sciences*, *105*, 18782-18787.
- Wu, Z., Puigserver, P., Andersson, U., Zhang, C., Adelmant, G., Mootha, V., Troy, A., Cinti, S., Lowell, B., Scarpulla, R. C. & Spiegelman, B. M. (1999). Mechanisms Controlling Mitochondrial Biogenesis and Respiration through the Thermogenic Coactivator PGC-1. *Cell*, *98*, 115-124.
- Wu, Z., Zhang, J. & Zhao, B. (2009). Superoxide Anion Regulates the Mitochondrial Free Ca<sup>2+</sup> Through Uncoupling Proteins. *Antioxidants & Redox Signaling*, *11*, 1805-1818.
- Xie, H., Valera, V., Merino, M., Amato, A., Signoretti, S., Linehan, W., Sukhatme, V. & Seth, P. (2009). LDH-A inhibition, a therapeutic strategy for treatment of hereditary leiomyomatosis and renal cell cancer *Mol Cancer Ther.*, *8*, 626-635.
- Youle, R. J. & Karbowski, M. (2005). Mitochondrial fission in apoptosis. *Nat Rev Mol Cell Biol*, *6*, 657-663.
- Yu, X., Mao, W., Zhong, A., Schow, P., Brush, J., Sherwood, S. W., Adams, S. H. & Pan, G. (2000). Characterization of novel UCP5/BMCP1 isoforms and differential regulation of UCP4 and UCP5 expression through dietary or temperature manipulation. *FASEB J.*, *14*, 1611-1618.
- Yuneva, M., Zamboni, N., Oefner, P., Sachidanandam, R. & Lazebnik, Y. (2007). Deficiency in glutamine but not glucose induces MYC-dependent apoptosis in human cells. *J. Cell Biol.*, *178*, 93-105.
- Zhang, C.-Y., Baffy, G., Perret, P., Krauss, S., Peroni, O., Grujic, D., Hagen, T., Vidal-Puig, A. J., Boss, O., Kim, Y.-B., Zheng, X. X., Wheeler, M. B., Shulman, G. I., Chan, C. B. & Lowell, B. B. (2001). Uncoupling Protein-2 Negatively Regulates Insulin Secretion and Is a Major Link between Obesity,  $\beta$  Cell Dysfunction, and Type 2 Diabetes. *Cell*, *105*, 745-755.
- Zhang, H., Gao, P., Fukuda, R., Kumar, G., Krishnamachary, B., Zeller, K. I., Dang, C. V. & Semenza, G. L. (2007). HIF-1 Inhibits Mitochondrial Biogenesis and Cellular Respiration in VHL-Deficient Renal Cell Carcinoma by Repression of C-MYC Activity. *Cancer Cell*, *11*, 407-420.
- Zhang, M., Wang, B., Ni, Y.-h., Liu, F., Fei, L., Pan, X.-q., Guo, M., Chen, R.-h. & Guo, X.-r. (2006). Overexpression of uncoupling protein 4 promotes proliferation and inhibits apoptosis and differentiation of preadipocytes. *Life Sciences*, *79*, 1428-1435.
- Zhou, S., Kachhap, S. & Singh, K. K. (2003a). Mitochondrial impairment in p53-deficient human cancer cells. *Mutagenesis*, *18*, 287-292.
- Zhou, S., Kachhap, S., Sun, W., Wu, G., Chuang, A., Poeta, L., Grumbine, L., Mithani, S. K., Chatterjee, A., Koch, W., Westra, W. H., Maitra, A., Glazer, C., Carducci, M., Sidransky, D., McFate, T., Verma, A. & Califano, J. A. (2007). Frequency and phenotypic implications of mitochondrial DNA mutations in human squamous cell cancers of the head and neck. *Proceedings of the National Academy of Sciences*, *104*, 7540-7545.
- Zhou, Z., Yon Toh, S., Chen, Z., Guo, K., Peng Ng, C., Ponniah, S., Lin, S.-C., Hong, W. & Li, P. (2003b). Cidea-deficient mice have lean phenotype and are resistant to obesity. *Nat Genet*, *35*, 49-56.
- Zinser, E., Sperka-Gottlieb, C. D., Fasch, E. V., Kohlwein, S. D., Paltauf, F. & Daum, G. (1991). Phospholipid synthesis and lipid composition of subcellular membranes in the unicellular eukaryote *Saccharomyces cerevisiae*. *J. Bacteriol.*, *173*, 2026-2034.

- Zu, X. L. & Guppy, M. (2004). Cancer metabolism: facts, fantasy, and fiction. *Biochemical and Biophysical Research Communications*, 313, 459-465.
- Zundel, W., Schindler, C., Haas-Kogan, D., Koong, A., Kaper, F., Chen, E., Gottschalk, A. R., Ryan, H. E., Johnson, R. S., Jefferson, A. B., Stokoe, D. & Giaccia, A. J. (2000). Loss of PTEN facilitates HIF-1-mediated gene expression. *Genes Dev.*, 14, 391-396.
- Žáčková, M., Skobisova, E., Urbankova, E. & Jezek, P. (2003). Activating {omega}-6 Polyunsaturated Fatty Acids and Inhibitory Purine Nucleotides Are High Affinity Ligands for Novel Mitochondrial Uncoupling Proteins UCP2 and UCP3. *J. Biol. Chem.*, 278, 20761-20769.

## ABBREVIATIONS

2-DG	2-deoxy glucose
Ac-CoA	acetyl-coenzymeA
ACL	ATP-citrate lyase
ADP	adenosine 5'-diphosphate
ALT	alanine aminotransferase
AMPK	AMP-activated protein kinase
AntA	antimycin A
ARNT	aryl-hydrocarbonyl receptor nuclear translocator
ATP	adenosine 5'-triphosphate
BAT	brown adipose tissue
BAX	Bcl-2-associated X protein
BSA	bovine serum albumin
cAMP	cyclic adenosine 3',5'- monophosphate
CIDE	DNA-fragmentation factor-like effector
CoQ	coenzyme Q (ubiquinone)
COX	cytochrome-c-oxidase
CREB	cAMP response element-binding protein
DFF	DNA-fragmentation factor
DMEM	Dulbecco's modified Eagle's medium
DMSO	dimethyl sulfoxide
EDTA	ethylenediaminetetraacetic acid
EGTA	ethylene glycol-bis(2-aminoethylether)-N,N',N'-tetraacetic
EPO	erythropoietin
ETC, ETS	electron transport chain/electron transport system
F6P	fructose-6-phosphate
FA	fatty acid
FAD, FADH <sub>2</sub>	flavin adenine dinucleotide
FASN	fatty acid synthase
FBP	fructose 1,6-bisphosphate
FCCP	carbonyl cyanide p-trifluoromethoxyphenylhydrazone
FDG	2-( <sup>18</sup> F) fluoro-2-deoxy-D-glucose
FH	fumarate hydratase
FIH	factor inhibiting HIF (hypoxia-inducible factor)
G6P	glucose-6-phosphate
GAPDH	glyceraldehyde-3-phosphate dehydrogenase
Glc	glucose
Gln/GAL	glutamine/galactose medium
GLS	glutaminase
GLUT	glucose transporter
GTP	guanosine 5'-triphosphate
HEPES	4-(2-hydroxyethyl)piperazine-1-ethanesulfonic acid
HER	human endothelial receptor
HIF	hypoxia-inducible factor
HK	hexokinase
HRE	hypoxia-responsive element
IBM	inner boundary membrane
ICM	intercristae membrane
ICS	cristae sacks interiors
IM	inner membrane
IMM	inner mitochondrial membrane

LDH	lactate dehydrogenase
MAPK	mitogen-activated protein kinase
ME	malic enzyme
MnSOD	manganese superoxide dismutase
mtDNA	mitochondrial DNA
NAD, NADH	$\beta$ -Nicotinamide adenine dinucleotide
NADPH	nicotinamide adenine dinucleotide phosphate
NF $\kappa$ B	nuclear factor- $\kappa$ B
NO	nitric oxide
NRF	nuclear respiratory factor
OAA	oxaloacetate
ODD	oxygen-dependent degradation
Oligo	oligomycin
OM	outer membrane
OMM	outer mitochondrial membrane
OXPHOS	oxidative phosphorylation
PDK	pyruvate dehydrogenase kinase
PDP	pyruvate dehydrogenase phosphatase
PFK	phosphofructokinase
PGC-1	PPAR $\gamma$ coactivator-1
PHD	prolyl-hydroxylase
PI3K	phosphoinositide 3-kinase
PK	pyruvate kinase
p $_{O_2}$	oxygen pressure
PPP	pentose-phosphate pathway
PUFA	polyunsaturated fatty acid
RCR	respiratory control ratio
ROS	reactive oxygen species
RT-PCR	real-time PCR
SCR	succinate control ratio
SDH	succinate dehydrogenase
TCA	tricarboxylic acid cycle
TFAM	mtDNA transcription factor A
UCP	uncoupling protein
UCPs, UCPn	uncoupling proteins, any uncoupling protein isoform
UCR	uncoupling control ratio
VDAC	voltage-dependent anion channel
VEGF	vascular endothelial growth factor
VHL	von Hippel-Lindau protein
WAT	white adipose tissue
$\alpha$ -KG	$\alpha$ -ketoglutarate

## LIST OF PUBLICATIONS

\*references not directly related to the thesis

1. **Recruitment of mitochondrial uncoupling protein UCP2 after lipopolysaccharide induction.**  
Růžička M, Škobisová E, Dlasková A, Šantorová J, **Smolková K**, Špaček T, Žáčková M, Modrianský M, Jezek P.  
*Int J Biochem Cell Biol.* 2005 Apr;37(4):809-21. **IF 4.009**
2. \* **Functional dynamic compartmentalization of respiratory chain intermediate substrates: implications for the control of energy production and mitochondrial diseases.**  
Benard G, Faustin B, Galinier A, Rocher C, Bellance N, **Smolkova K**, Casteilla L, Rossignol R, Letellier T.  
*Int J Biochem Cell Biol.* 2008;40(8):1543-54. Epub 2007 Dec 14. **IF 4.009**
3. **Redistribution of cell death-inducing DNA fragmentation factor-like effector-a (CIDEa) from mitochondria to nucleus is associated with apoptosis in HeLa cells.**  
Valousková E, **Smolková K**, Santorová J, Jezek P, Modrianský M.  
*Gen Physiol Biophys.* 2008 Jun;27(2):92-100. **IF 1.286**
4. **Absolute levels of transcripts for mitochondrial uncoupling proteins UCP2, UCP3, UCP4, and UCP5 show different patterns in rat and mice tissues.**  
Alán L, **Smolková K**, Kronusová E, Santorová J, Jezek P.  
*J Bioenerg Biomembr.* 2009 Feb;41(1):71-8. Epub 2009 Feb 26. **IF 2.634**
5. \* **Erythropoietin protects against local anesthetic myotoxicity during continuous regional analgesia.**  
Nouette-Gaulain K, Bellance N, Prévost B, Passerieux E, Pertuiset C, Galbes O, **Smolkova K**, Masson F, Miraux S, Delage JP, Letellier T, Rossignol R, Capdevila X, Sztark F.  
*Anesthesiology.* 2009 Mar;110(3):648-59. **IF 4.596**
6. **Bioenergetics of lung tumors: Alteration of mitochondrial biogenesis and respiratory capacity.**  
Bellance N, Benard G, Furt F, Begueret H, Smolková K, Passerieux E, Delage JP, Baste JM, Moreau P, Rossignol R.  
*Int J Biochem Cell Biol.* 2009 41, Aug 25. [Epub ahead of print]
7. **Mitochondrial bioenergetic adaptations of breast cancer cells to aglycemia and hypoxia.**  
**Smolková, K.**, Bellance, N., Scandurra, F., Genot, E. Gnaiger, E., Plecítá-Hlavatá, L., Ježek, P., Rossignol, R. *Int J Biochem Cell Biol.* 2009, 41, revised version submitted, 2009.
8. **Distinctions and similarities of cell bioenergetics and role of mitochondria in hypoxia, cancer, and embryonic development.**  
Ježek, P., Plecítá-Hlavatá, L., **Smolková, K.**, Rossignol, R.  
*Int J Biochem Cell Biol.* 2009, 41, invited review, submitted, 2009.
9. **Role of mitochondria in cancer and metabolic signaling.**  
**Smolková, K.**, Plecítá-Hlavatá, L., Benard, G., Rossignol, R., Ježek, P.,  
*Int J Biochem Cell Biol.* 2009, 41, invited review, 2009.

## **APPENDIX 1**

## MITOCHONDRIAL BIOENERGETIC ADAPTATIONS OF BREAST CANCER CELLS TO AGLYCEMIA AND HYPOXIA

Katarína Smolková<sup>1,2,6</sup>, Nadège Bellance<sup>1,2</sup>, Francesca Scandurra<sup>3</sup>, Elisabeth Genot<sup>4</sup>, Erich Gnaiger<sup>5</sup>, Lydie Plecítá – Hlavatá<sup>6</sup>, Petr Ježek<sup>6</sup>, and Rodrigue Rossignol<sup>1,2\*</sup>

1-INSERM U688, Bordeaux (France)

2-Université Victor Segalen Bordeaux 2, Bordeaux (France)

3-OROBOROS INSTRUMENTS, Innsbruck, Austria.

4-INSERM U889, IECB Pessac (France)

5-Medical University of Innsbruck, Department of General and Transplant Surgery, D. Swarovski Research Laboratory, Innsbruck, Austria;

6-Institute of Physiology, Dept. 75, Academy of Sciences of the Czech Republic (Prague, Czech Republic)

\* Email : rossig@u-bordeaux2.fr

**Abstract:** Breast cancer cells can survive and proliferate under harsh conditions of nutrient deprivation, including limitation in oxygen availability and glucose disponibility. We hypothesized that such environments could trigger metabolic adaptations of mitochondria promoting tumor progression. Here we mimicked aglycemia and hypoxia *in vitro* and compared the mitochondrial and cellular bioenergetic adaptations in human cancer (HTB-126) versus non cancer (HTB-125) cells, originating from breast tissue. Using high-resolution respirometry, we showed that glucose deprivation induced the enhancement of oxidative phosphorylation (OXPHOS) capacity (5 fold) in cancer cells, whereas it remained unchanged in control cells. Likewise, sustained hypoxia (1% oxygen during 6 days) improved cell respiration in non-cancer cells grown in glucose or glucose deprived medium (+34% and +26%, respectively). Conversely, under these conditions of oxygen limitation, routine respiration was strongly reduced in cancer cells (-36% in glucose medium, -24% in glucose deprived medium), and this effect disappeared when hypoxia was combined with glucose deprivation. This demonstrates that cancer cells behave differently than normal cells in bioenergetic adaptations to microenvironmental conditions. These differences in hypoxia and aglycemia tolerance of breast cancer cells compared to non-cancer predecessors may be important in the optimization of strategies for the treatment of breast cancer.

## **Introduction:**

To understand how cancer cells derive their vital energy from microenvironmental nutrients and oxygen is of fundamental importance for the elaboration of adapted anti-cancer therapies and diagnostic approaches (Kroemer and Pouyssegur, 2008). Recent developments indicate that bioenergetic features of cancer cells are highly variable, and could reflect both the primitive metabolic apparatus of cancer-initiating cells, and its ongoing modulation by the tumor microenvironment. The Warburg hypothesis (Warburg, 1930) of glycolytic-only cancer cells was recently challenged by biochemical studies that revealed the existence of a wide class of tumors where ATP is produced at a higher extent by mitochondrial oxidative phosphorylation (OXPHOS) rather than solely by glycolysis (Moreno-Sanchez et al., 2007). Hence, a survey of these studies showed that various tumors produce a significant part of their ATP (> 80%) by the mitochondrion (Zu and Guppy, 2004). Subsequently, an effort has been made in the last decade to propose a bioenergetic classification of cancer cells according to the relative contribution of sole glycolysis and OXPHOS to cellular ATP supply (Moreno-Sanchez et al., 2007). This was further supported by molecular studies which allowed to decipher the metabolic profile of various types of cancer cells, and provided evidence for a bioenergetic signature of human tumors (Cuezva et al., 2004, Cuezva et al., 2002). Yet, the determination of the expression level of key components of glycolysis and oxidative phosphorylation could be used for molecular diagnostics and prognostics. Further detailed investigations of the OXPHOS system in tumors revealed a broader range of modifications including decreased mitochondrial biogenesis (Pedersen, 1978, Cuezva et al., 1997), alterations in activity of the respiratory chain complexes (Simonnet et al., 2002, Simonnet et al., 2003), inhibition of the pyruvate dehydrogenase (PDH) complex (Kim et al., 2006), truncation of the Krebs' cycle with citrate extrusion (Hatzivassiliou et al., 2005), higher binding of hexokinase II to the mitochondrion (Pedersen, 2007), changes in organellar shape and size (Arismendi-Morillo and Castellano-Ramirez, 2008, Arismendi-Morillo, 2009) and the accumulation of mutations in mitochondrial DNA (Ishikawa et al., 2008, Chatterjee et al., 2006). These studies (see review article (Nadege et al., 2009)) helped to delineate the metabolic remodeling of cancer cells and brought inspiration for further investigations. It remains unknown whether the metabolic profile of cancer cells originates from a predefinite cancer initiating stem cell, and how the tumor microenvironment carves this pattern. In a previous study we showed that both the type and the availability of energy substrates participate in the determination of cancer cells bioenergetic profile (Rossignol et al., 2004). For instance, glucose deprivation led to a profound modification of energy pathways toward an oxidative metabolism, with upregulation of respiratory chain proteins and a higher branching, along with a constriction of the mitochondrial network in uterine cervix adenocarcinoma (HeLa), osteosarcoma (143B) or hepatocellular carcinoma (HEPG2) (Rossignol et al., 2004, Plecítá-Hlavatá et al., 2008). Such aglycemia-driven changes were less evident in non-cancer cells, suggesting a cancer specific adaptability to bioenergetic stresses (Rossignol et al., 2004). It is also well known that human primary cells excised from their tissue of origin and placed in cell culture dishes for artificial growth, rapidly shift toward a glycolytic phenotype (Gnaiger and Kemp, 1990, Gstraunthaler et al., 1999). Besides glucose, another key player in the definition of cancer cell's metabolic profile is oxygen tension ( $pO_2$ ). Hypoxia is a common feature of the microenvironment of cancer cells, and tumor

oxygenation can be severely compromised as compared to normal tissue (Vaupel et al., 2007). Thus, it seems more appropriate to investigate the impact of hypoxia and aglycemia on cancer cells which typically encounter this type of stress *in situ*. Therefore, we focused our study on breast cancer cells which have the adaptative capacity to survive under such microenvironmental substrate deprivation (Vaupel and Hockel, 2000). Accordingly, the group of Peter Vaupel obtained low values of intratumoral oxygen tension ranging between 3 to 10 mmHg in breast malignant tissue, while the non-cancer tissue presented with higher values close to 50 mmHg (Vaupel et al., 2003). The "Gatenby and Gillies" microenvironmental model of carcinogenesis (Gatenby and Gillies, 2004, Gatenby and Gillies, 2008) considers that pre-cancer cells are typically found in tissue regions where oxygen and glucose delivery is low. This might have pre-adapted energy metabolism to a life of uncontrolled growth and deregulated cell death. They further proposed that during tumor growth, angiogenesis leads to the elaboration of an inadequate microvasculature, which results in the set-up of intermittent oxygen and glucose deprivation to cancer cells, along with acidification of the extracellular space. Although the impact of aglycemia, hypoxia and acidification on cancer cells metabolic remodelling was analysed in parcellar studies, their combined interaction was insufficiently investigated. Different levels of hypoxia are observed in tumors, and Peter Vaupel proposed the "Janus face" model whereby metabolic adaptations are thought to occur when oxygen levels are decreased below 1%, while more drastic hypoxia (below 0.1%) could trigger the generation of new genetic variants and resistance to apoptosis (Vaupel, 2008, Vaupel and Mayer, 2005). In the present study, we conducted a longitudinal bioenergetic analysis of cancer cells adaptability to oxygen and glucose deprivation. We used human breast carcinoma cells (HTB-126) and their non-cancer counterpart (HTB-125). Our results evidence a bioenergetic improvement of the mitochondrial system of cancer cells after 6 days of growth in the absence of glucose. Conversely, the exposure to hypoxia at 1% O<sub>2</sub> triggered a large reduction of OXPHOS capacity, which resulted in cell death when growth was not supported by glycolysis. This demonstrates that cancer cells behave differently than normal cells in bioenergetic adaptations to microenvironmental conditions.

## Materials and Methods:

**Cell types and culture conditions:** HTB-126 (cell strain derived from the ductal carcinoma of the breast) and HTB-125 (control cell line, a normal fibroblast-like line from the same patient, from normal breast tissue peripheral to an infiltrating ductal carcinoma which was the source for HTB-126) were purchased from ATCC. The "glucose medium" consisted of High Glucose Dulbecco's Modified Eagle Media (DMEM; GIBCO, No [11995](#)), containing 25 mM glucose, supplemented with 10% fetal calf serum (*Hyclone*), 10 mM Hepes, 100 U/ml penicilin, and 100 U/ml of streptomycin. Alternatively, we used the "galactose medium" that consisted of DMEM deprived of glucose (GIBCO, No 11966), supplemented with galactose (10 mM final), and glutamine (6mM final), 10 mM Hepes, 1 mM sodium pyruvate, 100 U/ml penicilin, and 100 U/ml of streptomycin and 10% fetal calf serum - dialyzed (*Hyclone*, No SH30079). All cells were kept in 5% CO<sub>2</sub> at 37°C at air saturation. Hypoxia was obtained by growing the cells in a dedicated hypoxic chamber (Invivo 300 from Biotrace International) with 5% CO<sub>2</sub> and a controlled mixture of air/N<sub>2</sub> to reach stable 1% O<sub>2</sub>.

**Cell viability:** We used the neutral red assay to assess cell viability, as originally described in (Borenfreund and Puerner, 1985). Cells were grown in 96 well-plates in various conditions including aglycemia and hypoxia. They were washed with 0.9% NaCl and incubated with 1/60 v/v of a 4 mg/ml neutral red solution for 2 hours at 37°C. A washing of the cells was performed with 0.9% NaCl and cell fixation was obtained by a rapid washing with a formol-calcium solution (1 ml formaldehyde 40%, 10 ml of 10% calcium-chloride and 89 ml distilled water). Then, cell permeabilization and intracellular membrane lysis was obtained with a solution of 50% ethanol and 1% acetic acid. This results in the extraction of neutral red from the cell and homogenization was performed by stirring the plate. Absorbance was measured in a multi-well scanning spectrophotometer (SAFAS MP96) at a wavelength of 540 nm with a reference set at 630 nm. Tests were done in quadruplicate and repeated three times. The results of neutral red uptake (viability) were expressed as percent value of the control (untreated cells) absorbance.

**Respirometry:** Mitochondrial oxygen consumption assays were performed using the high-resolution respirometry system Oxygraph-2k (OROBOROS INSTRUMENTS, Austria). This instrument provides sufficient sensitivity and time resolution for analysis of the oxygen kinetics of mitochondrial and cellular respiration (Gnaiger, 2001). Cell respiration was measured at different cell densities (from  $2 \cdot 10^5$  to  $2 \cdot 10^6$  per ml according to volume-specific flux) at 37°C in 2 ml chambers containing culture medium (DMEM), at a stirring rate of 700 rpm. Data were digitally recorded using DatLab4 software where oxygen flux was calculated as the negative time derivative of oxygen concentration,  $c_{O_2}(t)$ . Oxygen sensors were calibrated routinely at air saturation and in oxygen depleted media. A standard correction was performed for instrumental background oxygen flux arising from oxygen consumption of the oxygen sensor and minimum back-diffusion into the chamber. Two types of polarographic investigations were performed: *i*) flux measurement on intact cells (as described in (Hutter et al., 2004, Gnaiger, 2008), and *ii*) oxygen kinetics with  $c_{50}$  (or  $P_{50}$ ) determination (as described in Steinlechner-Maran et al., 1996; Pecina et al.,

2004). For the oxygen kinetics measurements, respiration rate was recorded continuously along the entire oxygen range with a data recording interval of 1 s. The data were corrected for the response time of the oxygen sensor (usually 3 – 5 s (Gnaiger, 2001)).  $c_{50}$  and  $J_{\max}$  values were determined in the 1.1 kPa (about 10  $\mu\text{M}$ ) oxygen range, using a standard algorithm of DatLab2 software (Gnaiger et al., 1995). The apparent  $c_{50}$  is the oxygen concentration for half-maximum respiration measured on intact cells in a given condition. It gives a measure of the limitation of mitochondrial energy production by oxygen availability (Gnaiger et al., 1998). The factor for conversion of oxygen pressure to oxygen concentration is 9.5 ( $\text{O}_2$  solubility in DMEM [ $\mu\text{M}\times\text{kPa}^{-1}$ ]).

In our study, we determined various bioenergetic parameters to characterize the cellular state of aerobic energy production (Gnaiger, 2008).

Routine respiration ( $R$ ) was measured in intact cells (in a given culture medium, i.e glucose or galactose), in the coupled state of physiological respiratory control. Non-coupled resting respiration or leak respiration ( $L$ ) is obtained in the presence of oligomycin (2  $\mu\text{g}/\text{ml}$ ) which inhibit the mitochondrial phosphorylation system so that no ATP can be produced, and electron flow reflects the energy requirement to compensate for the proton leak. The maximal uncoupled respiratory activity measured in presence of optimum uncoupler concentration (0.5 steps, 1.5  $\mu\text{M}$  FCCP final in our study) provides a measure of the kinetic capacity of the electron transport system or ETS capacity ( $E$ ), under conditions of physiological substrate supply in the intact cell. Using ETS capacity as a common basis for normalization of coupling control ratios, the  $R/E$  reflects the level of mitochondrial activity relative to the maximal kinetic capacity of the electron transport system. Correspondingly, the  $L/E$  ratio reflects the level of leak respiration relative to ETS capacity and provides an estimate of intrinsic uncoupling. Finally, the fraction of respiration actually used for ATP production is estimated as the difference  $R/E-L/E$  or  $(R-L)/E$  (Hütter et al., 2004). The Crabtree effect was studied by addition to galactose medium of 2 M glucose (25 mM final, corresponding to the glucose concentration in high-glucose medium). Respiration of permeabilized cells was measured in respiration medium MiRO5 (0.5 mM EGTA, 3 mM  $\text{MgCl}_2\cdot 6\text{H}_2\text{O}$ , 65 mM KCl, 20 mM taurine, 10 mM  $\text{KH}_2\text{PO}_4$ , 20 mM HEPES, 110 mM sucrose, 1 g/l BSA, pH 7.1; Gnaiger et al., 2000). Respiratory substrates were 2 mM malate, 10 mM glutamate for Complex I respiration, with addition of 10 mM succinate to determine the additive effect of convergent electron input through Complex I+II (Gnaiger, 2009). OXPHOS capacity was measured with 4 mM ADP. Respiration was inhibited with rotenone (200 nM), antimycin A (2.5  $\mu\text{M}$ ) or KCN (0.5 mM).

**Microscopy:** The morphology of the mitochondrial network was studied by fluorescence confocal microscopy using Mitotracker Green (Invitrogen) 150 nM for 20 min at 37°C, on a FluoView laser scanning inverted microscope (Nikon). The reconstitution of three-dimensional images was performed using Imaris Software (Bitplane). Cells were grown in glucose or glucose-deprived medium, in normoxia or hypoxia (as précised in the results and legends) on glass chamber (Lab-Tek) and series of images were taken from three different chambers. Images were selected randomly and the analysis was performed using a double-blinded approach. The area of mitochondrial sections was determined using Scanview and ImageJ software. The total mitochondrial area was normalized to the cell nucleus area on each micrograph. For each biopsy, thirty images were analyzed.

**Western-Blotting:** Cell lysis was performed using 4% lauryl-maltoside, for 30 min on ice.

Sample preparation and electrophoresis were performed as described previously (Benard et al., 2006b). Antibody against the respiratory chain complexes were obtained from *Mitoscience* (Eugene, OR). Actin antibody were purchased from *SantaCruz Biotechnology*; The signal was detected using the chemiluminescent ECL Plus reagent (GE Healthcare) and a Chemidoc system (Biorad). It was quantified by densitometric analysis using Image J (*NIH*) software.

***Statistical analysis:*** All the data presented in this study correspond to the mean value of  $N$  experiments  $\pm$  SD, with  $N \geq 3$  (see figure legends). Comparison of the data sets was performed with the Student's t test, using SigmaPlot. Two sets of data were considered statistically different when  $P < 0.05$ .

## Results:

**1) Cell viability is supported by OXPHOS in glucose-deprived medium:** Breast cancer cells (HTB-126) and their non-cancer predecessors (HTB-125) were grown in cell culture medium with or without glucose, as previously described (Reitzer et al., 1979, Rossignol et al., 2004). The neutral red assay measures the active uptake of neutral red inside the cell. It can be used as a metabolic index related to cell viability, as discussed previously (Nouette-Gaulain et al., 2009). To assess the actual dependency of neutral red uptake on mitochondrial energy production we determined first the effect of inhibitors of the OXPHOS system (**Figure 1**). The results indicate a dose-dependent inhibition of the neutral red uptake by F<sub>1</sub>-F<sub>0</sub> ATPsynthase inhibitor oligomycin (Fig. 1A), complex I inhibitor rotenone (Fig. 1B), and complex III inhibitor antimycin A (Fig. 1C) in HTB-126 cancer cells grown in galactose-glutamine medium. No significant effect was observed for the same doses of inhibitors in HTB-126 cells grown in glucose medium (**Figure 1A,B,C**). This demonstrates that cancer cells viability is closely linked to mitochondrial energy production in glucose-deprived medium.

**2) The viability of cancer cells is controlled by glucose disponibility and oxygen availability:** The effect of hypoxia was studied while cells were incubated at normoxia, or at hypoxia (1% oxygen) during 1 or 6 days, and cell viability was assessed using the neutral red assay during the exponential phase of growth in glucose or galactose-glutamine medium (**Figure 1D**). We expressed the results as the ratio of the neutral red uptake measured in hypoxia to that measured at normoxia. A ratio of 1 means that viability was similar in hypoxia and normoxia; a ratio < 1 indicates a loss of viability in hypoxia. In HTB-125 non-cancer cells grown in glucose medium, hypoxia induced a decrease in cell viability at day 1 (20 ± 14% reduction), and no significant change at day 6. Conversely, in cancer cells (HTB-126), 6 days of hypoxia resulted in a large increase in cell viability (54 ± 6% increase). In glucose-deprived medium, 6 days of hypoxia induced a significant decrease of cell viability both in HTB-125 cells (51 ± 8% reduction after 6 days), or in cancer HTB-126 (all the cells died). This suggests that 6 days of growth at 1% O<sub>2</sub> hypoxia exerts opposite effects on cancer cells viability, depending on the presence or absence of glucose in the culture medium.

**3) Sustained glucose deprivation improves OXPHOS capacity in cancer cells:** We used high-resolution respirometry to assess the impact of glucose deprivation on routine respiration in intact cells (**Figure 2A**). We compared the respiratory activities obtained *i*) in glucose medium, *ii*) just after glucose removal and replacement by galactose-glutamine (indicated by the symbol "Gal 0"), and *iii*) after 4 days of growth in glucose deprived-medium (indicated by the symbol "Gal 4"). Routine respiration in glucose medium was lower ( $P < 0.05$ ) for the HTB-126 cancer cells ( $JO_2 = 24 \pm 4.8 \text{ pmol O}_2 \cdot \text{s}^{-1} \cdot 10^{-6} \text{ cells}$ ) versus the HTB-125 non-cancer cells ( $JO_2 = 41.4 \pm 1.6 \text{ pmol O}_2 \cdot \text{s}^{-1} \cdot 10^{-6} \text{ cells}$ ). The immediate removal of glucose ("Gal 0") induced no significant effect in non-cancer cells, while a doubling of the respiratory activity was measured in cancer cells (**Figure 2A**). This increase is known as the removal of Crabtree effect, describing glucose-mediated instant suppression of respiration (Crabtree, 1928). In another set of experiments we measured cell respiration after 4 days of growth in galactose medium (**Figure 2A**). We observed a large increase ( $P < 0.05$ ) of routine respiration in cancer cells ( $90.7 \pm 4.8 \text{ pmol O}_2 \cdot \text{s}^{-1} \cdot 10^{-6} \text{ cells}$ ), while no significant change ( $P < 0.05$ ) was measured in the non-cancer cells ( $49.9 \pm$

4.4 pmol O<sub>2</sub>·s<sup>-1</sup>·10<sup>-6</sup> cells). Under all conditions we also determined the oxygen pressure at 50% of maximum flux ( $c_{50}$ ), which gives a measure of the apparent affinity of the cell to oxygen (see traces of **Figure 2B**). The  $c_{50}$  was constant at 0.6 to 0.8 μM in HTB-125 cells under all substrate conditions (Glc, Gal 0 and Gal 4; Fig. 2C) when respiratory activity was unchanged (Fig. 2A). This value of the  $c_{50}$  agrees with the oxygen affinity observed in human umbilical vein endothelial cells and fibroblasts (Steinlechner-Maran et al., 1996; Pecina et al., 2004). The  $c_{50}$  increased significantly to 1.1 μM (affinity to oxygen decreased) in HTB-126 cells (Gal 4) when respiration per cell doubled in comparison to HTB-125 cells (Fig. 2). Such an increase of  $c_{50}$  is expected with increasing turnover of cytochrome *c* oxidase (Gnaiger et al., 1998). It was surprising, therefore, that the  $c_{50}$  did not decline in HTB-126 cells in the presence of glucose under conditions of suppressed respiration (Fig. 2C). The constant  $c_{50}$ , therefore, indicates a regulatory mechanism related to the Crabtree effect, the nature of which is not resolved.

**4) Short-term glucose deprivation illustrates the reversible Crabtree effect:** While considering the peculiarities of the bioenergetics of HTB-126 cancer cells, one must distinguish the adaptative features (as the enhancement of cell respiration observed only after 4 days of growth in glucose deprived medium; see above) from the negative properties. The Crabtree effect does not require adaptations to occur, and was previously defined as the inhibition of mitochondrial ATP production by high concentrations of glucose in yeast (Crabtree, 1928), and subsequently in cancer cells. We observed such a control of OXPHOS by glucose in the HTB-126 cancer cells, since the addition of glucose (“Glc”) to these cells grown in glucose-deprived medium (“Gal0”) triggered a large (39%,  $P < 0.05$ ) reduction of cell respiration (**Figure 3A**). This phenomenon was fully recovered when cells grown in glucose medium were shifted to a glucose-deprived medium (**Figure 3B**). This Crabtree effect was also observed on the uncoupled flux of respiration (**Figure 3C**), indicating that glucose did not interact with the phosphorylation system. Hence, our data reveal a kinetic inhibition of the electron transport system by glucose in cancer cells. This effect was not observed in the non-cancer HTB-125 cells (data not shown). The  $c_{50}$  remained unchanged when the Crabtree effect was removed. After 4 days of growth in glucose deprived medium (“Gal4”), adaptations occurred and routine respiration was increased (**Figure 3A**).

**5) Long-term glucose deprivation leads to increased cell respiration without change in R/E and L/E coupling control ratios, or Complex I/Complex II utilization:** The actual state of mitochondrial respiration in culture medium can be determined in intact cells by the evaluation of two parameters: the *L/E* coupling control ratio which reflects the extent of intrinsic uncoupling, and the *R/E* coupling control ratio which expresses the routine respiration relative to maximal electron transport chain (ETS) capacity. The fraction of oxygen consumption used for ATP production is the  $(R-L)/E$  ratio (see Methods). In HTB-125 non cancer cells we observed a significantly lower *L/E* ratio ( $0.07 \pm 0.02$ ) as compared to the HTB-126 cancer cells ( $0.17 \pm 0.07$ ) (**Figure 4A**). This demonstrates a higher proton leak in cancer cells, which did not vary significantly upon glucose removal in the two cell types. The *R/E* ratio was higher ( $p < 0.05$ ) in cancer cells ( $0.51 \pm 0.05$ ) as compared to non-cancer cells ( $0.40 \pm 0.05$ ), indicating a lower apparent excess capacity of the ETS in cancer cells. Yet, the  $(R-L)/E$  ratios presented no difference between the two cell types nor after glucose removal (Figure 4A), suggesting that ETS was used at the same extent to produce ATP. Moreover, the utilization of specific substrates and inhibitors can be used in

permeabilized cells to describe the respiratory system. In HTB-126 cells previously grown in glucose medium, or adapted to long-term growth in glucose deprived medium, we observed a similar increase in cell respiration when the energy substrates for Complex I respiration (glutamate+malate) were complemented by addition of succinate for determination of convergent Complex I+II respiration (**Figure 4C**). The constant substrate control ratios demonstrate that the entire respiratory system was upregulated upon adaptation to glucose-deprivation, hence suggesting an activation of mitochondrial biogenesis in response to sustained glucose deprivation.

**6) Glucose deprivation stimulates the expression of OXPHOS proteins in cancer cells:** The expression levels of respiratory chain proteins (subunits of complex I, complex II and complex IV) were measured by westernblots on cell lysates prepared from HTB-125 and HTB-126 cells, grown in glucose medium (“Glc”) or glucose deprived medium for 4 days (“Gal4”). An example of westernblot is given in (**Figure 4D inset**), and the results of the densitometric analysis are summarized in the histogram of (**Figure 4D**). We expressed the ratios of the protein band densities measured in samples from glucose-deprived medium, to those obtained in glucose medium (for the same content of cell lysate proteins). A value of 1 means no change in the expression level of complex I, II and IV in glucose deprived medium, while a value >1 indicates the upregulation of these proteins. The results show an increase ( $P < 0.05$ ) of protein expression levels with a mean factor of  $1.26 \pm 0.098$ ,  $1.88 \pm 0.48$  and  $2.39 \pm 0.15$  for CI, CIV and CII in non-cancer cell grown in absence of glucose, respectively. In cancer cells, this increase was more pronounced and the mean factor values were of  $1.28 \pm 0.01$ ,  $4.17 \pm 0.34$  and  $5.97 \pm 1.7$  for CI, CIV and CII, respectively. These data evidence a stronger induction of OXPHOS proteins expression in glucose-deprived medium of cancer cells.

**7) Opposite effect of oxygen limitation on mitochondrial respiration in cancer cells versus non-cancer cells:** The routine cell-specific respiration of HTB-125 and HTB-126 cells grown in glucose or glucose-deprived medium for prolonged time (full adaptation is reached after 4 days), was measured after 6 days in normoxia or 1% hypoxia, as was the pH value of the cell culture medium (**Figure 5**). In non-cancer cells grown in glucose medium, 1% O<sub>2</sub> hypoxia significantly enhanced cell respiration measured at normoxia ( $P < 0.05$ ) by 34% after 6 days. This reflects the increased capacity of the respiratory system. This was also observed in glucose deprived medium (26% increase). Conversely, in cancer cells 1% O<sub>2</sub> hypoxia led to a reduction of routine respiration measured in normoxia, both in glucose medium or glucose-deprived medium (36% and 24% reduction, respectively). The pH measurement revealed a significant ( $P < 0.05$ ) medium acidification in cancer cells grown under aglycemia and hypoxia. This argues for a different sensitivity and a variable response of cell energy metabolism toward hypoxia, in cancer cells versus the non-cancer counterpart.

**8) Determination of mitochondrial network morphology and area in breast cancer versus non-cancer cells:** Mitochondrial bioenergetic capacity is intimately linked to the configuration of the mitochondrial network (Benard et al., 2007, Rossignol et al., 2004, Plecitá-Hlavatá et al., 2008), so we analyzed this feature in living HTB-125 and HTB-126 cells by confocal microscopy (**Figure 6**). In non-cancer HTB-125 cells, neither the removal of glucose nor the limitation of oxygen availability separately triggered a change of the

mitochondrial network morphology and total area. Interestingly, the combination of aglycemia and 1% O<sub>2</sub> hypoxia induced a wider spreading of this network, with a significant increase in the total organellar area (by a factor of 1.93 as compared to normoxic HTB-125 in glucose medium). In HTB-126 cancer cells these changes were more sensitive, as the sole removal of glucose triggered an increase in mitochondrial total area (by a factor of 1.51). Yet, the combination of aglycemia and 1% O<sub>2</sub> hypoxia induced further changes (total mitochondrial area was increased by a factor of 1.91), comparable with what was observed in the non-cancer HTB-125 cells. In all conditions, the mitochondrial network remained in the tubular configuration and no excessive fragmentation was observed (data not shown).

## Discussion:

To study the ability for bioenergetic adaptation of breast cancer cells, along with their consequences for cell viability, we mimicked *in vitro* the tumor microenvironmental conditions of tumor oxygen limitation (1% O<sub>2</sub>;  $p_{O_2} < 7$  mmHg or 1 kPa) and glucose deprivation (no glucose; replaced by galactose and glutamine (Reitzer et al., 1979, Rossignol et al., 2004)). In HTB-126 cancer cells and their non-cancer predecessors (HTB-125) we assessed mitochondrial oxidative capacity and affinity for oxygen after 1 or 6 days of hypoxia, aglycemia, or a combination of both stresses.

Prior to the analysis of the bioenergetic adaption of cancer cells to environmental substrate limitations, it was necessary to study the mitochondrial respiratory capacity of cancer cells and non-cancer cells. To this aim, we compared the rate of respiration of these cells placed in the same conditions of energy substrate availability, pH and temperature. In glucose medium, the rate of respiration was lower for cancer cells as compared to non-cancer cells. It could therefore be concluded that mitochondrial respiratory capacity is reduced in cancer cells. However, the rate of routine respiration of cancer cells measured in the absence of glucose ("Gal 0" conditions), was similar to that of non-cancer cells. This discrepancy is known as the Crabtree effect according to which high concentrations of glucose inhibit mitochondrial respiration in cancer cells (Crabtree, 1928). In our study we give a demonstration of this reversible phenomenon in breast cancer cells. The underlying mechanisms still remain unresolved, and current theories suggest that some intermediates of glucose oxidation could inhibit mitochondrial oxidative phosphorylation. Biochemical studies performed on yeast suggest that fructose 1,6-bisphosphate could play a determinant role in this process (Diaz-Ruiz et al., 2008). Hepatoma cells show a 50-fold increase of this metabolite concentration following 5 mM glucose addition to the cells (Rodriguez-Enriquez et al., 2001). Interestingly, the addition of galactose did not change the level of fructose 1,6-bisphosphate in this previous study, and we observed the removal of this Crabtree effect when glucose was replaced by galactose. It is important to note that galactose is not used as a fuel by cancer cells, but serves for nucleic acids synthesis, while glutamine is consumed by the mitochondria to produce ATP. This was demonstrated on HeLa cells using C<sub>13</sub> labelled glucose and glutamine (Reitzer et al., 1979, Donnelly and Scheffler, 1976). Thus, to compare the bioenergetic status of cancer cells versus non cancer cells while taking into consideration the Crabtree effect, it is required to compare the cells placed in the "Glc" and the "Gal 0" conditions, as defined in our study. Moreover, the rapid loss of HTB-126 cancer cell viability induced by various inhibitors of the OXPHOS system was observed only in glucose-deprived medium, further emphasizing the fact that ATP is derived from OXPHOS in this medium.

Yet, the sole rate of intact cell respiration (routine respiration) is not sufficient to delineate the bioenergetic status, since it gives no information on the actual extent of oxygen consumption used for ATP synthesis. This is reflected more by the L/E ratio, the R/E ratio, and the (R-I)/E ratio. Accordingly, we evidenced i) a higher proton leak in cancer cells (which might be explained by difference in membrane composition and fluidity or slipping of the OXPHOS components), ii) a lower apparent excess capacity of the ETS in cancer cells (which might be explained by differences in the kinetic parameters and the specific regulation of the OXPHOS components), and iii) the same extent of ETS utilization for ATP production. This might allow to reconsider or refine the hypothesis of dysfunctional mitochondria in tumors (Warburg, 1930, John, 2001), as our results indicate

a significant part (around 35 %) of mitochondrial respiration used for ATP synthesis in both cell types, and an important role of the OXPHOS system for energy production and cell survival in situations of glucose limitation. This strengthens the need for a thorough evaluation of the metabolic profile of tumors, along with a characterization of their microenvironment, in order to derive adapted therapies (Moreno-Sanchez et al., 2007, Zu and Guppy, 2004, Nadege et al., 2009).

Our study further demonstrates the determinant role of mitochondrial oxidative phosphorylation in cancer cell energetics, as we observed a significant upregulation of mitochondrial OXPHOS proteins in glucose deprived medium. For instance, the expression level of complex IV subunit one was increased by a factor of 6, after only 4 days of growth in aglycemia, and this was associated with a 3-fold increase of respiration in the HTB-126 cancer cells, while no significant change was measured in the corresponding non-cancer cells. Given the higher energy needs of cancer cells for supporting their deregulated growth and extensive biosyntheses, one could hypothesize that cancer cells have to enhance their OXPHOS system when the fuel for energy production switches from glycolytic to oxidative-only. In non-stringent conditions, glucose is the preferential energy substrate of cancer cells, and its consumption is typically enhanced by the expression of more rapid and irreversible isoforms of the glycolytic pathway (Mathupala et al., 1997). In our study, we observed the enhancement of the OXPHOS pathway when glucose was replaced by glutamine. This could suggest that the strong energy demand of cancer cells dictates the upregulation of whatever energy pathway is used, as determined by the type and availability of the energy substrate. This peculiarity was observed for other cancer cells (HeLa, 143B (Rossignol et al., 2004) and HepG2 (Plecitá-Hlavatá et al., 2008)), and could designate the underlying pathway of metabolic remodeling as a potential target for anti-cancer therapy. These regulatory pathways could involve HIF1 $\alpha$  and PGC1 $\alpha$ , which are the two main orchestrators of the pseudo-hypoxic metabolic changes (Pollard et al., 2005, Bratslavsky et al., 2007, King et al., 2006), and the energy-dependent control of mitochondrial biogenesis (Ventura-Clapier et al., 2008), respectively. In addition to glucose deprivation which drives the above discussed metabolic adaptations, cancer cells are also confronted to oxygen limitation. Thus, we looked at the bioenergetic changes triggered by 1% O<sub>2</sub> hypoxia in HTB-126 and HTB-125 cells. We found that 1% O<sub>2</sub> hypoxia induced a 30% reduction of mitochondrial respiration (measured at normoxia) in HTB-126 cancer cells, while it triggered a 30% increase in HTB-125 non-cancer cells. These differences were explained by downregulation and the upregulation of respiratory chain protein expression, respectively. Such a striking difference in the response to hypoxia provides evidence specific features of cancer cells, which might be used for deriving therapeutic strategies. For instance, our observation could explain why hypoxia increases tumor cell sensitivity to glycolytic inhibitors as we observed a metabolic shift towards this pathway for cellular energy production (Liu et al., 2002). Yet, cancer cells have developed a highly (de)regulated oxygen sensing system whereby the factor HIF1 $\alpha$  has become the target of a complex pseudo-hypoxic regulatory mechanism (Bratslavsky et al., 2007). This might alter the sensitivity of cancer cells to oxygen levels, and could explain the opposite response as compared to non-cancer cells, where oxygen limitation triggers the up-regulation of OXPHOS (see model of **Figure 7**). Such enhancement of OXPHOS is a compensatory adaptative response typically observed in normal tissues, and was described in physiological conditions of hypoxia, such as exercise training or high altitude (Dufour et al., 2006, Essop, 2007). In our study, we further measured a lower sensitivity of mitochondrial respiration toward a decrease in oxygen concentration, as we observed

higher  $C_{50}$  values (lower apparent affinity to oxygen) in HTB-126 cells, as compared to the HTB-125s. Again, this might be related to the existence of an interfering pseudo-hypoxic regulatory pathway in cancer cells. To complete our analysis, we combined glucose deprivation with oxygen limitation to analyze the bioenergetic adaptations which may occur, since tissue nutrient deprivation due to inadequate blood supply occurs very early during tumor development. We observed that the specific downregulation of OXPHOS triggered by hypoxia in cancer cells did no longer occur when glutamine was the only substrate for growth, i.e when ATP can only be produced by mitochondria. Hence, under conditions of increased mitochondrial energy demand, 1%  $O_2$  hypoxia cannot downregulate the OXPHOS system, as it occurred in glucose medium. This evidences an interaction and coordination between nutrient sensing and oxygen sensing, for the ultimate determination of cancer cells metabolic apparatus. Our observations might therefore explain in part the existence of two classes of tumors, the glycolytic and the OXPHOS class, as proposed by Zu et al. (Zu and Guppy, 2004), Moreno-Sanchez (Moreno-Sanchez et al., 2007) or Bellance et al. (Nadege et al., 2009). In non-cancer cells, glucose-deprivation did not change the stimulatory effect of hypoxia, so that OXPHOS remained improved by 6 days of growth in 1%  $O_2$ . Noteworthy, the stimulation of OXPHOS by glucose deprivation and by hypoxia were additive in cancer cells. While the changes observed in our study demonstrate a profound remodelling of cancer cells metabolic profile by energy substrate limitation, the analysis of cell viability revealed the importance of these modifications for tumor progression. Hypoxia alone improved greatly cancer cell viability in glucose medium (+54%), while it killed these cells in the absence of glucose. Hence, sustained hypoxia stimulates cell metabolism, possibly via the upregulation of glycolysis and the consecutive enhancement of glucose oxidation. Numerous studies showed that sustained hypoxia stabilizes the transcription factor HIF $\alpha$ , which activates the expression of more rapid and irreversible glycolytic genes, with downstream proliferative and anabolic effects (Denko, 2008). In HTB-125 non-cancer cells, no improvement of cell viability was observed after 6 days of hypoxia, which indicates that solely cancer cells can improve their growth under hypoxia. In glucose-deprived medium, 1%  $O_2$  hypoxia killed all cancer cells, and reduced strongly cell viability in the HTB-125 non-cancer cells (-51%). This further demonstrates that cancer or non-cancer cells rely essentially on glycolysis to survive under 1%  $O_2$  hypoxia. Thus, solely hypoxia without glucose deprivation allows to distinguish cancer cells and non-cancer cells, with regard to their differences in metabolic adaptative capacities. This emphasizes the need for a better fundamental description of the pathways involved in the concertation between oxygen sensing and nutrient sensing in cancer cells. These mechanisms will reveal important difference between cancer and non-cancer cells that could be targeted to inhibit cancer cell's metabolic adaptations and subsequent survival under conditions of glucose and oxygen limitation.

**Acknowledgments:** We thank the French National Institute for Scientific and Medical Research (INSERM), Université Victor Segalen Bordeaux 2, Région Aquitaine, Cancéropôle Grand Sud-Ouest (GSP) and Association contre les Maladies Mitochondriales (Ammi) for financial support. KS was supported by the grants from the Academy of Sciences No. IAA500110701 (to PJ), and AV0Z50110509; she performed a PHD thesis in “co-tutelle” between France and the Czech Republic, supported by a grant from the French Government.

**Abbreviations:** **ADP**, adenosine diphosphate ; **ANT**, adenine nucleotide translocator; **ATP**, adenosine triphosphate; **COX**, cytochrome c oxidase; **Cyt c**, cytochrome c; **CoQ**, coenzyme Q; **ETS**: electron transport chain; **OXPHOS**, oxidative phosphorylation.

## References:

- Arismendi-Morillo, G. (2009). Electron microscopy morphology of the mitochondrial network in human cancer. *The International Journal of Biochemistry & Cell Biology, In Press*.
- Arismendi-Morillo, G. J. & Castellano-Ramirez, A. V. (2008). Ultrastructural mitochondrial pathology in human astrocytic tumors: potentials implications pro-therapeutics strategies. *J Electron Microsc (Tokyo)*, 57, 33-39.
- Benard, G., Bellance, N., James, D., Parrone, P., Fernandez, H., Letellier, T. & Rossignol, R. (2007). Mitochondrial bioenergetics and structural network organization. *J Cell Sci*, 120, 838-848.
- Benard, G., Faustin, B., Passerieux, E., Galinier, A., Rocher, C., Bellance, N., Delage, J. P., Casteilla, L., Letellier, T. & Rossignol, R. (2006a). Physiological diversity of mitochondrial oxidative phosphorylation. *Am J Physiol Cell Physiol*, 291, C1172-1182.
- Benard, G., Faustin, B., Passerieux, E., Galinier, A., Rocher, C., Bellance, N., Delage, J. P., Casteilla, L., Letellier, T. & Rossignol, R. (2006b). Physiological diversity of mitochondrial oxidative phosphorylation. *Am J Physiol Cell Physiol*.
- Borenfreund, E. & Puerner, J. A. (1985). Toxicity determined in vitro by morphological alterations and neutral red absorption. *Toxicol Lett*, 24, 119-124.
- Bratslavsky, G., Sudarshan, S., Neckers, L. & Linehan, W. M. (2007). Pseudohypoxic pathways in renal cell carcinoma. *Clin Cancer Res*, 13, 4667-4671.
- Chance, B. & Williams, G. R. (1955). Respiratory enzymes in oxidative phosphorylation. III. The steady state. *J Biol Chem*, 217, 409-427.
- Chatterjee, A., Mambo, E. & Sidransky, D. (2006). Mitochondrial DNA mutations in human cancer. *Oncogene*, 25, 4663-4674.
- Crabtree, H. G. (1928). The carbohydrate metabolism of certain pathological overgrowths. *Biochem J*, 22, 1289-1298.
- Cuezva, J. M., Chen, G., Alonso, A. M., Isidoro, A., Misek, D. E., Hanash, S. M. & Beer, D. G. (2004). The bioenergetic signature of lung adenocarcinomas is a molecular marker of cancer diagnosis and prognosis. *Carcinogenesis*, 25, 1157-1163.
- Cuezva, J. M., Krajewska, M., de Heredia, M. L., Krajewski, S., Santamaria, G., Kim, H., Zapata, J. M., Marusawa, H., Chamorro, M. & Reed, J. C. (2002). The bioenergetic signature of cancer: a marker of tumor progression. *Cancer Res*, 62, 6674-6681.
- Cuezva, J. M., Ostronoff, L. K., Ricart, J., Lopez de Heredia, M., Di Liegro, C. M. & Izquierdo, J. M. (1997). Mitochondrial biogenesis in the liver during development and oncogenesis. *J Bioenerg Biomembr*, 29, 365-377.
- Denko, N. C. (2008). Hypoxia, HIF1 and glucose metabolism in the solid tumour. *Nat Rev Cancer*, 8, 705-713.
- Diaz-Ruiz, R., Averet, N., Araiza, D., Pinson, B., Uribe-Carvajal, S., Devin, A. & Rigoulet, M. (2008). Mitochondrial oxidative phosphorylation is regulated by fructose 1,6-bisphosphate. A possible role in Crabtree effect induction? *J Biol Chem*, 283, 26948-26955.
- Donnelly, M. & Scheffler, I. (1976). Energy metabolism in respiration deficient and wild type chinese hamster fibroblasts in culture. *J.cell.Physiol*, 89, 39-52.
- Dufour, S. P., Ponsot, E., Zoll, J., Doutreleau, S., Lonsdorfer-Wolf, E., Geny, B., Lampert, E., Fluck, M., Hoppeler, H., Billat, V., Mettauer, B., Richard, R. & Lonsdorfer, J. (2006). Exercise training in normobaric hypoxia in endurance runners. I. Improvement in aerobic performance capacity. *J Appl Physiol*, 100, 1238-1248.
- Essop, M. F. (2007). Cardiac metabolic adaptations in response to chronic hypoxia. *J Physiol*, 584, 715-726.
- Gatenby, R. A. & Gillies, R. J. (2004). Why do cancers have high aerobic glycolysis? *Nat Rev Cancer*, 4, 891-899.
- Gatenby, R. A. & Gillies, R. J. (2008). A microenvironmental model of carcinogenesis. *Nat Rev Cancer*, 8, 56-61.
- Gnaiger, E. (2001). Bioenergetics at low oxygen: dependence of respiration and phosphorylation on oxygen and adenosine diphosphate supply. *Respir Physiol*, 128, 277-297.
- Gnaiger, E. (2008) Polarographic oxygen sensors, the oxygraph and high-resolution respirometry to assess mitochondrial function. In: *Mitochondrial Dysfunction in Drug-Induced Toxicity* (Dykens, J.A., Will, Y., eds.) John Wiley: 327-352.
- Gnaiger, E. (2009) Capacity of oxidative phosphorylation in human skeletal muscle. New perspectives of mitochondrial physiology. *Int J Biochem Cell Biol* doi:10.1016/j.biocel.2009.03.013

- Gnaiger, E. & Kemp, R. B. (1990). Anaerobic metabolism in aerobic mammalian cells: information from the ratio of calorimetric heat flux and respirometric oxygen flux. *Biochim Biophys Acta*, 1016, 328-332.
- Gnaiger, E., Kuznetsov, A.V., Schneeberger, S., Seiler, R., Brandacher, G., Steurer, W., Margreiter, R. (2000) Mitochondria in the cold. In: Life in the Cold (Heldmaier, G., Klingenspor, M., eds.) Springer, Heidelberg, Berlin, New York: 431-442.
- Gnaiger, E., Lassnig, B., Kuznetsov, A. V. & Margreiter, R. (1998). Mitochondrial respiration in the low oxygen environment of the cell. Effect of ADP on oxygen kinetics. *Biochim Biophys Acta*, 1365, 249-254.
- Gnaiger, E., Steinlechner-Maran, R., Mendez, G., Eberl, T. & Margreiter, R. (1995). Control of mitochondrial and cellular respiration by oxygen. *J Bioenerg Biomembr*, 27, 583-596.
- Gstraunthaler, G., Seppi, T. & Pfaller, W. (1999). Impact of culture conditions, culture media volumes, and glucose content on metabolic properties of renal epithelial cell cultures. Are renal cells in tissue culture hypoxic? *Cell Physiol Biochem*, 9, 150-172.
- Hatzivassiliou, G., Zhao, F., Bauer, D. E., Andreadis, C., Shaw, A. N., Dhanak, D., Hingorani, S. R., Tuveson, D. A. & Thompson, C. B. (2005). ATP citrate lyase inhibition can suppress tumor cell growth. *Cancer Cell*, 8, 311-321.
- Hutter, E., Renner, K., Pfister, G., Stockl, P., Jansen-Durr, P. & Gnaiger, E. (2004). Senescence-associated changes in respiration and oxidative phosphorylation in primary human fibroblasts. *Biochem J*, 380, 919-928.
- Ishikawa, K., Takenaga, K., Akimoto, M., Koshikawa, N., Yamaguchi, A., Imanishi, H., Nakada, K., Honma, Y. & Hayashi, J. (2008). ROS-generating mitochondrial DNA mutations can regulate tumor cell metastasis. *Science*, 320, 661-664.
- John, A. P. (2001). Dysfunctional mitochondria, not oxygen insufficiency, cause cancer cells to produce inordinate amounts of lactic acid: the impact of this on the treatment of cancer. *Med Hypotheses*, 57, 429-431.
- Kim, J. W., Tchernyshyov, I., Semenza, G. L. & Dang, C. V. (2006). HIF-1-mediated expression of pyruvate dehydrogenase kinase: a metabolic switch required for cellular adaptation to hypoxia. *Cell Metab*, 3, 177-185.
- King, A., Selak, M. A. & Gottlieb, E. (2006). Succinate dehydrogenase and fumarate hydratase: linking mitochondrial dysfunction and cancer. *Oncogene*, 25, 4675-4682.
- Kroemer, G. & Pouyssegur, J. (2008). Tumor cell metabolism: cancer's Achilles' heel. *Cancer Cell*, 13, 472-482.
- Liu, H., Savaraj, N., Priebe, W. & Lampidis, T. J. (2002). Hypoxia increases tumor cell sensitivity to glycolytic inhibitors: a strategy for solid tumor therapy (Model C). *Biochem Pharmacol*, 64, 1745-1751.
- Mathupala, S. P., Rempel, A. & Pedersen, P. L. (1997). Aberrant glycolytic metabolism of cancer cells: a remarkable coordination of genetic, transcriptional, post-translational, and mutational events that lead to a critical role for type II hexokinase. *J Bioenerg Biomembr*, 29, 339-343.
- Moreno-Sanchez, R., Rodriguez-Enriquez, S., Marin-Hernandez, A. & Saavedra, E. (2007). Energy metabolism in tumor cells. *Febs J*, 274, 1393-1418.
- Nadege, B., Patrick, L. & Rodrigue, R. (2009). Mitochondria: from bioenergetics to the metabolic regulation of carcinogenesis. *Front Biosci*, 14, 4015-4034.
- Nouette-Gaulain, K., Bellance, N., Prevost, B., Passerieux, E., Pertuiset, C., Galbes, O., Smolkova, K., Masson, F., Miraux, S., Delage, J. P., Letellier, T., Rossignol, R., Capdevila, X. & Sztark, F. (2009). Erythropoietin protects against local anesthetic myotoxicity during continuous regional analgesia. *Anesthesiology*, 110, 648-659.
- Passerieux, E., Rossignol, R., Letellier, T. & Delage, J. P. (2007). Physical continuity of the perimysium from myofibers to tendons: involvement in lateral force transmission in skeletal muscle. *J Struct Biol*, 159, 19-28.
- Pecina, P., Gnaiger, E., Zeman, J., Pronicka, E. & Houstek, J. (2004). Decreased affinity for oxygen of cytochrome-c oxidase in Leigh syndrome caused by SURF1 mutations. *Am J Physiol Cell Physiol*, 287, C1384-1388.
- Pedersen, P. (1978). Tumor mitochondria and the bioenergetic of cancer cells. In S. Karger (Ed.) *Progress in experimental tumor research*. pp. 190-274). Basel, New York.
- Pedersen, P. L. (2007). Warburg, me and Hexokinase 2: Multiple discoveries of key molecular events underlying one of cancers' most common phenotypes, the "Warburg Effect", i.e., elevated glycolysis in the presence of oxygen. *J Bioenerg Biomembr*, 39, 211-222.

- Plecita-Hlavata, L., Lessard, M., Santorova, J., Bewersdorf, J. & Jezek, P. (2008). Mitochondrial oxidative phosphorylation and energetic status are reflected by morphology of mitochondrial network in INS-1E and HEP-G2 cells viewed by 4Pi microscopy. *Biochim Biophys Acta*, 1777, 834-846.
- Pollard, P. J., Briere, J. J., Alam, N. A., Barwell, J., Barclay, E., Wortham, N. C., Hunt, T., Mitchell, M., Olpin, S., Moat, S. J., Hargreaves, I. P., Heales, S. J., Chung, Y. L., Griffiths, J. R., Dalglish, A., McGrath, J. A., Gleeson, M. J., Hodgson, S. V., Poulson, R., Rustin, P. & Tomlinson, I. P. (2005). Accumulation of Krebs cycle intermediates and over-expression of HIF1alpha in tumours which result from germline FH and SDH mutations. *Hum Mol Genet*, 14, 2231-2239.
- Reitzer, L., Wice, B. & Kennel, D. (1979). Evidence that glutamine, not sugar, is the major energy source for cultured HeLa cells. *JBC*, 254, 2669-2676.
- Rodriguez-Enriquez, S., Juarez, O., Rodriguez-Zavala, J. S. & Moreno-Sanchez, R. (2001). Multisite control of the Crabtree effect in ascites hepatoma cells. *Eur J Biochem*, 268, 2512-2519.
- Rossignol, R., Gilkerson, R., Aggeler, R., Yamagata, K., Remington, S. J. & Capaldi, R. A. (2004). Energy substrate modulates mitochondrial structure and oxidative capacity in cancer cells. *Cancer Res*, 64, 985-993.
- Simonnet, H., Alazard, N., Pfeiffer, K., Gallou, C., Beroud, C., Demont, J., Bouvier, R., Schagger, H. & Godinot, C. (2002). Low mitochondrial respiratory chain content correlates with tumor aggressiveness in renal cell carcinoma. *Carcinogenesis*, 23, 759-768.
- Simonnet, H., Demont, J., Pfeiffer, K., Guenaneche, L., Bouvier, R., Brandt, U., Schagger, H. & Godinot, C. (2003). Mitochondrial complex I is deficient in renal oncocytomas. *Carcinogenesis*, 24, 1461-1466.
- Steinlechner-Maran, R., Eberl, T., Kunc, M., Margreiter, R. & Gnaiger, E. (1996). Oxygen dependence of respiration in coupled and uncoupled endothelial cells. *Am J Physiol*, 271, C2053-2061.
- Vaupel, P. (2008). Hypoxia and aggressive tumor phenotype: implications for therapy and prognosis. *Oncologist*, 13 Suppl 3, 21-26.
- Vaupel, P. & Hockel, M. (2000). Blood supply, oxygenation status and metabolic microenvironment of breast cancers: characterization and therapeutic relevance. *Int J Oncol*, 17, 869-879.
- Vaupel, P., Hockel, M. & Mayer, A. (2007). Detection and characterization of tumor hypoxia using pO<sub>2</sub> histography. *Antioxid Redox Signal*, 9, 1221-1235.
- Vaupel, P. & Mayer, A. (2005). Effects of anemia and hypoxia on tumor biology. In C. Bokemeyer & H. Ludwig (Eds.) *Anemia in Cancer. European School of Oncology Scientific Updates*. pp. 47-54.
- Vaupel, P., Mayer, A., Briest, S. & Hockel, M. (2003). Oxygenation gain factor: a novel parameter characterizing the association between hemoglobin level and the oxygenation status of breast cancers. *Cancer Res*, 63, 7634-7637.
- Ventura-Clapier, R., Garnier, A. & Veksler, V. (2008). Transcriptional control of mitochondrial biogenesis: the central role of PGC-1{alpha}. *Cardiovasc Res*, 79, 208-217.
- Warburg (1930). *Metabolism of tumors*, (Editor ed.). London: Arnold Constable.
- Zu, X. L. & Guppy, M. (2004). Cancer metabolism: facts, fantasy, and fiction. *Biochem Biophys Res Commun*, 313, 459-465.

## Figures legends:

**Figure 1: Cell viability.** Effect of mitochondrial inhibition on cell viability of cancer cells HTB-126 grown in glucose medium (HTB-126 Glc) and in glucose-deprived medium (HTB-126 Gal) in the presence of mitochondrial inhibitors oligomycin (**A**), rotenone (**B**), and antimycin A (**C**) incubation for 8 hours, measured by the neutral red assay. Data are expressed as the ratio of the neutral red uptake measured in cells treated with OXPHOS inhibitors to that obtained in absence of inhibitors. Values are means  $\pm$  SD with  $N=3$ . (**D**) Cell viability of HTB-125 and HTB-126 grown in glucose (Glc) or glucose-deprived (Gal) medium under normoxia (21% O<sub>2</sub>) and hypoxia (1% O<sub>2</sub>). Data are expressed as neutral red uptake ratios of normoxic to hypoxic cells at day 1 (black) and 6 (white) in 1% oxygen. Values are means  $\pm$  SD.  $N=5$ .

**Figure 2: Cell respiration in glucose/glucose-deprived medium.** (**A**) Routine respiration of HTB-125 and HTB-126 cells in glucose (Glc), after glucose removal (Gal 0) and grown in glucose-deprived medium (Gal 4). Values are means  $\pm$  SD. \*  $P<0.05$  glucose-deprived compared to glucose; \*\*  $P<0.05$  cancer cell line (HTB-126) compared to control cell line (HTB-125). Values are means  $\pm$  SD with  $N>5$ . (**B**) Cell specific respiratory flux as a function of  $p_{O_2}$  of cancer HTB-126 cells in glucose medium (lower lines), after glucose removal (middle line) and in galactose medium (upper line). Representative traces of  $10^6$  cells/ml in culture medium. Dots represent single data points. Data recording interval was 1 s. Solid lines represent hyperbolic fit calculated in the low-oxygen range  $<1.1$  kPa. (**C**) Influence of cultivation conditions on cell respiration of normal and breast cancer cells –  $c_{50}$ .  $c_{50}$  of HTB-125 and HTB-126 cells in glucose (Glc), after glucose removal (Gal 0) and grown in glucose-deprived medium (Gal 4). Values are means  $\pm$  SD.  $N>5$ . \*  $P<0.05$  glucose-deprived compared to glucose; \*\*  $P<0.05$  cancer cell line (HTB-126) compared to control cell line (HTB-125).

**Figure 3: Crabtree effect in breast cancer cells.** Effect of glucose addition (**A**) and glucose removal (**B**) on ROUTINE respiration of intact cells expressed as cell-specific oxygen flow per  $10^6$  cells as a function of  $p_{O_2}$ . Corresponding  $p_{50}$  values are shown in the graph. (**C**) Respiration of cancer cells upon glucose addition and removal, comparison of ROUTINE respiration (full bars) and ETS capacity of uncoupled respiration (empty bars) per  $10^6$  cells. Cells grown in glucose medium (Glc), after glucose removal (Glc/Gal), grown in glucose deprived medium (Gal) and after glucose addition to cells grown in glucose-deprived conditions (Gal/Glc). Values are means  $\pm$  SD.  $N>5$ . \*  $P<0.05$  of Glc/Gal group compared to Glc group; \*\*  $P<0.05$  Gal/Glc group compared to Gal group.

**Figure 4: Respiratory ratios of HTB-125 and HTB-126 intact cells Glc vs. Gal; components of cell respiration in intact cells.** (**A**) Respiratory ratios calculated from polarographic measurements on intact cell using substrates present in the growth medium, and some inhibitors. L/E ratio (white bars) was calculated as the oligomycin-inhibited respiratory rate (leak respiration, L) over the maximal respiratory rate obtained with an uncoupler (ETS capacity, E); R/E ratio (grey bars) was calculated as the routine respiratory rate (R) over the maximal respiratory rate (E); and (R-L)/E ratio gives the part of respiration that is used under routine conditions to produce ATP. Values are means  $\pm$  SD.  $N>5$ . (**B**) State 3 respiration of complex I (CI) and complex I+II (CI+II) of permeabilized cells, quantified by addition of substrates glutamate and malate (CI) and succinate-rotenone

(CI+II) in the presence of ADP. Values are means  $\pm$  SD.  $N>5$ . (C) Western-blot quantification of the respiratory chain content of normal and breast cancer cells upon glucose deprivation. Contents of respiratory complexes I, II and IV were determined using whole cell lysates of HTB-125 and HTB-126 cells grown in glucose or glucose-deprived medium. Results are expressed as ratios of band intensities normalized to beta-actin of the corresponding glucose-deprived to glucose sample pairs. Band intensity was quantified by densitometry. Values are means  $\pm$ SD  $N=3$ . *Graph inset* shows an exemplar western-blot; note band designation and molecular weight (kDa, number in right). \*  $P<0.05$  glucose-deprived compared to glucose; \*\*  $P<0.05$  cancer cell line (HTB-126) compared to control cell line (HTB-125).

**Figure 5: Effect of hypoxia on respiratory flux and medium pH of normal and breast cancer cells.** Respiratory flux of intact HTB-125 and HTB-126 cells in glucose (Glc) or glucose-deprived medium (Gal) in normoxia (open columns) and after exposure to 1% O<sub>2</sub> for six days (full columns) expressed as a cell-specific flow per 10<sup>6</sup> cells (Y1 axis). #  $p<0.05$ . pH of the culture medium was measured after cultivation (Y2 axis). Symbols and bars are means  $\pm$ SD;  $N=3$ .

**Figure 6: Mitochondrial network in HTB-125 and HTB-126 in normoxia and hypoxia.** Images obtained by confocal microscopy were analyzed using Imaris Software (Bitplane). The total mitochondrial area (green) and the nucleus area (black) were measured on 3D projections, and the ratio mitochondria/nucleus was expressed as the normalized mitochondrial compartment. \*  $p<0.05$  Glc compared to Gln for the same cell type, #  $p<0.05$  normoxia compared to hypoxia. Values are means  $\pm$ SD.  $N=100$ .

**Figure 7: Different bioenergetic thresholds in cancer versus non-cancer cells.** Cancer cells adapt their OXPHOS machinery when glucose availability is decreased, while non-cancer cells survive with less intensive adaptations. This indicates a higher sensitivity of the HTB-126 cancer cells toward glucose limitation, and this is represented by a higher "Bioenergetic threshold 1" in these cells. This level of energy impairment below which OXPHOS upregulation arises determines cancer cells survival in situation of glucose low disponibility. It could be explained by a high energy demand of cancer cells, and a less efficient OXPHOS system, as compared to the HTB-125. When hypoxia is combined with aglycemia, the ratio of energy demand to energy supply increases, and cancer cells die more than non-cancer cells. This is represented by a higher "Bioenergetic threshold 2", which indicates the limit below which a limitation of energy substrates (*i.e* glucose and oxygen together) leads to cell death. This might be explained by an already activated hypoxic sensing (pseudo-hypoxic activation of HIF) which artificially increases the sensitivity of cancer cells toward a limitation of oxygen disponibility.

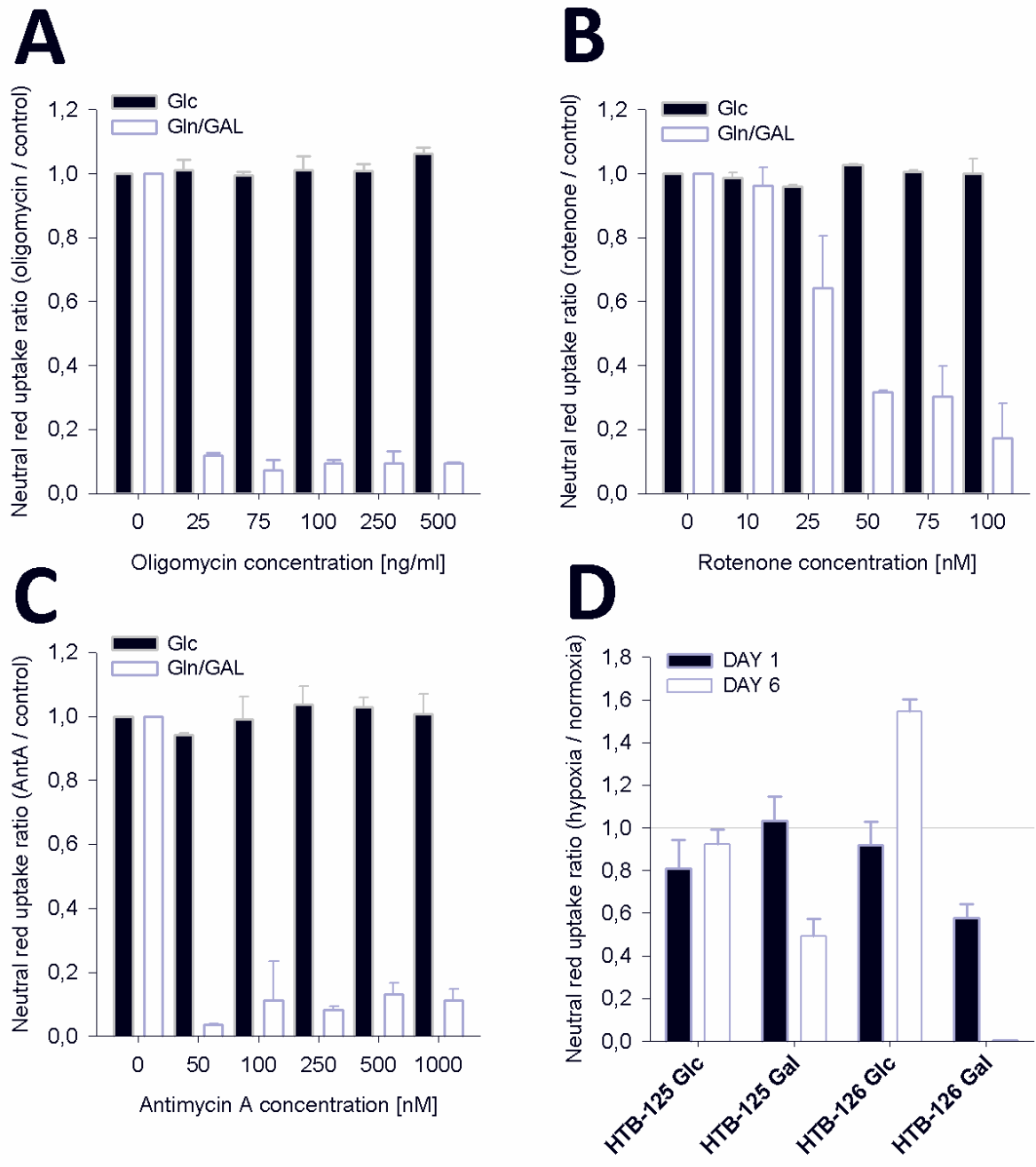


Fig. 1

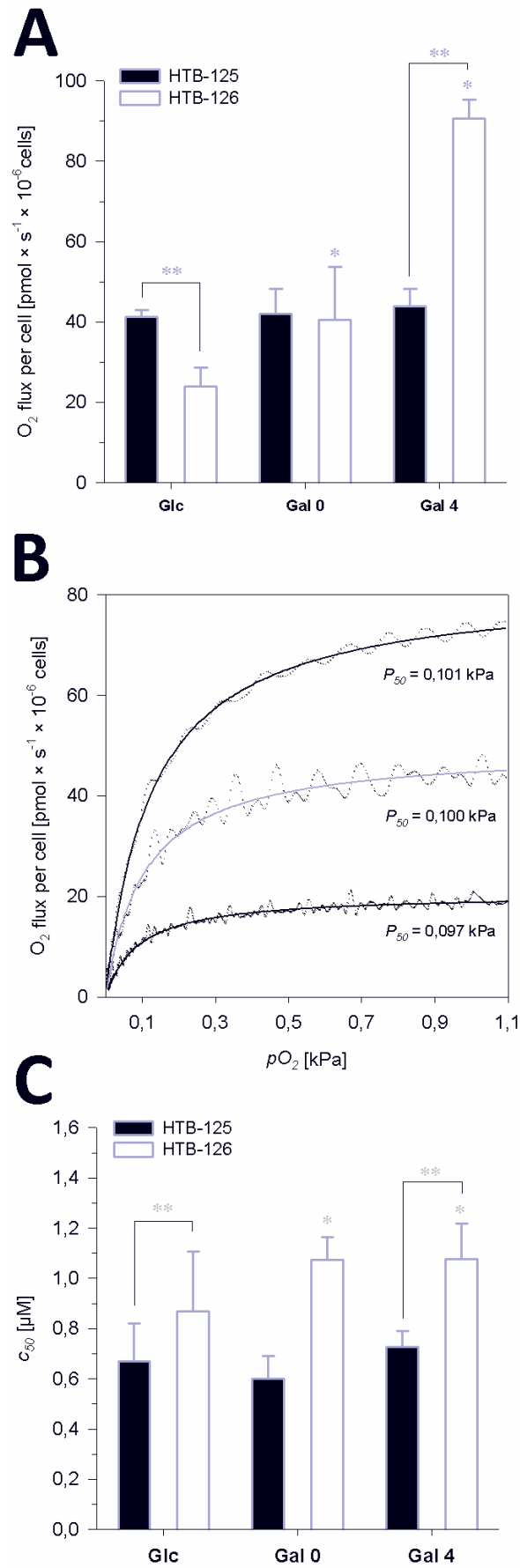


Fig. 2Fig.1

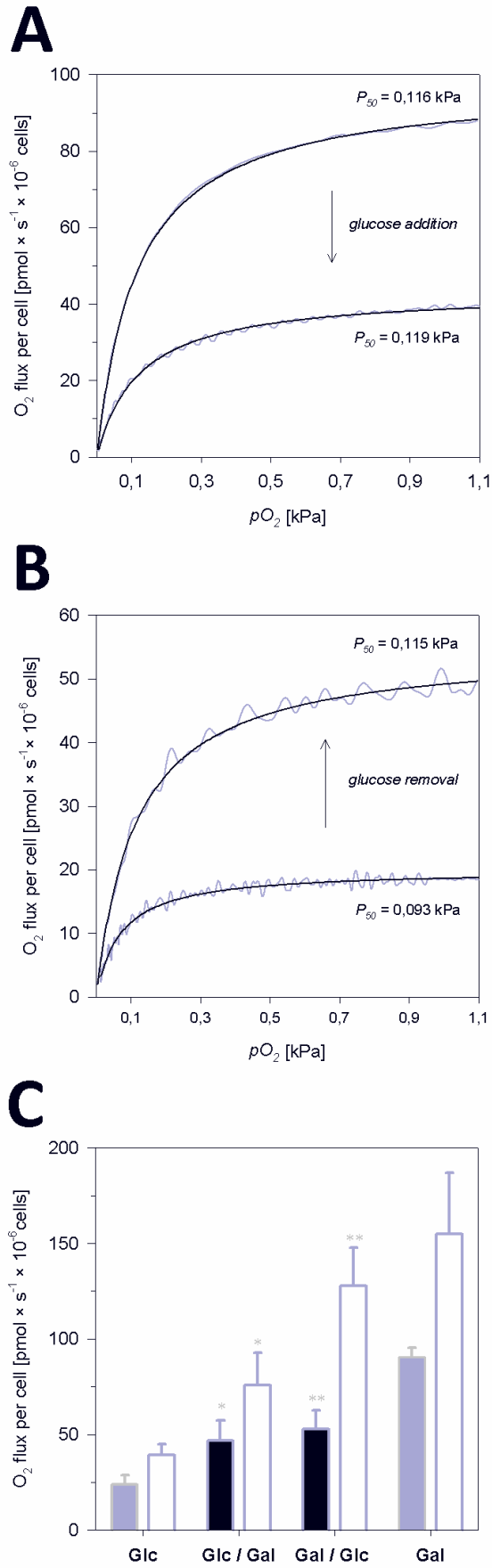


Fig. 3

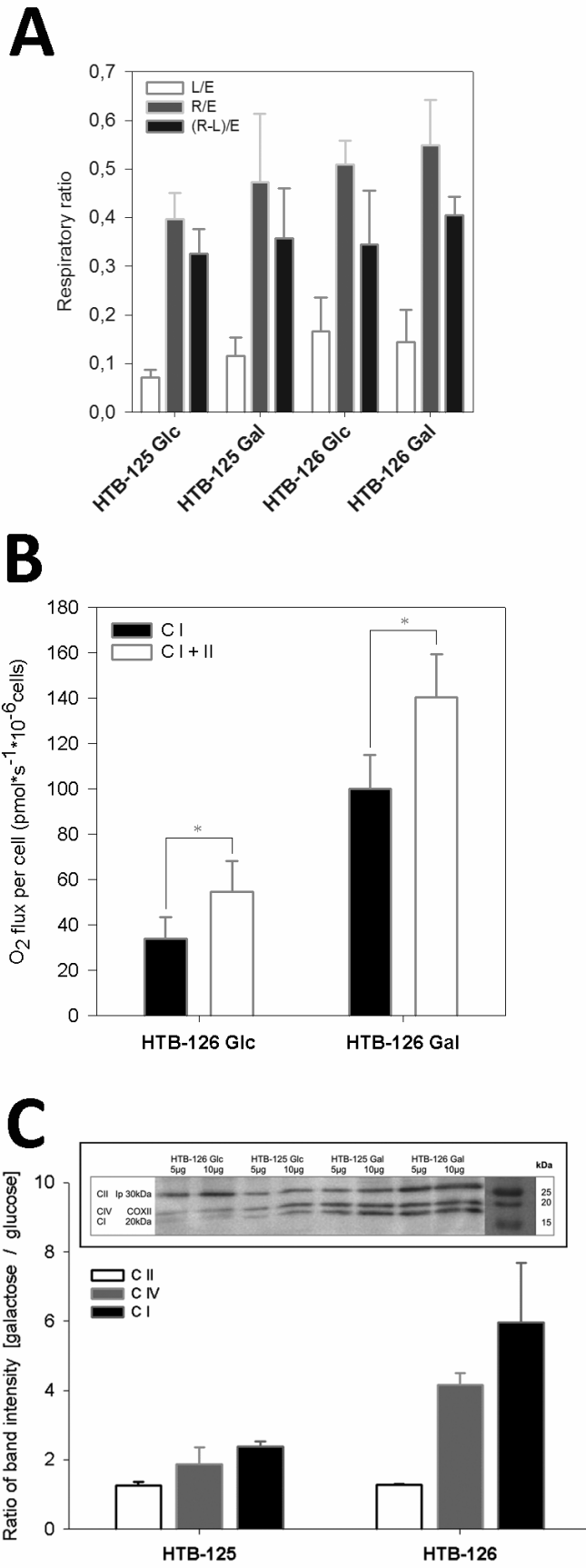


Fig. 4

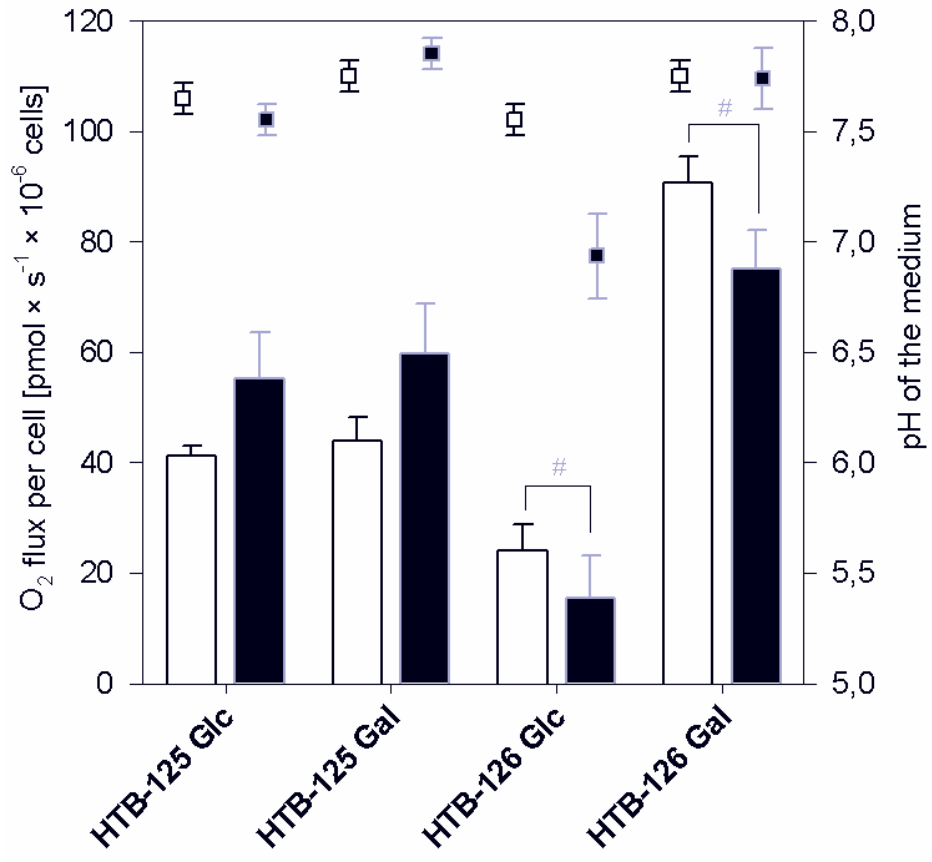


Fig. 5

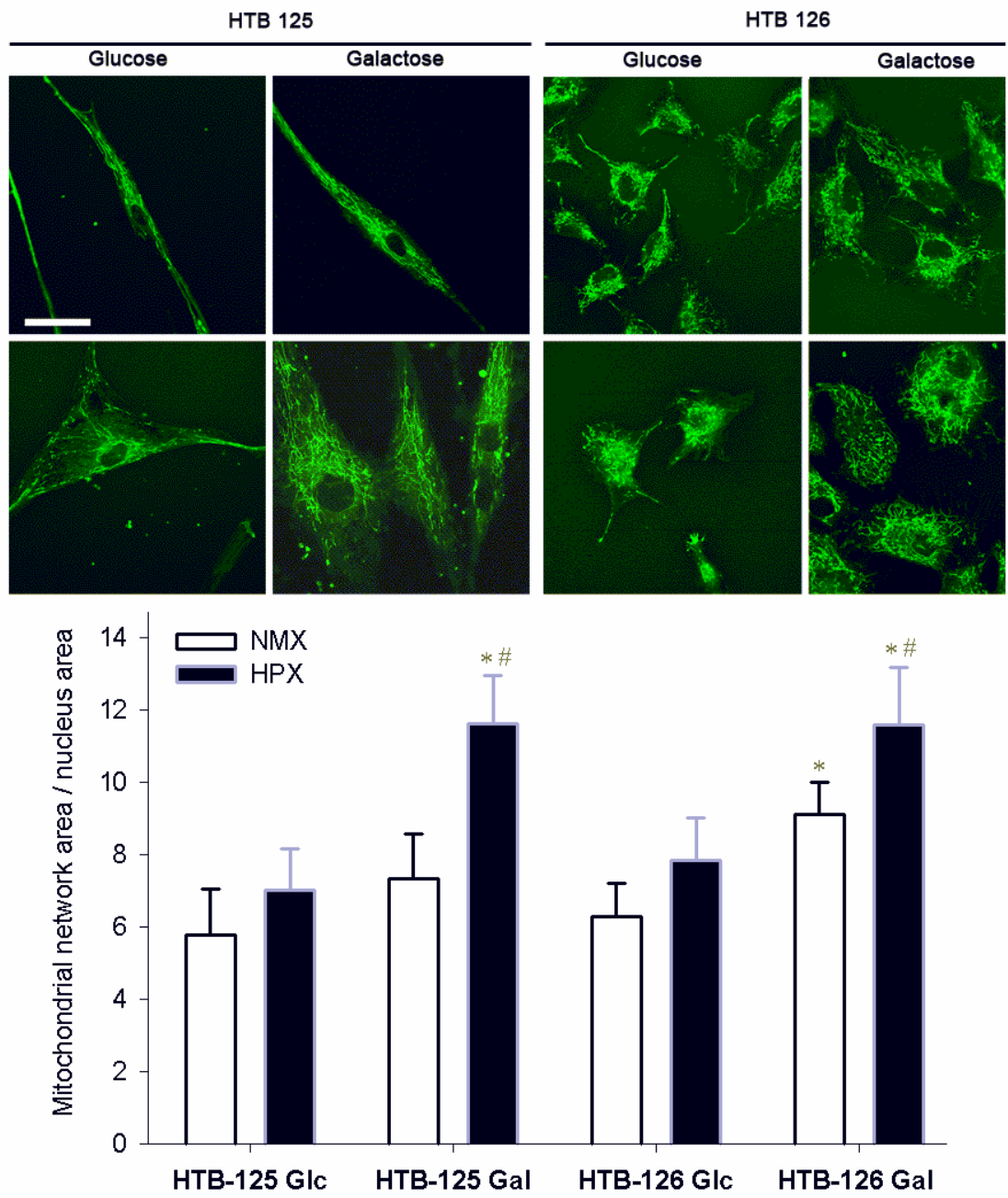


Fig. 6

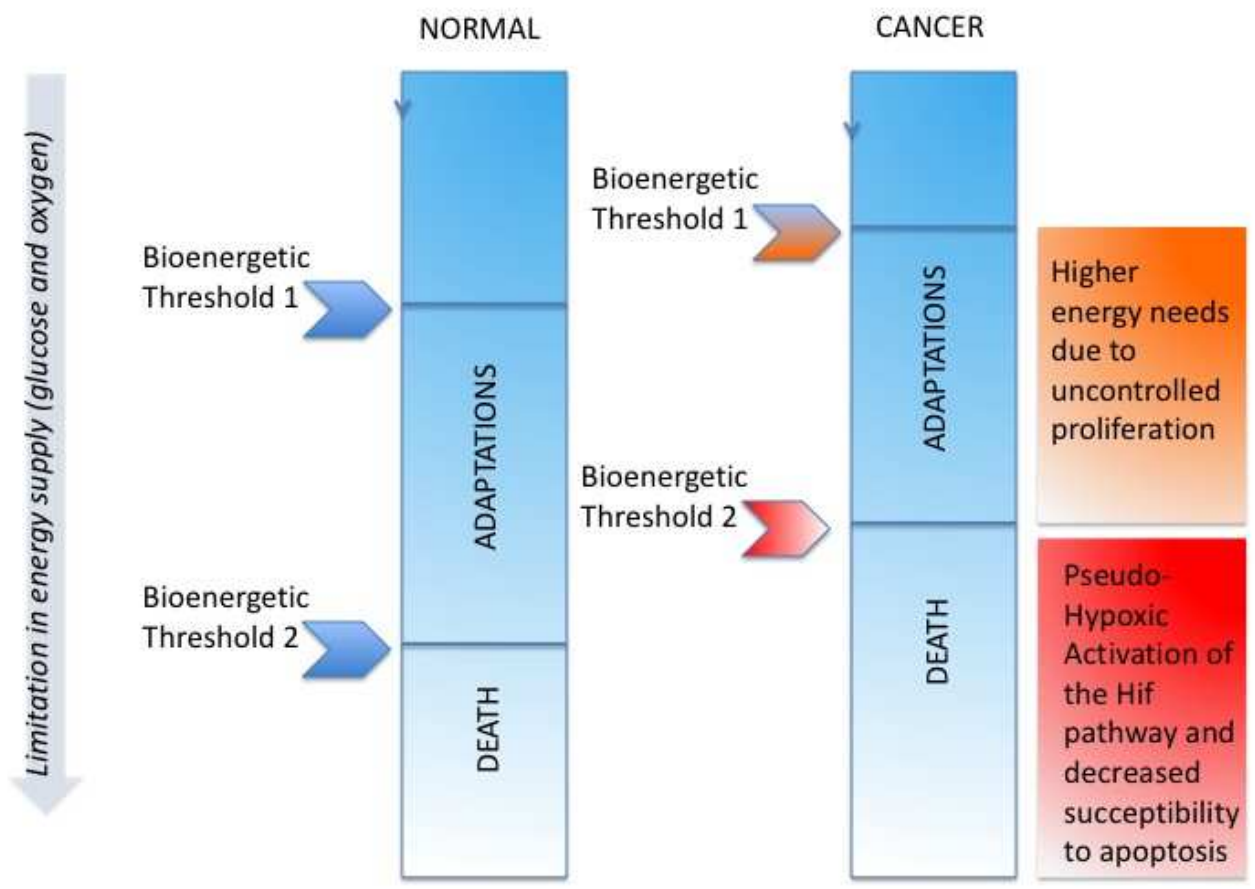


Fig. 7.

## **APPENDIX 2**

# Absolute levels of transcripts for mitochondrial uncoupling proteins UCP2, UCP3, UCP4, and UCP5 show different patterns in rat and mice tissues

Lukáš Alán · Katarína Smolková · Eva Kronusová ·  
Jitka Šantorová · Petr Ježek

Received: 7 November 2008 / Accepted: 29 January 2009 / Published online: 26 February 2009  
© Springer Science + Business Media, LLC 2009

**Abstract** Existing controversies led us to analyze absolute mRNA levels of mitochondrial uncoupling proteins (UCP1–UCP5). Individual UCP isoform mRNA levels varied by up to four orders of magnitude in rat and mouse tissues. UCP2 mRNA content was relatively high (0.4 to 0.8 pg per 10 ng of total mRNA) in rat spleen, rat and mouse lung, and rat heart. Levels of the same order of magnitude were found for UCP3 mRNA in rat and mouse skeletal muscle, for UCP4 and UCP5 mRNA in mouse brain, and for UCP2 and UCP5 mRNA in mouse white adipose tissue. Significant differences in pattern were found for rat vs. mouse tissues, such as the dominance of UCP3/UCP5 vs. UCP2 transcript in mouse heart and vice versa in rat heart; or UCP2 (UCP5) dominance in rat brain contrary to 10-fold higher UCP4 and UCP5 dominance in mouse brain. We predict high antioxidant/antiapoptotic UCP function in tissues with higher UCP mRNA content.

**Keywords** Mitochondrial uncoupling proteins · UCP2 · UCP3 · UCP4 · UCP5 · Absolute mRNA levels

## Introduction

With the exception of mitochondrial uncoupling protein 1 (UCP1), controversies in the research on UCPs cover all aspects including their putative function, i.e. doubts exist whether these proteins really uncouple mitochondria (Affourtit et al. 2007; Cannon et al. 2006; Esteves and Brand 2005). Their physiological roles in tissues will be undoubtedly given by the extent of uncoupling they induce when activated (Esteves and Brand 2005; Ježek et al. 2004). The lack of consensus on UCP function, even after a decade of research since the discovery of UCP2 and UCP3 isoforms, stems from the rather minute amounts expressed (with exception of UCP1) and imported into the inner membrane and from the lack of a clear understanding of isoform-specific tissue distribution. From a bioinformatics viewpoint, UCP1, UCP2, UCP3, UCP4, and UCP5 form a distinct subfamily within the gene family of mitochondrial anion carriers (Hanák and Ježek 2001; Ježek and Ježek 2003; Ježek and Urbánková 2000; Klingenspor et al. 2008). The carrier most sequentially similar to UCPs is the oxoglutarate carrier, which, however, lacks the unique uncoupling protein signature sequences (Hanák and Ježek 2001; Ježek and Ježek 2003; Ježek and Urbánková 2000). Functionally, *in vivo* uncoupling was demonstrated unequivocally for the first known member, UCP1, originally considered to be specific for brown adipose tissue (BAT), where it serves as the final molecular component of catabolic cascade of nonshivering thermogenesis (Cannon et al. 2006). However, UCP1 has also been detected in thymocytes (Adams et al. 2008a, b; Carroll et al. 2005),

Lukáš Alán and Katarína Smolková contributed equally to this work.

L. Alán · K. Smolková · E. Kronusová · J. Šantorová · P. Ježek  
Department of Membrane Transport Biophysics, No.75, Institute  
of Physiology, Academy of Sciences of the Czech Republic,  
Prague, Czech Republic

L. Alán  
e-mail: alan@biomed.cas.cz

K. Smolková  
e-mail: smolkova@biomed.cas.cz

J. Šantorová  
e-mail: santor@biomed.cas.cz

P. Ježek (✉)  
Dept. No.75, Membrane Transport Biophysics,  
Institute of Physiology, Academy of Sciences  
of the Czech Republic, Vídeňská 1083,  
14220 Prague 4, Czech Republic  
e-mail: jezek@biomed.cas.cz

where its thermogenic role is probably replaced by a regulatory role in apoptosis due to its ability to attenuate production of mitochondrial reactive oxygen species (ROS) (Dlasková et al. 2006). ROS facilitate apoptosis, and hence UCP1 activation would have a preventive effect on apoptosis whereas UCP1 inhibition would promote apoptosis. UCP1 was recently detected in skin (Mori et al. 2008), where it is proposed to function (as in thymocytes) as a suppressor of mitochondrial ROS production.

Attempts to derive physiological roles for distinct UCPs also have been based on their expression pattern in various tissues. Owing to their low expression levels (with the exception of UCP1 in BAT), their thermogenic function is rather excluded and as the most relevant function seems to be the attenuation of mitochondrial ROS production (Affourtit et al. 2007; Arsenijevic et al. 2000; Cannon et al. 2006; Esteves and Brand, 2005; Jabůrek et al. 2004; Ježek et al. 2004). Indeed the mild uncoupling is able to attenuate both superoxide formation within Complex III (Ježek and Hlavatá, 2005) as well as Complex I (Dlasková et al. 2008a, b). The extent of such an “antioxidant” mechanism *in vivo* would depend not only on absolute UCP levels but also on the activation state of each UCP and the extent of inhibition by purine nucleotides (Beck et al. 2007). The absolute protein levels serve as a basic parameter for rough estimation of UCP functional relevance in a given tissue.

Determination of UCP expression patterns is difficult due to their extreme hydrophobicity and impossibility to raise antibodies, which would not cross-react with other UCPs (Pecqueur et al. 2001) or with other members of the anion carrier gene family. Hence, most studies have relied on methods quantifying UCP mRNA levels such as northern blotting and RT-PCR. Despite the translational down-regulation described for UCP2 (Hurtaud et al. 2006; Pecqueur et al. 2001) and UCP5 (Kim-Han et al. 2001), or the translational up-regulation of UCPs (Hurtaud et al. 2007), the precise determination of transcript levels still provides valuable information.

UCP2 is considered to be expressed ubiquitously in mammalian tissues (Fleury et al. 1997; Gimeno et al. 1997; Lengacher et al. 2004). In contrast, UCP3 mRNA has been detected in northern blots of human skeletal muscle and in rodent skeletal muscle, heart, and BAT (Boss et al. 1997; Vidal-Puig et al. 1997). The original reports for UCP5 and UCP4 mentioned their high expression in the central nervous system (Mao et al. 1999; Sanchis et al. 1998). Northern blotting also detected UCP5 mRNA in both mouse and human heart, kidney (Kim-Han et al. 2001; Sanchis et al. 1998; Yu et al. 2000) and skeletal muscle (Lengacher et al. 2004; Sanchis et al. 1998; Yu et al. 2000). These results were confirmed by UCP5 immunodetection (Kim-Han et al. 2001). However, Sanchis et al. (1998)

found even wider distribution of UCP5 mRNA, in the rat, mouse, and human gut, lung, testis, uterus, spleen, and white and brown adipose tissue. Additional findings were reported for the human prostate, pancreas, adrenal medulla and cortex, thyroid gland and liver, as well as for the mouse liver (but not spleen), lung, and skeletal muscle (Yu et al. 2000). Using quantitative RT-PCR with TaqMan probes, Lengacher et al. (2004) found not only UCP4 and UCP5 mRNA in the mouse brain cortex (together with a lower amount of UCP2 transcript), but also ~100 times lower levels of UCP3 and UCP1 mRNA. In BAT and skeletal muscle, Lengacher et al. (2004) also identified all five UCP mRNAs, with the UCP1 mRNA level in BAT being ~100-fold higher than all other isoforms, and with UCP3 mRNA level being at least 10-fold higher in skeletal muscle. It is unclear, however, whether the minute levels of UCP mRNAs become translated into mature proteins. If indeed they are translated, one must re-evaluate the molecular physiology of UCPs based on their tissue distribution in light of findings such as UCP1 mRNA in human pancreatic  $\beta$ -cells (Sale et al. 2007), UCP5 in endocrine cells (Ho et al. 2005, 2006), UCP4 mRNA in preadipocytes (Zhang et al. 2006), or of the emerging role of UCP4 and UCP5 in brain pathologies (Liu et al. 2006; Chan et al. 2006; Nakase et al. 2007; Naudí et al. 2007).

In this work, we used quantitative real-time RT-PCR to determine absolute levels of UCP mRNAs, except of UCP1, in selected tissues. The levels of different UCP mRNAs varied by up to four orders of magnitude in various rat tissues. Their distinct pattern was found in mouse tissues. Functional redundancy among UCPs was suggested by different dominance of certain isoforms in given rat and mouse tissues. Whereas UCP2 dominance was found in rat heart, UCP3 and UCP5 dominated in mouse heart. Similar UCP2 (UCP5) dominance in rat brain contrasted to UCP4 and UCP5 dominance in mouse brain with one order of magnitude higher levels of mRNAs.

## Materials and methods

### mRNA isolation

The total RNA was isolated from rat (Wistar, 250 to 275 g) and mouse (Balb/C, 20–25 g) tissues by a standard procedure (Chomczynski and Sacchi 1987). An RNase-free DNase-I was purchased from Top-Bio (Czech Republic). Routinely, mRNA was isolated from the DNase-I-treated total RNA, except for skeletal muscle and white adipose tissue (WAT), using an mRNA isolation kit (Roche Applied Science, USA) and Oligo(dT) 3'Bio-oligo(dT)<sub>20</sub> (Metabion, Czech Republic). Skeletal muscle and WAT mRNAs were extracted using a Fibrous Tissue and Regular Midi RNeasy

kit (Qiagen), respectively, including on-column DNase treatment. The samples of total RNA and mRNA were quantified from their spectra with a subtracted light scattering contribution using an Agilent 8453E UV-VIS spectroscopy system and 200- $\mu$ l quartz cuvettes. An mRNA sample was used for further analysis only when its purity was reflected by the  $A_{260}/A_{280}$  ratios of 1.7 to 1.9.

#### Design of primers and probes for real-time RT-PCR

We quantified UCP mRNAs using a reliable and specific RT-PCR procedure, based on fluorescence signal detection by hybridization probes. When the probes are in proximity, Förster resonance energy transfer proceeds between the probes and indicates their correct annealing to the amplicon cDNA in each PCR cycle. Sets of two primers and two fluorescent hybridization probes were designed as shown in the Table 1 for rat and mouse UCP2 (Růžička et al. 2005), UCP3, UCP4, and UCP5. A primer set for glyceraldehyde-3-phosphate dehydrogenase (*GAPDH*, a house-keeping gene) as well as primer and probe synthesis was provided by TIB MOLBIOL (Berlin, Germany).

Several essential criteria were kept for primer design in order to achieve the highest precision of mRNA quantification. Each PCR primer from a pair was designed to anneal to a different exon (corresponding to the unspliced mRNA molecule or to the gene sequence, where exons are separated by a long intron). This arrangement avoids any quantification of potential contaminating genomic DNA. PCR primers and hybridization probes were designed to hybridize the most variant part of the UCP sequence—the 5'-most—where various UCP isoforms differ (Ježek and Urbánková 2000). For example, in the case of rat UCP2 the amplicon spans 349 base pairs (i.e. bp 136–485). A 1-bp gap was usually left between adjacent hybridization probes (Table 1). We thus sacrificed to choose amplicons close to the 3' terminus, i.e. the way that also includes detection of mRNA that potentially could have been cut/damaged during isolation. In turn, our selected design for UCP3 and UCP5 covers all their splicing variants (Table 1). This is impossible to achieve with amplicons close to the 3' terminus.

#### Quantitative real-time RT-PCR

Routinely, 20–80 ng mRNA was used for real-time RT-PCR on a LightCycler (Roche) with 0.5  $\mu$ M primers and 0.2  $\mu$ M hybridization probes. Reverse transcription was performed (30 min at 55°C) followed by the reverse transcriptase inactivation for 30 s at 95°C, and then by 40 cycles of 2 s denaturation and annealing for 25 s at temperatures described in Table 1, and elongation for 25 s at 72°C. The  $MgCl_2$  content was optimized for each set of primers and

probes (see Table 1). The absolute mRNA amounts, in picograms, were calculated from crossing points of each run. Calibrations were provided by seven order of magnitude-spanning dilution series of the PCR-amplified amplicons, starting from an initial concentration of 10 ng/ $\mu$ l. The calculated calibration slopes (Table 1) approached the predicted theoretical slope of 3.3, meaning that if two starting mRNA samples differed in content by one order of magnitude then equivalent amplified levels would be achieved 3.3 cycles apart. This is equivalent to doubling the amplicon amount in each single cycle.

A series of control experiments were performed for each sample. PCR product length was confirmed by electrophoresis on 1.5% agarose gels. To verify that the genomic DNA was not amplified and thus did not contribute to the quantification, the reverse transcription step was omitted in control runs; in such controls, no fluorescence was detected. The specificity of the primers and hybridization probes for mouse UCP2 was verified with the various tissue mRNA samples of UCP2 (–/–) mice (donated by B.B. Lowell, Harvard Univ., School of Medicine; Zhang et al. 2001), and no fluorescence was observed. Similarly, there was no cross-amplification between particular UCP isoforms when a PCR reaction was performed with a vector containing a cDNA for any other UCP isoform.

## Results

### mRNA levels for UCP2

We have confirmed the presence of UCP2 mRNA in all eight rat tissues studied (Fig. 1a). The absolute amount of UCP2 mRNA (in pg per 10 ng of total isolated mRNA) decreased in the order of spleen > heart > lung > WAT > brain > skeletal muscle > kidney > liver, spanning a 30-fold difference in UCP2 transcript content (Fig. 1a). Only in the rat spleen and lung were the UCP2 transcript levels of the same order of magnitude as the control GAPDH transcript levels. With the exception of the heart UCP2 mRNA, a similar pattern was found for mouse tissues (Fig. 2a). The heart UCP2 transcript level in mouse was up to 40-fold lower than in the mouse lung. In turn, the heart and lung UCP2 transcript levels were equivalent in the rat.

### mRNA levels for UCP3

As expected (Boss et al. 1997; Vidal-Puig et al. 1997), we detected the highest UCP3 mRNA levels in rat and mouse skeletal muscle and intermediate levels in mouse heart (Fig. 1b, Fig. 2b), the latter being of the same order of magnitude as the UCP2 lung transcript levels. In contrast to the very high UCP2 mRNA levels found in the rat heart,

**Table 1** Primer sets and fluorescent hybridization probes used for RT-PCR quantification of UCP mRNAs Primers (forward, f, reverse, r) and probes P<sub>X</sub> and P<sub>LC</sub> were designed as follows. X denotes the fluorescein fluorophore (donor); Red 640 is a Roche fluorophore (acceptor). The annealing temperatures were calculated by the synthesizing company (TIB MOLBIOL, Berlin, Germany)

	Sequence (5'→ 3') / excluded intron	Exon	Amplicon length MgCl <sub>2</sub>	Annealing temperature	Calibration Slope	Calibration Intercept
<b>RAT</b>						
<b>UCP2</b>	<i>f</i> GAGAGTCAAGGGCTAGCGC	exon 2				
	<i>r</i> GCTTCGACAGTGCTCTGGTA	exon 2	350 bp	58°C	- 3.543	- 20.84
	P <sub>X</sub> TCAGAGCATGCAGGCATTGG X intron 1200 bp	exon 2/3				
	P <sub>LC</sub> LC Red640-CCGCCTCCTGGCAGGTAGC p	exon 3	4 mM			
<b>UCP3</b>	<i>f</i> GTTGGACTTCAGCCATCAGAA	exon 1				
	<i>r</i> GTGGGTTGAGCACAGGTC	exon 3	418 bp	58°C	- 3.089	- 18.08
	P <sub>X</sub> GAACGGACCACTCCAGCGTC X intron 1986 bp	exon 2/3				
	P <sub>LC</sub> LC Red640-CCATCAGGATTCTGGCAGGCT p	exon 3	6 mM			
<b>UCP4</b>	<i>f</i> TGGCCGAGCTAGCAACC intron 3023 bp	exon 1/2				
	<i>r</i> CAGAGGGGATAATGTTTCATCTTCA	exon 3	289 bp	58°C	- 3.061	- 17.13
	P <sub>X</sub> CCATTTACAGACACGTAGTGTACTCTGGA X intron 2421 bp	exon 2/3				
	P <sub>LC</sub> LC Rec 640-GTCGGATGGTCACCTACGAACAT p	exon 3	4 mM			
<b>UCP5</b>	<i>f</i> GATTGTAAGCGGACATCAG intron 4713 bp	exon 1/2				
	<i>r</i> GGTTGGCAATAGTAGATGAAATC see Footnote 1	exon 5	419 bp	58°C	- 3.170	- 18.15
	P <sub>X</sub> CGCCATACACAAAAGGTTTCCA X	exon 2				
	P <sub>LC</sub> LC Red640-TTCAGACCAGACATCTCATGGCTTAA p	exon 2	4 mM			
<b>GAPDH</b>	<i>f</i> AACTCCCTCAAGATTGTCAGCAA					
	<i>r</i> ATGTCAGATCCACAACGGATACA		316 bp	58°C	- 3.201	- 18.88
	P <sub>X</sub> CAGTCTTCTGAGTGGCAGTGATGGCA X					
	P <sub>LC</sub> LC Red705-ACTGTGGTCATGAGCCCTTCCACG p		4 mM			
<b>MOUSE</b>						
<b>UCP2</b>	<i>f</i> GAGAGTCAAGGGCTAGTGC	exon 2				
	<i>r</i> GCTTCGACAGTGCTCTGGTA	exon 3	349 bp	56°C	- 3.341	- 18.57
	P <sub>X</sub> TCAGAGCATGCAGGCATCGG X intron 772 bp	exon 2/3				
	P <sub>LC</sub> LC Red640-CCGCCTCCTGGCAGGTAGC p	exon 3	4 mM			
<b>UCP3</b>	<i>f</i> GTTTACTGACAACCTCCCCT intron 62 bp	exon 3/4				
	<i>r</i> CTCCTGAGCCACCATCT	exon 4	165 bp	56°C	- 3.363	- 18.96
	P <sub>X</sub> AAGACCCGATACATGAACGC X	exon 4				
	P <sub>LC</sub> LC Red640-CCCCTAGGCAGGTACCGCp	exon 4	5 mM			
<b>UCP4</b>	<i>f</i> GGACGAGCAAGTTCCTACTG	exon 1				
	<i>r</i> CCCTCCAATGACCGATTTTC see Footnote 2	exon 4	346 bp	56°C	- 3.470	- 16.05
	P <sub>X</sub> CCATTTACAGACACGTAGTGTACTCTGGA X	exon 4				
	P <sub>LC</sub> LC Red640-GTCGGATGGTCACCTATGAACATCTAC p	exon 4	6 mM			
<b>UCP5</b>	<i>f</i> CAGTGATTCATCAGAAAAGTTCCA intron 1/2 5054 bp	exon 1				
	<i>r</i> CCGTGTTTTAGTAAGATCCACAG intron 2/3 1543 bp	exon 3	133 bp	56°C	- 3.37	- 16.89
	P <sub>X</sub> CGCCATACACAAAAGGTTTCCA X	exon 2				
	P <sub>LC</sub> LC Red640-TTCAGACCAGACATCTCATGGCTTAA p	exon 2	5 mM			
<b>GAPDH</b>	<i>f</i> AATGGTGAAGGTTCGGTGTGA					
	<i>r</i> CTGGAAGATGGTATGGGGC		229 bp	56°C	- 3.364	- 21.57
	P <sub>X</sub> GGCAAATTCAACGGCACAGTCAAG X					
	P <sub>LC</sub> LC Red705-CCGAGAATGGGAAGCTTGTCATCAAC p		4 mM			

Footnote 1: intron 4/5 2083 bp, intron 3/4 2813, intron 2/3 1749 bp; Footnote 2: intron 1/2 2634 bp, intron 3/4 3809 bp, intron 2/3 2375 bp

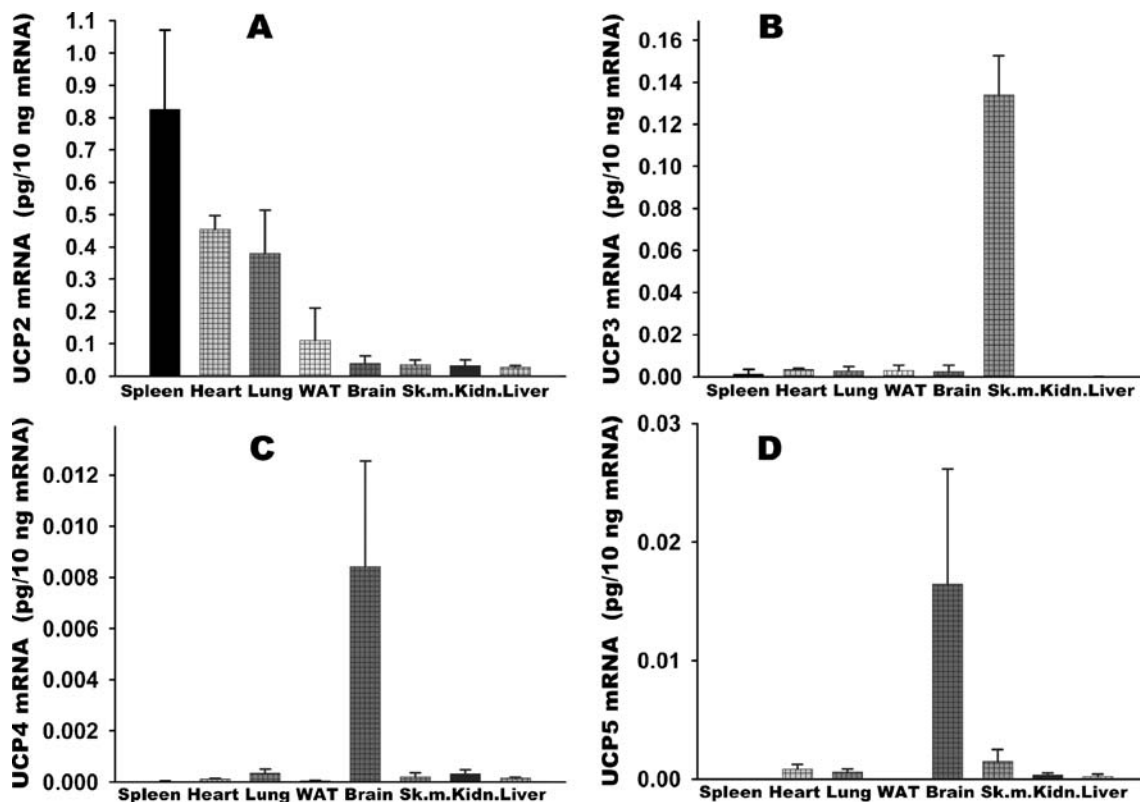


**Fig. 1** Real-time RT-PCR quantification of UCP2 mRNA in rat tissues. The absolute amounts of transcripts (pg per 10 ng of total isolated mRNA) encoding UCP2 **a**, UCP3 **b**, UCP4 **c**, and UCP5

mRNA per day are plotted for selected rat tissues. Quantification, performed as described in Materials and methods, was derived according the calibrations with parameters listed in Table 1

the UCP3 mRNA was much less abundant. The other UCP3 transcript levels reached only  $\sim 10^{-3}$  pg per 10 ng of total isolated mRNA with the exception of rat liver ( $\sim 10^{-5}$ ) and rat kidney (not detectable, Fig. 1b). A similar pattern was found for mouse tissues, with the exception of higher levels of UCP3 transcript in the spleen and WAT (Fig. 2b). There was no compensatory increase in UCP3 transcript level in the heart of the UCP2 (-/-) mice (not shown).

mRNA levels for UCP4

The absolute mRNA levels of the UCP4 isoform in rat tissues were generally among the lowest determined (Fig. 1c). They were by up to three orders of magnitude lower than the UCP2 mRNA levels. As expected (Mao et al. 1999), the maximum UCP4 mRNA level was in the brain, but still two orders of magnitude lower than the UCP2 mRNA level. In turn, UCP4 transcript abundance in the rat brain (similarly for UCP5, see below) was similar to that of UCP2 mRNA in the mouse lung (Fig. 2c vs. Fig. 2a). The mouse skeletal muscle UCP4 transcript level exceeded that of UCP2. Similarly, mouse WAT contained nearly equivalent levels ( $\sim 0.05$  pg per 10 ng of total isolated mRNA) of UCP2, UCP3, and UCP4 transcripts. The UCP4 transcript level was not increased in the brain of

the UCP2 (-/-) mice compared with wild-type mice (not shown).

mRNA levels for UCP5

Similar to the rat UCP3 and UCP4 mRNAs, rat UCP5 mRNA was primarily expressed in a single tissue, namely brain. Whereas in the case of rat UCP3 such an apparent exclusivity was found in the skeletal muscle, in the case of rat UCP5 it was the brain (Fig. 1d). In other tissues the levels of UCP5 mRNA ( $\sim 10^{-3}$  pg per 10 ng of total isolated mRNA) transcript levels of UCP5 were similar to the UCP3 levels. The rat UCP5 mRNA levels were still at least three-fold higher than those of UCP4. The tissue distribution of mouse UCP5 mRNA expression was somewhat more heterogeneous compared with the other UCPS, although UCP5 mRNA levels in brain were highest among the tested tissues (Fig. 2d). Notably,  $\sim 0.5$  pg per 10 ng of total isolated mRNA was found for the UCP5 and UCP4 transcripts in the mouse brain, as well as for UCP2 mRNA in mouse lung and UCP3 mRNA in mouse skeletal muscle. The mouse heart UCP5 mRNA level was equivalent to that of UCP3. UCP5 mRNA in WAT and spleen was even more abundant than UCP3 mRNAs in these tissues and UCP2 mRNA in WAT. Although only at levels of  $\sim 0.05$  pg per

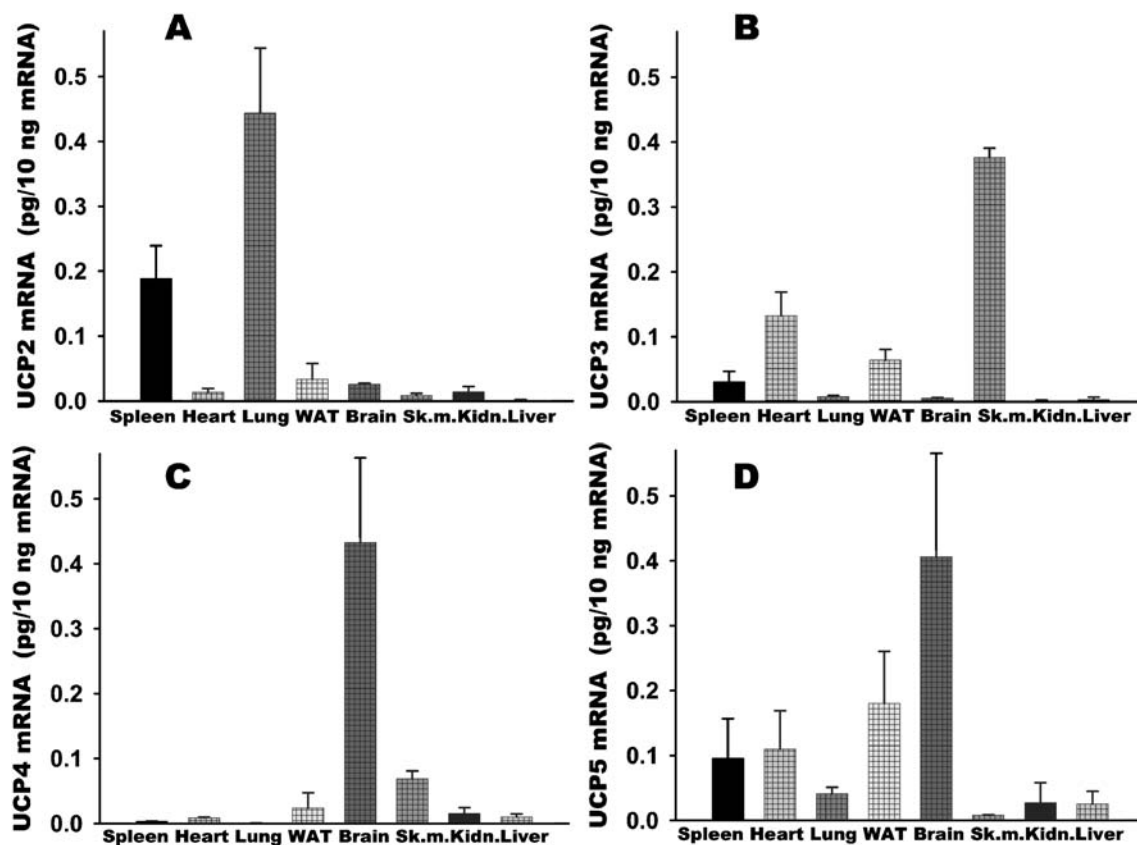


**Fig. 2** Real-time RT-PCR quantification of UCP2 mRNA in mouse tissues. The absolute amounts of transcripts (pg per 10 ng of total isolated mRNA) encoding UCP2 **a**, UCP3 **b**, UCP4 **c**, and UCP5

mRNA per day are plotted for selected mouse tissues. Quantification, performed as described in Materials and methods, was derived according the calibrations with parameters listed in Table 1

10 ng of total isolated mRNA, UCP5 was the predominant isoform in the mouse liver and kidney. The UCP5 transcript was not elevated in the brain of UCP2 ( $-/-$ ) mice.

## Discussion

For the first time this work presents a unified quantification of UCP transcripts (with the exception of UCP1) in the heart, liver, kidney, brain, skeletal muscle, and WAT. The results clearly show that the tissue-specific expression pattern of individual isoforms is quite distinct between rat and mouse and that the levels of mouse UCP4 and UCP5 transcripts, previously considered to be very low, are in fact quite high. This finding sheds new light on previous studies in mice in which one isoform, UCP2 or UCP3, was ablated. Their reported interpretations might be yet inconclusive due to the possible expression of other UCP isoforms, if one considers the possibility of functional redundancy among UCPs.

The advantage of quantitative real-time PCR with properly designed primers and probes lies in the unsurpassed selectivity and resolution that are not achievable by northern blotting or “chip screening”. Thus we provide

reference data for the four UCP isoform transcript levels that span four to five orders of magnitude. The major question remains how the translation machinery deals with transcripts of such varying and distinct abundance. Is the resulting translation only 10,000-fold less frequent when the transcript is of  $10^{-4}$  relative abundance? Alternatively, is there a threshold under which translation is nil for a very-low-abundance transcript? One could also speculate on the existence of a mechanism that upregulates the translation of low-abundance transcripts. Indeed, the observed disparity between the abundance of certain mRNAs and their corresponding protein products has been attributed to both translational down-regulation (Pecqueur et al. 2001; Hurtaud et al. 2006) and up-regulation (Hurtaud et al. 2007).

We have chosen a reference unit that is quite versatile and has practical implications, namely the unit of picograms of a given transcript per 10 ng of total isolated mRNA. One unit is close to the expected average transcription of 10,000 genes if all genes were transcribed equivalently. Only the level of the UCP2 transcript in the rat spleen approached one such unit. The selected reference gene, *GAPDH*, was transcribed in different tissues at levels between 1 and 10 pg per 10 ng of total isolated mRNA, corresponding to 0.01% to 0.1% of average gene represen-

tation (mRNA abundance). The finding that UCP2 transcript abundance was highest in the spleen points to important physiological role of UCP2 in macrophages (Arsenijevic et al. 2000; Giardina et al. 2008) and other white blood cell types, resident in the spleen. Similarly, the second highest UCP2 transcript amount, found in the rat and mouse lung, may reflect its predominating expression in the alveolar macrophages.

Attempting at least to find the order of magnitude proportionality between the measured levels of UCP mRNAs and their corresponding protein products, we can compare data for mouse spleen. These data show that UCP2 accounts for ~0.03% of all mitochondrial proteins (Pecqueur et al. 2001). Compare this to our finding of 0.002% for UCP2 transcript abundance (Fig. 2a). Considering on average 10,000 transcribed genes as 100%, these data would match only, if approximately each tenth transcribed protein in general was mitochondrial. The reported mouse lung UCP2 protein level (~0.002% of rat mitochondrial proteins, Pecqueur et al. 2001) seems to correlate with a rather high estimated transcript abundance of 0.004% (Fig. 2a). Also, our [<sup>3</sup>H]GTP binding study reflecting UCP2 protein amounts (Žáčková et al. 2003) correlated better with the rat UCP2 transcript quantification (Fig. 1a), indicating rather high amounts of UCP2 protein in rat lung mitochondria, and 10-fold lower levels in rat liver mitochondria (Žáčková et al. 2003). Indeed, the UCP2 mRNA was one order of magnitude greater in lung than in liver (Fig. 1a).

With the precision of calibrated real-time RT-PCR, we can claim that when no amplification proceeds within a sample there is definitively no transcript present, unless it exists in the range of attograms per 10 ng of total isolated mRNA. With such sensitivity, we identified UCP5 and UCP4 transcripts in all tested rat tissues, and we confirmed previous findings of UCP5 mRNA in mouse liver, lung, kidney, and spleen (Sanchis et al. 1998), heart (Kim-Han et al. 2001; Sanchis et al. 1998; Yu et al. 2000), and skeletal muscle (Lengacher et al. 2004; Sanchis et al. 1998; Yu et al. 2000). In the mouse these transcripts levels were very high (0.1 pg per 10 ng of total isolated mRNA, Fig. 2d). Also surprising was the rather high UCP4 mRNA level in mouse skeletal muscle (up to 0.1 pg per 10 ng of total isolated mRNA), being only five times lower than the UCP4 transcript level in mouse brain (Fig. 2d).

Patterns of the four studied UCP isoforms are remarkable for the heart and brain. In the rat heart, UCP2 mRNA was present at up to 0.5 units (i.e. pg per 10 ng of total isolated mRNA, the second highest level measured in our tissue set), exceeding by the two to three orders of magnitude the levels of UCP3, UCP4, and UCP5 transcripts. In turn, among mouse UCP mRNAs, UCP3 and UCP5 mRNAs were the most abundant and nearly

equivalent, whereas UCP2 mRNA was 10-fold less abundant. For reason unknown, UCP2 seems to have been phylogenetically selected for its role in the rat heart, and likewise for UCP3 and UCP5 in the mouse heart. This finding puts into context the previous striking reports demonstrating the importance of UCP2 function in the rat heart (Bo et al. 2008; McLeod et al. 2005).

In the rat brain, the predominant rat UCP2 transcript and roughly half-abundant UCP5 transcript exceeded 10-fold the UCP4 mRNA levels, whereas, on the contrary, in the mouse brain the UCP4 transcript and the equally abundant UCP5 transcript outnumbered UCP2 mRNA by 10-fold. In conclusion, the tissue distribution of UCP isoform mRNAs differs between rat and mouse. As such, researchers must heed caution when extrapolating the findings/conclusions for one of these rodent species onto the other and when reporting on studies of single-gene knockout mice.

**Acknowledgement** The project was supported by grants of the Grant Agency of the Czech Republic (No. 303/07/0105), the Internal Grant Agency of the Academy of Sciences of the Czech Republic (No. A500110701); the Czech Ministry of Education (No. 1P05ME794) and the research project AV0Z50110509. We gratefully acknowledge the excellent technical assistance of Dr. M. Růžicka with regard to tissue removal.

## References

- Adams AE, Carroll AM, Fallon PG, Porter RK (2008a) *Biochim Biophys Acta* 1777:772–776
- Adams AE, Hanrahan O, Nolan DN, Voorheis HP, Fallon P, Porter RK (2008b) *Biochim Biophys Acta* 1777:115–117
- Affourtit C, Crichton PG, Parker N, Brand MD (2007) *Novartis Found Symp* 287:70–80
- Arsenijevic D, Onuma H, Pecqueur C, Raimbault S, Manning BS, Miroux B, Couplan E, Alves-Guerra MC, Goubern M, Surwit R, Bouillaud F, Richard D, Collins S, Ricquier D (2000) *Nat Genet* 26:435–439
- Beck V, Jabůrek M, Demina T, Rupprecht A, Porter RK, Ježek P, Pohl EE (2007) *FASEB J* 21:1137–1144
- Bo H, Jiang N, Ma G, Qu J, Zhang G, Cao D, Wen L, Liu S, Ji LL, Zhang Y (2008) *Free Radic Biol Med* 44:1373–1381
- Boss O, Samec S, Paoloni-Giacobino A, Rossier C, Dulloo A, Seydoux J, Muzzin P, Giacobino JP (1997) *FEBS Lett* 408:39–42
- Cannon B, Shabalina IG, Kramarova TV, Petrovic N, Nedergaard J (2006) *Biochim Biophys Acta* 1757:449–458
- Carroll AM, Haines LR, Pearson TW, Fallon PG, Walsh CM, Brennan CM, Breen EP, Porter RK (2005) *J Biol Chem* 280:15534–15543
- Chan SL, Liu D, Kyriazis GA, Bagsiyao P, Ouyang X, Mattson MP (2006) *J Biol Chem* 281:37391–37403
- Chomezynski P, Sacchi N (1987) *Anal Biochem* 162:156–159
- Dlasková A, Hlavatá L, Ježek P (2008a) *Int J Biochem Cell Biol* 40:2098–2109
- Dlasková A, Hlavatá L, Ježek J, Ježek P (2008b) *Int J Biochem Cell Biol* 40:1792–1805
- Dlasková A, Špaček T, Škobisová E, Šantorová J, Ježek P (2006) *Biochim Biophys Acta* 1757:467–473
- Esteves TC, Brand MD (2005) *Biochim Biophys Acta* 1709:35–44

- Fleury C, Neverova M, Collins S, Raimbault S, Champigny O, Lévi-Meyrueis C, Bouillaud F, Seldin MF, Surwit RS, Ricquier D, Warden CH (1997) *Nat Genet* 15:269–272
- Giardina TM, Steer JH, Lo SZ, Joyce DA (2008) *Biochim Biophys Acta* 1777:118–129
- Gimeno RE, Dembski M, Weng X, Shyjan AW, Gimeno CJ, Iris F, Ellis SJ, Deng N, Woolf EA, Tartaglia LA (1997) *Diabetes* 46:900–906
- Hanák P, Ježek P (2001) *FEBS Lett* 495:137–141
- Ho PW, Chu AC, Kwok KH, Kung MH, Ramsden DB, Ho SL (2006) *J Neurosci Res* 84:1358–1366
- Ho PW, Chan DY, Kwok KH, Chu AC, Ho JW, Kung MH, Ho SL (2005) *J Neurosci Res* 81:261–268
- Hurtaud C, Gelly C, Bouillaud F, Lévi-Meyrueis C (2006) *Cell Mol Life Sci* 63:1780–1789
- Hurtaud C, Gelly C, Chen Z, Lévi-Meyrueis C, Bouillaud F (2007) *Cell Mol Life Sci* 64:1853–1860
- Jabůrek M, Miyamoto S, Di Mascio P, Garlid KD, Ježek P (2004) *J Biol Chem* 279:53097–53102
- Ježek P, Hlavatá L (2005) *Int J Biochem Cell Biol* 37:2478–2503
- Ježek P, Ježek J (2003) *FEBS Lett* 534:15–25
- Ježek P, Urbánková E (2000) *IUBMB Life* 49:63–70
- Ježek P, Žáčková M, Růžička M, Škobisová E, Jabůrek M (2004) *Physiol Res* 53:S199–S211
- Kim-Han JS, Reichert SA, Quick KL, Dugan LL (2001) *J Neurochem* 79:658–668
- Klingenspor M, Fromme T, Hughes DA Jr, Manzke L, Polymeropoulos E, Riemann T, Trzcionka M, Hirschberg V, Jastroch M (2008) *Biochim Biophys Acta* 1777:637–641
- Lengacher S, Magistretti PJ, Pellerin LJ (2004) *J Cereb Blood Flow Metab* 24:780–788
- Liu D, Chan SL, de Souza-Pinto NC, Slevin JR, Wersto RP, Zhan M, Mustafa K, de Cabo R, Mattson MP (2006) *Neuromolecular Med* 8:389–414
- Mao W, Yu XX, Zhong A, Li W, Brush J, Sherwood SW, Adams SH, Pan G (1999) *FEBS Lett* 443:326–330
- McLeod CJ, Aziz A, Hoyt RF Jr, McCoy JP Jr, Sack MM (2005) *J Biol Chem* 280:33470–33476
- Mori S, Yoshizuka N, Takizawa M, Takema Y, Murase T, Tokimitsu I, Saito M (2008) *J Invest Dermatol* 128:1894–1900
- Nakase T, Yoshida Y, Nagata K (2007) *Neuropathology* 27:442–447
- Naudí A, Caro P, Jové M, Gómez J, Boada J, Ayala V, Portero-Otín M, Barja G, Pamplona R (2007) *Rejuvenation Res* 10:473–484
- Pecqueur C, Alves-Guerra M-C, Gelly C, Lévi-Meyrueis C, Couplan E, Collins S, Ricquier D, Bouillaud F, Miroux B (2001) *J Biol Chem* 276:8705–8712
- Růžička M, Škobisová E, Dlasková A, Šantorová J, Smolková K, Špaček T, Žáčková M, Modrianský M, Ježek P (2005) *Int J Biochem Cell Biol* 37:809–821
- Sale MM, Hsu FC, Palmer ND, Gordon CJ, Keene KL, Borgerink HM, Sharma AJ, Bergman RN, Taylor KD, Saad MF, Norris JM (2007) *BMC Endocr Disord* 30:7–1
- Sanchis D, Fleury C, Chomiki N, Goubern M, Huang Q, Neverova M, Grégoire F, Easlick J, Raimbault S, Lévi-Meyrueis C, Miroux B, Collins S, Seldin M, Richard D, Warden C, Bouillaud F, Ricquier D (1998) *J Biol Chem* 273:34611–34615
- Vidal-Puig A, Solanes G, Grujic D, Flier JS, Lowell BB (1997) *Biochem. Biophys. Res. Commun* 235:79–82
- Yu XX, Mao W, Zhong A, Schow P, Brush J, Sherwood SW, Adams SH, Pan G (2000) *FASEB J* 14:1611–1618
- Zhang CY, Baffy G, Perret P, Krauss S, Peroni O, Grujic D, Hagen T, Vidal-Puig AJ, Boss O, Kim YB, Zheng XX, Wheeler MB, Shulman GI, Chan CB, Lowell BB (2001) *Cell* 105:745–755
- Zhang M, Wang B, Ni YH, Liu F, Fei L, Pan XQ, Guo M, Chen RH, Guo XR (2006) *Life Sci* 79:1428–1435
- Žáčková M, Škobisová E, Urbánková E, Ježek P (2003) *J Biol Chem* 278:20761–20769

## **APPENDIX 3**

## Redistribution of cell death-inducing DNA fragmentation factor-like effector-a (CIDEa) from mitochondria to nucleus is associated with apoptosis in HeLa cells

E. Valoušková<sup>1</sup>, K. Smolková<sup>2</sup>, J. Šantorová<sup>2</sup>, P. Ježek<sup>2</sup> and M. Modrianský<sup>1</sup>

<sup>1</sup> *Institute of Medical Chemistry and Biochemistry, Faculty of Medicine and Dentistry, Palacký University, Olomouc, Czech Republic. E-mail: walouch@email.cz*

<sup>2</sup> *Institute of Physiology, Dept. 75, Academy of Sciences of the Czech Republic, Prague, Czech Republic*

**Abstract.** Cell death-inducing DFF[DNA fragmentation factor]-like effector-a (CIDEa), may initiate apoptosis by disrupting a complex consisting of 40-kDa caspase-3-activated nuclease (DFF40/CAD) and its 45-kDa inhibitor (DFF45/ICAD). CIDEa, however, was found to be localized in mitochondria. We have performed immunodetection of CIDEa in whole cells and subcellular fractions of HeLa cells adapted for a tetracycline-inducible CIDEa expression. Using immunocytochemistry we observed redistribution, enhanced upon treatment with camptothecin or valinomycin, of CIDEa to nucleus. Similarly, CIDEa content increased in the nuclear fraction but decreased in cytosolic fraction in cells treated to initiate apoptosis. We hypothesize that CIDEa is sequestered in mitochondria while transfer of this potentially dangerous protein from mitochondria into nucleus intensifies or even initiates apoptosis.

**Key words:** CIDEa — Mitochondria — Apoptosis — Migration to nucleus — HeLa cells

**Abbreviations:** BSA, bovine serum albumin; CAD, caspase-activated DNase; CCCP, carbonyl cyanide trifluoromethoxyphenylhydrazone; DFF, DNA fragmentation factor; CIDEa, cell death-inducing DFFa-like effector; DTT, dithiothreitol; EDTA, ethylenediaminetetraacetic acid; ICAD, inhibitor of CAD; PBS, phosphate buffered saline; PKC, protein kinase C; PMSF, phenylmethanesulfonyl fluoride; TUNEL, TdT-mediated dUTP nick end labeling.

### Introduction

Besides their function as metabolic powerhouses, mitochondria are one of major “decision makers” in apoptosis initiation and as gatekeepers of other ways of cell death (Cheng et al. 2006; Kim et al. 2006). Relay of information signaling that involves mitochondria is mediated by proteins possessing the ability to migrate between mitochondria and cytosol or other cell organelles or compartments, notably to the nucleus where subsequent signaling cascades may be initiated. On one hand, a “regular” protein import proceeds into mitochondrion (import of nuclear-coded mitochondrial proteins) bringing in either executive or regulatory proteins

(Baker et al. 2007). Among the latter, PKC-, tyrosine- and other kinases were found to access at least the intermembrane space (Salvi et al. 2005). On the other hand, an export of signaling proteins into the cytosol or other cell organelles exists and plays an essential role in life and death (Cheng et al. 2006; Garrido et al. 2006; Kim et al. 2006). Thus, protein export mechanisms for apoptosis mediators such as cytochrome c, Smac/Diablo, apoptosis-inducing factor or EndoG serve as well established, but not completely understood examples (Cheng et al. 2006; Kim et al. 2006; Varecha et al. 2007).

Bearing in mind the above principles, it is not surprising that proteins called cell death-inducing DFFa (DNA fragmentation factor a)-like effector-a,b,3 (CIDEa, CIDEb, CIDE3/FSP27) have been found in mitochondria (Inohara et al. 1998). The three CIDE proteins have different tissue distributions for their mRNA and their physiological roles specific to given tissues are unknown. CIDE proteins display high homology to the N-terminal sequence of both subunits of the

Correspondence to: Martin Modrianský, Institute of Medical Chemistry and Biochemistry, Faculty of Medicine and Dentistry, Palacký University, Hněvotínská 3, 775 15 Olomouc, Czech Republic  
E-mail: oregon@tunw.upol.cz

heterodimeric DFF, which consists of the 40-kDa caspase-3-activated nuclease (DFF40/CAD), and its 45-kDa inhibitor (DFF45/ICAD). The DFF45/DFF40 complex is cleaved by caspase-3 during apoptosis and thereafter free DFF40 causes apoptotic DNA fragmentation and chromatin condensation (Inohara et al. 1999; Bayascas et al. 2004). CIDE-induced apoptosis is not sensitive to caspase inhibitors but is inhibited by DFF45 (Inohara et al. 1998). The N-domain of CIDE proteins most probably binds to the homologous domain of DFF45 opposing the factor's inhibitory as well as chaperone effect on DFF40 (Lugovskoy et al. 1999; Neimanis et al. 2007). The nuclease is then able to cleave DNA. It is not yet fully established, whether the DFF45/DFF40 complex is formed in the nucleus or in the cytosol. However, nuclear import studies suggested that the DFF45/DFF40 complex is imported more readily than its components (Neimanis et al. 2007), thus preferring the model of cytosolic formation of the complex. If this was exclusive *modus operandi* of DFF, then CIDEa must migrate to nucleus in order to bind DFF45 and induce apoptosis. If sole DFF40 nuclease could migrate into the nucleus, apoptosis might be induced by CIDE-mediated dissociation of the DFF45/DFF40 complex in the cytosol.

The situation is more complex, because several studies localized CIDEa (Zhou et al. 2003), CIDEb (Chen et al. 2000) and CIDE3 (Liang et al. 2003) in mitochondria. A consensus has been found that while the N-CIDE domain located within the N-terminal is required for binding to DFF45 or DFF40 (Inohara et al. 1998; Lugovskoy et al. 1999; Chen et al. 2000), the C-CIDE domain within the C-terminal is required for mitochondrial localization and apoptosis (Inohara et al. 1998; Chen et al. 2000). The latter finding contrasts with the obligatory N-terminal localization of mitochondrial addressing sequences (presequences or scattered motifs). Employing dedicated software, e.g. <http://psort.ims.u-tokyo.ac.jp>, we were unable to locate a mitochondrial addressing sequence within either CIDEa or CIDEb amino acid sequences. We may assume that docking in mitochondria is just ensured by the C-CIDE domain. Migration of tagged CIDEb, for example, from mitochondria to nucleus (or to cytosol) was missing in case of apoptosis induced by staurosporine and etoposide (Chen et al. 2000). Because the two drugs affect primarily Bak/Bax-dependent apoptosis, we selected other effectors, including camptothecin and valinomycin, and endeavored to investigate the issue of CIDEa migration.

## Materials and Methods

### *Inducible CIDEa expression*

An open reading frame clone of human CIDEa in an entry vector pENTR221 (Invitrogen) has been transposed using a clonase reaction into a vector T-Rex pDEST30 (Invitrogen)

for a tetracycline-induced expression, obtaining pDEST30-CIDEa plasmid containing the full open reading frame for CIDEa inserted downstream from *tet* repressor binding site. The HeLa cell line overexpressing the tetracycline repressor (Invitrogen) was cultured in the presence of antibiotic Blastidicin (1 µg/ml) at 37°C in a humidified incubator with 5% CO<sub>2</sub> in the Eagle's minimum essential medium supplemented with 2 mmol/l L-glutamine, 10% fetal calf serum, 100 IU/ml penicillin, and 100 µg/ml streptomycin. Transfections were performed using 1 µl Lipofectamine 2000™ (Roche) per 1 µg DNA with estimated efficiency up to 50%. Following transfection cells were allowed to stabilize for 24 h and then subjected to further treatments.

### *Initiation of apoptosis*

The pDEST30-CIDEa-transfected T-Rex-HeLa cells were subjected to tetracycline (1 µg/ml) for defined time intervals, thus obtaining a time-course of induced CIDEa expression. In experiments where apoptosis initiators were used, cells were subjected to tetracycline treatment for 8 h followed by 2 h incubations with following apoptosis initiators: a DNA-topoisomerase I complex inhibitor camptothecin (2 µmol/l); a protonophore CCCP (2 µmol/l); a potassium ionophore valinomycin (2 µmol/l); and a calcium ionophore A23187 (2 µmol/l). Extent of apoptosis was assayed using caspase-3 activity, TUNEL assay and cell death assay assessing cell morphology.

### *Preparation of subcellular fractions*

Minor modifications of previously described method (Carcamo et al. 2002) have been adapted. T-Rex-HeLa cells were washed twice with 2 ml of ice-cold PBS and scraped into 1 ml of PBS. Suspension was centrifuged (1500 × g/5 min/4°C), the pellet was resuspended by gentle pipetting in 300 µl of ice-cold buffer A (10 mmol/l HEPES, pH 7.9; 10 mmol/l KCl; 1.5 mmol/l MgCl<sub>2</sub>; 0.5 mmol/l DTT; 0.1% (v/v) NP-40), incubated for 10 min on ice, and centrifuged (5500 × g/10 min/4°C). Following collection of supernatant, which contains cytosolic and mitochondrial fraction, the pellet was vigorously resuspended by syringe/needle in 3 volumes of ice-cold buffer B (20 mmol/l HEPES, pH 7.9; 420 mmol/l NaCl; 0.2 mmol/l EDTA; 1.5 mmol/l MgCl<sub>2</sub>; 0.5 mmol/l DTT; 0.5 mmol/l PMSF; 25% (v/v) glycerol) and incubated for 30 min on ice. Following centrifugation (12,000 × g/20 min/4°C), the supernatant (nuclear extract) was collected. Both extracts were stored in -80°C until further use. Protein content in extracts was determined by the Bradford method (Bradford 1976).

### *Caspase-3 activity*

The PBS-washed cells were lysed in 50 µl of ice-cold lysis buffer (50 mmol/l HEPES, pH 7.4; 0.5% Triton X-100,

a protease inhibitor cocktail tablet, 5 mmol/l DTT; 4°C; 15 min). The lysate was cleared by centrifugation (14,000 × g; 4°C; 15 min) and the supernatant total protein determined by the Bradford method (Bradford 1976). The lysate was assayed in 20 mmol/l HEPES, pH 7.1, 2 mmol/l EDTA, 5 mmol/l DTT, containing a protease inhibitor cocktail tablet and caspase-3 fluorescent substrate (Ac-DEVD-AMC; 50 μmol/l) by incubation at 37°C for 60 min. Background fluorescence was subtracted, as obtained in parallel samples with a caspase-3 inhibitor (Ac-DEVD-CHO; 2 μmol/l). The fluorescence was measured at 380/450 nm using an LS 50 B spectrofluorometer (Perkin-Elmer).

#### *Western blot detection of CIDEa*

Cells were collected by scraping off in the growth medium to ensure the detached cells are not lost in the rinsing procedure. The cell suspension was centrifuged and the pellet was resuspended in 50 μl of the lysis buffer. Following addition of SDS-PAGE sample buffer (50 μl) it was boiled for 5 min at 95°C. 20–30 μg of total protein/lane was run on 12% SDS-PAGE, blotted onto PVDF membrane and the CIDEa antigen was detected using primary antibody developed in rabbit (ProSci). Horseradish peroxidase-conjugated secondary anti-rabbit antibody and Luminol reagent (Santa Cruz Biotechnology) were used for visualization.

#### *In situ detection of apoptosis (TUNEL)*

Detection of apoptosis by TUNEL assay was performed as per manufacturer instructions (Roche). Samples were evaluated under fluorescent microscope Olympus IX70 (Olympus).

#### *Immunocytochemistry*

Cells were fixed by adding ice cold methanol and the whole plate was placed overnight into a -20°C freezer. Upon thawing, cells were rinsed twice with PBS and permeabilized by incubating in 0.2% Triton TX-100/PBS (v/v) for 30 min at room temperature. Blocking was performed by incubation for 15 min at room temperature in 3% BSA/PBS (w/v) and was followed by incubation with anti-CIDEa primary antibody (ProSci) diluted 1 : 100 in 3% BSA/PBS (w/v) for 45 min at 37°C. After rinsing three times in PBS, cells were incubated for 30 min at room temperature in fluorescein-conjugated secondary anti-rabbit antibody (Molecular Probes) suspended in 3% BSA/PBS (w/v). Following three washes in PBS, the slides were mounted using fluorescent mounting medium (Dako Cytomation). Confocal microscope FluoView FV1000 (Olympus) was used for evaluation of the slides.

#### *Confocal microscopy*

The inverted fluorescent microscope Olympus IX81 with FluoView FV1000 laser scanning unit was employed for single photon microscopy with an Argon laser (457 nm, 488, 515 nm, 30 mW total output) for excitation (Olympus). A pinhole unit (50–800 μm) was used to set confocal conditions.

#### *Cell death assay*

Slides for immunocytochemistry were also used for identifying apoptotic cells. Approximately 300 cells total and 100 CIDEa positive cells were counted in random fields of each slide under fluorescent/phase contrast microscope. Apoptotic cells were distinguished based on typical morphological alteration of adherent cells undergoing apoptosis including becoming rounded and condensed. Condensation of cells was also readily apparent after nuclear staining by Hoechst 33258 dye. Cell numbers were then used for estimation of apoptotic cell percentages.

#### *Statistical analysis*

Student's *t*-test was used to establish statistically significant differences.

## **Results**

#### *CIDEa overexpression leads to apoptosis in HeLa cells*

Previous studies on CIDE proteins stated that overexpression of the protein causes apoptosis (Chen et al. 2000). We have employed T-REx HeLa cells, a cell line stably expressing tetracycline repressor, transfected with pDEST30-CIDEa, which allows regulated and timed CIDEa expression under control of *tet* repressor binding element. First a time course of tetracycline incubation was studied. Time point 0 h clearly shows no expression of CIDEa, indicated that expression of the protein is suppressed in the absence of tetracycline during the 24 h stabilization period post transfection. We found that the maximum expression was reached at 12 h post tetracycline (1 μg/ml) addition, but afterwards expression was declining (Fig 1A). It may imply that overexpression of CIDEa induces apoptosis resulting in cell death, a fact corresponding with previous reports (Chen et al. 2000). The disappearance of CIDEa in the cell population suggests that the transfected cells die, whereas the non-transfected do not. In our case, the majority of transfected cells would perish between 12 and 24 h post-tetracycline addition. Such a short time required for the cells to die may reflect the amount of CIDEa plasmid used for transfection, also shown by others (Inohara et al. 1998), and sensitivity of the cells. While caspase-3 activity varied throughout the time course (data not shown), the percentage

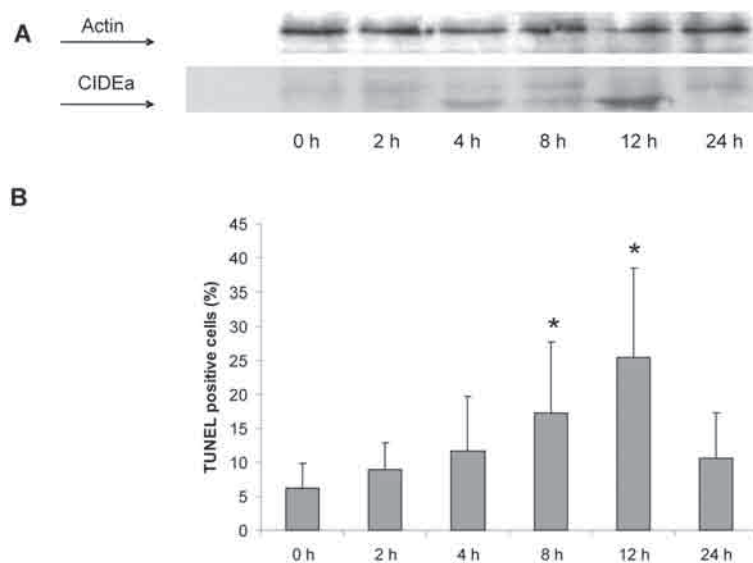


**Figure 1.** Time-course of CIDEa overexpression and apoptosis in T-Rex HeLa cells. T-Rex HeLa cells were transfected with pDEST-CIDEa plasmid and following 24 h stabilization subjected to tetracycline (1  $\mu\text{g/ml}$ ) treatment for indicated time periods. **A.** Representative immunoblot of CIDEa presence in samples of transfected HeLa cells treated with tetracycline for 0, 2, 4, 8, 12, and 24 h. Actin served as loading control. **B.** Cells found TUNEL positive were counted and compared with total number of cells. Error bars represent standard deviation determined from three independent experiments. \*  $p < 0.05$ .

of TUNEL positive cells displayed an apparent maximum at 8–12 h with both time points showing significantly higher percentage than time point 0 (Fig. 1B). Hence further experiments conducted used 8 h of tetracycline (1  $\mu\text{g/ml}$ ) treatment followed by 2 h in the presence of apoptosis initiators.

#### Localization of CIDEa in HeLa cells overexpressing the protein

CIDEb was shown to be localized in mitochondria when overexpressed in Chinese hamster ovary cells (Chen et al. 2000) and CIDEa in brown fat mitochondria (Zhou et al. 2003). We also found that CIDEa was localized in mitochondria upon its tetracycline-regulated expression in HeLa cells (data not shown). Immunocytochemistry of CIDEa-overexpressing T-Rex HeLa cells shows both nuclear as well as extranuclear localization of CIDEa (Fig. 2). Quantification of CIDEa-positive cells over four independent experiments (100 CIDEa-positive cells counted *per* experiment) yielded higher number of cells displaying either nuclear or mixed, i.e. nuclear as well as extranuclear, CIDEa localization in camptothecin- and valinomycin-treated cells, 50 and 80%, respectively, versus the DMSO-treated cells – 40%.

#### CIDEa redistribution is associated with treatment of HeLa cells with apoptosis initiators

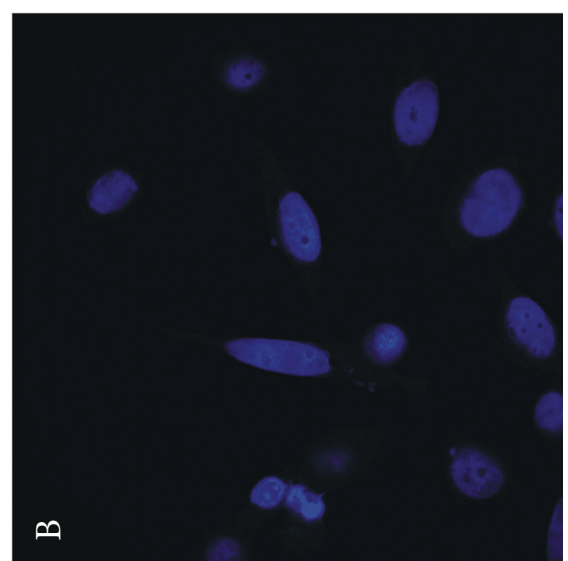
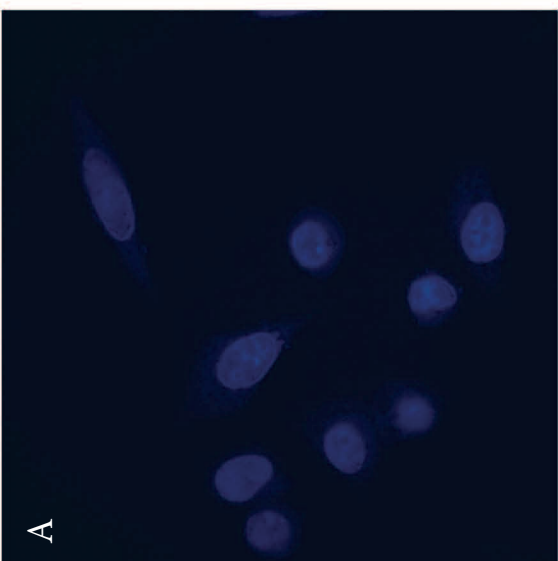
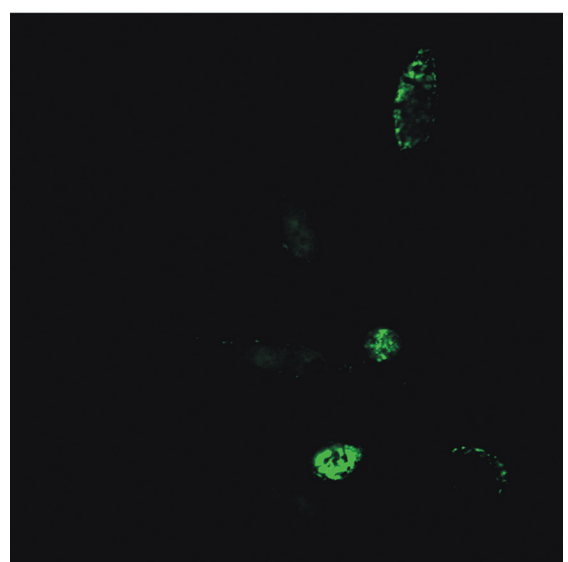
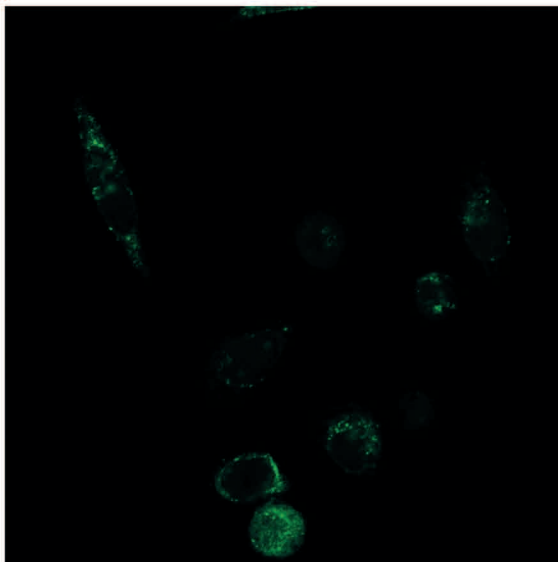
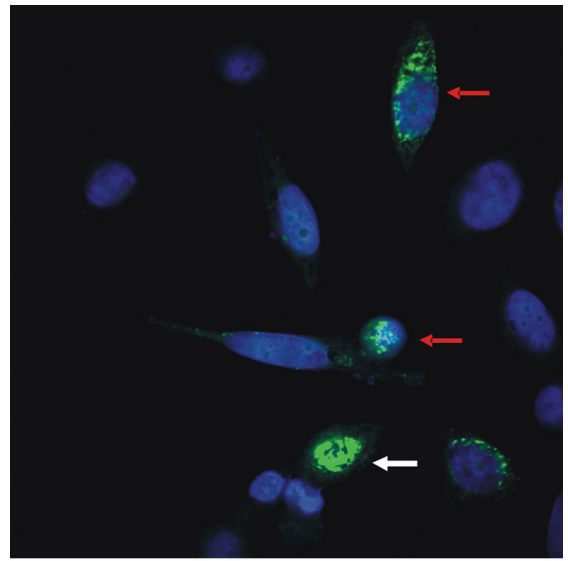
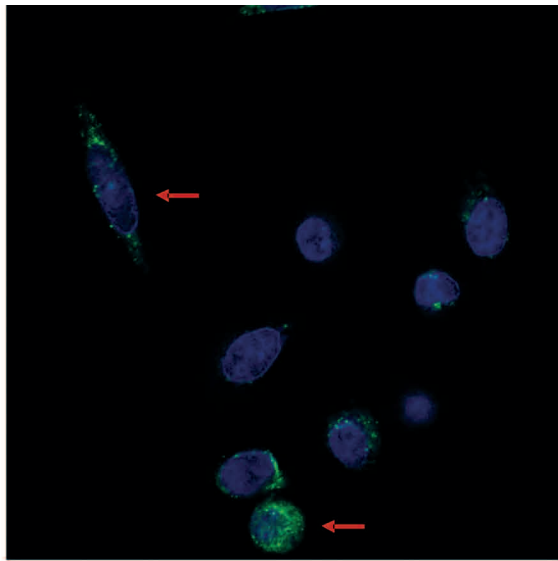
CIDEa expressed under *tet* repressor regulation appears to localize in both extranuclear and nuclear space as shown in

confocal microscopy images (Fig. 2). Despite the plausibility of confocal images, we used CIDEa immunodetection in subcellular fractions of CIDEa-overexpressing T-Rex HeLa cells to reveal the presence of the protein in general cytosolic, containing mitochondria, as well as nuclear fractions (Fig. 3). Valinomycin effect on CIDEa redistribution is more apparent than in the case of camptothecin and corresponds with the quantification of CIDEa-positive cells displaying at least some nuclear localization of CIDEa (*vide supra*).

Heterogeneous cell population was present in our experiments with variable percentage of cells undergoing apoptosis. Pretreatment of cells with pan caspase inhibitor z-VAD-fmk did not significantly alter the percentage of CIDEa positive cells displaying apoptotic morphology, i.e. cells displaying shrinkage and/or nuclear fragmentation, thus demonstrating the caspase-independence of the process (Fig. 4). On the contrary, the percentage of CIDEa positive/apoptotic cells in samples treated with valinomycin was significantly higher than those treated with DMSO (78 vs. 40%) thus supporting the link between redistribution of CIDEa and apoptosis.

#### Discussion

Original branding of CIDE proteins as pro-apoptotic factors stems from homology of their N-terminal domain with the corresponding domains of the DFF40/CAD and DFF45/ICAD proteins (Inohara et al. 1998; Lugovskoy et al. 1999).



A

B

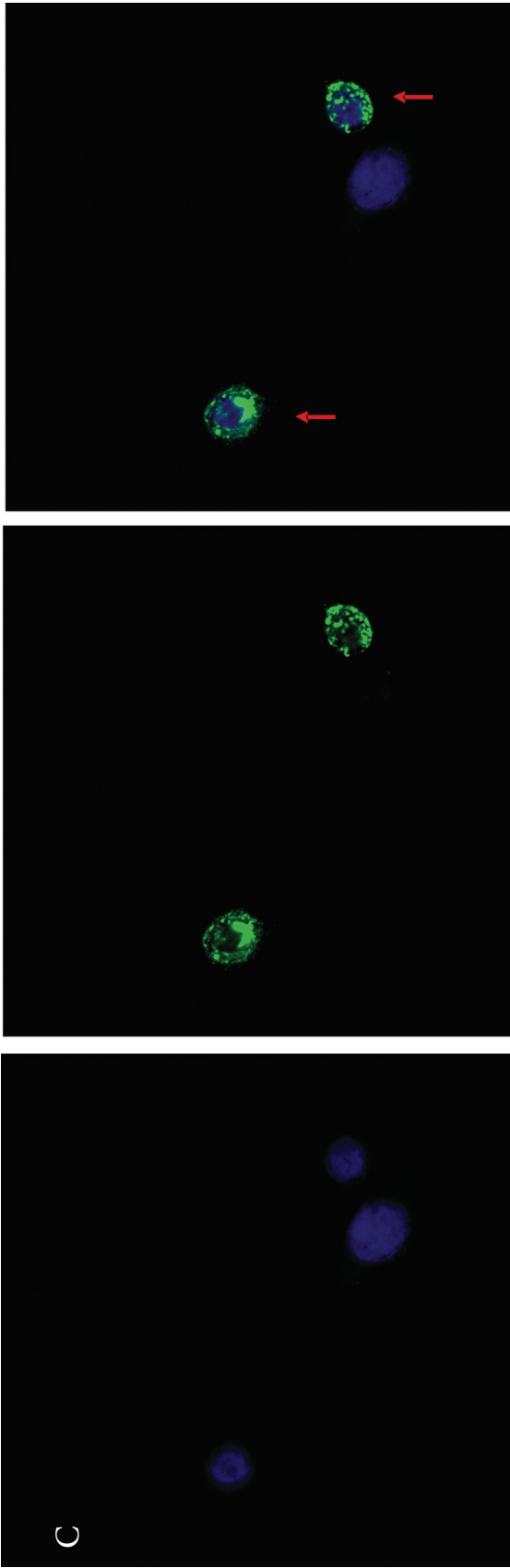


**Figure 2.** Subcellular localization of CIDEa. T-REx HeLa cells were transfected with pDEST-CIDEa plasmid and following 24 h stabilization subjected to tetracycline (1  $\mu\text{g}/\text{ml}$ ) treatment for 8 h followed by 2 h of treatment with DMSO (A), camptothecin (2  $\mu\text{mol}/\text{l}$ ; B) or valinomycin (2  $\mu\text{mol}/\text{l}$ ; C). Cells were fixed and probed with antiCIDEa antibody followed by AlexaFluor 488-conjugated secondary antibody and Hoechst 33258 dye. Fields shown were visualized under confocal microscope (magnification 400 $\times$ ) using the appropriate wavelengths for AlexaFluor 488 (green fluorescence) and Hoechst (blue fluorescence) dyes, and the two images were merged. White arrows indicate cells showing predominantly nuclear localization of CIDEa, red arrows show cells with nuclear as well as extranuclear localization of CIDEa.

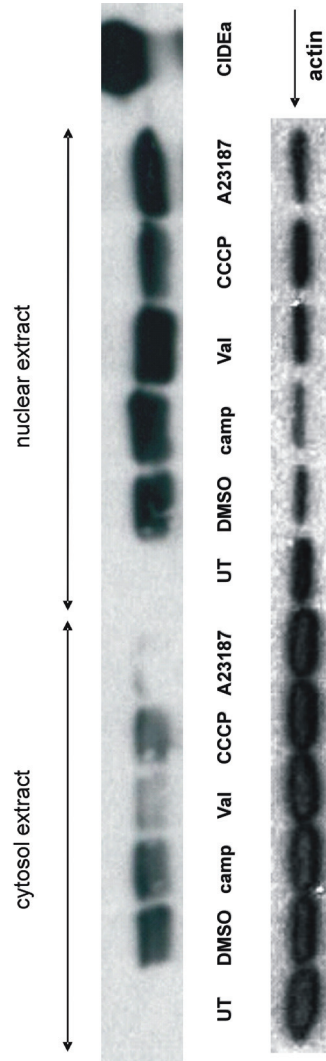


**Figure 3.** Redistribution of CIDEa from cytosol to the nucleus following apoptosis initiation. T-REx HeLa cells were transfected with empty pDEST or pDEST-CIDEa plasmid and following 24 h stabilization subjected to tetracycline (1  $\mu\text{g}/\text{ml}$ ) treatment for 8 h followed by 2 h of treatment with the indicated effector. Cells were then collected and cytosolic and nuclear fractions were prepared. 30  $\mu\text{g}$  of total protein from each fraction/lane were separated on SDS-PAGE, blotted onto PVDF membrane and subjected to immunodetection. Primary antiCIDEa antibody was followed by secondary horseradish peroxidase-conjugated antibody to allow chemiluminescent detection. Actin was used as a loading control. UT, empty vector without further treatment; DMSO, pDEST-CIDEa vector treated with DMSO only as vehicle control; camp, 2  $\mu\text{mol}/\text{l}$  camptothecin; Val, 2  $\mu\text{mol}/\text{l}$  valinomycin; CCCP, 2  $\mu\text{mol}/\text{l}$  CCCP; A23187, 2  $\mu\text{mol}/\text{l}$  calcium ionophore; CIDEa, recombinant human CIDEa prepared from inclusion bodies.

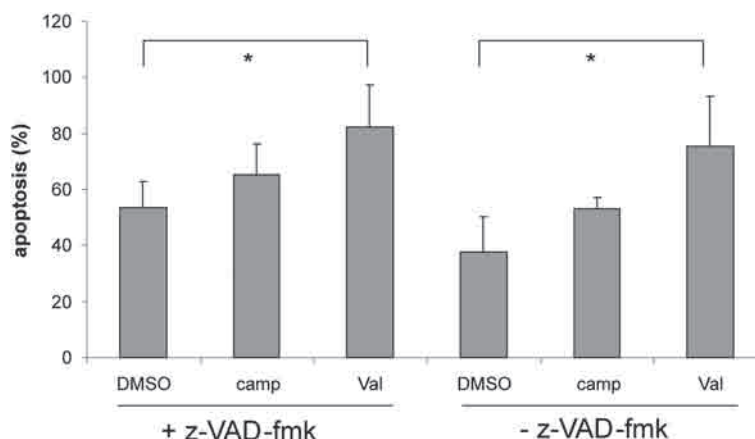


**Figure 4.** Effect of pan-caspase inhibitor on apoptosis induced by CIDEa overexpression. T-Rex HeLa cells were transfected with pDEST-CIDEa plasmid and following 24 h stabilization subjected to tetracycline (1  $\mu\text{g/ml}$ ) treatment for 8 h. After brief rinse with PBS, cells were treated for 30 min with 50  $\mu\text{mol/l}$  pan-caspase inhibitor z-VAD-fmk and then further 2 h with the indicated effector. Cells were probed with CIDEa antibody followed by AlexaFluor 488-conjugated secondary antibody and Hoechst 33258 dye. CIDEa positive and apoptotic cells were quantified from random fields, at least 100 cells displaying apoptotic morphology per experiment. Percentage of apoptosis was then calculated as a ratio of CIDEa positive apoptotic cells versus total number of apoptotic cells. Error bars are standard deviations determined from at least three independent experiments. DMSO, cells treated with DMSO only as vehicle control; camp, 2  $\mu\text{mol/l}$  camptothecin; Val, 2  $\mu\text{mol/l}$  valinomycin; \*  $p < 0.05$ .

The final proof that CIDE binds to the homologous domain on DFF45 hence opposing its inhibitory effect on the DFF40 nuclease, which subsequently cleaves DNA, is still missing. Our findings of CIDEa redistribution during incumbent apoptosis, induced either by CIDEa overexpression or in synergy with other apoptotic initiators, make the model, in which the DFF45/DFF40 complex enters the nucleus and CIDEa has to migrate therein to initiate its dissociation, more plausible. This model is also supported by the finding that the whole DFF45/DFF40 complex is imported more readily into the nucleus than its components separated (Neimanis et al. 2007). If CIDEa could disrupt the complex in the cytosol, migration of the free DFF40 nuclease into the nucleus might not be as intense. We found that migration of CIDEa into the nucleus is more apparent during apoptosis initiation by camptothecin and valinomycin and is independent of caspase activity. Hence, in some cell types (Gummeson et al. 2007), CIDEa may constitute another mitochondria-mediated apoptotic pathway alternative to others well-known, e.g. cytochrome c release (Garrido et al. 2006).

Exact pathway leading to CIDEa redistribution is unclear, however, we perceive the different mode of action for each stimulus as the culprit for more pronounced redistribution of CIDEa after valinomycin treatment (Fig. 3). Main target of camptothecin, DNA : topoisomerase I complex, is clearly located in the nucleus. Result of the interaction, i.e. DNA strand breaks, could lead to release of mitochondrial proteins, including CIDEa, only *via* indirect means and after nuclear signaling to mitochondria. On the other hand, valinomycin is a potassium uniporter that causes collapse

of mitochondrial membrane potential and its whole transformation into  $\Delta\text{pH}$  (Dlaskova et al. 2008), hence it likely triggers release of mitochondrial proteins as a result of mitochondrial network transformation. Pro-apoptotic proteins Bax and Bak were shown to be involved in normal as well as apoptotic mitochondrial morphogenesis (Karbowski et al. 2006). But we think that role of CIDEa in apoptosis resembles that of cytochrome c rather than that of Bax/Bak.

Previously, the overexpression of CIDEb in COS-1 cells was linked to apoptosis and those studies supported the pro-apoptotic role of the protein (Chen et al. 2000). Our data agree with the pro-apoptotic role of CIDEa, if present in high amounts in HeLa cells, where expression of native CIDEa is absent. In contrast, induction of CIDEa in mouse liver (Viswakarma et al. 2007) or brown fat (Liang et al. 2003; Zhou et al. 2003) was not accompanied by an increase in apoptosis. This can be explained by the existence of a hypothetical co-factor of mitochondrial origin present in certain cell types and capable of preventing CIDEa-dependent apoptosis, suggesting regulation of CIDEa export from mitochondria. A co-factor could be a protein binding CIDEa. Previously, CIDEa was reported to interact with mitochondrial uncoupling protein UCP1 present nearly exclusively in brown adipose tissue, a tissue in which CIDEa did not induce apoptosis (Zhou et al. 2003). Our attempts to verify the proposed interaction between CIDEa and UCP1 using surface plasmon resonance spectroscopy are so far inconclusive (Jezek and co-workers, unpublished data). Similarly, we do not have any evidence that CIDEa may interact with UCP1 homolog, UCP2, despite the pres-

ence of UCP2 in HeLa cells (Valoušková and co-workers, unpublished results). Nevertheless, our data (Fig. 2) support the mitochondrial origin of the postulated co-factor, since overexpressed CIDEa was found to be predominantly localized in mitochondria (Zhou et al. 2003), similarly to its homolog CIDEb (Chen et al. 2000; Liang et al. 2003) or CIDE3 (Liang et al. 2003).

Mitochondrial localization of CIDE proteins may thus serve as sequestering of potentially dangerous proteins much like others previously demonstrated (Kim et al. 2006) that would otherwise put cells into peril of an unavoidable apoptosis. Release of CIDEs from mitochondria and their migration to the nucleus would be then linked to apoptosis. The “resting position” would be represented by CIDE association with the postulated co-factor. Mechanisms of CIDE release from their supposed location within an intermembrane space of mitochondria are unknown, but hitching a ride on small mitochondrial “rafts” as proposed by Skulachev (Skulachev et al. 2004) and hypothesized for ganglioside GD3 (Garofalo et al. 2007) is possible. One can also speculate that CIDE export across the outer mitochondrial membrane may be accomplished by a reverse mode of transport by translocase of outer membrane complexes, by transport through multimers of Bax/Bak or through voltage-dependent anion channel complexes with ceramide, a mechanism either similar or distinct from the ways used by other pro-apoptotic messengers such as cytochrome c, apoptosis-inducing factor, or endonuclease G (Kim et al. 2006). The CIDE transfer into the nucleus should have serious consequences. It would represent important feedback information signaling of e.g. energetic status towards modulation or even execution of apoptosis. As we demonstrated, the CIDE pathway is caspase-independent.

**Acknowledgements.** This work was supported by the grants GACR 301/05/0121 and MSM6198959216.

## References

- Baker M. J., Frazier A. E., Gulbis J. M., Ryan M. T. (2007): Mitochondrial protein-import machinery: correlating structure with function. *Trends Cell Biol.* **17**, 456–464
- Bayascas J. R., Yuste V. J., Sole C., Sanchez-Lopez I., Segura M. F., Perera R., Comella J. X. (2004): Characterization of splice variants of human caspase-activated DNase with CIDE-N structure and function. *FEBS Lett.* **566**, 234–240
- Bradford M. M. (1976): A rapid and sensitive method for the quantitation of microgram quantities of protein utilizing the principle of protein-dye binding. *Anal. Biochem.* **72**, 248–254
- Carcamo J. M., Pedraza A., Borquez-Ojeda O., Golde D. W. (2002): Vitamin C suppresses TNF $\alpha$ -induced NF $\kappa$ B activation by inhibiting I $\kappa$ B $\alpha$  phosphorylation. *Biochemistry* **41**, 12995–13002
- Dlaskova A., Hlavata L., Jezek P. (2008): Oxidative stress caused by blocking of mitochondrial Complex I H<sup>+</sup> pumping as a link in aging/disease vicious cycle. *Int. J. Biochem. Cell Biol.* [Epub ahead of print]
- Garofalo T., Tinari A., Matarrese P., Giammarioli A. M., Manganeli V., Ciarlo L., Misasi R., Sorice M., Malorni W. (2007): Do mitochondria act as “cargo boats” in the journey of GD3 to the nucleus during apoptosis? *FEBS Lett.* **581**, 3899–3903
- Garrido C., Galluzzi L., Brunet M., Puig P. E., Didelot C., Kroemer G. (2006): Mechanisms of cytochrome c release from mitochondria. *Cell Death Differ.* **13**, 1423–1433
- Gummesson A., Jernas M., Svensson P. A., Larsson I., Glad C. A., Schele E., Gripeteg L., Sjöholm K., Lystig T. C., Sjöstrom L., Carlsson B., Fagerberg B., Carlsson L. M. (2007): Relations of adipose tissue CIDEA gene expression to basal metabolic rate, energy restriction, and obesity: population-based and dietary intervention studies. *J. Clin. Endocrinol. Metab.* **92**, 4759–4765
- Chen Z., Guo K., Toh S. Y., Zhou Z., Li P. (2000): Mitochondria localization and dimerization are required for CIDE-B to induce apoptosis. *J. Biol. Chem.* **275**, 22619–22622
- Cheng W. C., Berman S. B., Ivanovska I., Jonas E. A., Lee S. J., Chen Y., Kaczmarek L. K., Pineda F., Hardwick J. M. (2006): Mitochondrial factors with dual roles in death and survival. *Oncogene* **25**, 4697–4705
- Inohara N., Koseki T., Chen S., Wu X., Nuñez G. (1998): CIDE, a novel family of cell death activators with homology to the 45 kDa subunit of the DNA fragmentation factor. *Embo J.* **17**, 2526–2533
- Inohara N., Koseki T., Chen S., Benedict M. A., Nuñez G. (1999): Identification of regulatory and catalytic domains in the apoptosis nuclease DFF40/CAD. *J. Biol. Chem.* **274**, 270–274
- Karbowski M., Norris K. L., Cleland M. M., Jeong S. Y., Youle R. J. (2006): Role of Bax and Bak in mitochondrial morphogenesis. *Nature* **443**, 658–662
- Kim R., Emi M., Tanabe K. (2006): Role of mitochondria as the gardens of cell death. *Cancer Chemother. Pharmacol.* **57**, 545–553
- Liang L., Zhao M., Xu Z., Yokoyama K. K., Li T. (2003): Molecular cloning and characterization of CIDE-3, a novel member of the cell-death-inducing DNA-fragmentation-factor (DFF45)-like effector family. *Biochem. J.* **370**, 195–203
- Lugovskoy A. A., Zhou P., Chou J. J., McCarty J. S., Li P., Wagner G. (1999): Solution structure of the CIDE-N domain of CIDE-B and a model for CIDE-N/CIDE-N interactions in the DNA fragmentation pathway of apoptosis. *Cell* **99**, 747–755
- Neimanis S., Albig W., Doenecke D., Kahle J. (2007): Sequence elements in both subunits of the DNA fragmentation factor are essential for its nuclear transport. *J. Biol. Chem.* **282**, 35821–35830
- Salvi M., Brunati A. M., Toninello A. (2005): Tyrosine phosphorylation in mitochondria: a new frontier in mitochondrial signaling. *Free Radic. Biol. Med.* **38**, 1267–1277
- Skulachev V. P., Bakeeva L. E., Chernyak B. V., Domnina L. V., Minin A. A., Pletjushkina O. Y., Saprunova V. B., Skulachev I. V.,

- Tsyplenkova V. G., Vasiliev J. M., Yaguzhinsky L. S., Zorov D. B. (2004): Thread-grain transition of mitochondrial reticulum as a step of mitoptosis and apoptosis. *Mol. Cell. Biochem.* **256-257**, 341–358
- Varecha M., Amrichova J., Zimmermann M., Ulman V., Lukaso-ova E., Kozubek M. (2007): Bioinformatic and image analyses of the cellular localization of the apoptotic proteins endonuclease G, AIF, and AMID during apoptosis in human cells. *Apoptosis* **12**, 1155–1171
- Viswakarma N., Yu S., Naik S., Kashireddy P., Matsumoto K., Sarkar J., Surapureddi S., Jia Y., Rao M. S., Reddy J. K. (2007): Transcriptional regulation of Cidea, mitochondrial cell death-inducing DNA fragmentation factor  $\alpha$ -like effector A, in mouse liver by peroxisome proliferator-activated receptor  $\alpha$  and  $\gamma$ . *J. Biol. Chem.* **282**, 18613–18624
- Zhou Z., Toh S. Y., Chen Z., Guo K., Ng C. P., Ponniah S., Lin S.-C., Hong W., Li P. (2003): Cidea-deficient mice have lean phenotype and are resistant to obesity. *Nat. Genet.* **35**, 49–56

Final version accepted: March 17, 2008

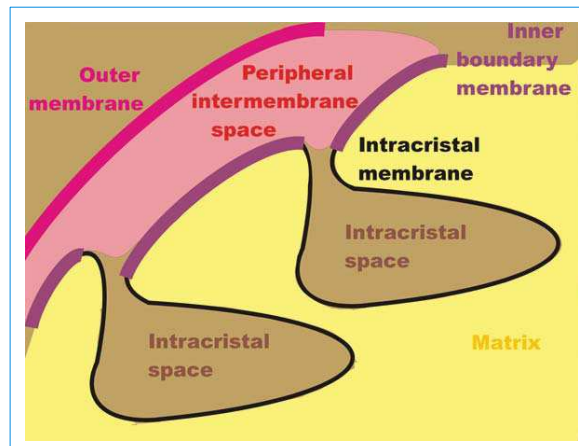


**FIG 2-1. Compartmentalization of a mitochondrion.** Outer membrane (OM), peripheral intermembrane space (PIMS) and its part within the cristae sacks, the intracristal space (ICS) are recognized, as well as two parts of the inner membrane, the peripheral, i.e. inner boundary membrane (IBM), and the intracristal membrane (ICM), and finally the matrix. Sectioning the tubule, one can view either a unique peripheral sandwich OM–PIMS–IBM–matrix; or below OM one may point to cristae (sack) outlets and ICS, below which ICM and finally matrix layers are recognized (Ježek and Plecítá-Hlavatá 2009).

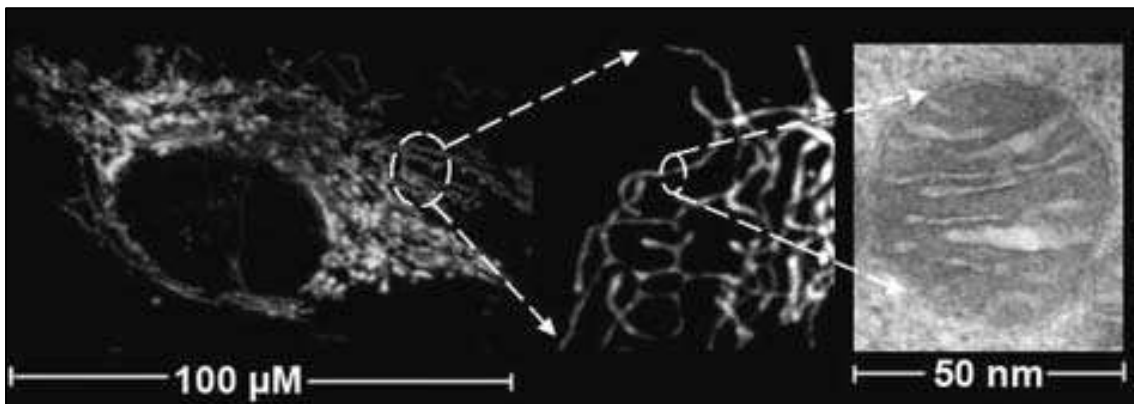


**FIG 2-2. Mitochondrial network.** Shows the traditional view of mitochondria (*right panel*), intersection of the mitochondrial tubules (*middle panel*) and typical mitochondrial network (Benard and Rossignol 2008).

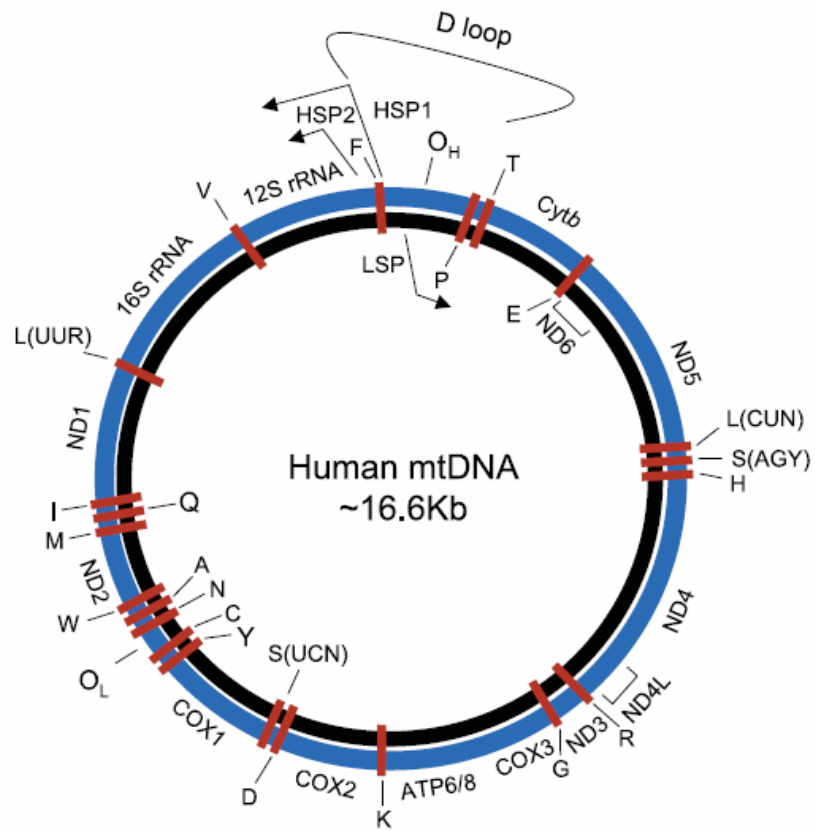


**FIG 2-3. Mitochondrial DNA.** Human mitochondrial DNA with designated encoded genes and non-coding regions (*Scarpulla 2008*).

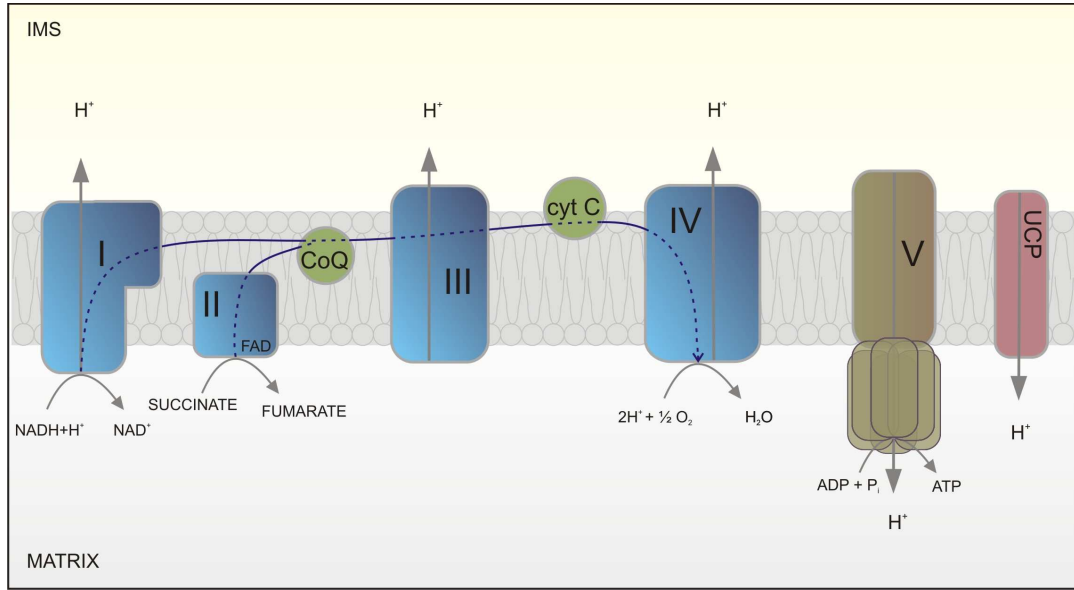


**FIG 2-4. Mitochondrial respiratory chain.** Schematic view of mitochondrial electron transport chain with substrates. Uncoupling protein (UCP) dissipate proton gradient of IMM.

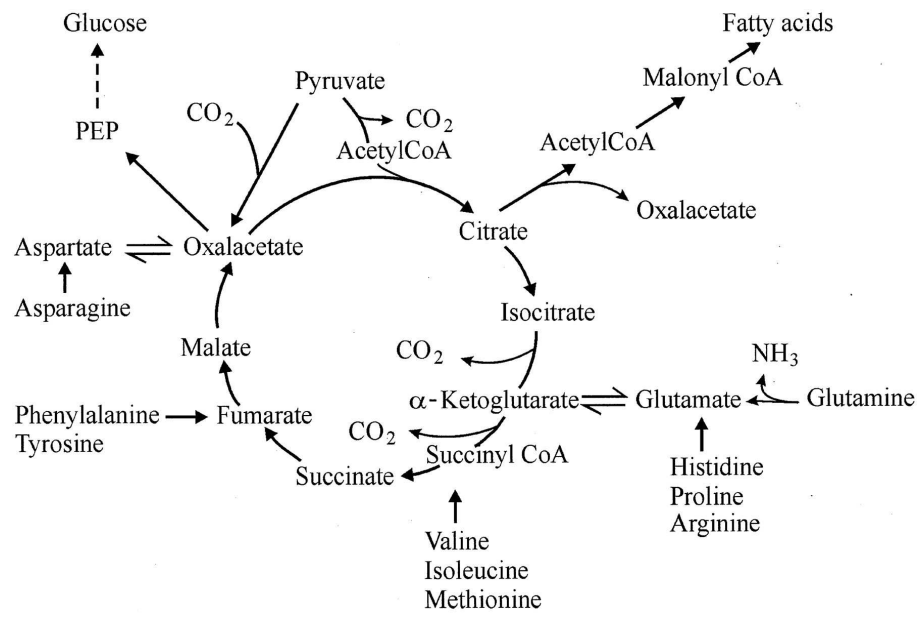


**FIG 2-5. Anaplerotic and cataplerotic flux of the TCA cycle.** Metabolic pathways that commonly utilize or replenish intermediates of the TCA are depicted (*Owen et al. 2002*).

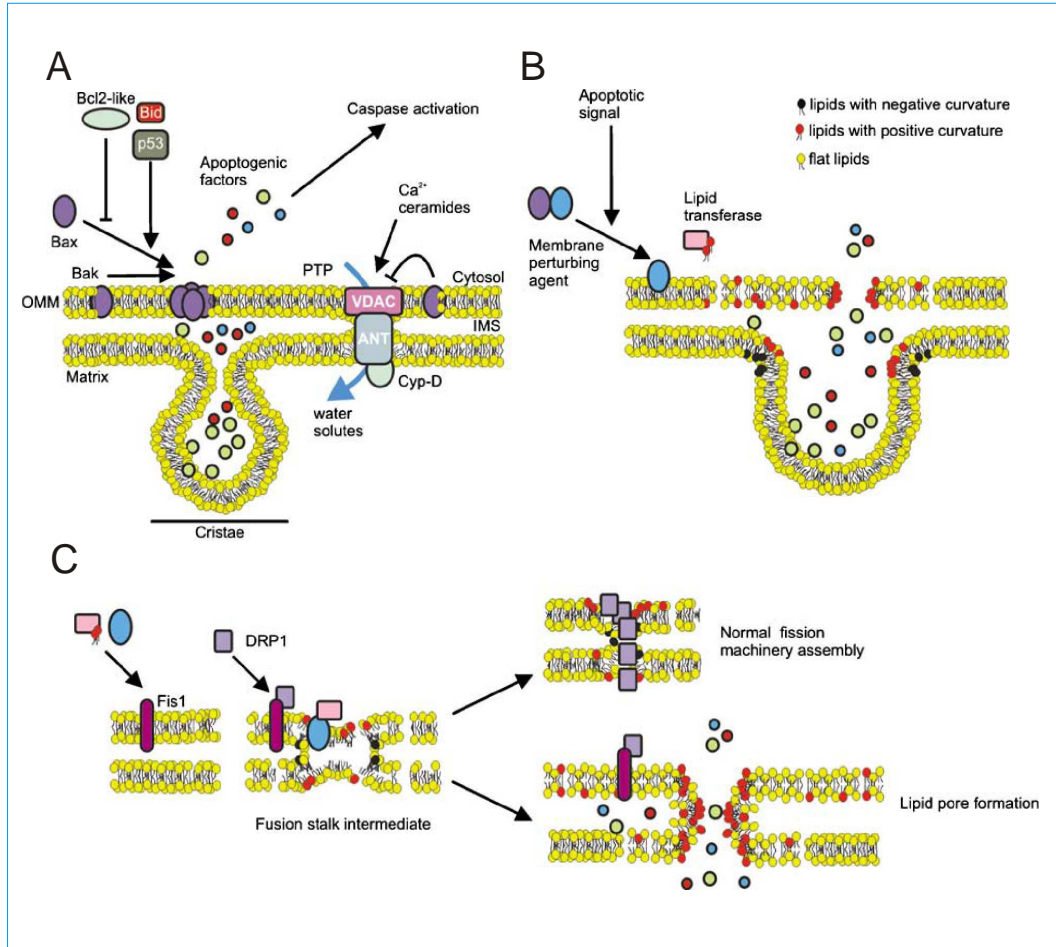


**FIG 2-6. Models of mitochondrial permeability transition.** (A) Classic model of PTP opening and formation of channels by proapoptotic Bcl2-family members. (B) An alternative scenario with a membrane-perturbing agent (either tBid, Bax or a protein that controls mitochondria morphology) translocates to the mitochondria and destabilizes the lipid bilayer. (C) Proposed model for mitochondrial division process and fission induced PTP (Alirol and Martinou 2006).

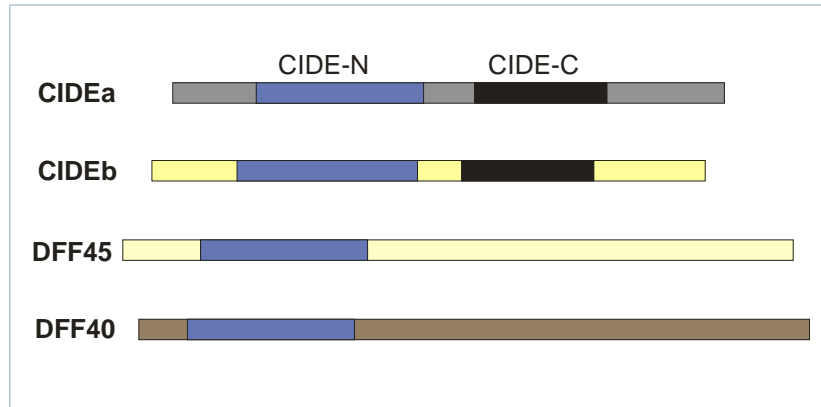


**FIG 2-7. Distribution of CIDE domains in CIDE and DFF proteins.** Figure shows that CIDE-N domains being present both in CIDE proteins as well as in DFF 40/45 protein since CIDE-C domain is present specifically in CIDE proteins.

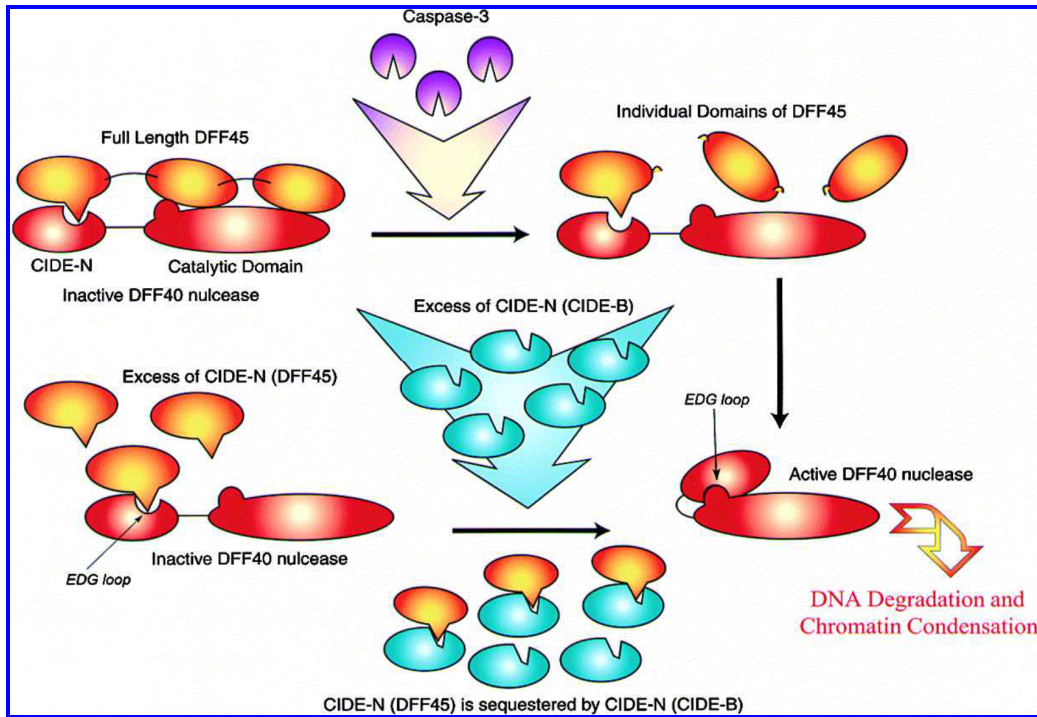


**FIG 2-8. Model for the inhibition and activation of DFF40.** Caspase 3 cleaves DFF45 into three domains that dissociate from the DFF40/DFF45 complex (top). Subsequently, the EDG loop of the CIDE-N domain of DFF40 interacts with the catalytic domain of nuclease, triggering DNA degradation and chromatin condensation. DFF40 can be inhibited by an excess of CIDE-N (DFF45). However, excess CIDE-N (CIDE-B) can sequester the CIDE-N domain of DFF45, making the EDG loop of DFF40 available for the interaction with nuclease catalytic domain (bottom) (*Lugovskoy et al. 1999*).

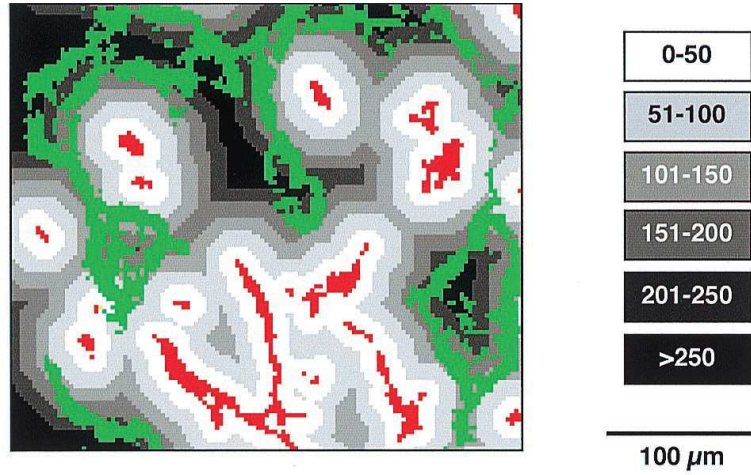


**FIG 2-9. Distribution of hypoxic regions within tumor.** Section from human glioma xenograft in mice shows hypoxic regions (green) and zones of oxygen supply (grey scale) around perfused vessel (red). Oxygen declines with increased distance from the perfused vessel (*Rijken et al. 2000*).

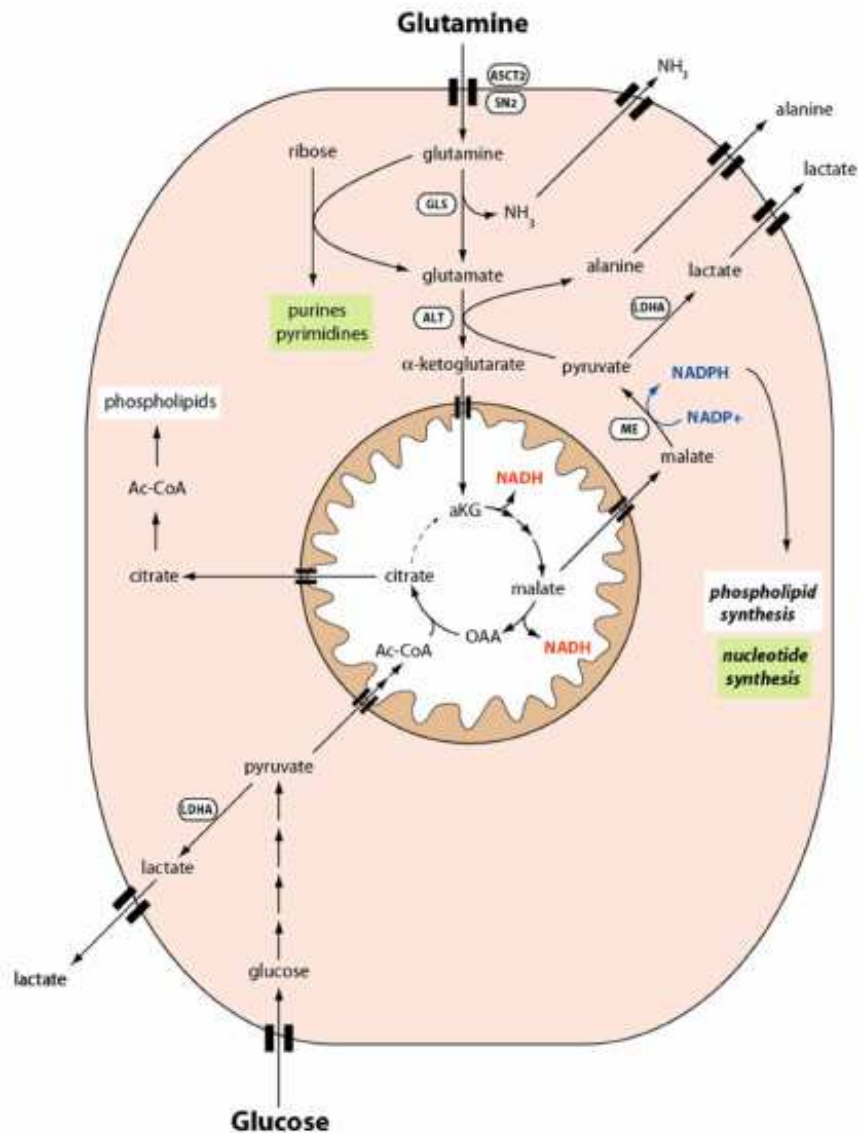


**FIG 2-10. Scheme of glutaminolysis.** High affinity glutamine transporters (ASCT2, SN2) import glutamine into the cell. Glutaminolysis involves enzymes glutaminase (GLS) alanine aminotransferase (ALT), production of malate, the oxidation of malate to pyruvate via malic enzyme (ME), and the reduction of pyruvate to lactate via lactate dehydrogenase A (LDH-A). The steps of glutamine to glutamate to  $\alpha$ -ketoglutarate may take place in the mitochondria. Glutaminolysis drives NADPH production, which fuels nucleotide and fatty acid biosynthesis (*DeBerardinis et al. 2007*).

NORMAL TISSUE mmHg	TUMORAL TISSUE mmHg	REF	NOTE
	<b>Brain</b>		
59.8	15.3	<i>(Kayama et al. 1991 )</i>	mean general anesthesia, high grade/low grade tumor; mean values local anesthesia, high grade/low grade tumor
17.9	9.2*	<i>(Beppu et al. 2002)</i>	
5.9	5.6 / 10.3*	<i>(Collingridge et al. 1999)</i>	
11.1	11.1 / 33.1*		
	<b>Breast</b>		
65	30	<i>(Collingridge et al. 1999)</i>	
	10	<i>(Auer et al. 2007)</i>	
57	42	<i>(Hohenberger et al. 1998)</i>	
52	3 - 15	<i>(Vaupel et al. 2006)</i>	
37	3 - 15	<i>(Vaupel et al. 2003)</i>	
	<b>Uterine cervix</b>		
	12.5	<i>(Hockel et al. 1996)</i>	adenocarcinoma/squamous cell carcinoma
51	5	<i>(Lyng et al. 1997)</i>	
	14.5	<i>(Vaupel et al. 2006)</i>	
	1 - 44		
	<5	<i>(Sundfor et al. 1997)</i>	
	(0 - 75)		
	1.4 - 44.1	<i>(Hockel et al. 1999)</i>	
	<b>Head and neck</b>		
	4,1 ± 1,2*	<i>(Brizel et al. 1997)</i>	recurrent tumor
	0 – 95	<i>(Nordsmark et al. 2007)</i>	
	HF2.5 22%		
	0 – 85.5	<i>(Rudat et al. 2000)</i>	
	HF2.5 26.8%		
	HF5 41.8%		
	0 - 76	<i>(Stadler et al. 1999)</i>	
	HF2.5 24%		
	HF5 30%		

**TAB 2-1. Overview of tumor oxygenation of selected tumor types 1.** Measurement were performed with oxygraphic pO2 needle exclusively. Values are median, usually introduced also with range of measured values. \* are designated mean values. HF5 – hypoxic fraction bellow 5 mmHg, expressed in %. HF2.5 hypoxic fraction bellow 2.5 mmHg, expressed in %.

<b>NORMAL TISSUE</b> <i>mmHg</i>	<b>TUMORAL TISSUE</b> <i>mmHg</i>	<b>REF</b>	<b>NOTE</b>
	<b>Melanoma</b>		
40.5	11.6 17.1 6.7 3 / 9	<i>(Lartigau et al. 1997)</i>   <i>(Lyng et al. 1997)</i>	tumor node metastasis skin metastasis xenograft
	<b>Sarcoma</b>		
9 (5 - 20)	2  10 (1 - 34) 18 (7 - 50)  4 20 7,5  19 (1 - 58)  18	<i>(Mayer et al. 2008)</i>  <i>(Bentzen et al. 2003)</i>   <i>(Cardenas-Navia et al. 2004)</i> <i>(Brizel et al. 1996)</i>  <i>(Nordsmark et al. 2001)</i>  <i>(Nordsmark et al. 1996)</i>	myometrium / leiomyosarcoma  malign  benign  fibrosarcoma, xenograft recurrent nonrecurrent
	<b>Pancreas</b>		
0 - 5.3 HF2.5 24-94	24.3 - 92.7	<i>(Koong et al. 2000)</i>	

**TAB 2-2. Overview of tumor oxygenation of selected tumor types 2.** Measurements were performed with oxygraphic pO<sub>2</sub> needle exclusively. Values are median, usually introduced also with range of measured values. \* are designated mean values. HF5 – hypoxic fraction bellow 5 mmHg, expressed in %. HF2.5 hypoxic fraction bellow 2.5 mmHg, expressed in %.

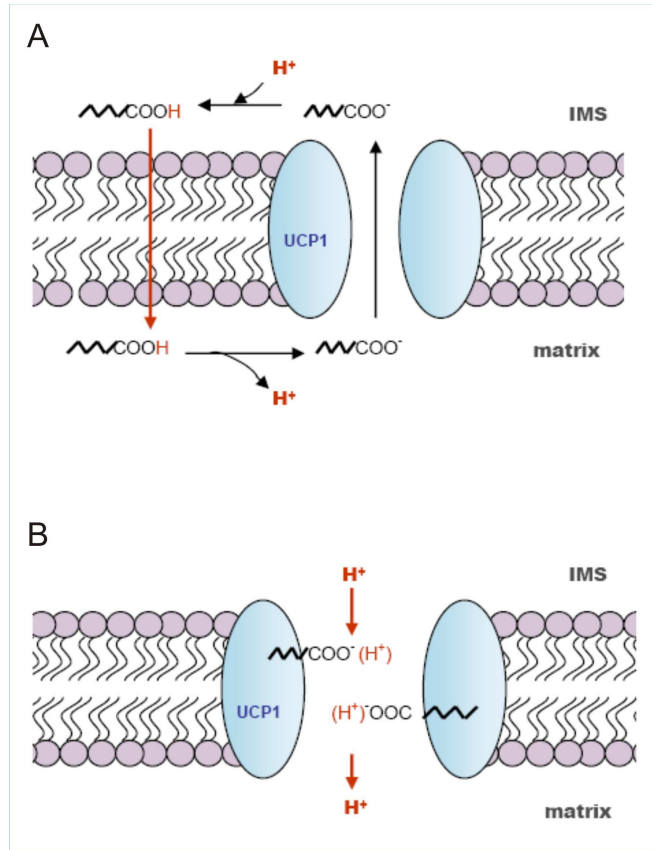


**FIG 2-11. Uncoupling of respiration by uncoupling proteins, proposed models.** FA cycling mechanism (A) and proton buffering model (B).

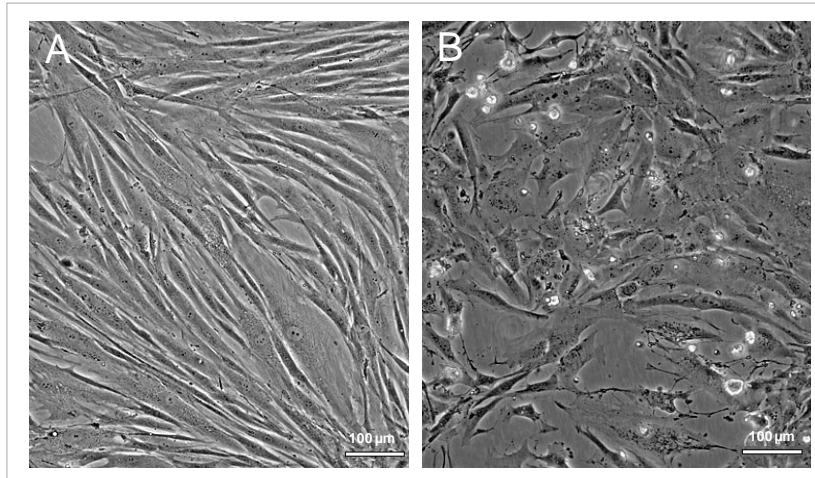


**FIG 3-1. HTB-125 and HTB-126.** Cell cultures used; control cell line HTB-125 (A) and breast cancer cell line HTB-126 (B).

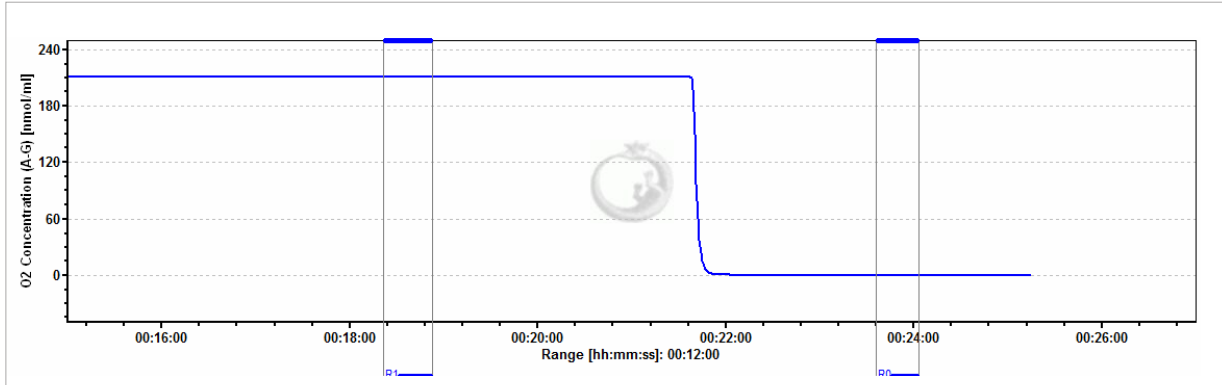


**FIG 3-2. Oxygen signal calibration.** Two-point calibration of oxygen signal at air saturation (R1) and zero calibration (R0) after depletion of oxygen by concentrated solution of sodium dithionate.

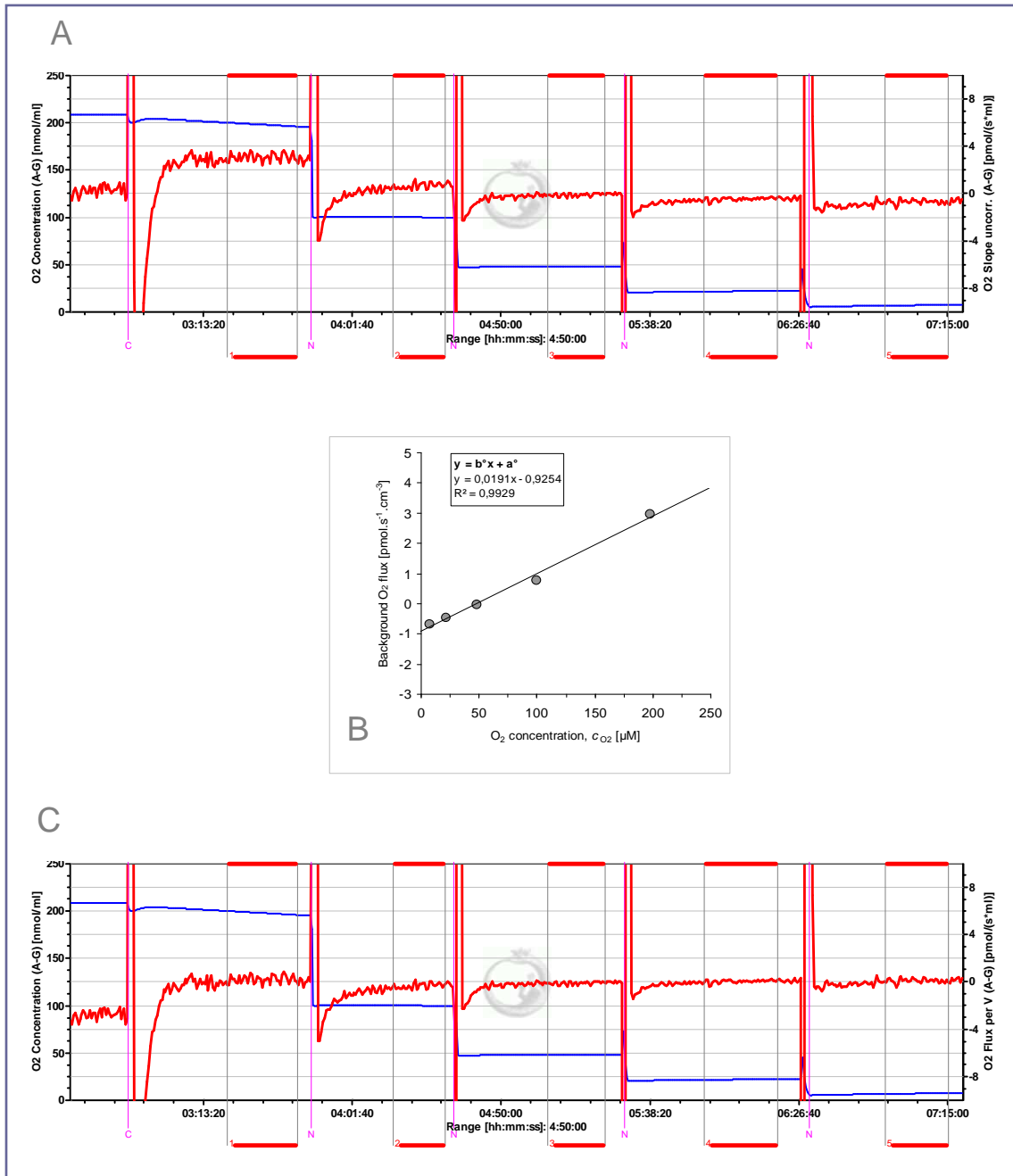


**FIG 3-3. Background calibration.** Background calibration experiment (A) performed on five levels of oxygen concentration (marked) shown without background correction. (B) Linear dependence of background oxygen flux from oxygen concentration. (C) Corrected background flux.

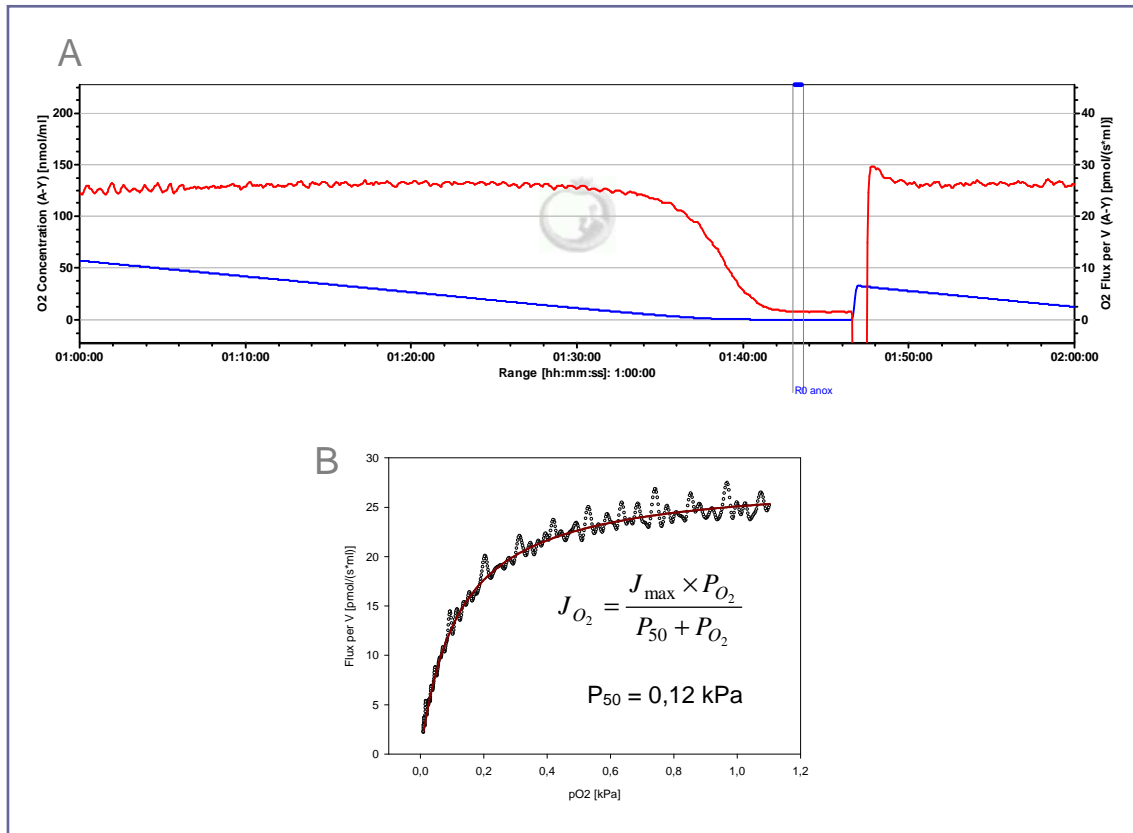


**FIG 3-4. Oxygen kinetics measurement measurement.** (A) Measurement of cellular respiration in low oxygen range followed by reoxygenation. After complete depletion of oxygen, zero calibration of oxygen signal can be performed (RO anox). (B) Hyperbolic fit of cellular respiration over 1,1 kPa range of oxygen pressure.  $P_{50}$  is calculated.

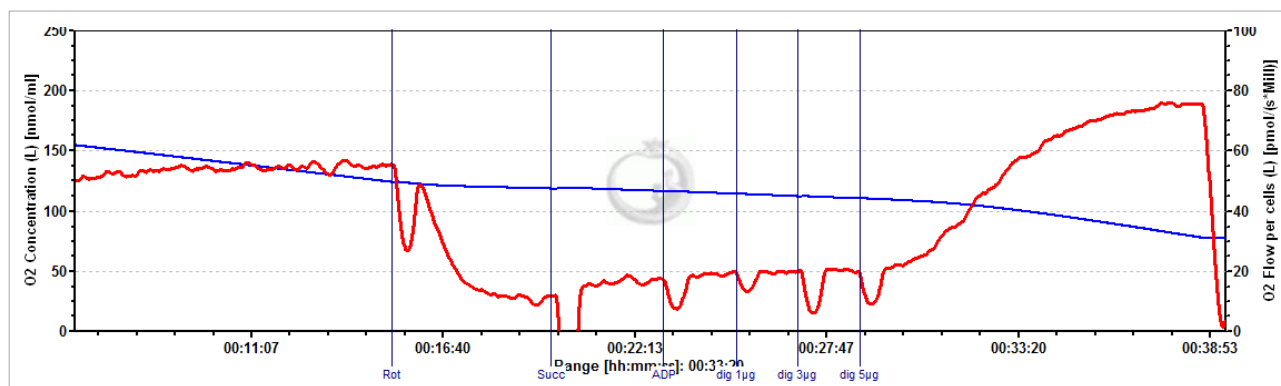


**FIG 3-5. Cell permeabilization of HTB-126 GAL.** Cellular respiration in respiratory medium, flux inhibited by rotenone addition (Rot), succinate and ADP addition, followed by digitonin titration. After 5  $\mu$ g, permeabilization was observed as indicated by rapid increase of respiratory flux.

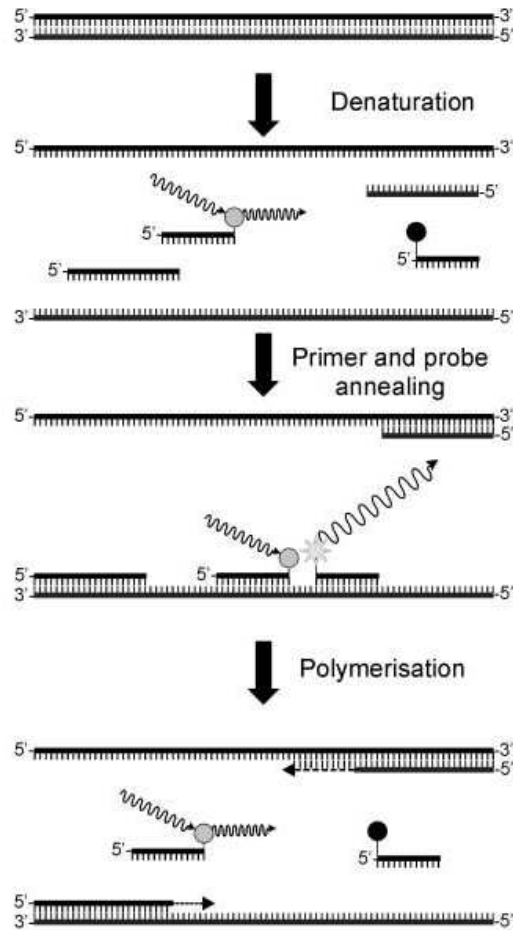


**FIG 3-6. Schematic model of real-time PCR quantification using fluorescent hybridization probes.**

One of the probes carries at its 3' end a fluorescein donor, which emits green fluorescent light when excited by the Lightcycler's light source. Its emission spectrum overlaps the excitation spectrum of an acceptor fluorophore that is attached to the 5' end of the second probe (LC-Red 640 or LC-Red 705). This probe must be blocked at its 3' end to prevent its extension during the annealing step. Excitation of the donor results in fluorescence resonance energy transfer to the acceptor and the emission of red fluorescent light. In solution, the two dyes are apart, and because the energy transfer depends on the spacing between the two dye molecules, only background fluorescence is emitted by the donor. After the denaturation step, both probes hybridize to their target sequence in a head-to-tail arrangement during the annealing step. This brings the two dyes in close proximity to one another and the fluorescein can transfer its energy at high efficiency. The intensity of the light of longer wavelength emitted by the second dye is measured, with increasing amounts of measured fluorescence proportional to the amount of DNA synthesized during the PCR reaction. A fluorescent signal is detected only as a result of two independent probes hybridizing to their correct target sequence. This increases specificity and generates additional flexibility for probe design (Bustin 2000).

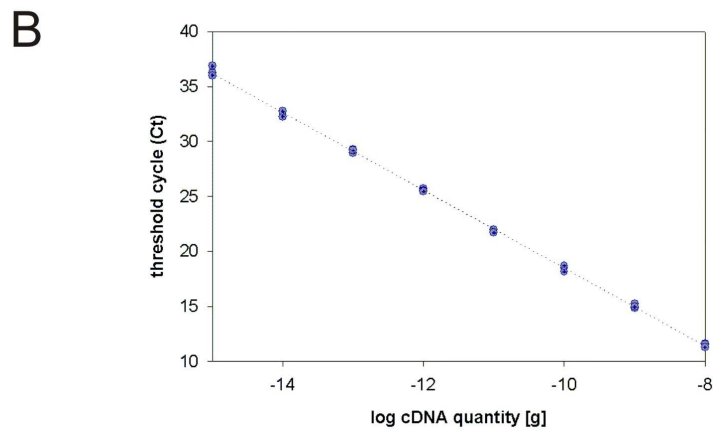
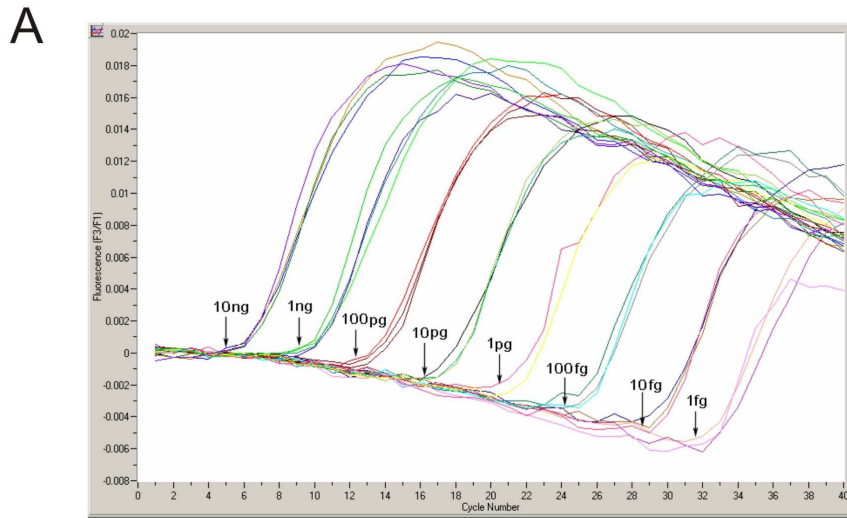


**FIG 3-7. Calibration for absolute quantification.** Lightcycler output of the calibration experiment (A) and subsequent calibration curve (B). Note that figures A and B do not represent corresponding set of data.

		Sequence (5' → 3')	Amplicon length	Annealing temperature	Calibration Slope	Calibration Intercept
			MgCl <sub>2</sub>			
<b>RAT</b>						
<b>UCP2</b>	<i>f</i> <i>r</i> P <sub>X</sub> P <sub>LC</sub>	GAGAGTCAAGGGCTAGCGC GCTTCGACAGTGCTCTGGTA TCAGAGCATGCAGGCATTGG X LC Red640-CCGCCTCCTGGCAGGTAGC p	350 bp 4 mM	58°C	- 3.543	- 20.84
<b>UCP3</b>	<i>f</i> <i>r</i> P <sub>X</sub> P <sub>LC</sub>	GTTGGACTTCAGCCATCAGAA GTGGGTTGAGCACAGGTC GAACGGACCACTCCAGCGTC X LC Red640-CCATCAGGATTCTGGCAGGCT p	418 bp 6 mM	58°C	- 3.089	- 18.08
<b>UCP4</b>	<i>f</i> <i>r</i> P <sub>X</sub> P <sub>LC</sub>	TGGCCGAGCTAGCAACC CAGAGGGGATAATGTTTCATCTTCA CCATTTACAGACACGTAGTGTACTCTGGA X LC Rec 640-GTCGGATGGTCACCTACGAACAT p	289 bp 4 mM	58°C	- 3.061	- 17.13
<b>UCP5</b>	<i>f</i> <i>r</i> P <sub>X</sub> P <sub>LC</sub>	GATTGTAAGCGGACATCAG GGTTGGCAATAGTAGATGAAATC CGCCATACACAAAAGGTTTCCA X LC Red640-TTCAGACCAGACATCTCATGGCTTAA p	419 bp 4 mM	58°C	- 3.170	- 18.15
<b>GAPDH</b>	<i>f</i> <i>r</i> P <sub>X</sub> P <sub>LC</sub>	AACTCCCTCAAGATTGTCAGCAA ATGTCAGATCCACAACGGATACA CAGTCTTCTGAGTGGCAGTGATGGCA X LC Red705-ACTGTGGTCATGAGCCCTCCACG p	316 bp 4 mM	58°C	- 3.201	- 18.88
<b>MOUSE</b>						
<b>UCP2</b>	<i>f</i> <i>r</i> P <sub>X</sub> P <sub>LC</sub>	GAGAGTCAAGGGCTAGTGC GCTTCGACAGTGCTCTGGTA TCAGAGCATGCAGGCATCGG X LC Red640-CCGCCTCCTGGCAGGTAGC p	349 bp 4 mM	56°C	- 3.341	- 18.57
<b>UCP3</b>	<i>f</i> <i>r</i> P <sub>X</sub> P <sub>LC</sub>	GTTTACTGACAACTTCCCCT CTCCTGAGCCACCATCT AAGACCCGATACATGAACGC X LC Red640-CCCCTAGGCAGGTACCGCp	165 bp 5 mM	56°C	- 3.363	- 18.96
<b>UCP4</b>	<i>f</i> <i>r</i> P <sub>X</sub> P <sub>LC</sub>	GGACGAGCAAGTTTCTACTG CCCTCCAATGACCGATTTC CCATTTACAGACACGTAGTGTACTCTGGA X LC Red640-GTCGGATGGTCACCTATGAACATCTAC p	346 bp 6 mM	56°C	- 3.470	- 16.05
<b>UCP5</b>	<i>f</i> <i>r</i> P <sub>X</sub> P <sub>LC</sub>	CAGTGATTCATCAGAAAAGTTCCA CCGTGTTTTAGTAAGATCCACAG CGCCATACACAAAAGGTTTCCA X LC Red640-TTCAGACCAGACATCTCATGGCTTAA p	133 bp 5 mM	56°C	- 3.37	- 16.89
<b>GAPDH</b>	<i>f</i> <i>r</i> P <sub>X</sub> P <sub>LC</sub>	AATGGTGAAGGTCGGTGTGA CTGGAAGATGGTGATGGGC GGCAAATTCACGGCACAGTCAAG X LC Red705-CCGAGAATGGGAAGCTTGTTCATCAAC p	229 bp 4 mM	56°C	- 3.364	- 21.57

**TAB 3-1. Primer sets and fluorescent hybridization probes used for RT-PCR quantification of UCP mRNAs.** Primers (forward, *f*, reverse, *r*) and probes P<sub>X</sub> and P<sub>LC</sub> were designed as follows. X denotes the fluorescein fluorophore (donor); Red 640 is a Roche fluorophore (acceptor). The annealing temperatures were calculated by the synthesizing company (TIB MOLBIOL, Berlin, Germany).

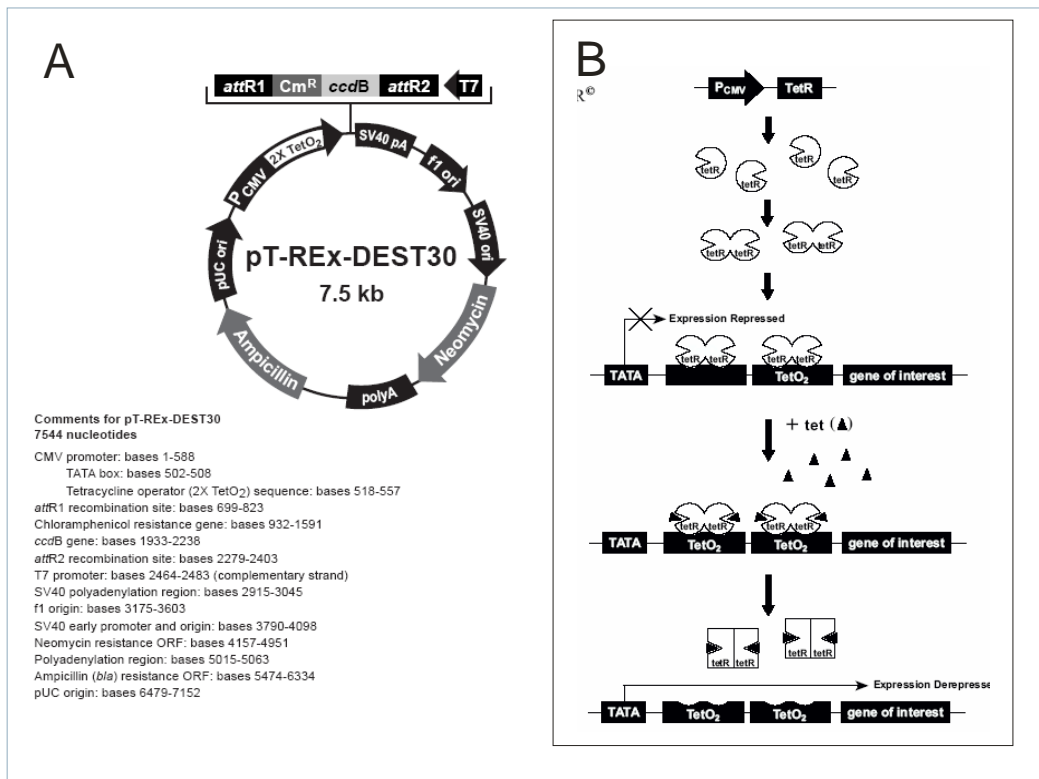


**FIG 3-8. Tetracycline-inducible expression.** (A) Map of pT-Rex-DEST30 vector that was used for tetracycline-inducible expression of CIDEa protein. (B) Vector bears 2 x TetO<sub>2</sub> sequences within promoter, that bind tetracycline repressor protein (tet-R). Tetracycline repressor protein is unbound after tetracycline binding and expression is derepressed.

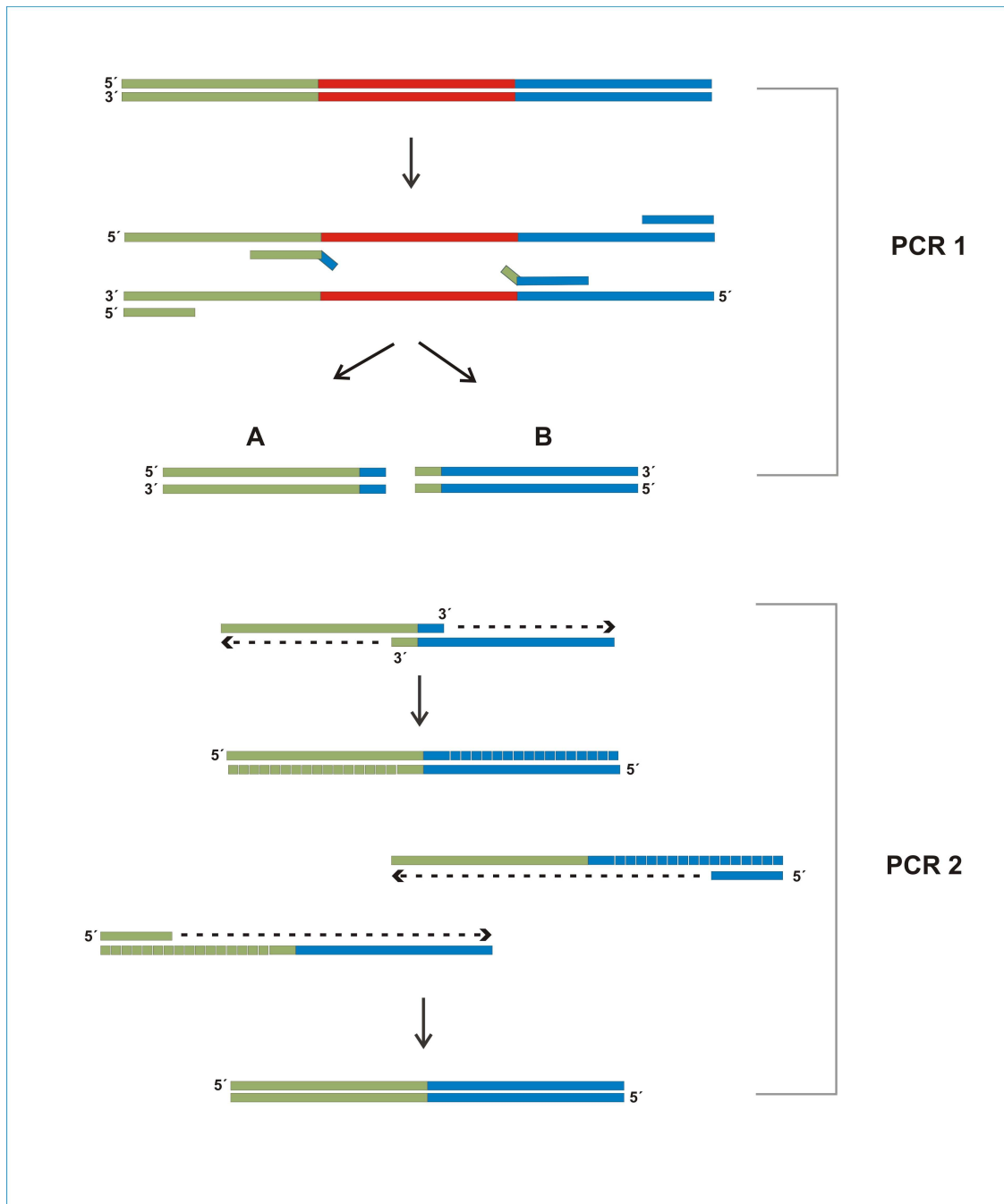


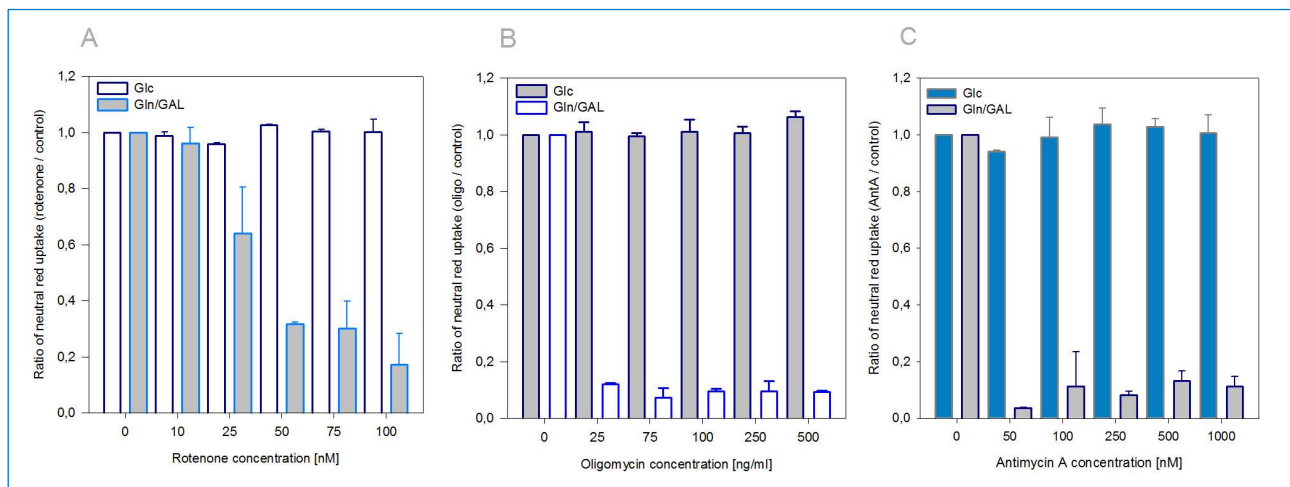
**FIG 3-9. Scheme of CIDE-N and CIDE-C domain deletion by PCR.** In PCR 1, primers are designed to produce two PCR products A and B with overlapping and complementary terminal sequences. Desired domain is not quantified. In the first cycle of the PCR 2 reaction, complementary ends of PCR products A and B serve as a primer for 3' → 5' extension by DNA polymerase. This step is necessary for annealing the external primers, which are the only primers present in PCR 2 reaction mix. Resulting PCR product do not contain the domain (*red*). Such a PCR product can be used to be subcloned into the desired vector.

construct / primer sequence 5' → 3'	
<b>pENTR</b>	
<b>attb 1</b>	GGGGACAAGTTTGTACAAAAAAGCAGGCTTC ATGCGAGGGGACCGGGCTTCTGG
<b>attb 2</b>	GGGGACCACTTTGTACAAGAAAGCTGGGTC CTATCCACACGTGAACCTGCCC
<b>CIDEΔC</b>	
<b>inside 1</b>	TTGCTCGCCGCCGAAGAGGTCG CAGTTTCTCATCTATCTGGGCA
<b>inside 2</b>	TGCCCAGATAGATGAGAAACTG CGACCTCTTCGGCGGCGAGCAA
<b>CIDEΔN</b>	
<b>inside 1</b>	ACCCCGCTCATGCATCCAGCT CAGCACGTCCCCACTTGCTCG
<b>inside 2</b>	CGAGCAAGTGGGGACGTGCTG AGCTGGATGCATGAGCGGGGT
<b>DsRed-MonomerC1</b>	
<b>Fw</b>	AACATTATCTCGAGGAGGCACCATGCGA
<b>Rev</b>	GGCCGTCGAATTCTAGTTCTATCCACACG

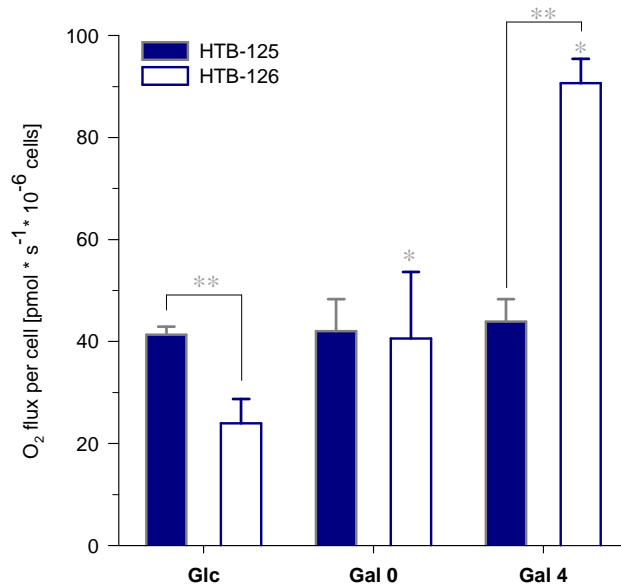
**TAB 3-2. Primer sequences used for expression plasmids preparation.** Primers *attb* were used for cloning into pDonr221. Primers *Fw* and *Rev* were used for protein fusion with DsRED fluorescent protein. Primers *inside* were used for CIDE domains deletion.

PRIMER / PROBE		Tm
<b>CIDEa #1</b>	ATCAgCAAgACTCTggATgTC	21mer 57,0°C
<b>CIDEa#2</b>	ggCCTTgAAgCTTgTgCA	18mer 55,6°C
<b>CIDEa HP#1</b>	gAgTCACCTTCgACCTATACAggCTgAA X	28mer 67,2°C
<b>CIDEa HP#2</b>	LC Red604-CCCAAggACTTCCTCggCTgTCTCAAT p	27mer 66,8°C

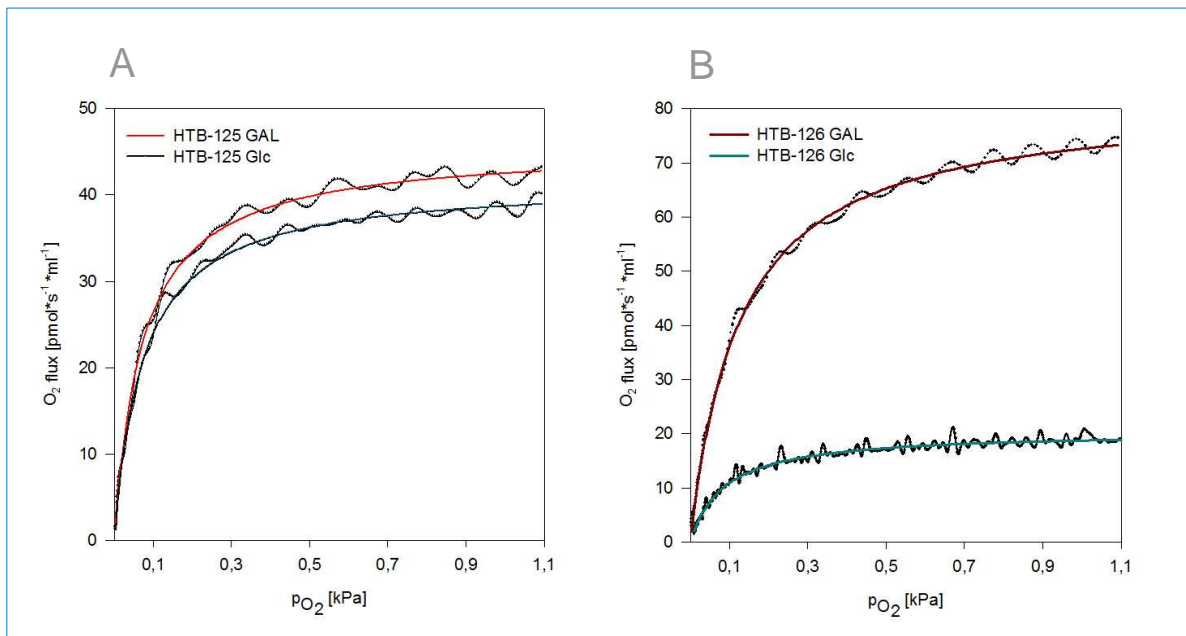
**TAB 3-3. Primers and probes sequences used for Real-time quantification of rat CIDEa.** X- fluorescein, p- 3' phosphate, Tm – primer-specific melting temperature.



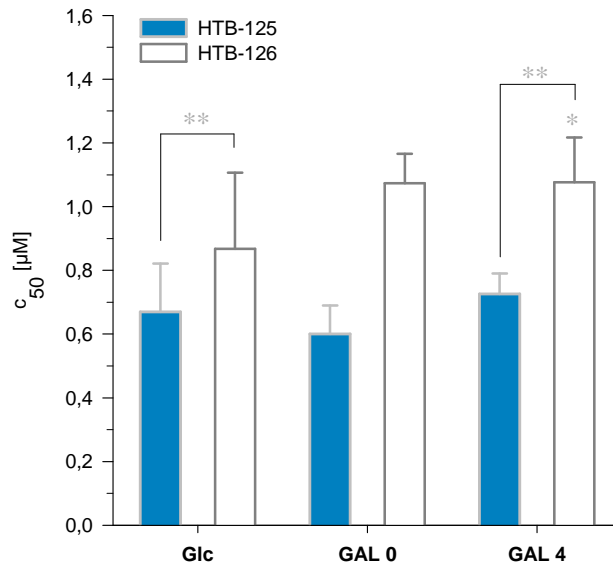
**FIG 4-1. Effect of mitochondrial inhibition on cell viability of cancer HTB-126 cells.** Cell viability of cancer HTB-126 Glc and HTB-126 GAL cells in the presence of mitochondrial inhibitors rotenone (A), oligomycin (B), and antimycin A (C) incubation for 8 hours, measured by neutral red assay. Values are means  $\pm$  SD  $n=2$ .



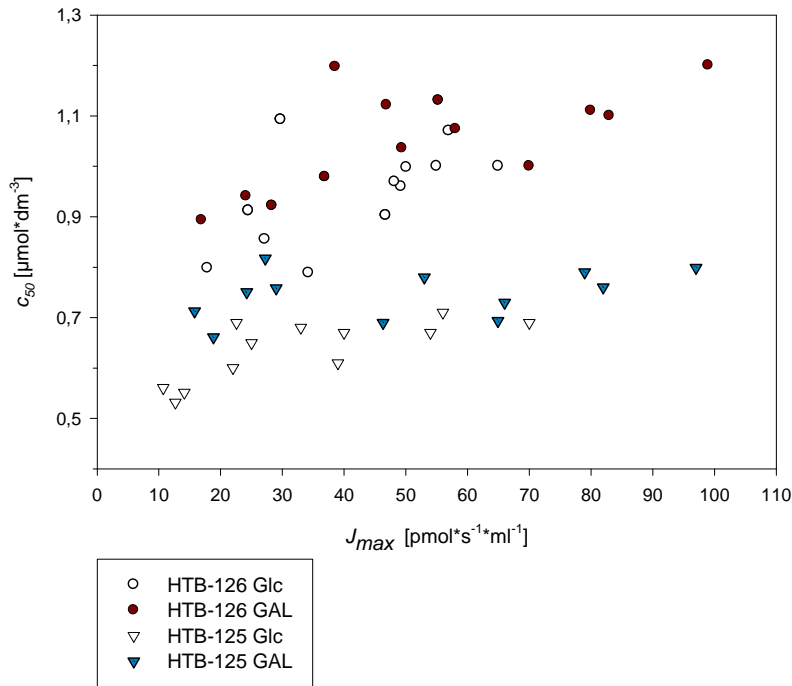
**FIG 4-2. Influence of cultivation conditions on cell respiration of normal and breast cancer cells.** Cell specific respiration of HTB-125 and HTB-126 cells in glucose (Glc) vs. glucose-deprived medium (Gal 0, Gal 4).  $\pm$ SD. \*  $p < 0,05$  compared to glucose; \*\*  $p < 0,05$  compared to control cell line. Values are means  $\pm$  SD,  $n > 5$ .



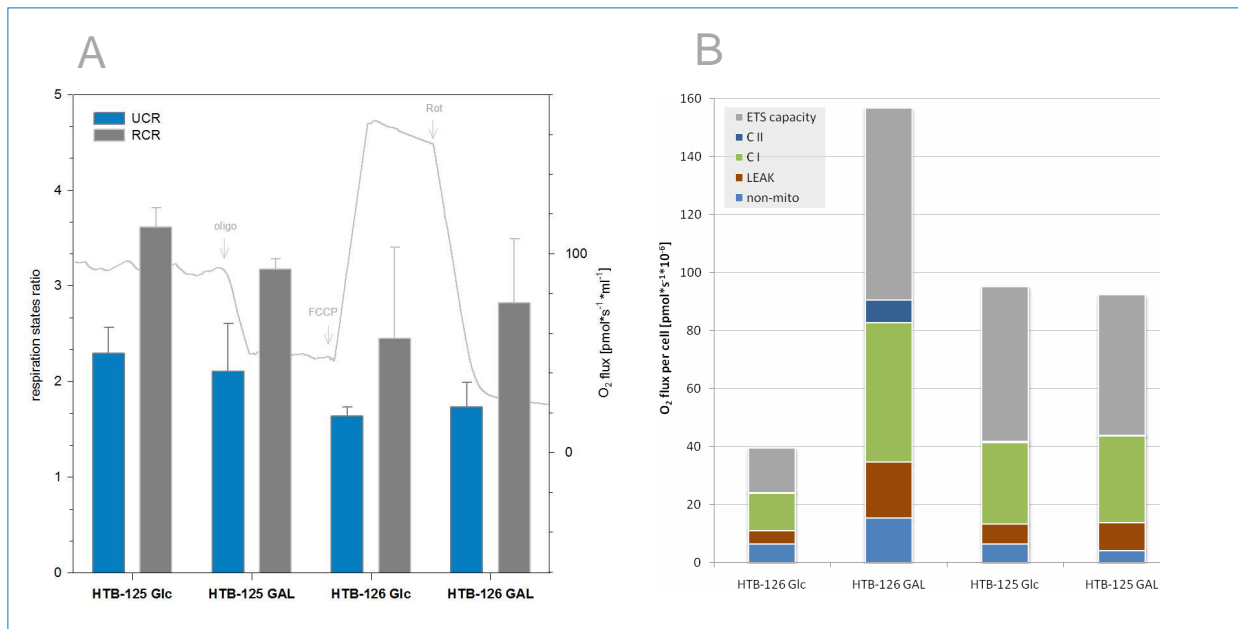
**FIG 4-3. Influence of cultivation conditions on cell respiration of normal and breast cancer cells – oxygen kinetics.** Cell specific respiratory flux as a function of  $p_{O_2}$  of control cells (A) and cancer cells (B) - representative traces of  $10^6$  cells in culture medium. Dots represents single data points. Data recording interval was 1 s. Solid lines represent hyperbolic fit calculated in the low-oxygen range  $< 1,1$  kPa.



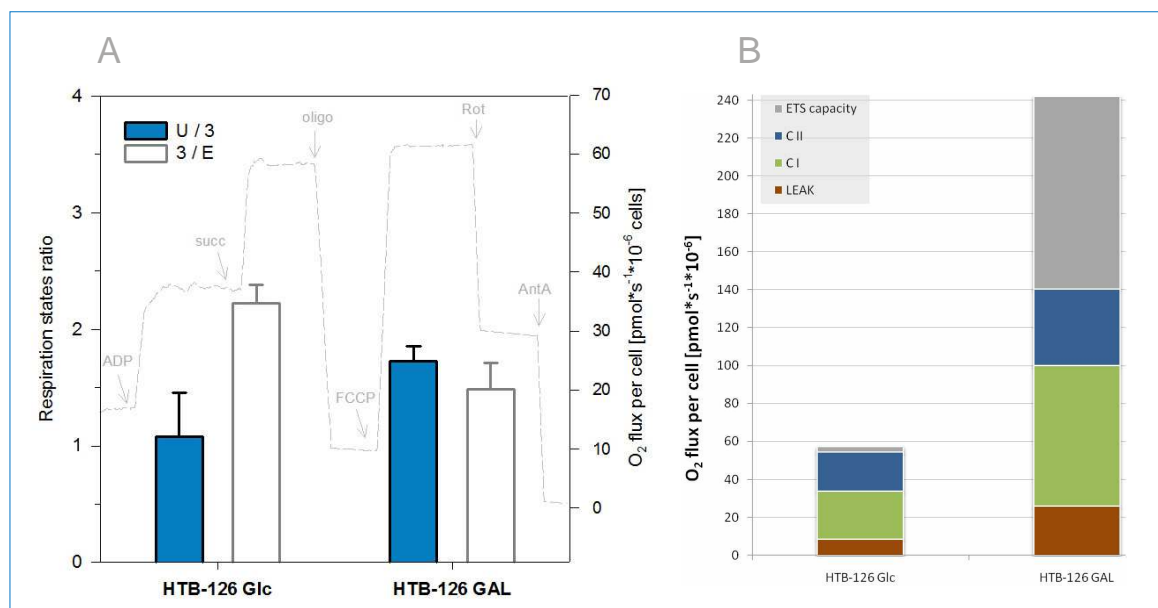
**FIG 4-4. Influence of cultivation conditions on cell respiration of normal and breast cancer cells –  $c_{50}$ .**  $c_{50}$  of HTB-125 and HTB-126 cells in glucose (Glc) vs. glucose-deprived medium (Gal 0, Gal 4). \*  $p < 0,05$  compared to glucose; \*\*  $p < 0,05$  compared to control cell line. Values are means  $\pm$  SD  $n > 5$ .



**FIG 4-5. Variation of  $c_{50}$  with respiratory flux.**  $c_{50}$  of intact cells is plotted as a function of  $J_{max}$ , where  $J_{max}$  results from measurements at different cells densities. Different symbols represent different cell lines. Open symbols: cells grown in Glc/GAL medium. Each point represents a single measurement. Within each group, we can see an increase of  $c_{50}$  with cell density, resulting in increase of  $J_{max}$  (linear slopes, calculated from linear regression fits, are 0.0028, 0.0030, 0.0024, and 0.0006, respectively for HTB-126 Glc, HTB-126 GAL, HTB-125 Glc and HTB-125 GAL, cells respectively). Oxygen diffusion is a factor controlling  $c_{50}$  more in HTB-126 than HTB-125 cells.



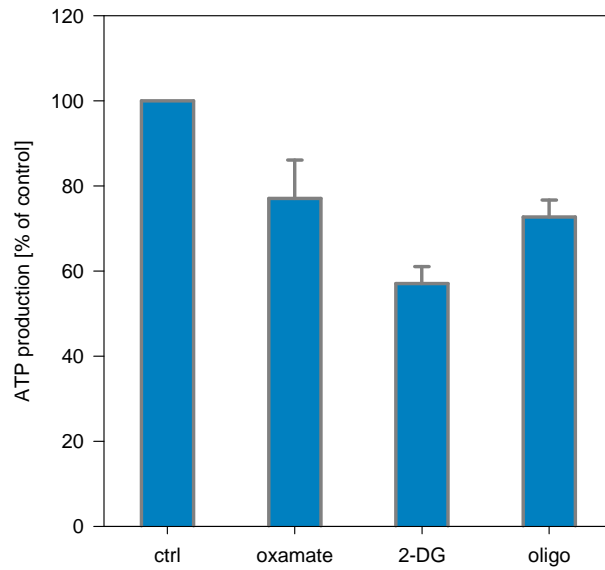
**FIG 4-6. Respiratory ratios of HTB-125 and HTB-126 intact cells Glc vs. Gln/GAL; components of cellular respiration in intact cells.** (A) Respiratory ratios calculated of intact cells respiration with inhibitors; uncoupling control ratio (UCR, blue bars) calculated of uncoupled respiration (U) over routine respiration (R) and coupling ratio, (RCR, grey bars), calculated of routine flux over oligomycin-inhibited flux. Experiments were performed according to the protocol as illustrated (grey line, Y2 axis), expressed as volume-specific flux of random sample. Arrows indicate events for an addition of inhibitors. Values are means  $\pm$  SD  $n > 5$ . (B) Quantification of individual elements of respiratory flux as integrate to cellular respiration of intact cells, expressed as cell-specific flux per  $10^6$  cells. Each color represents particular respiratory state; non-mitochondrial part of routine flux (*non-mito*), leak respiration (*LEAK*), rotenone-sensitive flux (*CI*), antimycine-sensitive part (*CII*), and reserve capacity after uncoupling (*ETS capacity*). Columns represent cell type under glucose or glucose-deprived conditions. Each column consists of particular respiratory state expressed per  $10^6$  cells.



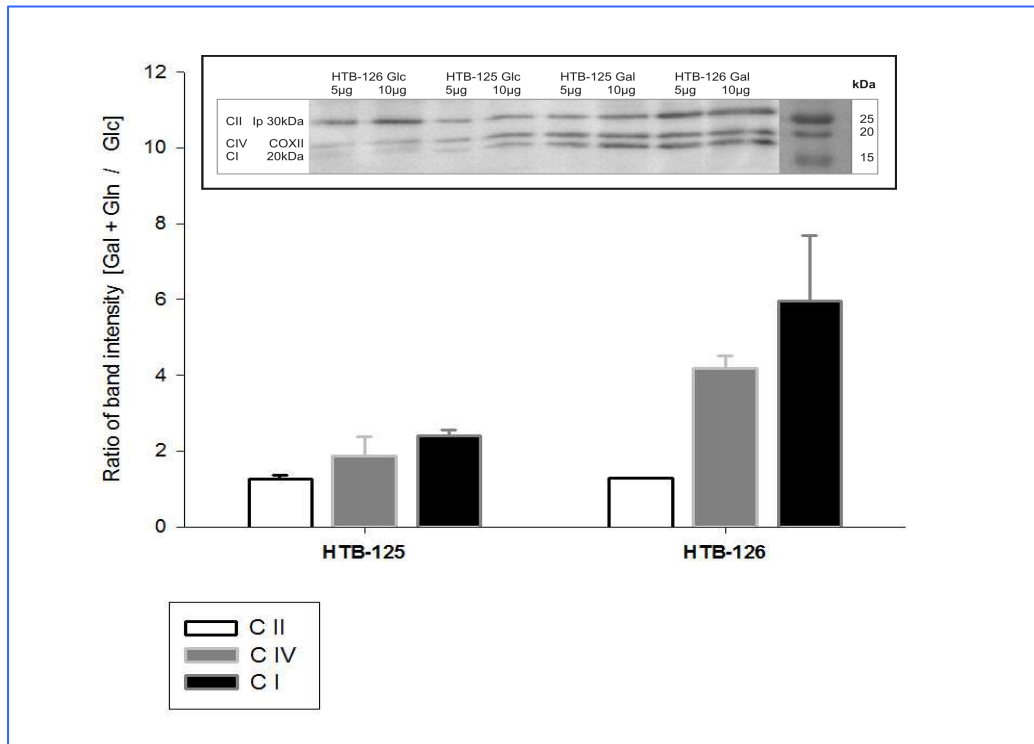
**FIG 4-7. Respiratory ratios of permeabilized cancer cells; components of mitochondrial respiration in permeabilized cells.** (A) Respiration of permeabilized cells was performed as illustrated (grey line, Y2 axis) at the example of  $10^6$  of HTB-126 Glc cells. Arrows indicate substrate/inhibitors addition. Blue bars is RCR values calculated as uncoupled flux over state 3 flux with complex I + II substrates. White bars express ratio of state 3 respiration and corresponding routine respiration. Values are means  $\pm SD$   $n \geq 4$ . (B) Quantified contribution of particular elements of respiratory flux expressed per  $10^6$  cells as described in the text; bars consist of leak respiration (LEAK), complex I related flux (CI), complex II – related flux (CII), and reserve capacity of respiratory system (ETS capacity).

	U/3	3/endo	SCR	$U_{perm}/U_{int}$
HTB-126 Glc	1,08 $\pm$ 0,38	2,23 $\pm$ 0,15	2,67 $\pm$ 0,40	1,47 $\pm$ 0,12
HTB-126 GAL	1,73 $\pm$ 0,12	1,49 $\pm$ 0,22	1,40 $\pm$ 0,15	1,55 $\pm$ 0,16

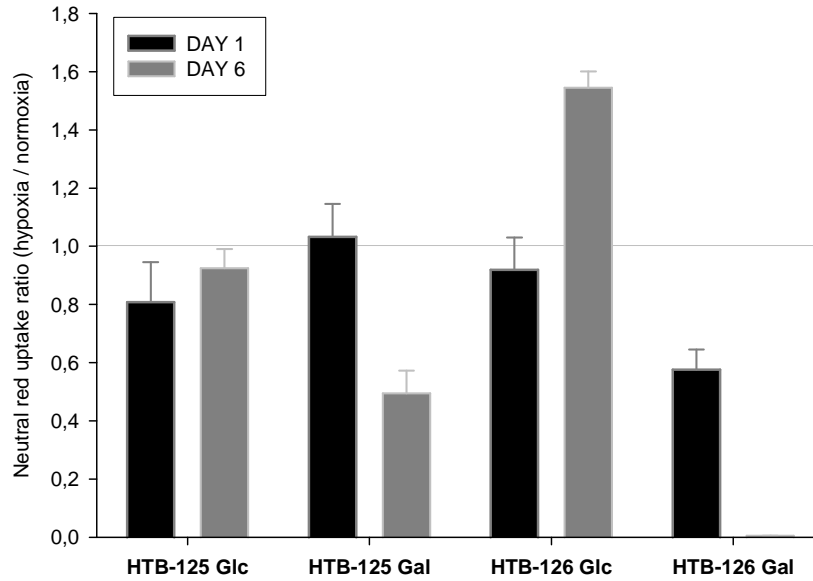
**TAB 4-1. Quantification of respiratory ratios of permeabilized cells.** Ratio  $U/3$  is UCR of permeabilized cells. It expresses the ratio of uncoupled state to state 3 respiration with complex I+II input. Ratio  $3/endo$  expresses the state 3 respiration with complex I+II input over the corresponding routine respiration. SCR, succinate control ratio, expresses the increase of respiration after succinate addition.  $U_{perm}/U_{int}$  expresses the ratio of fully uncoupled states of permeabilized to intact cells. Values are means  $\pm SD$ .  $n \geq 4$ .



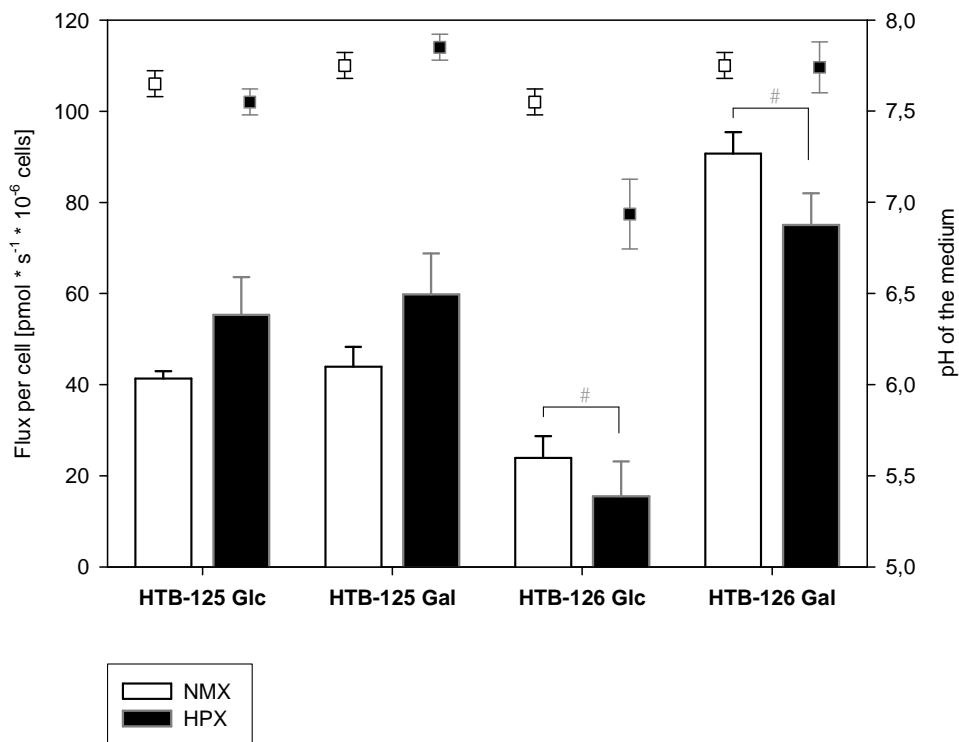
**FIG 4-8. ATP synthesis in HTB-126 Glc.** Measurement of ATP synthesis with glycolytic inhibitors 2-deoxy glucose (2-DG) and oxamate, and oligomycine. Results we expressed in pmols/mg of cellular protein and further correlated to control value with no inhibitor (ctrl). Values are means  $\pm$  SD  $n=3$ .



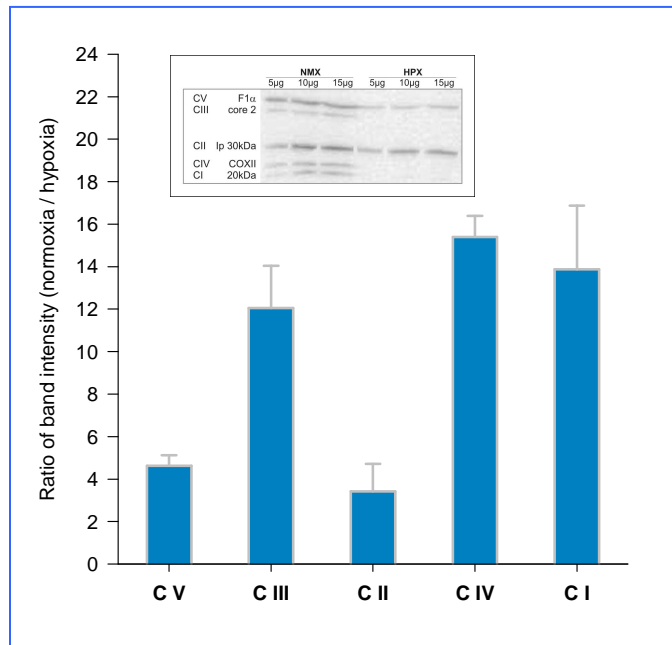
**FIG 4-9. Western-blot quantification of the respiratory chain content of normal and breast cancer cells upon glucose deprivation.** Contents of respiratory complexes I, II and IV were determined using whole cell lysates of HTB-125 and HTB-126 cells grown in Gln or Gln/GAL medium. Results are expressed as ratios of band intensities of the corresponding Gln/GAL to Glc sample pairs. Band intensity was quantified by densitometry. Values are means  $\pm$  SD  $n=3$ . *Graph inset* shows an exemplar Western-blot; note band designation and molecular weight (kDa, number in right).



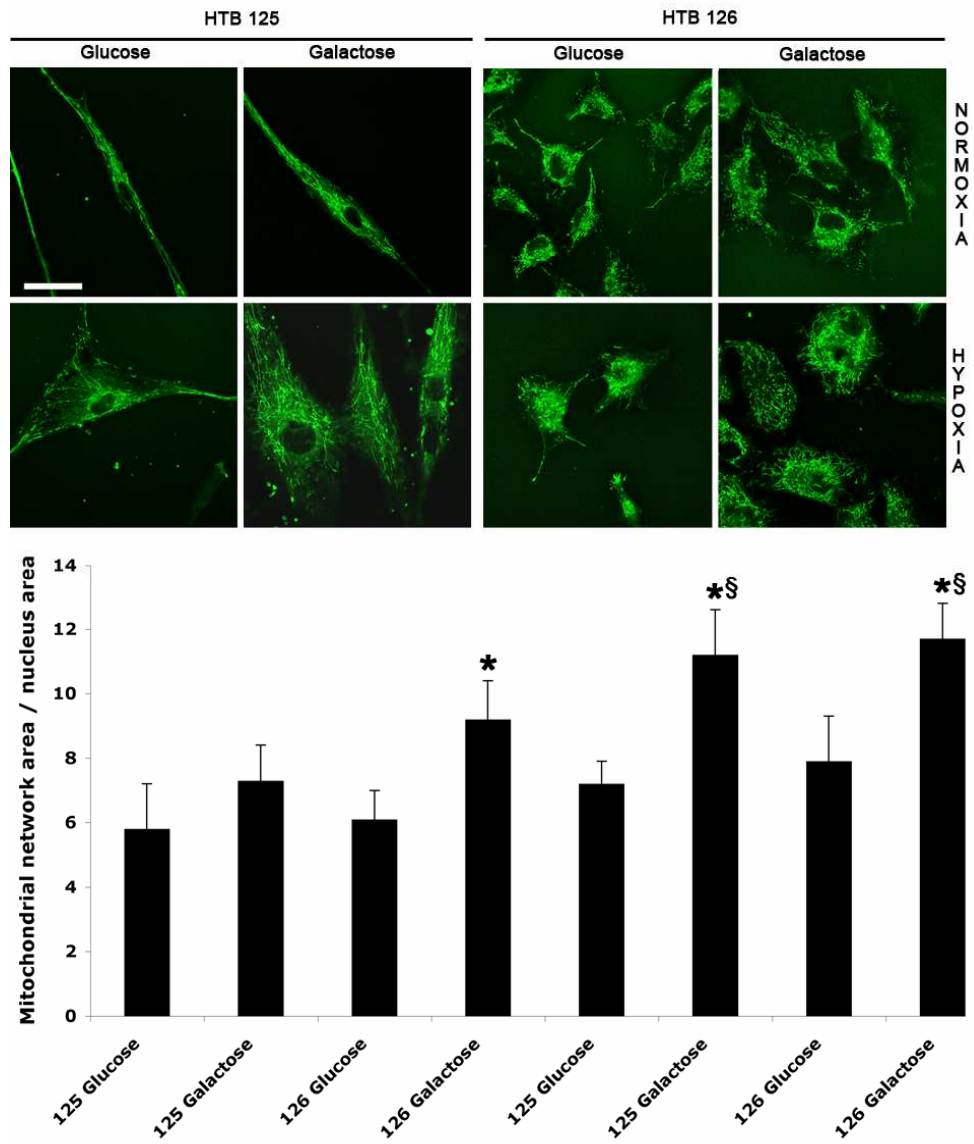
**FIG 4-10. Cell viability of HTB-125 and HTB-126 under normoxia and hypoxia.** Data are expressed as neutral red uptake ratios of normoxic to hypoxic cells at day 1 (black) and 6 (grey) in 1% oxygen. Values are means  $\pm$ SD  $n=5$ .



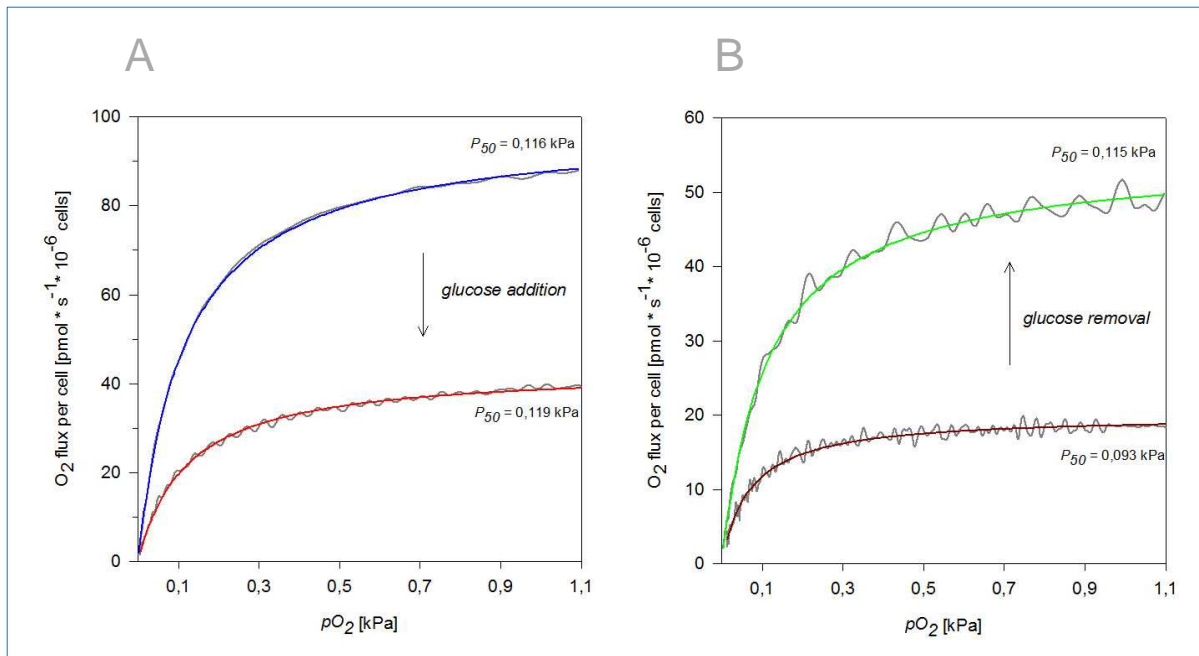
**FIG 4-11. Effect of hypoxia on respiratory flux and medium pH of normal and breast cancer cells.** Respiratory flux of intact HTB-125 and HTB-126 cells in glucose (Glc) or glucose-deprived medium (Gal) in normoxia (NMX) and after exposure to 1% O<sub>2</sub> for six days (HPX) expressed as a cell-specific flux per 10<sup>6</sup> cells (columns, Y1 axis). #  $p < 0,05$ . pH of the culture medium was measured after cultivation (Y2 axis). Values are means  $\pm$ SD  $n=3$ .



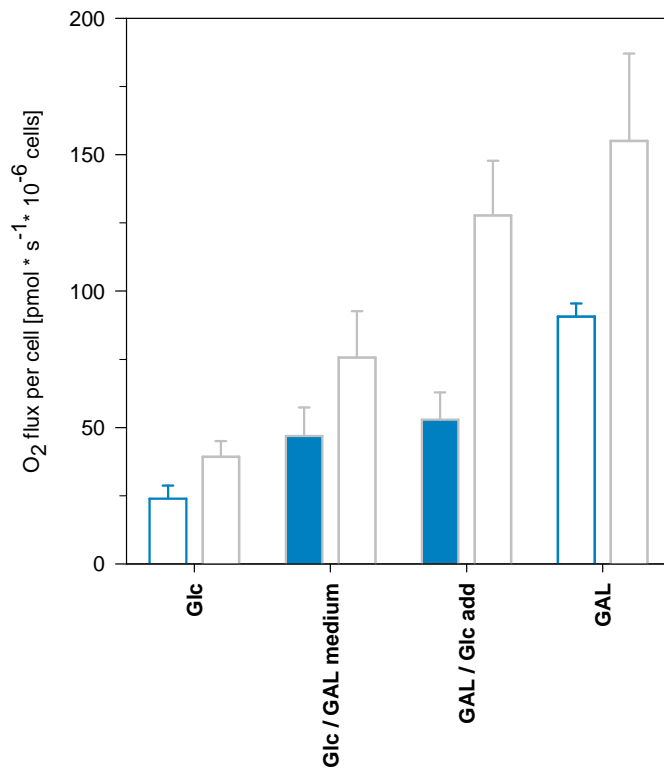
**FIG 4-12. Western-blot quantification of the respiratory chain content of breast cancer cells HTB-126 Glc grown under hypoxia.** Quantification of respiratory chain complexes I - V in whole cell lysates of cells grown in 1% oxygen and 21% oxygen expressed as ratios of normoxia to hypoxia of the corresponding sample pair. Values are means  $\pm$ SD  $n=3$ .



**FIG 4-13** Mitochondrial network in HTB-125 and HTB-126 in normoxia and hypoxia. Images obtained by confocal microscopy were analyzed and total mitochondrial area was related to nucleus area. \*  $p < 0.05$  Glc compared to GAL, §  $p < 0.05$  normoxia compared to hypoxia. Values are means  $\pm$ SD  $n=100$ .



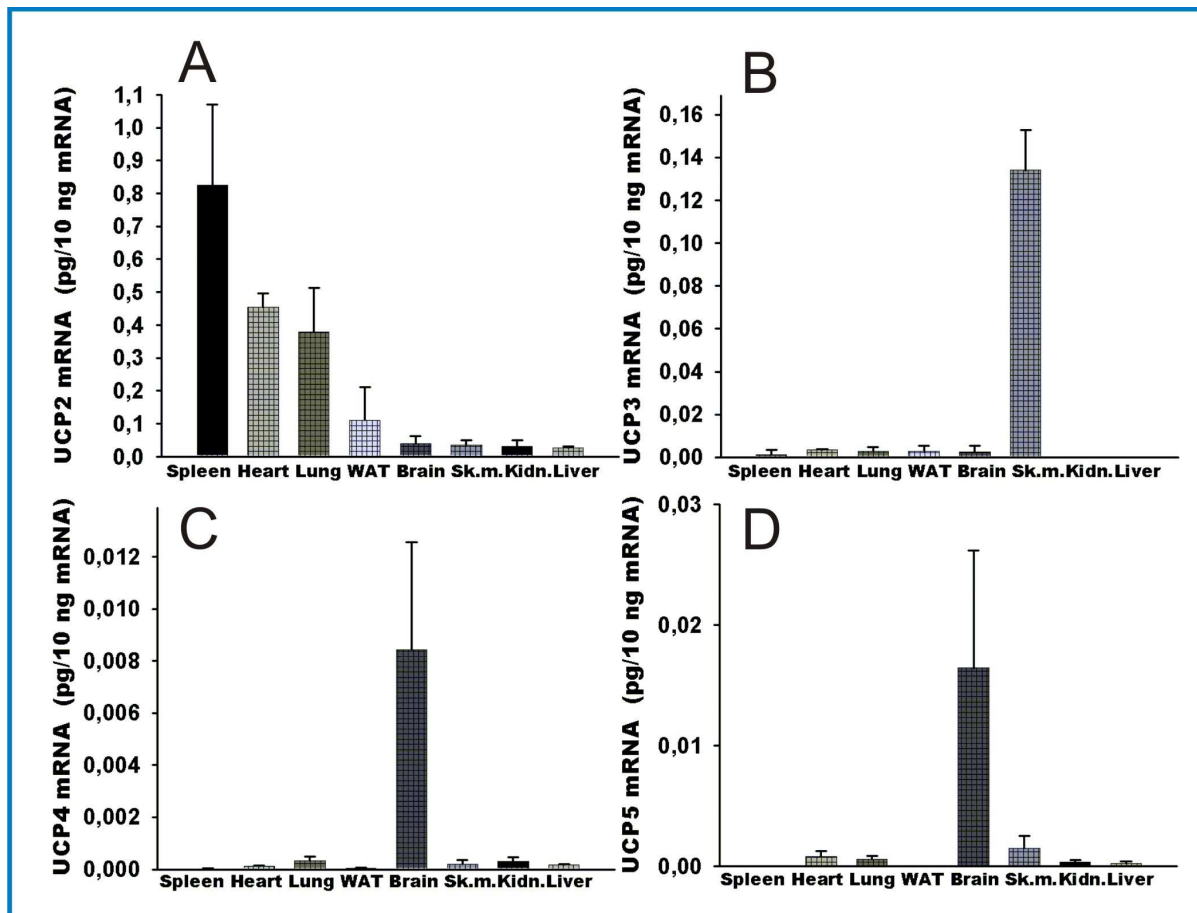
**FIG 4-14. Demonstration of Crabtree effect occurring in breast cancer cells.** Effect of glucose addition (A) and glucose removal (B) on cellular respiration of intact cells expressed as cell-specific flux of  $10^6$  cells as a function of  $p_{O_2}$ . Corresponding  $P_{50}$  is shown in the graph.



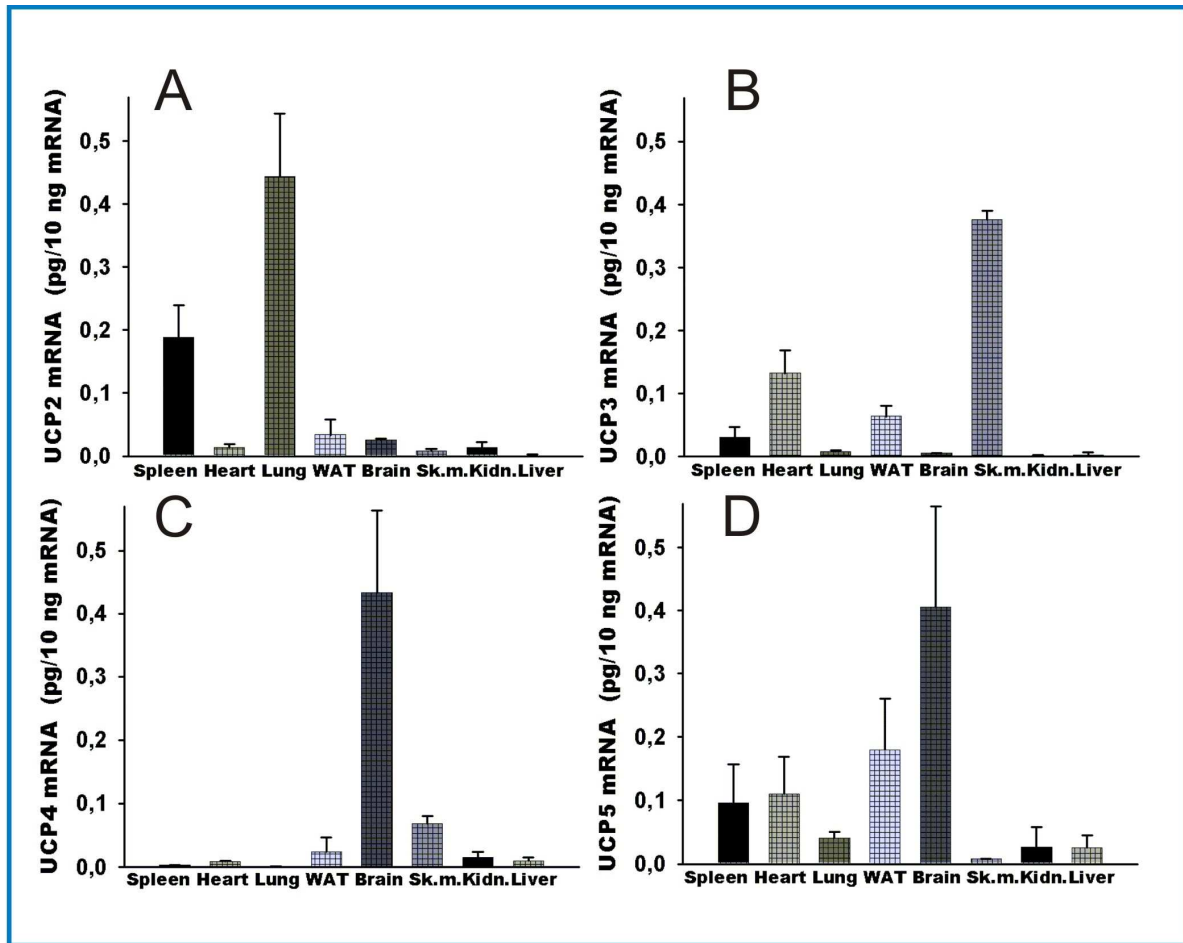
**FIG 4-15. Respiration of cancer cells upon glucose addition and removal, comparison of routine and uncoupled flux.** Respiration of  $10^6$  HTB-126 cells in designated conditions (blue bars) and corresponding uncoupled flux (grey bars). Values are means  $\pm$  SD.  $n > 5$ .

	Glc	Glc / GAL	GAL / Glc	GAL
$c_{50}$ [ $\mu\text{mol}\cdot\text{l}^{-1}$ ]	0,94 $\pm$ 0,20	1,07 $\pm$ 0,09	1,07 $\pm$ 0,11	1,09 $\pm$ 0,16
UCR U/R	1,64 $\pm$ 0,09	1,53 $\pm$ 0,22	2,52 $\pm$ 0,16	1,76 $\pm$ 0,26

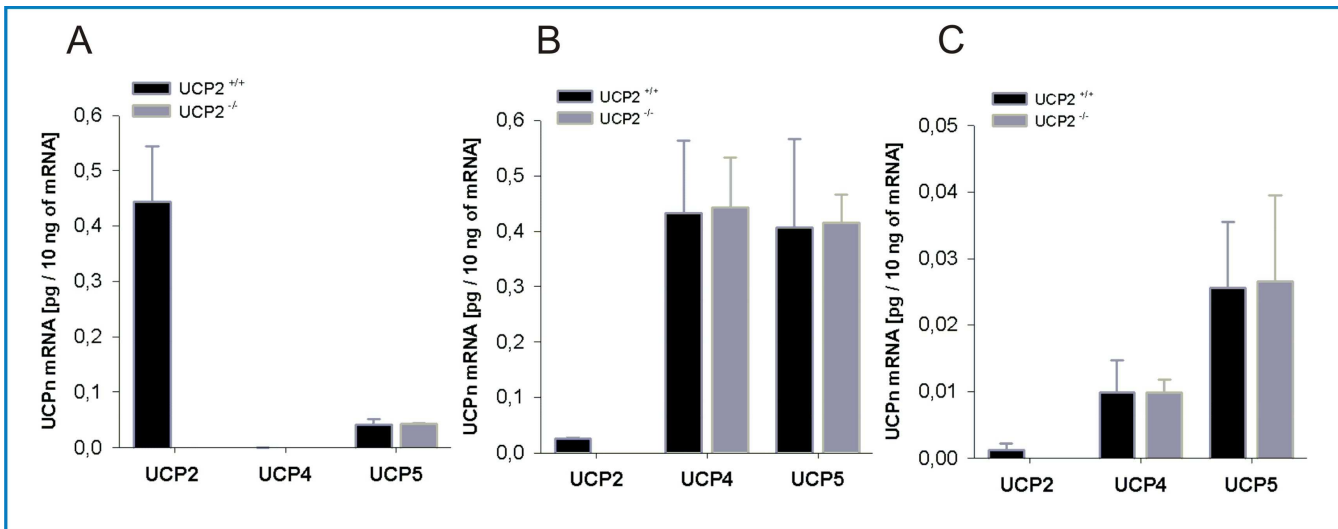
**TAB 4-2. Quantified  $c_{50}$  values and uncoupling phosphorylation ratios in response to glucose presence.**  $c_{50}$  values and UCR values derived of cellular respiration of intact HTB-126 cells; values in glucose medium (*Glc*), after glucose removal and replacement by Gln/GAL medium (*Glc/GAL*), after glucose addition to GAL cells (*GAL/Glc*) and GAL cells (*GAL*). Values are means  $\pm$  SD.  $n > 5$ .



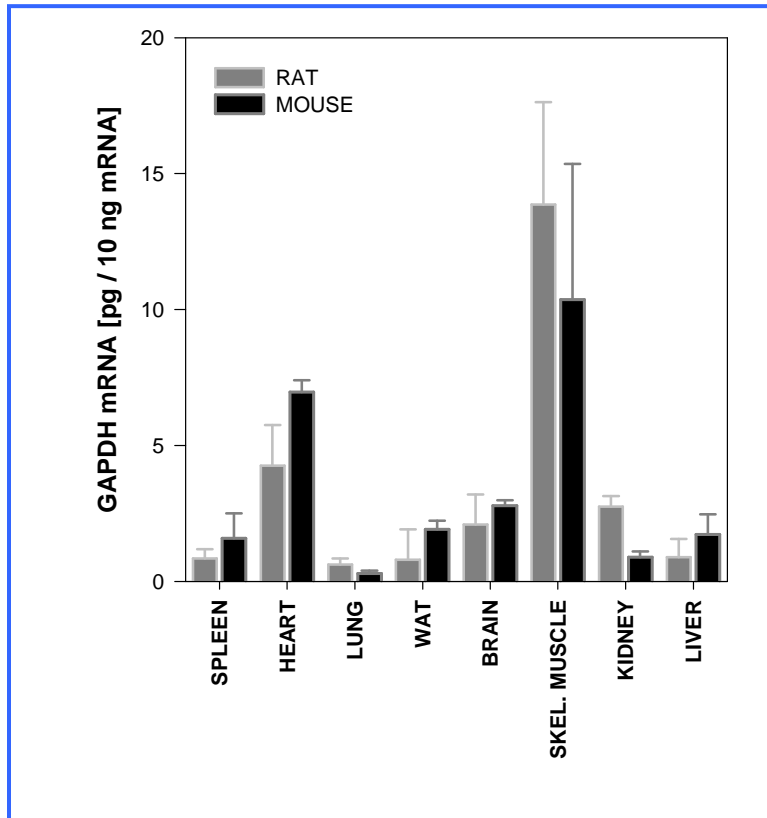
**FIG 4-16. Quantification of UCPn mRNA in rat tissues.** Transcript quantification is expressed as pg of UCPn mRNA per 10 ng of overall transcript in PCR reaction. Quantification of UCP 2 (A), UCP 3 (B), UCP 4 (C) and UCP 5 (D) mRNA. Values are means  $\pm$  SD.  $n \geq 5$ .



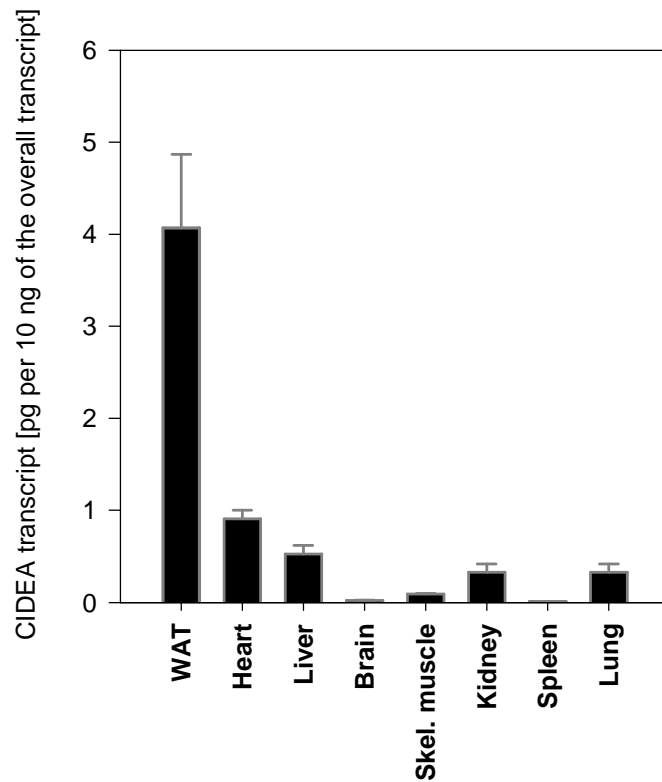
**FIG 4-17. Quantification of UCPn mRNA in mouse tissues.** Transcript quantity is expressed as pg of UCPn mRNA per 10 ng of overall transcript in PCR reaction. Quantification of UCP 2 (A), UCP 3 (B), UCP 4 (C) and UCP 5 (D) mRNA. Values are means  $\pm$  SD.  $n \geq 5$ .



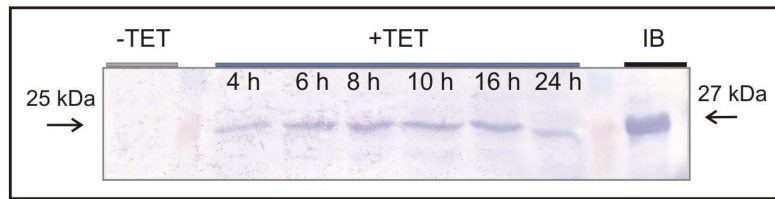
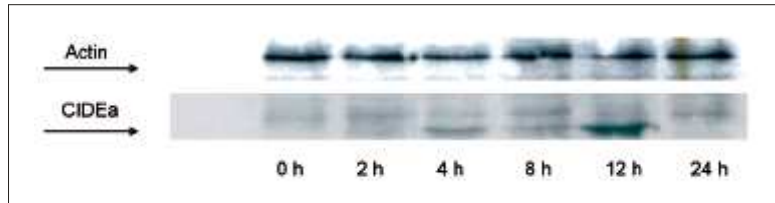
**FIG 4-18. Quantification of UCPn mRNA in control and UCP2<sup>-/-</sup> mouse.** Quantification of transcripts of UCP2, UCP4 and UCP5 in UCP2-null (grey) and control (black) mouse in lung (A), brain (B) and liver (C) to follow theoretical compensatory expression of other isoforms after genetic ablation of UCP2. Values are means  $\pm$  SD.  $n = 4$ .



**FIG 4-19. Quantification of GAPDH mRNA in mouse and rat tissues.** Quantification of GAPDH transcripts in rat (*grey*) and mouse (*black*) tissues for comparison with UCPs in corresponding tissues.



**FIG 4-20. Absolute quantification of mRNA transcripts of CIDEA in rat tissues.** Values are means  $\pm$  SD.  $n=3$ .

**A****B**

**FIG 4-21. Induction of CIDEa expression – western blot.** (A) Induction of hCIDEa expression by tetracycline in 293-HEK cells. Cells were subjected to tetracycline for desired time course. Western-blot of isolated mitochondrial fraction is presented; -TET means no addition of tetracycline, where no induction of expression occurs. IB is positive control of bacterially-expressed hCIDEa His-tagged. (B) Expression of CIDEa in HeLa cells by tetracycline.

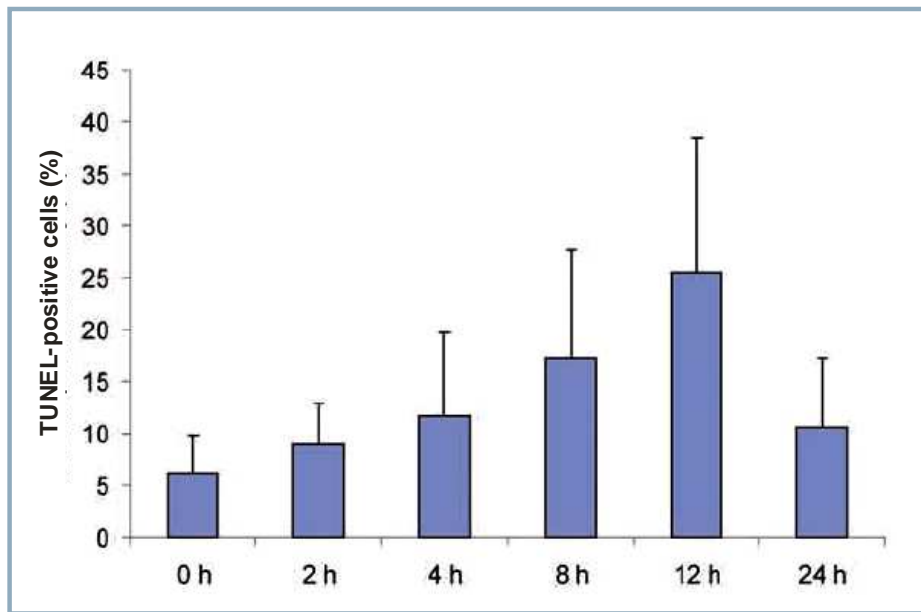


**FIG 4-22. TUNEL assay of HeLa cells expressing CIDEa.** Results are expressed as a percentage of TUNEL-positive cells. Values are means  $\pm$  SD.  $n=3$ .

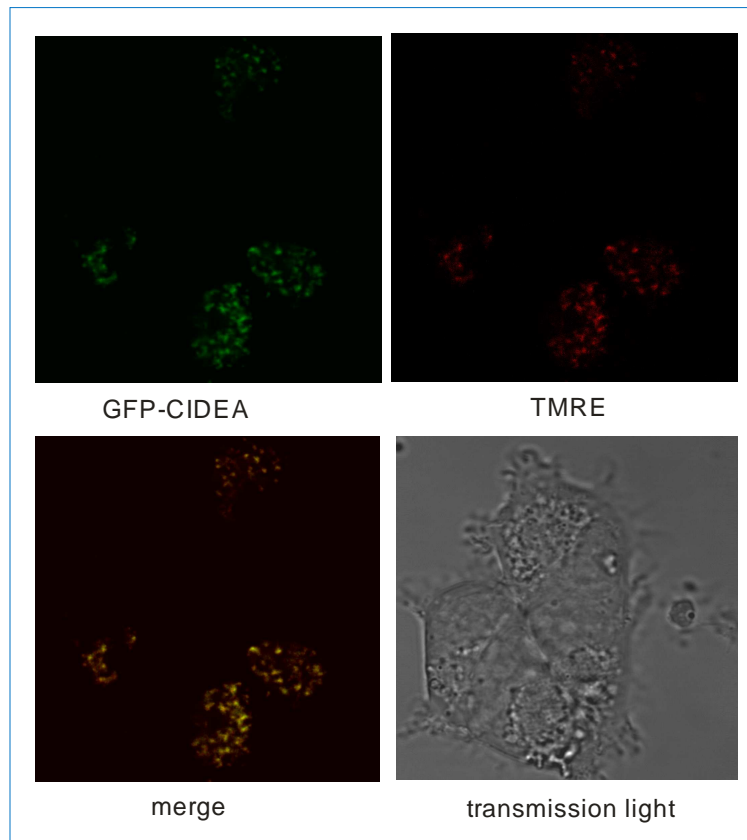


**FIG 4-23. Mitochondrial localization of CIDEa in 293-HEK cells – confocal microscopy.** CIDEa was tagged with N-terminal GFP (DEST53) and mitochondrial localization was analyzed by colocalization with mitochondrial-specific dye TMRE. CIDEa localized to mitochondria (yellow merge).

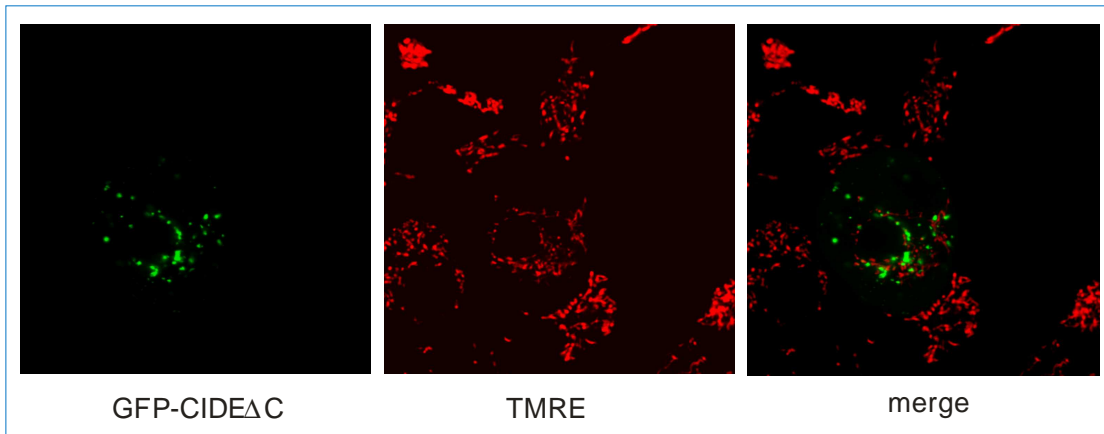


**FIG 4-24. Subcellular localization of CIDE $\Delta$ C in 293-HEK cells – confocal microscopy.** CIDE $\Delta$ C was tagged with N-terminal GFP (DEST53) and mitochondrial localization was analyzed by colocalization with mitochondrial-specific dye TMRE. CIDEA localized to mitochondria (merge).

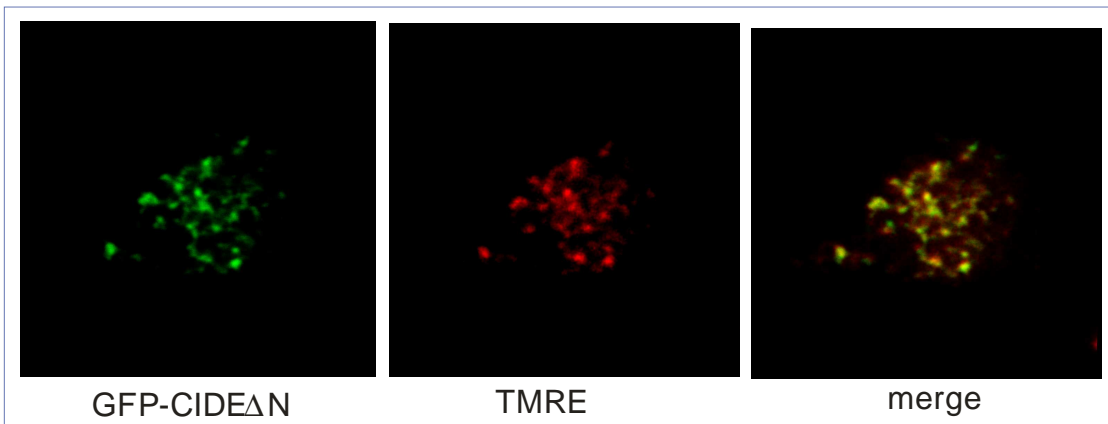


**FIG 4-25. Subcellular localization of CIDE $\Delta$ N in 293-HEK cells – confocal microscopy.** CIDE $\Delta$ N was tagged with N-terminal GFP (DEST53) and mitochondrial localization was analyzed by colocalization with mitochondrial-specific dye TMRE. CIDEA localized to mitochondria (yellow merge).

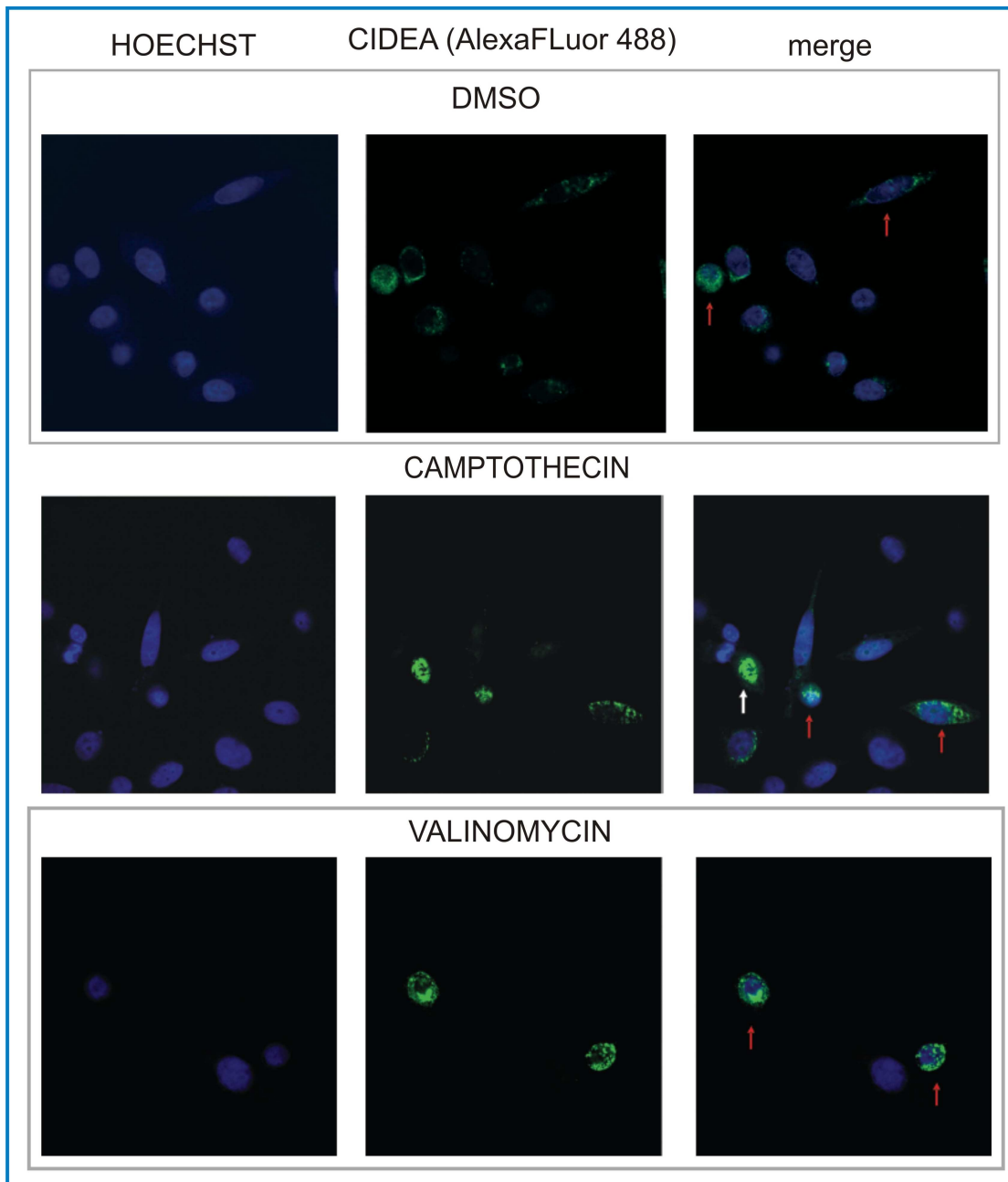


**FIG 4-26. Subcellular localization of CIDEa in HeLa cells treated with valinomycin and camptothecin.** T-REx HeLa cells were transfected with pDEST-CIDEa plasmid and following 24 h stabilization subjected to tetracycline (1  $\mu\text{g}/\text{ml}$ ) treatment for 8 h followed by 2 h of treatment with DMSO (*top*), camptothecin (2  $\mu\text{M}$ ; *middle*) or valinomycin (2  $\mu\text{M}$ ; *bottom*). Cells were fixed and probed with antiCIDEa antibody followed by AlexaFLuor 488-conjugated secondary antibody and Hoechst 33258 dye. Fields shown were visualized under confocal microscope (magnification 400 $\times$ ) using the appropriate wavelengths for AlexaFLuor 488 (green fluorescence) and Hoechst (blue fluorescence) dyes, and the two images were merged. White arrows indicate cells showing predominantly nuclear localization of CIDEa, red arrows show cells with nuclear as well as extranuclear localization of CIDEa.

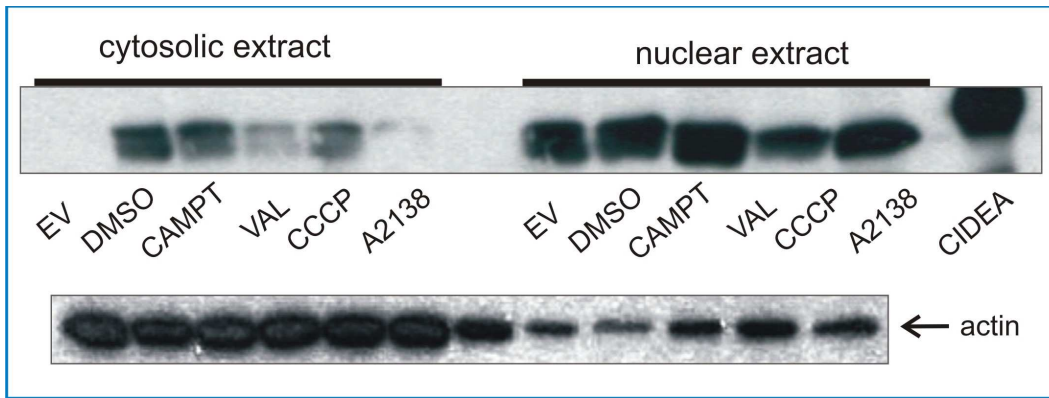


**FIG 4-27. Redistribution of CIDEa from cytosolic to nuclear fraction of HeLa cells– western-blot.** Redistribution of CIDEa of cytosolic to nuclear extract after apoptotic stimuli. EV – negative control usány empty vector, DMSO(dimethyl sulfoxid) – negative control, CAMPT – capmtothecin (2  $\mu$ M), VAL – valinomycin (2  $\mu$ M), A23187 – calcium ionophore, CIDEA – positive control positive control of bacterially-expressed hCIDEa His-tagged.

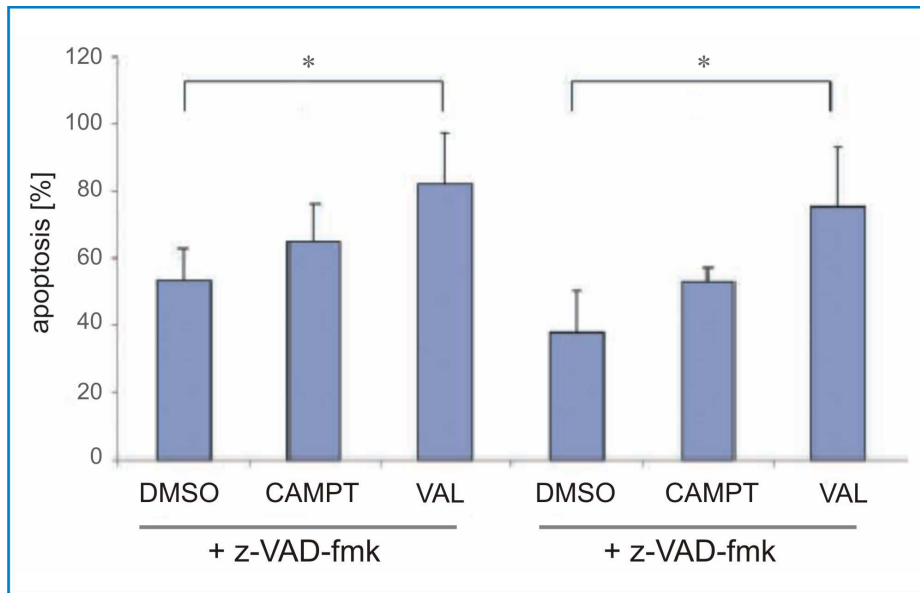


**FIG 4-28. Effect of pan-caspase inhibitor on apoptosis induced by CIDEa overexpression.** T-REx HeLa cells were transfected with pDEST-CIDEa plasmid and following 24 h stabilization subjected to tetracycline (1  $\mu$ g/ml) treatment for 8 h. After brief rinse with PBS, cells were treated for 30 min with 50  $\mu$ mol/l pan-caspase inhibitor z-VAD-fmk and then further 2 hours with the indicated effector. Cells were probed with CIDEa antibody followed by AlexaFluor 488-conjugated secondary antibody and Hoechst 33258 dye. CIDEa positive and apoptotic cells were quantified from random fields, at least 100 cells displaying apoptotic morphology per experiment. Percentage of apoptosis was then calculated as a ratio of CIDEa positive apoptotic cells versus total number of apoptotic cells. Error bars are standard deviations determined from at least three independent experiments. DMSO, cells treated with DMSO only as vehicle control; CAMPT, 2  $\mu$ M camptothecin; VAL, 2  $\mu$ M valinomycin. Values are means  $\pm$  SD.  $n=3$ . \*  $p < 0.05$ .

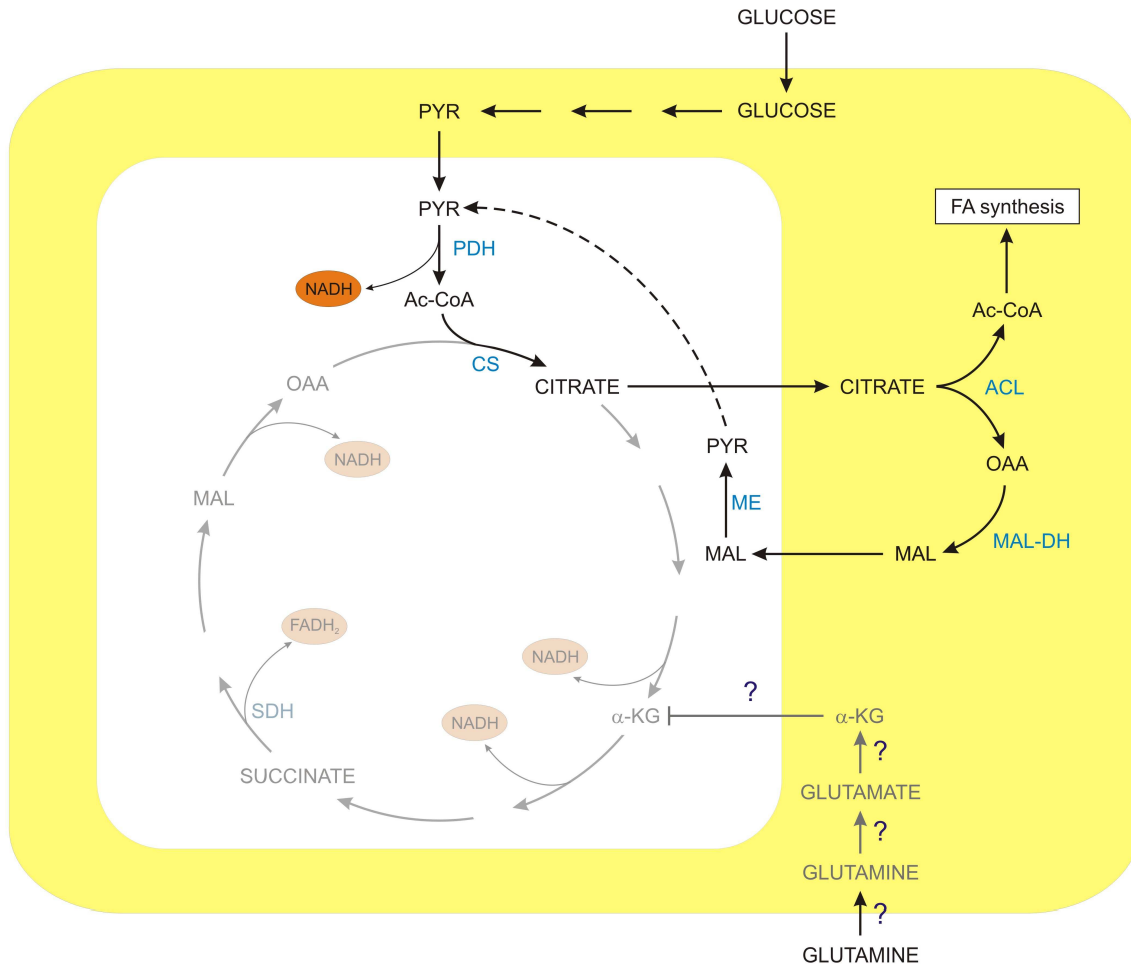


**FIG 5-1.** Proposed mechanism of downregulation of mitochondrial respiration in HTB-126 Glc. Glucose medium is a source of glucose as well as glutamine. Pyruvate entering mitochondria is metabolized in TCA cycle. High rate of citrate efflux probably take place, thus attenuating TCA cycle and NADH production. *ACL* – ATP citrate lyase, *MAL-DH* – malate dehydrogenase, *ME* – malic enzyme, *PDH* – pyruvate dehydrogenase, *CS* – citrate dehydrogenase.

